Neural circuit plasticity underlying learning and memory in *Drosophila melanogaster*: from synaptic connections to behavior

“Doctor rerum naturalium”

of the Georg-August-Universität Göttingen

within the doctoral program “Sensory and Motor Neuroscience”,

Göttingen Graduate School for Neurosciences, Biophysics, and Molecular Biosciences (GGNB)

submitted by

El Yazid Rachad

from Tetouan, Morocco

Göttingen, February 3rd, 2023

Thesis Committee:

Prof. Dr. André Fiala
(Department of Molecular Neurobiology of Behaviour, Johann-Friedrich-Blumenbach Institute for Zoology and Anthropology, Georg-August University, Göttingen)

Prof. Dr. Ralf Heinrich
(Department of Cellular Neurobiology, Johann-Friedrich-Blumenbach Institute for Zoology and Anthropology, Georg-August University, Göttingen)

Prof. Dr. Siegrid Löwel
(Department of Systems Neuroscience Johann Friedrich Blumenbach Institute for Zoology and Anthropology Göttingen Campus Institute for Dynamics of Biological Networks, Georg-August University, Göttingen)

Members of the Examination Board:

Reviewer: **Prof. Dr. André Fiala**
(Department of Molecular Neurobiology of Behaviour, Johann-Friedrich-Blumenbach Institute for Zoology and Anthropology, Georg-August University, Göttingen)

Second Reviewer: **Prof. Dr. Ralf Heinrich**
(Department of Cellular Neurobiology, Johann-Friedrich-Blumenbach Institute for Zoology and Anthropology, Georg-August University, Göttingen)

Prof. Dr. Carolin Wichmann
(Molecular Architecture of Synapses Group, Institute of Auditory Neuroscience, University Medical Centre, Göttingen)

Prof. Dr. Thomas Dresbach
(Department of Anatomy and Embryology, University Medical Centre, Göttingen)

Prof. Dr. Gregor Bucher
(Department of Evolutionary Developmental Genetics, Johann-Friedrich-Blumenbach Institute for Zoology and Anthropology, Georg-August University, Göttingen)

Prof. Dr. Jochen Staiger
(Department of Neuroanatomy, University Medical Centre, Göttingen)

Date of the oral examination: March 17th, 2023

Table of Contents

I. General introduction

Drosophila melanogaster, conversationally known as the fruit fly, was and is still being used exhaustively as a model organism in life sciences throughout the last century (Arias, 2008; Bellen et al., 2010). Its abundance, low costs and rapid reproduction cycle along with its vast and elaborate genetic toolkit have made the fly of the essence in scientific research (Tolwinski, 2017). The incessant generation and development of a plethora of molecular and genetic tools has allowed this model organism to keep pace with the latest advances. Its application in research ranges from dissection of cellular morphogenesis (Cong et al., 2001; Oshima et al., 2006; Li et al., 2007), mapping neuronal circuitries underlying a variety of behaviors (Aso et al., 2014a; Owald et al., 2015; Hige et al., 2015), aging and cell death (Pandey et al., 2016; Pihán et al., 2021; Takeuchi et al., 2022) to human disease modeling (Issa et al., 2018; Yost et al., 2020; Jung et al., 2020; Wang et al., 2021). This introduction covers some useful strategies, mainly utilized in the proposed manuscripts, for identifying and mapping neuronal circuitries and their functioning in integrating sensory signals and translating them to adaptive behavior.

1. The life cycle of *Drosophila*

Drosophila melanogaster is a holometabolous insect that has a short life cycle containing four stages from the embryo to the adult fly. The female fly has the innate capacity to lay around 100 eggs daily for about 20 days (Fernández-Moreno, 2007). Under optimal laboratory conditions (25°C and 60% humidity), a *Drosophila* egg hatches in the first day into a first instar larva that feeds on the surface of the media to then molt after approximately 24 hours into a second instar larva, which by then burrows through the food for another day. A second molt marks the transformation to

a feeding third instar larva that crawls out of the medium once satiety has been achieved to undergo metamorphosis, and wanders up the vial's wall between 24 to 48 hours searching for a suitable pupariation spot. During metamorphosis, the pupa undergoes a series of larval tissue degradation along with neo-adult organs development for around 84 hours. Finally, the adult fly ecloses (detaches from the pupa's cuticle). The whole developmental process takes approximately 10 days in the mentioned optimal conditions (twice as long at 18°C), allowing researchers to conduct a panoply of experimental procedures and genetic manipulations in a matter of a couple of weeks (Figure 1).

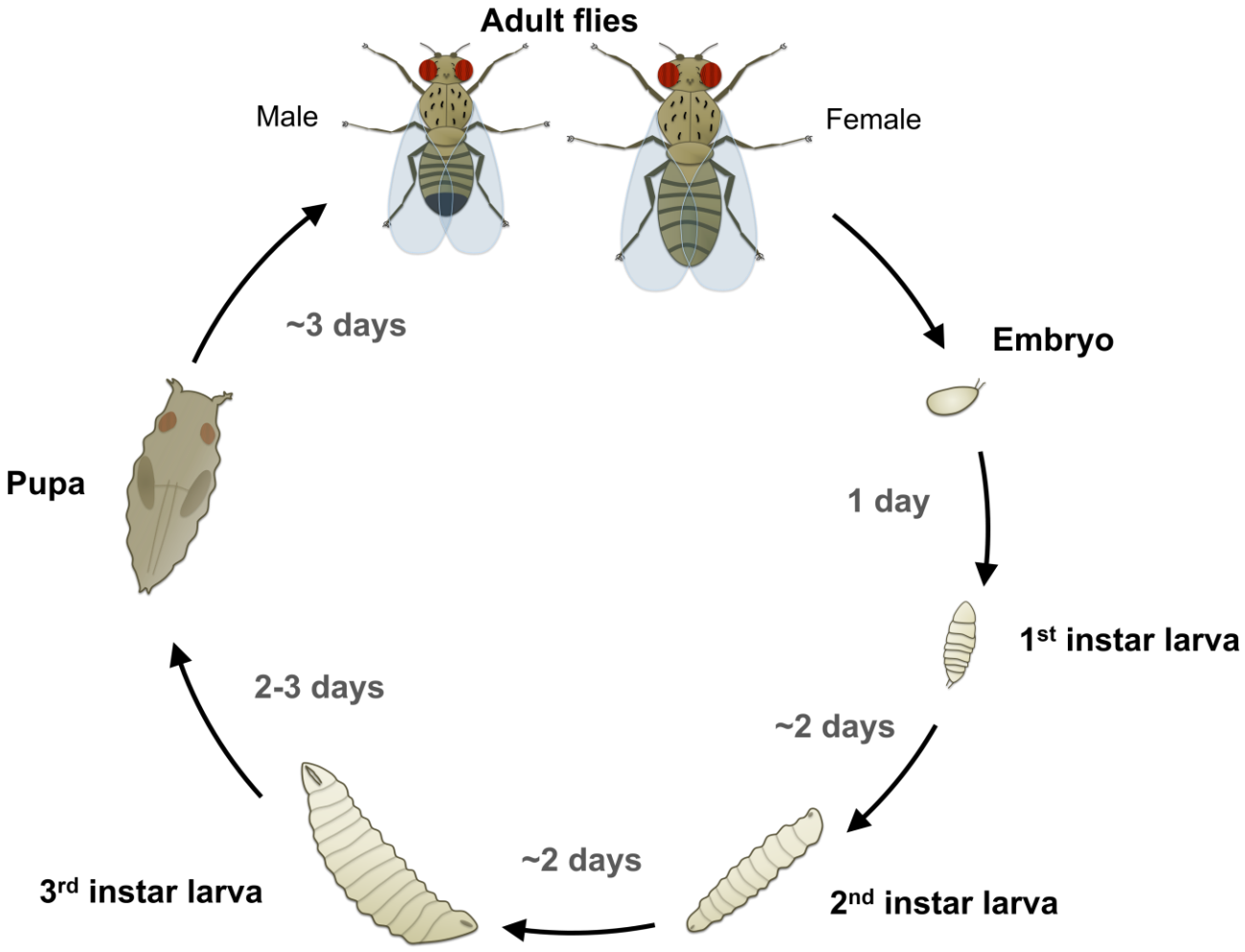

Figure 1: *The fruit fly Drosophila melanogaster life cycle is succinct. It takes a fly around 10 days to develop from an embryo to an adult at 25°C and 60% humidity. Four main phases mark Drosophila's development: embryo, larva (first, second and third instar), pupa and adult (modified from Ong et al., 2015).*

It has been shown that pupariation is initiated by a significant surge of the hormone ecdysone (Yamanaka et al., 2013). This steroid hormone, secreted from the ring gland, is the key regulator to all insect developmental transitions. During metamorphosis, the nervous system of a fly is highly remodeled and reorganized (Tissot & Stocker, 2000). Recent new advances in the understanding of ecdysone action have relied on the use of genetic tools in *Drosophila melanogaster* to study metamorphosis (Yu et al., 2013; Yamanaka et al., 2013; Rabinovich et al., 2016; Mayseless et al., 2018).

In particular, neuronal remodeling during development is crucial to establish neural circuits and is essential for the development of both vertebrate and invertebrate nervous systems (Luo & O'Leary, 2005). It starts with degenerative processes, such as synapse degradation and neurite pruning, and ends with stabilizing regenerative processes, in particular axon and dendrite regrowth (Watts et al., 2003). Studies on fruit flies remodeling properties during development are of importance to understand human diseases and disorders. It has been recently established that defects in neuronal remodeling determine the progression of multiple neuropsychiatric disorders, such as autism (Thomas et al., 2016) and schizophrenia (Cocchi et al., 2016). In addition, studies have shown that molecular mechanisms underlying developmental synaptic elimination play a role in the development of disorders such as schizophrenia (Sekar et al., 2016) and neurodegenerative diseases, notably Alzheimer's disease (Hong et al., 2016). In some physio-

pathological conditions such as dying back neurodegenerative diseases (Yaron & Schuldiner, 2016), neurites degeneration has been shown to play important roles in development and are detected at the final stages of said diseases. In spite of the fact that remodeling and neurodegenerative diseases do not share cell death as a common denominator, the mechanistic similarities that they exhibit elucidate an opportunity to a better understanding of the mechanism of degeneration in some neurological and neuropsychiatric disorders. The fruit fly represents a favorable model to study fundamental principles of neuronal remodeling and its role, however and in the scope of this thesis, our overall interest in this aspect is the mushroom body's pruning and remodeling.

In the adult *Drosophila* brain, the mushroom body (MB) is the focal structure of associative learning and memory (Heisenberg et al., 1985; de Belle & Heisenberg, 1994; Fiala, 2007; Liu et al., 2016). Each of the two MBs (one per hemisphere) consists of approximately 2000 neurons (Heisenberg, 2003; Aso et al., 2009), named Kenyon cells (KCs), proliferating from four distinct neuroblasts (Ito et al., 1997). These neurons form into neuropils that can be subdivided into two vertical (α and α′) and three horizontal lobes (β, β′ and γ) (Crittenden et al., 1998). A high density dendritic area, called the calyx, represents the site where these KCs are sparsely activated by mainly, but not exclusively, olfactory sensory input that is mostly conveyed by the olfactory PNs (Gruntman & Turner, 2013). The modulation from the GABAergic anterior paired lateral (APL) and the serotonergic dorsal paired medial (DPM) neurons plays a role in the sparse activity of the KCs that leads to a better odor discrimination and processing in the adult brain (Yu et al., 2005; Lin et al., 2014; Jürgensen et al., 2021). The olfactory information encoded by the KCs is further modulated by dopaminergic neurons (DANs) innervating different compartments of

the MB. Activation of DANs through a reinforcement stimulus (rewarding or punishing) shifts the valence of a sensory information while it is integrated and transferred to higher somato-sensory regions by MB output neurons (MBONs) (Aso & Rubin, 2016) (more details in the olfactory pathway section of this thesis, page 16).

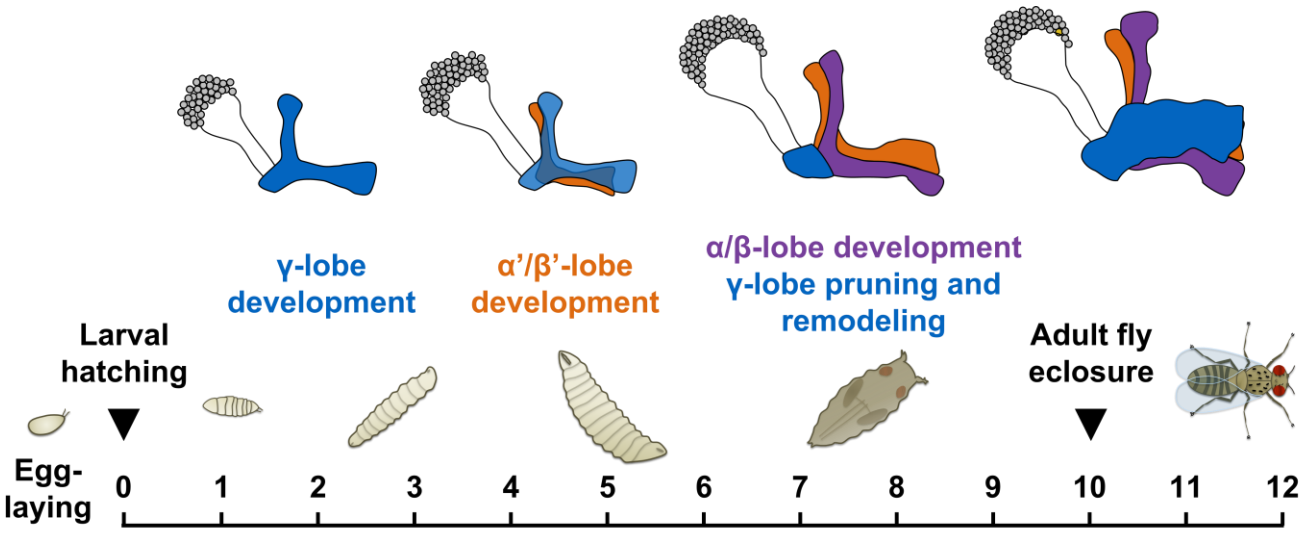

Figure 2: *Pruning and remodeling of γ-KCs allows strong and stable regrowth of the adult MB. Larval γ-KCs extend their dendrite arborizations in the calyx and project axonal terminal to form the MB lobes. During metamorphosis, γ-KC dendrites and axons degrade to a certain extent and later regrow to find and form connections with their respective synaptic partners (adopted from Mayseless et al., 2018).*

The remodeling of the γ-lobe of the MB during development is crucial for establishing strong, stable and precise connectivity with its synaptic partners (Figure 2). It has been previously established that inhibition of γ-lobe KCs pruning resulted in a pruning defect of the APL neuron, suggesting that inhibiting remodeling of one neuronal population can affect the functional wiring of the entire circuitry (Mayseless et al., 2018). In addition, recent studies demonstrate that pruning deficits of the developing MB lead to an impairment of courtship memory (Redt-Clouet et al., 2012),

associative odor learning, and cause hyperactivity (Poppinga et al., 2022). As cited above, studies on developmental remodeling and its role in circuitry reconstruction along with a proper functioning of the MB has been elucidated, but the cellular and sub-cellular mechanisms allowing such phenomenon remain unknown. Therefore, Is neuronal activity in terms of de- and/or hyperpolarization together with calcium dynamics important for MB pruning and circuit remodeling? This question will be addressed in the first manuscript of this thesis (Mayseless et al., 2023, page 36).

2. The repertoire for genetic engineering in *Drosophila*

The genome of *Drosophila* contains a pair of sex chromosomes, X/X or X/Y, and three pairs of autosomes described as II, III, and IV, which was fully sequenced and published in the year 2000 (Adams et al., 2000). Due to its simplicity and the relatively modest number of neurons when compared with mammals, the nervous system of *Drosophila* allows arrays of state-of-the-art genetic manipulations. A collection of various genetic tools allows the study of the complexity of the nervous system both anatomically and functionally in immaculate detail. With the use of such an enhanced genetic toolkit, researchers progressed in the last few decades in understanding various functions and behaviors such as aspects of development of the nervous system (Hartenstein et al., 2008; Mayseless et al., 2018), synaptic connectivity (Li et al., 2020; Scheffer et al., 2020), exocytosis and endocytosis at synapses (Bellen et al., 2010), and the neuronal circuits underlying complex behaviors such as feeding, sleep and courtship (Knapp et al., 2022), and learning and memory (Widmann et al., 2016; Bilz et al., 2020). These unremitting developed methods allow neuroscientists to tackle almost any fundamental biological question,

and the 60% genome homology that flies and humans share facilitates the translational properties of this knowledge (Mirzoyan et al., 2019).

To genetically manipulate neuronal gene expression and neuronal activity, the most reliable and employed technique is the binary expression GAL4/UAS system (Brand & Perrimon, 1993). This system targets gene expression that promotes a specific activation of any cloned gene in cell-specific patterns (Figure 3A). GAL4 is a transcriptional activator derived from yeast and inserted in various locations of *Drosophila*'s genome to then drive expression from one specific genomic enhancer of interest. Due to its exclusive expression in yeast, it does not alter or interfere with any endogenous gene expression in *Drosophila* and can be used unequivocally. To generate these GAL4 drivers, the original P-elements (also known as P-element enhancer detectors or enhancer traps) were modified by substituting the lacZ reporter with GAL4 by cloning and inserted into the genome (Brand & Perrimon, 1993).

The dual nature of this system necessitates the presence of another component that consists of GAL4-responsive target genes, also referred to as upstream activation sequence (UAS). Any reporter sequence of a gene of interest can be replicated and inserted into a vector downstream of the UAS sequence. Each of the GAL4 and UAS sequences are usually carried in different transgenic lines, separating the target gene from its transcriptional activator, and only bind in the progeny to express the desired reporter. For creating drivers with more restricted expression patterns, small fragments of DNA are cloned into plasmids upstream of a promoter and GAL4, and then inserted at a specific docking site in the fly genome using the ΦC31 integrase (Groth et al., 2004). Another element that can be added to the GAL4/UAS system, making it a ternary system, is the GAL4 repressor GAL80 (Ma & Ptashne, 1987) (Figure 3B). The introduction of this repressor that prevents the

initiation of GAL4 transcription by binding to it, adds another layer of gene expression manipulations. For example, the function of GAL4 can be temporally controlled using a temperature-sensitive GAL80 in the TARGET system (McGuire et al., 2004), or used in stochastic yet sparse labeling of fewer cells in desired neuronal populations by flipping out the GAL80 (positioned behind Flipase recognition targets FRT) *via* a heat-shock Flipase (hsFLP) during development (e.g. MARCM technique) (Lee & Luo, 1999).

The generation of the GAL4 system was extensively exploited in the Janelia Farm Flylight Project (Jenett et al., 2012) and the Vienna Tile library (VT) (Pfeiffer et al., 2010) that led to the creation and characterization of thousands of GAL4 driver lines. The availability of such an arsenal of GAL4 driver lines is certainly useful, but often the insertion of such a sequence can lead to unspecific cell targeting due the expression of the promoter in other cells. This of course generates some complications in the context of investigating the role of specific cell types in different forms of behaviors by genetically manipulating them. Thus, assigning functions to cell populations might be difficult if one cannot differentiate between the GAL4 targeted cells. Therefore, an introduction of more specific strategy that permits positive selection was introduced and derived from the Gal4-UAS system called Split Gal4 (Luan et al., 2006). GAL4 consists of two separable and functional domains for specific DNA-site recognition (DNA binding domain (DBD)), and transcription activation (the activation domain (AD)). Inserted alone, these two domains are inoperative and incapable of promoting gene expression, but reconstitute the transcriptional activity of GAL4 when fused (Figure 3C).

The split-GAL4 system was obtained by fusing both the DBD and AD domains of GAL4 to strong heterodimerizing leucine zippers and may independently express in

different cell populations using different enhancers (Luan et al., 2006). Only cells that express both enhancers and thus would express both DBD and AD can reconstruct GAL4 activity and become transcriptionally active. The cell-specific targeting nature of the split-GAL4 technique made it one of the most platitudinous systems in mapping and manipulating the fly nervous system. With an array of accessible genetic constructs and manipulation tools, this system is employed in various studies ranging from investigating neural circuits and connectomics (Aso et al., 2014a; Aso et al., 2014b; Eichler et al., 2017; Li et al., 2020), to dissecting simple and complex behaviors, notably feeding (Lau et al., 2021), locomotion (Bidaye et al., 2014) and learning and memory (Aso et al., 2014b; Saumweber et al., 2018).

In addition to the GAL4/UAS technique, other binary systems have been described and utilized in *Drosophila* such as LexA/lexAop (Szüts & Bienz, 2000) and QF/QUAS (Potter & Luo, 2011). These systems can be simultaneously expressed with each other allowing non-overlapping cell targeting, manipulation and activity monitoring (Lai & Lee, 2006) using various reporters and indicators. As the LexA and QF systems have been recently developed and introduced, the existence of a library of drivers is yet to be made. These binary expression systems are used (separately or even in combination) to a great extent in the proposed studies of this thesis (manuscript 1, 2 and 3). This allowed us to address our questions by employing different strategies ranging from the use of such systems to express various transgenes to alter, enhance or monitor the functional activity of the target neuronal populations.

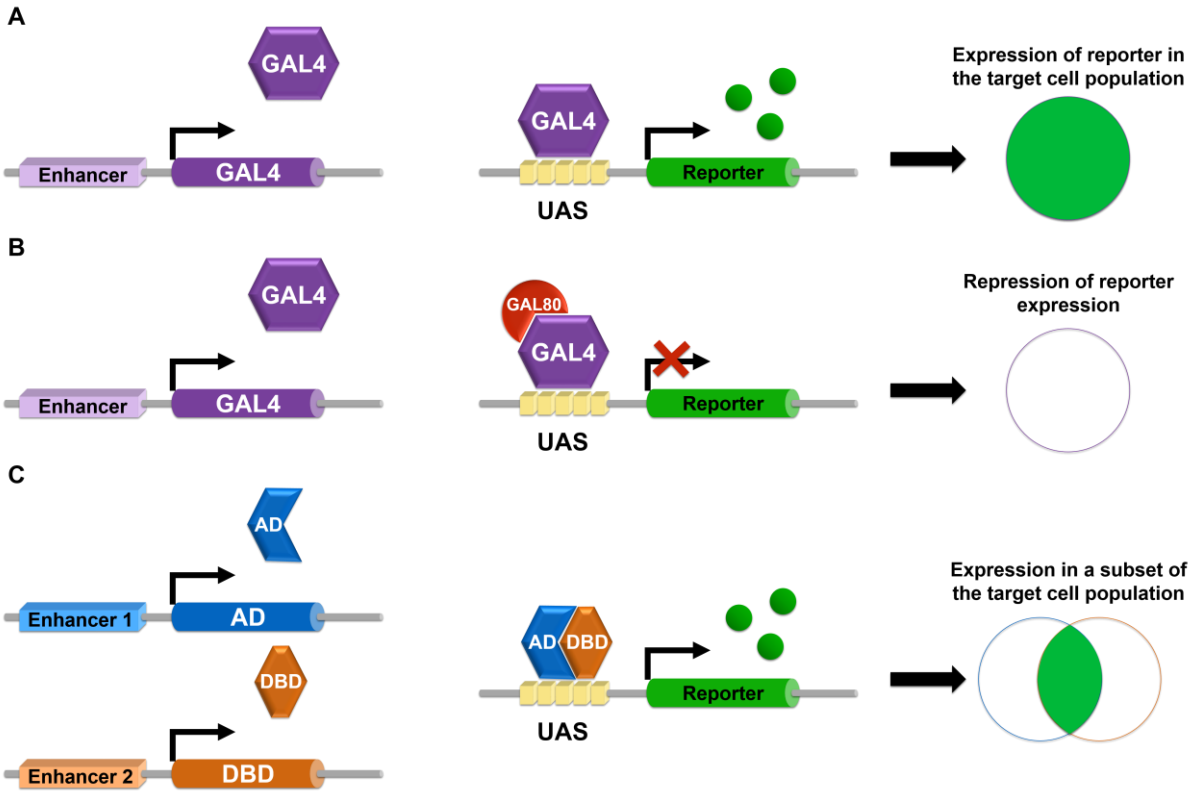

Figure 3: *Most common genetic expression techniques in Drosophila. (**A**) The binary GAL4/UAS expression system that allows specific transgene expression in distinct neuronal cell types. A cell specific enhancer is upstream of the insertion site of the yeast transcription factor GAL4 that is exclusively expressed in cells in which this promoter is active. UAS (upstream activation sequence) is inserted before a reporter gene and leads to its expression only in the presence of GAL4. (**B**) The GAL4 repressor GAL80 can be added to this binary system, making it a ternary expression system, to allow another layer of temporal control in gene expression techniques. **(C)** GAL4 can be separated into two distinct fragments called DBD (DNA-binding domain) and AD (activation domain), each inserted downstream of a distinct enhancer that allows specific targeted gene expression in different cell types. Alone, these two domains are inoperative and only when the two enhancers are expressed in the same cell type, the GAL4 transcriptional activity is restored and expression is initiated in the cells of interest.*

These cell-specific gene expression systems can be used to drive the production of various reporters ranging from ion channels or toxins that block or facilitate neuronal activity, to indicators for various compounds of the cell that are implicated in

determining the effect on behavior (Venken et al., 2011). *Drosophila*'s nervous system is able to generate complex coordinated behavioral sequences in response to diverse sensory cues and previously learned experiences. The implementation of such elaborate neural activity and gene expression manipulation tools can aid in identifying specific neuronal circuits that are necessary and sufficient for decoding particular sensory modalities or integrating different behaviors. Experiments have shown that one of the ways to assess the role of a certain neuron or neuronal population in a behavior is to eliminate their function by causing cell death and quantify the generated effects (Hidalgo et al., 1995). Less extreme approaches, that do not include killing cells, were created to block neurotransmission by interfering with synaptic vesicle release. The first tool that was developed is the light chain of tetanus toxin (TNT) that cleaves neuronal synaptobrevin (nSyb) and blocks vesicle release leading to neuronal silencing (Sweeney et al., 1995). In spite of the many perks of UAS-TNT, it presents a few disadvantages that result in cell damage, developmental defects and possible neuronal circuitry compensation due to its chronic expression. This might alter assaying phenotypic consequences in response to neuronal manipulations. Furthermore, the introduction of a new transgenic construct that permits temporally controlled and reversible neuronal silencing, named *Shibire*^{ts} allowed circumventing such inconveniences (Figure 4A). UAS-*Shibire*^{ts} is a temperature-sensitive dominant negative mutation of *Drosophila* orthologous form Dynamin (GTPase necessary for vesicle recycling) ortholgue. In restrictive temperatures (30°C), the protein product of this gene is ineffective resulting in blocking chemical neurotransmitter release thus blocking the output of the targeted cells (Kitamoto, 2001; Kitamoto, 2002). This versatile tool has been described in numerous studies investigating neuronal circuits underlying different behaviors,

especially the dissection of micro-circuits responsible for different forms of learning and memory (Kasuya et al., 2009; Owald et al., 2015; Zhao et al., 2019; Hancock et al., 2022, manuscript 2, page 73; Suzuki et al., 2022; Rachad et al., manuscript 3, page 88). Another construct to block membrane depolarization by ion channel manipulation is the inwardly rectifying potassium channel Kir2.1. UAS-Kir2.1 prevents neuronal depolarization by increasing K^+ ions conductance (Paradis et al., 2001). In contrast, a reliable tool that was described to increase neuronal activity using ion channels is the temperature inducible cation channel UAS-dTrpA1 (Rosenzweig et al., 2005, Hamada et al., 2008). Both of these ion channel manipulation constructs have been utilized in many experiments, e.g. assessing the MB activity during metamorphosis in the first manuscript of this thesis (Mayseless et al., 2023, page 36).

Instead of silencing or increasing neuronal activity, other transgenes are employed to probe neuronal functional, especially in the context of optical functional *in vivo* imaging, e.g. to identify distinct neurons that respond to various sensory stimuli correlating with behavioral responses. Based on the fact that firing an action potential leads to local increases in calcium levels, a collection of genetically encoded calcium indicators is available to monitor neuronal activity. One of these calcium sensors, the single-fluorophor GCaMP (Nakai et al., 2001; Wang et al., 2003), has been significantly developed in many generations varying in kinetic properties and calcium binding affinity, making it the reagent of choice (Figure 4B). To dive even further in localized calcium level changes, this sensor has been fused with pre- and post-synaptic proteins for a better readout in investigating synaptic activities. A study introduced two UAS-GCaMP sensors coupled with either the C-terminus of rat Synaptophysin (forming the pre-synaptic Syp-GCaMP3) or the C-terminus of the post-synaptic protein *dHomer* (forming the post-synaptic dHomer-GCaMP3) for a

highly-localized monitoring of the calcium activity (Pech et al., 2015) (Figure 4C-D). In addition to calcium, different cell components linked to neuronal activity changes can be monitored. The two candidates that can be exemplified are the neurotransmitter vesicle release indicator (pH-sensitive fluorescent protein) pHluorin (Miesenböck et al., 1998) (fused to the first intravesicular domain of rat Synaptophysin in the lumen of synaptic vesicles and forming Syp-pHTomato) (Pech et al., 2015) and the highly responsive circularly permuted GFP (cpGFP)-based cAMP sensor G-Flamp1 (green fluorescent cAMP indicator 1) (Wang et al., 2022) (Figure 4E-F). All of these sensors show robust and reliable fluorescence changes in the context of investigating the neuronal circuitry underlying a complex form of higher-order olfactory learning in *Drosophila* (Rachad et al., manuscript 3, page 88).

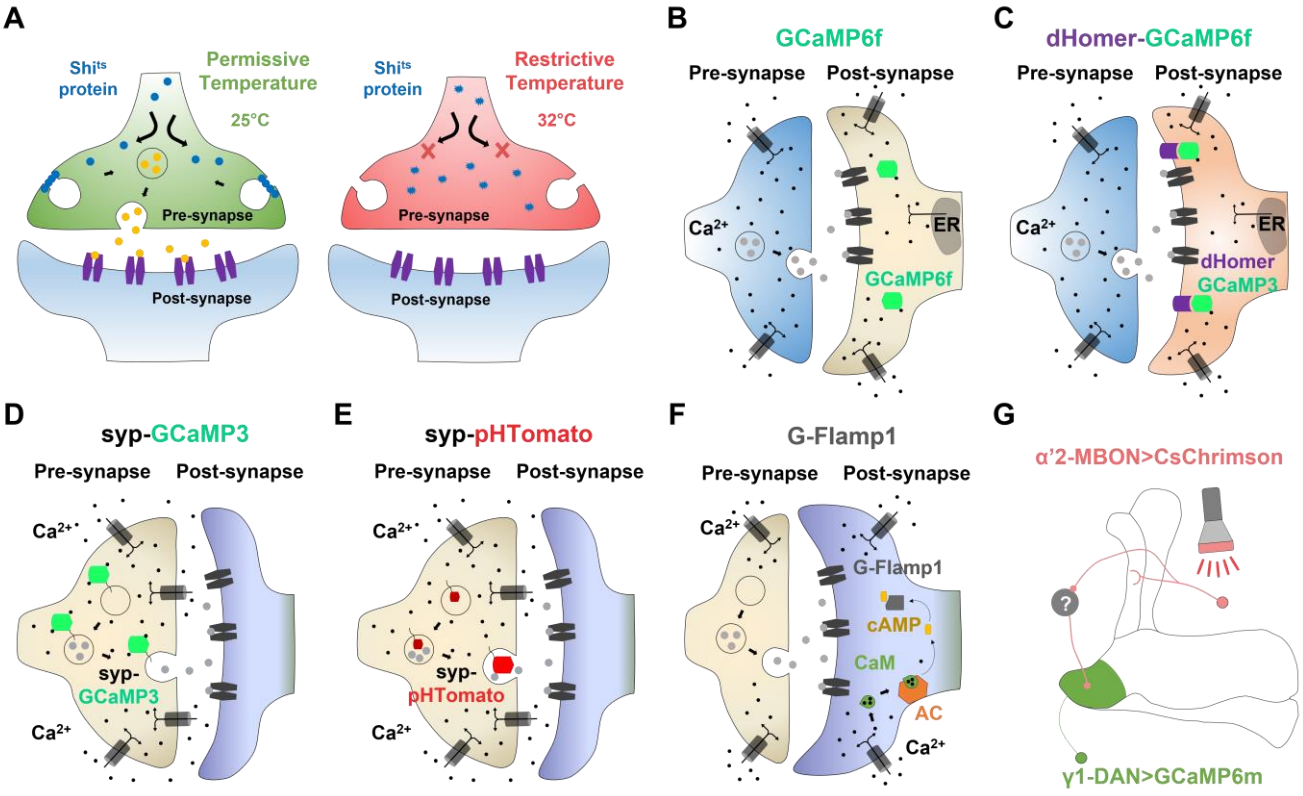

Figure 4: *Examples of various transgenic tools utilized in dissecting neuronal circuits and activity in Drosophila. (**A**) Mirrored illustrations representing the dynamics of the temperature-*

*sensitive mutation Shibire^{ts}. During permissive conditions (left), the dynamin orthologue Shi^{ts} plays a role in vesicle recycling for a normal functioning of synaptic transmission. On the other hand, raising the temperature in the restrictive conditions (right) leads to an impairment of Shi^{ts} role, thus blocking the output of the manipulated neuron (Kitamoto, 2002). (**B-D**) Different calcium sensors exemplified by their expression sites. These calcium indicators can be cytosolic (**B**)* (*Dana et al., 2019), localized in the pre- (**D**) or post-synaptic (**C**) site due to their fusion to pre- or post-synaptically expressed proteins (Pech et al., 2015). (**E**) Neurotransmitter vesicle release sensor Synapto-pHluorin (UAS-Syp-pHTomato) inserted into the first domain of rat Synaptophysin in the lumen of synaptic vesicles (Pech et al., 2015). (**F**) Green fluorescent cAMP indicator 1 (G-Flamp1) has immensely high kinetics and affinity to cAMP and is circularly permuted GFP-based (Wang et al., 2022). (**G**) Example drawing of simultaneous optogenetics with calcium monitoring in a target neuronal population. Expression of CsChrimson allows optogenetic activation of distinct neurons with specific illumination wavelengths and record calcium levels upon this activation in other neurons to verify and existence of synaptic or functional connectivity (for more details, Rachad et al., manuscript 3, page 88).*

Working independently or in addition to the various mentioned sensors, a generation of genetically encoded proteins that activate or silence neural activity in response to light stimulation has been an exciting extension for research in the neuroscience field. Optogenetics *in Drosophila*, kick-started by UAS-P2X2 (Lima & Miesenböck, 2005) (a cation channel activated by caged ATP released by light) and developed into various photoactivatable opsins, is a versatile method allowing neuronal simultaneous manipulations acting in synergy to answer a precise biological question (Venken et al., 2011). Another subfamily of these opsins is the ChannelRhodopsin sub-family that functions as sensory photoreceptors in unicellular green algae to control phototaxis (Nagel et al., 2002), but allows light to control different aspects of neuronal activity when expressed in other organisms (Schroll et al., 2006).Furthermore, CsChrimson, a CsChannelRhodopsin-Chrimson chimera replacing the Chrimson N terminus in the CsChR N terminus, has the same spectral

and kinetic properties as Chrimson (Klapoetke et al 2014). Activation of this red light-sensitive channelrhodopsin culminates in reliable light-triggered action potentials in targeted neurons (Figure 4G). Due to the controllability of light delivery, these optogenetic tools allow us to input or disrupt information in the precision of neurons themselves, thus creating an opportunity to scrutinize neurons' activity in their networks.

Determining the neuronal candidates implicated in encoding specific stimuli based on their activity is merely the first piece in mapping neuronal circuitries underlying behaviors. The further steps would logically imply linking these neurons into circuits by determining their anatomical and functional connectivity. Transgenetic tools that label the connectivity across synaptic partners are referred to as transsynaptic tools. One of the most recognized transsynaptic tools is GRASP (GFP Reconstitution Across Synaptic Partners), that was initially developed in *C. elegans* and has been used to identify synaptic connections in *Drosophila* (Feinberg et al., 2008). This construct contains two split-GFP fragments, spGFP1-10 and spGFP11, that are membrane-bound and expressed in presynaptic and postsynaptic neurons (Gordon & Scott., 2009). Expressed alone, neither fragment emits fluorescence. Only when two neurons synaptically connect, GFP is reconstructed across these synaptic partners and can be visualized by fluorescence microscopy. Reports show the existence of other chemical synapse detecting techniques besides GRASP such as trans-Tango (Talay et al., 2017), TRACT (TRAnsneuronal Control of Transcription) (Huang et al., 2017), and BAcTrace (Botulinum-Activated Tracer) (Cachero et al., 2020). In addition, an electrical synapse (formed by gap junctions) detecting technique named PARIS (Pairing Actuators and Receivers to optically ISolate gap junction) has been recently published (Wu et al., 2019).

In summary, the myriad of transgenic constructs for spatio-temporal gene expression to specific neurons, manipulation and monitoring of their activity, and evaluation of behavioral consequences can be used in the context of understanding the mechanisms by which the nervous system develops and computes particularly complex behaviors (e.g. higher-order olfactory conditioning), together with the synaptic plasticity underlying such phenomena.

3. The olfactory processing pathways in the *Drosophila* brain

Given the complexity of the compound eyes of insects, one could assume that their elaborate visual system that allows them to integrate cues from a large three-dimensional field of vision might be of great interest in studying insect learning processes. The adult fruit fly visual system perceives multiple optical points in a wide space by retinal cells classified by their photoreceptors (from R1 to R8), regularly arranged from ommatidia, and detect light stimuli from UV to green (Heisenberg & Buchner, 1977). The visual message is then transferred through different layer of the visual system (lamina, medulla, lobula, and lobula plate) to higher centers responsible for motion and color related behaviors (Rachidi et al., 1997; Zhu, 2013). Multiple behavioral studies have been utilized in vision research ranging from investigating phototaxis behaviors such as in the Buridan's paradigm (Bülthoff et al., 1982; Han et al., 2021), motion related assays featuring the use complicated optomotor mazes (Heisenberg & Götz, 1975; Rister et al., 2007; Buchner & Wu, 2009; Zhu et al., 2009), to higher-order behaviors such as second-order motion (Theobald et al., 2008; Theobald et al., 2010; Zhang et al., 2013).

However, olfactory associative learning has been the main target of investigation in all forms of learning and memory in the fruit fly. This potent domination in learning

literature stems from *Drosophila*'s ability to reliably achieve quantifiable and reliable results of learning and memory along with odor discrimination (Tully & Quinn, 1985). In addition, the olfactory primary processing hub, the antennal lobe (AL), is curiously similar in structural architecture and function to that of vertebrates (Boeckh et al., 1990). Moreover, downstream of the olfactory bulb in mammals, the piriform cortex receives odor input and is the equivalent in function and hierarchy to the mushroom body (MB) of insects (Davis & Han, 1996). Previous studies demonstrate the similarities in the expression of specific sub-cellular compounds that play fundamental roles in learning and memory such as the adenylyl cyclase and the protein kinase A in the mammalian piriform cortex (Cadd & McKnight, 1989; Xia et al., 1991) as well as the MB of the fruit fly (Nighorn et al., 1991; Han et al., 1992; Skoulakis et., 1993). The similarities that these two structures exhibit in function, odor processing hierarchy and cell-type specific markers provide concrete evidence that learned behaviors can be transposed from insects to mammals. Furthermore, a fly can rapidly and easily learn about the association between an odor and a reinforcing stimulus (punishment e.g. electric shocks or reward e.g. sugar). The nature of the reinforcement imposes a valence on the innate stimulus and creating an aversive or attractive memory. This provides for a field of studies for researches to investigate different phases of memory formation, consolidation, decay, and retrieval along with a functional dissection of the mechanisms underlying these phases (Xia et al., 1997; Busto et al., 2010; Johnson & Nichols, 2011; Lagasse et al., 2012; Siegenthaler et al., 2019; Inami et al., 2020; Zatsepina et al., 2021; Sabandal et al., 2021; Zhang et al., 2021; Rachad et al., manuscript 3, page 88).

Reception of odor molecules occurs at the level of the olfactory sensory neurons (OSNs) at the antennae and the maxillary palps, where the funiculus, the third

antennal segment, gives base to the sensilla (Shanbhag et al., 2000). In *Drosophila*, males and females possess approximately 1200 OSNs. In every OSN, olfactory receptors (ORs) are pretty unique with a common expression of the ubiquitous receptor Or83b or ORCO, and can be co-expressed (up to three conventional ORs) to determine a specific molecular response profile to different odorants and keep their identities (Galizia & Sachse, 2010). Another type of receptors expressed in the OSNs is the ionotropic glutamate receptors in (IRs) (Benton et al., 2009). When odors bind to their respective receptors, OSNs expressing the same type of ORs or IRs are potentiated and transmit the sensory information to a single glomerulus in the antennal lobe (AL), which represents the first olfactory neuropil in the insect brain. The expression pattern and functional differences between these olfactory receptors (ORs and IRs) explains the distinct separation of glomeruli innervated by them (Silbering et al., 2011). ORs are conserved in their expression pattern in *Drosophila* as well as in mammals (Galizia & Sachse, 2010). Nevertheless, it has been described that in a few cases of 1:2 and 2:1 innervation ratios from OSNs to the glomeruli of the AL in *Drosophila* exist as well (Couto et al. 2005; Fishilevich & Vosshall 2005). The AL consists mainly of ~50 glomerular groups per hemisphere (in the fruit fly), which are the structures where OSNs, local neurons (LNs) and projection neurons (PNs) form synaptic connections and interact. Optical imaging of intracellular calcium activity in flies shows that stimulation with an odor leads to distinct spatiotemporal glomerular activity patterns (Fiala et al. 2002). In addition, it has been shown that the AL glomeruli respond to odors in broad and mostly specific activity patterns, with odors being represented in multiple glomeruli at once (Seki et al., 2017). Downstream of the OSNs, PNs receive odor information reliably in 1:1 (and rarely 1:2) connection, and convey it then to the lateral horn (LH) and the MB for

behavioral olfactory processing. While the MB encodes the information of the odor in the context of a conditioned behavioral response, the lateral horn integrates innate odor-related behavior (Heisenberg et al., 1985) (Figure 5).

The MB receives odor information from ~150 uni-glomerular PNs in the MB calyces, which are large protuberances consisting of dense dendritic arborizations. Each PN axon traverses along significant areas of the calyx, forming connections by their pre-synaptic sites, called boutons, with many intrinsic KCs (Marin et al., 2002). Around three uni-glomerular PNs innervate each glomerulus and project in the same manner to the MB and the LH, suggesting a functional stereotypy (Wong et al., 2002). Despite the fact that PNs and KCs exhibit a highly intermingled crosswise interconnections, the latter possess a high firing threshold that translates into a sparse activity. This means that only a small subset of KCs respond to a distinct odor (5-8%) (Turner et al., 2008; Luo et al., 2010), and thus favoring associative olfactory learning (Fiala, 2007; Bilz et al., 2020). The KCs spike only if multiple PNs are activated simultaneously (Gruntman & Turner, 2013). Studies suggest that one of the mechanisms that induce this high firing threshold and thus the sparse activity of the KCs is the modulation from the GABAergic APL and the serotonergic DPM neurons. This results in fine-tuned odor discriminations at the level of the MB (Yu et al., 2005, Lin et al., 2014; Eichler et al., 2017). The KCs project elongated and uniformly aligned axonal branches that merge in the peduncle of the MB and then diverge into three neuropils called the MB lobes. There are three lobes in the MB as mentioned above (α/β, α′/β′ and γ) that can be separated into different compartments according to the innervation pattern of the modulatory neurons DANs and the MBONs (Aso et al., 2014; Li et al., 2020). A connectomics study of the adult *Drosophila* MB further classifies KCs based on anatomical and functional characteristics to then suggest the

presence of seven different layers (Li et al., 2020). Even though multiple types of KCs that constitute these layers were described, the main neurotransmitter of these cells is acetylcholine (ACh) (Barnstedt et al., 2016), with a co-localization with the short neuropeptide F (sNPF) in parts of the α/β lobe and all γ-KCs (Johard et al., 2008).

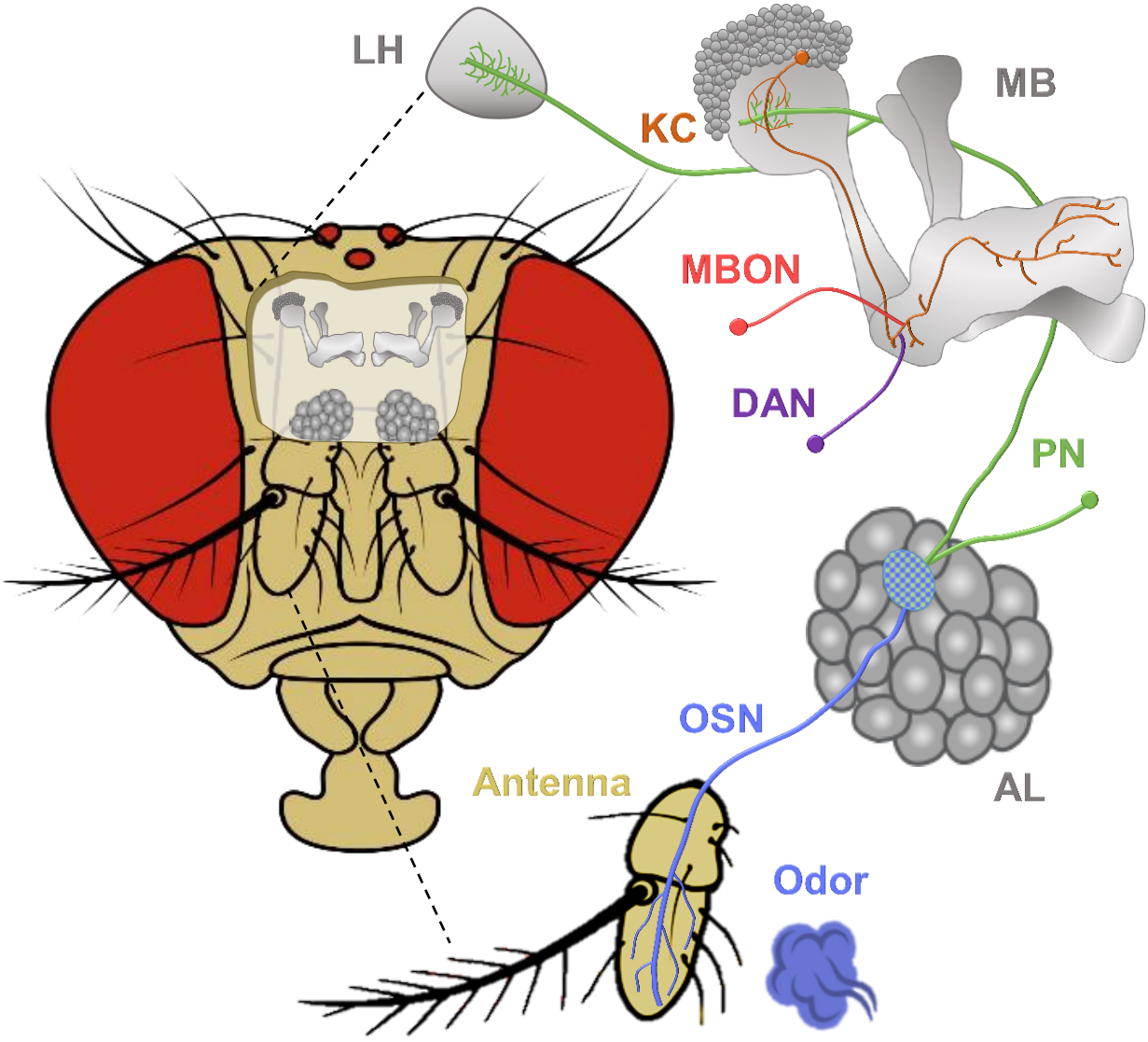

Figure 5: *Simplified cartoon representation of the Drosophila olfactory system. The left of the figure represents the frontal view of the Drosophila with an opening that exposes the central brain, especially the MB and the AL. On the right, portrayed is the odor information pathway in Drosophila brain. The odor bind to its olfactory receptors (ORs) at the dendrites of olfactory sensory neurons (OSNs) that express the same OR and converge in the first brain center of the olfactory pathway, the antennal lobe (AL). At this structure, the projections*

neurons (PNs) form glomeruli with the dendrites of the OSNs. Most PNs convey odor information to the mushroom body (MB) via bouton-like axon terminals that connect to the dendritic synapses of the MB intrinsic neurons, Kenyon cells (KCs). The PNs axons project further and terminate in the lateral horn (LH) in addition to few projections that bypass the mushroom. Modulatory dopaminergic neurons (DANs) and mushroom body output neurons (MBONs) innervate different compartments of the MB lobes. (Inpired from Bilz et al., 2018)

Synapses between KCs and MBONs are efficaciously modulated by MB input neurons, most commonly known as DANs, which mediate reinforcement signals (Aso et al., 2014a). Electron microscopy reconstruction studies reveal a conical circuit that defines every compartment of the MB independently from the neurotransmitters of DANs or MBONs (Li et al., 2020; Scheffer et al., 2020). Dopamine (DA) has been assigned many prominent roles in the vertebrate and invertebrate nervous systems. In mammals, this ubiquitous neuromodulator is involved in motor control, reinforcement, motivation, memory, arousal and attention (Schultz et al., 1997; Dayan & Balleine, 2002; Montague et al., 2004; Wise, 2004; Joshua et al., 2009). It has been extensively shown that a deteriorated, and thus dysfunctional, DA system is associated with neurodegenerative diseases and psychiatric disorders such as idiopathic Parkinson's disease, schizophrenia, depression, drug addiction and attention deficit disorder (Montague et al., 2004; Wise, 2004; Heinz & Schlagenhauf, 2010). In addition, DA plays a role in various physiological processes such as locomotion (Pendleton et al., 2002; Lima & Miesenböck 2005, Kong et al., 2010), reinforcement (Schwaerzel et al., 2003), feeding behaviors and motivation (Krashes et al., 2009), memory (Tempel et al., 1984; Schwaerzel et al., 2003; Aso & Rubin, 2016), and arousal (Lebestky et al., 2009) in *Drosophila*. Due to these similarities in the roles of DA in behavioral decision-making and adaptation from humans to simpler

invertebrates, along with the developed techniques to monitor and manipulate neuronal activity and circuits, *Drosophila* as a model organism allows a better apprehension of the modulatory role of DANs in complex behaviors in higher brain centers (Riemensperger et al. 2013; Tomchik, 2013; DasGupta et al. 2014; Owald et al. 2015; Owald & Waddell 2015; Felsenberg et al. 2018; Aimon et al. 2019; Boto et al. 2019).

At least eight DAN clusters in the fruit fly are characterized and project to various regions of the brain while mediating different behaviors and implicated in various functions (Mao & Davis, 2009). Innervating the different compartments of the MB lobes, DANs were sorted into two clusters that transmit modulatory information about reward and punishment from sensory neurons to KCs (Figure 6). Neurons located in the protocerebral anterior medial (PAM) cluster that projects its axon terminals in the horizontal lobes was shown to play a critical role in forming appetitive odor memory (Liu et al., 2012). On the other hand, the protocerebral posterior lateral 1 (PPL1) cluster, innervating the vertical lobes, was mapped as the origin of reinforcement signals for aversive odor memory (Riemensperger et al., 2005; Claridge-Chang et al., 2009; Aso et al., 2010) (Figure 6). The MB connectome data determines the presence of 6 PPL1 cell types and 15 PAM cell types (Li et al., 2020; Scheffer et al., 2020). It has been shown that blocking the neurotransmission of PPL1 DANs in the context of the training of an olfactory conditioned memory impaired aversive olfactory memory (Schwaerzel et al., 2003). Furthermore, studies confirm that an ineffective functioning of PAM DANs leads to an impairment of an appetitive memory formation (Ichinose et al., 2015). Therefore, DANs are crucial for mediating the reinforcement in the context of an olfactory associative conditioning. The main DA receptor that was described to play a crucial role in aversive conditioning is the D1-type GPCR (G-

protein coupled receptor) (Dop1R1), which is expressed in the MB (Aso et al., 2012; Qin et al., 2012). KCs of the MBs express an adenylyl cyclase translated from the *rutabaga* gene and activated by Gs-proteins and the calcium/calmodulin complex (Levin et al., 1992). This activation results in an increase of the second messenger 3’5’ cyclic adenosine monophosphate (cAMP) and instigates a transduction cascade leading to shaping neuronal connections by ameliorating synaptic plasticity (Gao et al., 2022). In the context of olfactory aversive learning, the adenylyl cyclase Rutabaga is activated by the dual activity of odor-conveying KCs through ACh receptors and punishment-mediating DANs *via* Dop1R1, thereby inducing the synaptic plasticity behind associative odor learning (Tomchik & Davis, 2009; Gervasi et al., 2010). In *Aplysia*, the two mainly described intracellular second messengers, calcium and cAMP, act in synergy and exhibit an increase in their levels respectively by activation of modulatory neurons mediating the reinforcing stimulus (US) and sensory neurons (CS1), thus enhancing synaptic changes (Abrams & Kandel, 1998). This means that monitoring cAMP is an excellent strategy to achieve a localized readout of synaptic changes induced by associative learning, thus investigating restricted plasticity in different compartments of the MB that are innervated by modulatory DANs in the context of higher-order olfactory learning (Rachad et al., manuscript 3, page 88). Another G-protein coupled DA receptor, Dop1R2, was described to be expressed in the MB to stabilize appetitive olfactory memory, and follows an additional signaling cascade (Raf/MAPK pathway) than Dop1R1 (Sun et al., 2020). Dop1R1 and Dop2R are the functional homologs of the mammalian D1 and D2 receptors (Sugamori et al., 1995; Hearn et al., 2002).

KCs, and much less DANs, output into the extended dendrites of 34 MBONs of 21 different types in the MB lobes (Aso et al., 2014a). These MBONs are separated by

type, neurotransmitter, innervation pattern of the 15 different compartments of the MB, and valence to behavioral output (Aso et al., 2014b) (Figure 6). One to five MBONs innervate each compartment of the MB and project afferent axon terminal to different neuropils outside the MB and thus mediating behavioral output (Aso et al., 2014a; Li et al., 2020). Three predominant neurotransmitters were described in MBONs: acetylcholine, glutamate, and GABA. It has been shown that a simultaneous presentation of an odor and a reinforcement that activate respectively KCs and DANs leads to presynaptic plasticity at the level of KC-MBON connectivity, either reducing or strengthening the synapses' activity (Hige et al., 2015). Moreover, the odor input from KCs along with the reinforcement modulation from DANs onto the highly plastic synapses of MBONs has been proposed to skew the representation of odor identity such as the valence after olfactory conditioning (Owald & Waddell, 2015). Contrary to KCs, MBONs have a low firing threshold and broadly tuned odor responses that translate into a response in most MBONs amid any odor presentation. Nevertheless, the weight of odor responses in MBONs varies dependently on cell types and innervation patterns (Cassenaer & Laurent, 2012). Unlike the hard-wired odor-evoked responses in PNs, the convergence of ~2000 KCs projecting onto a significantly smaller number of MBONs indicates that these output neurons are not responsible for maintaining and encoding odor identity but rather provide an integrative representation that may influence behavioral responses (Aso et al., 2014b). It is only fair to speculate that the learned olfactory information pattern follows a general unidirectional path originating from ORNs and conveyed to PNs, KCs and then later to MBONs with a behavior-dependent modulatory activity from DANs.

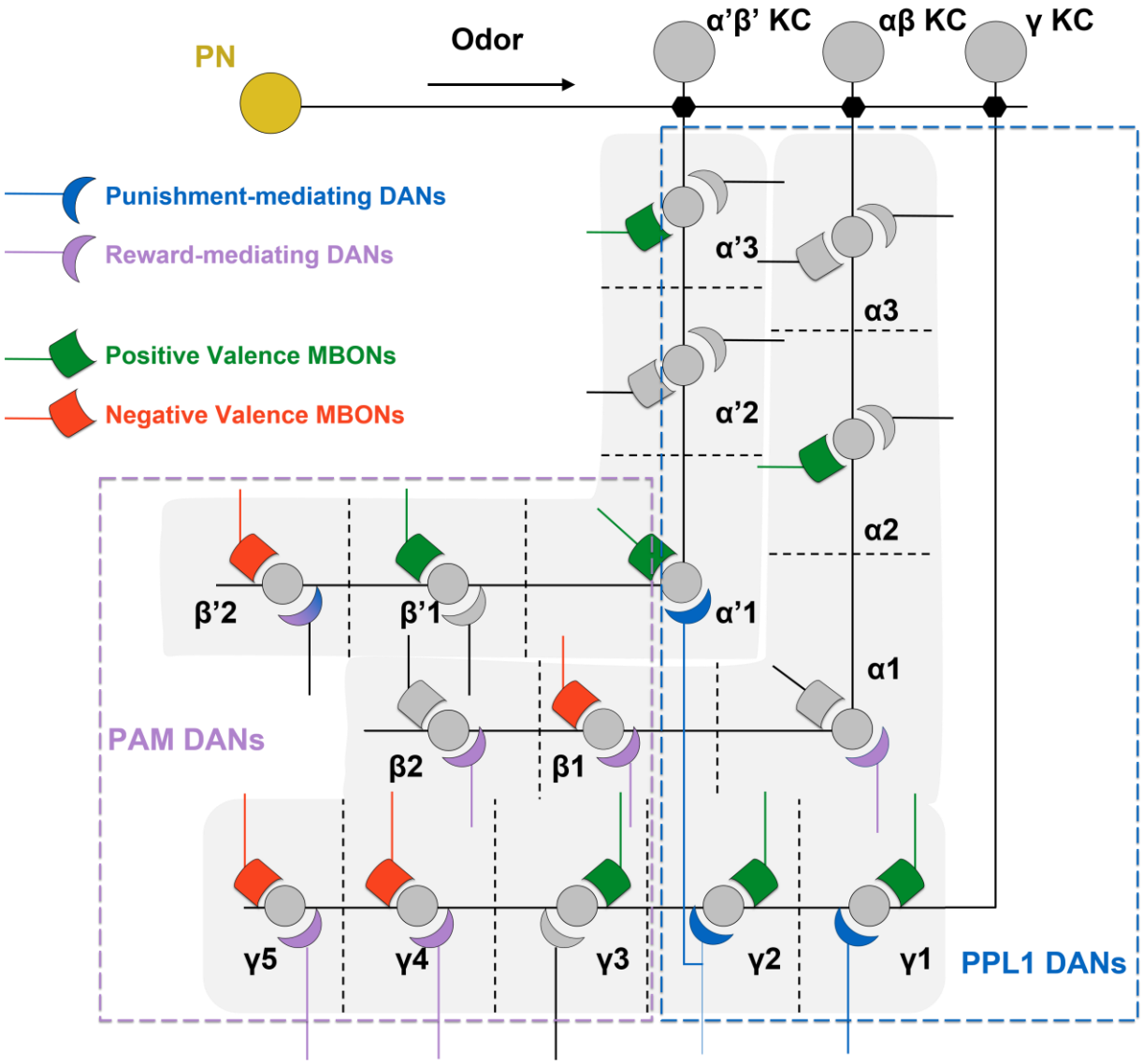

Figure 6: *Schematic representation of the innervation patterns of DANs and MBONS in the MB that defines 15 compartments in the MB lobes. The MB compartments are separated in the illustration by black dashed lines, DANs are half-moons and MBONS are concave rectangles. DANs and MBONs are color-coded based on the type of modulation (for DANs: blue for punishment and purple for reward) and their learned valences (for MBONs: green for positive and red for negative valence). Projection neurons (yellow circle) receive odor information from the AL and transmit olfactory sensory input to the MB calyx where they connect to the dendritic arborizations of KCs. The parallel axon fibers of the KCs form dense neuropils also referred to as the lobes (α/β, α'/β' and γ: gray background structures) where MBONs and DANs innervate the different MB compartments. Dashed color-coded rectangles outline the innervation areas of PPL1 (blue rectangle) and PAM (purple rectangle) cluster DANs in the MB lobes (Inspired from Aso et al., 2014b).*

MBONs form connections amongst each other and with other neuronal populations within and across-compartments (Aso et al., 2014a). A study proposes that DANs receive monosynaptic feedback from a variety of MBONs in the ipsi- and contralateral sides, using excitatory and inhibitory neurotransmitters (Li et al., 2020). The same study also shows that the majority of MB compartments possess at least one direct ipsilateral MBON-DAN feedback along with interneuron-indirect connections. It seems that all punishment-mediating PPL1 DANs and 66% of reward-mediating PAM DANs receive direct feedback from the majority of the typical and atypical MBON cell types (Li et al., 2020). Experiments highlighting numerous roles of MBON to DAN feedback suggest that within the same compartment, MBONs modulate the activity of DANs in multiple forms of memory consolidation and stabilization. For example, the consolidation of feeding-related appetitive long-term memory requires the within-compartment feedback from the MBON innervating the α1 compartment to its appropriate DAN (Ichinose et al., 2015). In addition, the GABAergic MBON innervating the γ1pedc>αβ plays a role in consolidating long-term appetitive memory by inhibiting the γ1pedc PPL1 DAN after associative olfactory learning (Pavlowsky et al., 2018). This feedback has also been described as a facilitation mechanism to a hunger-dependent food odor seeking memory (Sayin et al., 2019). Taken together, these results suggest that feedback from MBONs onto DANs allows previously established odor-reinforcement associations that modify the plastic synapses of KC-MBON connections, to affect future learning. In outline, feedback from MBON to DAN might presumably justify the neuronal mechanisms underlying diverse forms of learning beyond first-order associations, notably second-order conditioning, sensory-preconditioning and reinforcement learning.

4. Numerically simple yet behaviorally elaborate: *Drosophila* mushroom body as model circuit in behavioral neuroscience

Through associative learning, animals and humans engender a series of behavioral processes to cope with encountering diverse environmental stimuli, which they integrate to differentiate between vital and hazardous life situations. While Twitmyer discovered classical conditioning during the studies of the patellar tendon reflex, Pavlov observed the same phenomenon during research in salivation of dogs in response to food (Pavlov, 1927; Twitmyer, 1905). The fruit fly's potential to form associative chains in the context of an olfactory learning paradigm is studied with a variety of assays in flies, and was pioneered in 1985 by Tully and Quinn to be described as olfactory classical conditioning. In this report (Tully & Quinn, 1985), flies were exposed to odorants as conditioned stimuli paired (CS^+) or not (CS^-) with an unconditioned stimulus (US) representing punishing electric shock pulses as reinforcement in this case. After training, the learning index was assayed in a T-maze, in which flies are given the choice between the CS^+ and CS^- odorants, to evaluate the conditioned response i.e. the avoidance of the CS^+ formerly associated to the electric shock during the memory formation phase (Figure 7). Since then, this simple form of olfactory associative learning was featured in many studies dissecting the neuronal mechanisms behind it. Models for olfactory associative learning all point to the implication of the MB in processing and storing memory traces in the brain, with the first compelling experimental evidence being shown first in the honeybee (Menzel & Erber, 1978), and then in *Drosophila* (Heisenberg et al., 1985). By chemical, thermal, or genetic manipulations of the MB, these experiments propose that an alteration of the MB function results in a drastically decreased performance in associative learning. Several investigations confirm the modifications of the tripartite

circuitry between the odor-encoding mushroom body KC, the modulatory DANs and the MBON output to higher behavioral structures is responsible for establishing classical conditioning (Zars et al., 2000; Schwaerzel et al., 2003; Bilz et al., 2020; Hancock et al., 2022, manuscript 2, page 73; Rachad et al., manuscript 3, page 88). It has also been established that blocking synaptic output of the KCs of the α/β lobe is not required for memory formation in classical conditioning, but rather critically required for long term recalling the learned aversive behavior (Dubnau et al., 2001; McGuire et al., 2001; Schwaerzel et al., 2003; Krashes & Waddell, 2008; Kasuya et al., 2009). On the contrary, the α'/β' lobe plays a role only in memory formation and consolidation of early memories, but not in the retrieval (Krashes et al., 2007; Wang et al., 2008). In addition, it has been established that neurotransmission of KCs of the horizontal γ lobe is mainly responsible for short-term memory formation (Zars et al., 2000; Bilz et al., 2020), and for retrieving said memory (Xie et al., 2013). Furthermore, several DANs and MBONs were described to be implicated in different memories, ranging from immediate to long-term (Claridge-Chang et al., 2009; Hancock et al., 2022, manuscript 2, page page 73; Rachad et al., manuscript 3, page 88). The micro-circuitries where KC, MBONs and DANs interact are compact densities called boutons. It has been shown that these boutons show decorrelation after aversive conditioning in different compartments of the same lobe even though they are part of the same cell, meaning that these densities are individually modifiable and act as functional units (Bilz et al., 2020). In addition, the odor-evoked activity we see in the KC boutons demonstrates that the compartment that they belong to is as influential, if not more, than the cell they belong to (Bilz et al., 2020). Behavioral evaluation of different phases of memory formation and retrieval of classical conditioning reveals the implication of single neurons or neuronal cell types

in these particular phases (Ueoka et al., 2017; Hancock et al., 2022, manuscript 2, page 73; Rachad et al., manuscript 3, page 88). These findings led to an even further investigation of precise and localized learning-induced synaptic plasticity in the post-synaptic sites of MBONs showing that synaptic changes due to classical olfactory conditioning is restricted to one γ-lobe compartment (Hancock et al., 2022, manuscript 2, page 73). Another form of classical conditioning is acuity learning where flies can discriminate between two similar and strongly generalized odors if they are subjected to a discriminative training procedure during which one odor is paired with a punishment and the other one not (Barth et al., 2014). KCs encode odors in terms of sparsely distributed activity pattern of ~5-8% of this neuronal population. The more overlapping activated KCs the more similar are the stimuli perceived in terms of eliciting behavior, but the cellular mechanisms of differential synaptic plasticity underlying acuity learning remain unknown.

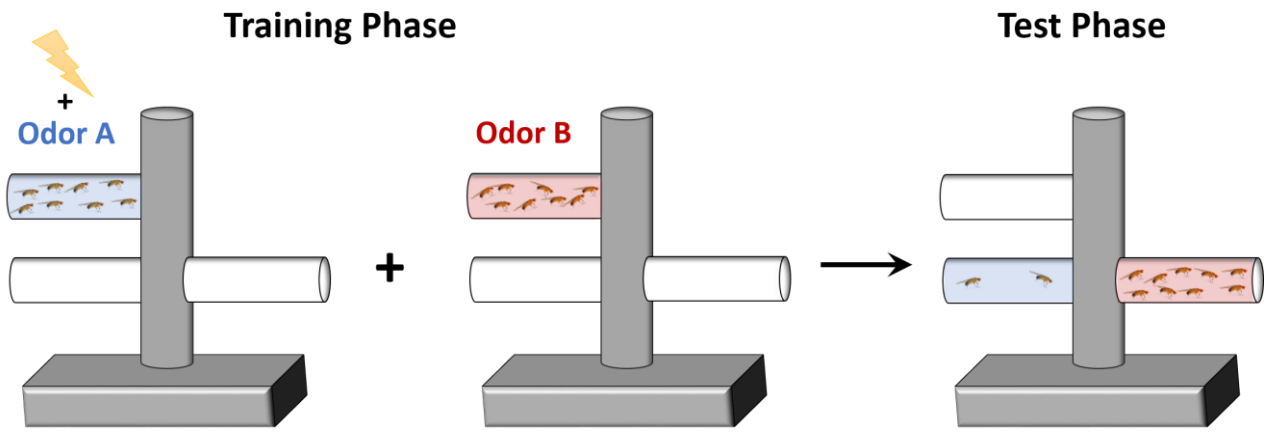

Figure 7: *Classical Pavlovian conditioning in Drosophila melanogaster. The schematic illustrations represent the different training and test phases of aversive olfactory learning paradigm in a T-maze as described by Tully and Quinn in 1985. On the left, the flies are presented with odor A (CS1) along with 12 pulses 90 volts for one minute, then after a break of another minute, these same flies receive odor B (CS^-) alone for another 60 seconds (middle drawing). Finally the flies are given the choice between the two odorants in the test phase for of two minutes duration, thus exhibiting avoidance to CS1 (right drawing).*

Due to its simplicity, classical conditioning allows the investigation of molecular and cellular mechanisms of learning and memory relying on one association of sensory cues. However in nature, animals and humans learning depends on a sequence of enforced and innate associative chains leading to complex behaviors with difficult-to-asses modalities. Many forms of higher-order learning, where a valence of a neutral stimulus is modified by reinforcement from another conditioned stimulus, were described in *Drosophila*, notably sensory preconditioning (SPC) (Giurfa, 2013; Martinez-Cervantes et al., 2022) and second-order conditioning (SOC) (Tabone & de Belle, 2011). In the fruit fly, SOC is a higher-order form of associative olfactory learning in which a neutral stimulus can generate a conditioned behavioral response when paired with a previously conditioned stimulus (Tabone & de Belle, 2011). This paradigm consists of two training phases; an initial training, also referred to as first-order or classical conditioning, requires an association of a conditioned stimulus (CS1) with a reinforcer or unconditioned stimulus (US). Then, a second training phase follows in which CS1 is paired with a neutral stimulus, CS2 (Figure 8). This second-order association engenders a conditioned aversion to CS2, regardless of the fact that no association has occurred between the original reinforcement from the US and CS2 (Tabone & de Belle, 2011). The SOC paradigm, first described by Pavlov in 1927, has spawned in many studies covering different organisms such as sea slugs or *Aplysia californica* (Hawkins et al., 1998), gold fish (Amiro & Bitterman, 1980), honeybees (Hussaini et al. 2007), pigeons (Stanhope, 1992), rats (Rescorla, 1976; Jennings & Kirkpatrick, 2018), and humans (Lee & Livesey, 2012; Craddock et al., 2018). This complex form of associative learning chains allows a better understanding of the previously established roles of neuronal substrates and connections to unravel complex “cognitive” processes.

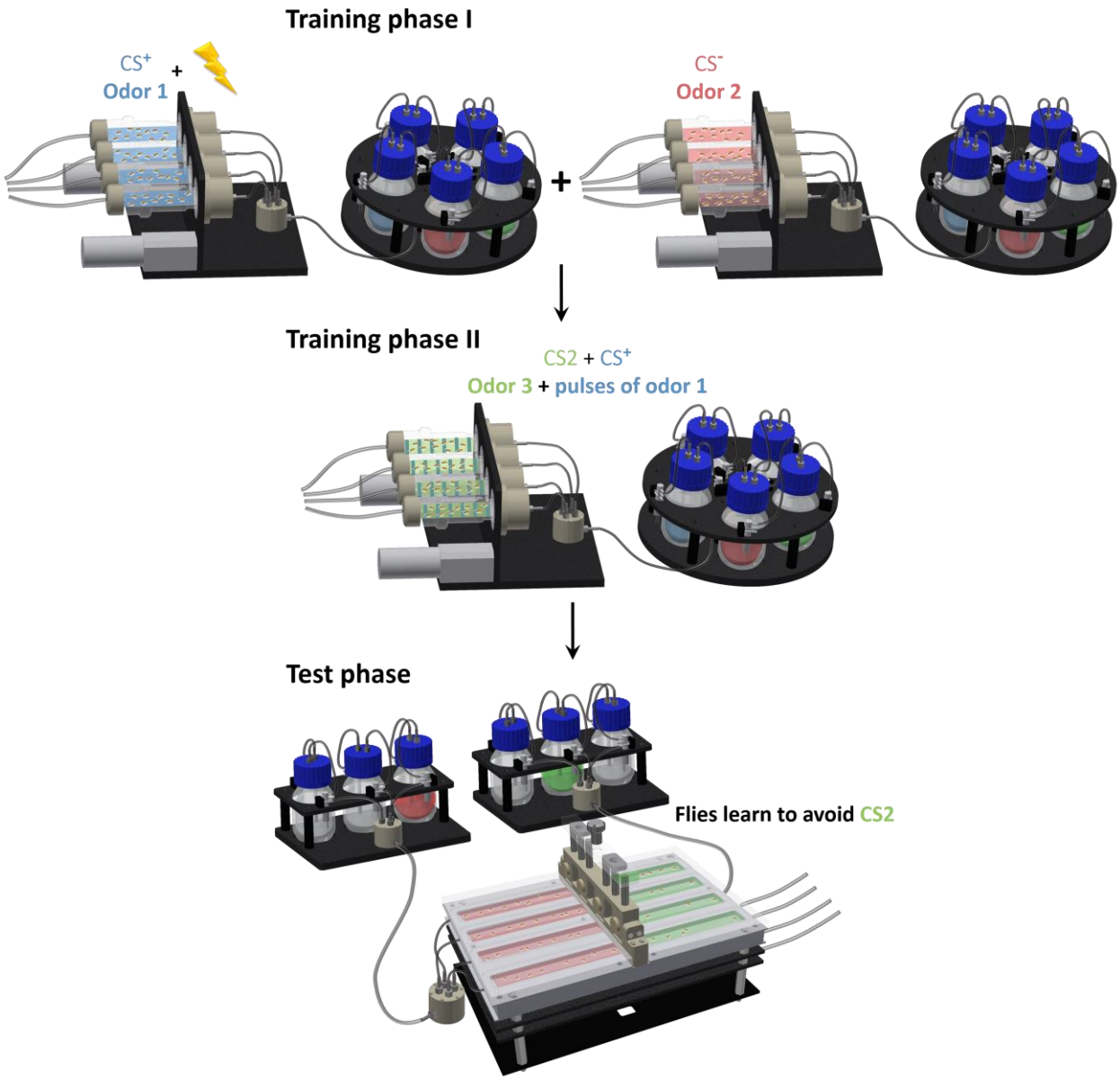

Figure 8: *Second-order conditioning in Drosophila melanogaster. The top and middle drawings represent the training apparatus containing the training tubes placed in a holder that connects to an olfactometer. The bottom illustration exemplifies the test machine composed of two olfactometers that dispense odor from their respective side into the test arena in the middle. Both of these devices are automatized and custom-built for fly higher-order leaning in the fruit fly (as described in Rachad et al, manuscript 3). SOC paradigm involves two training phases with the first one being classical aversive conditioning (see Figure 7), and pairing a novel odor (CS3 in green) with pulses of the conditioned odor (CS1 in blue) in the second training phases. Flies are then tested for their preference to CS- vs CS2 and show and avoidance to the latter.*

Dissecting the neuronal mechanisms and circuits underlying SOC is a key element into understanding higher-order associative learning. In rats, a study has shown that excitatory glutamatergic signaling from the pyramidal neurons back to the basolateral amygdala is responsible for aversive second-order memory formation (Holmes et al., 2013). The same study reports that administration of glutamate receptor NMDA antagonists during the pairing of a stimulus and reinforcement prevents the establishment of SOC (Holmes et al., 2013). Since the basolateral amygdala is described for its role in sensory associations between stimuli and their outcomes rather than their general valence (Corbit & Balleine, 2005; Prévost et al., 2012), the implication of this structure in SOC is rather unusual. Thus, either these results may speculate on the fact that SOC might not result from the transfer of general valences of the used stimuli, or more plausibly multiple sequential associations supported by the basolateral amygdala drive SOC. In *Drosophila*, It appears likely that not only associative olfactory learning induced by classical conditioning depends on the MB neuronal populations functioning, but also SOC. Recent reports suggest that SOC is enabled by specific interactions between dopaminergic circuits upon optogenetic manupilations in the context of an appetitive memory formation (Yamada et al., 2023). However, the suggested hypothesis stating the implication of MB neuronal circuitries and the mechamisms by which SOC is achieved has never been tested and is the rationale to the third manuscript of this study, at least in the scope of aversive olfactory learning.

5. Overview, manuscript introduction and contributions

In this study, we are covering three aspects of the neuronal mechanisms underlying associative olfactory conditioning in *Drosophila*, extending from development to synaptic changes in learning, along with my personal contributions in this scientific agenda.

In the first manuscript entitled “Neuronal excitability as a regulator of circuit remodeling”, I have worked in collaboration with Prof. Dr. Oren Schuldiner, Dr. Oded Mayseless and Gal Shapira who are affiliated to the Weizmann institute of Science in Rehovot-Israel, as well as Prof. Dr. André Fiala as my doctoral thesis supervisor, to demonstrate that neuronal activity of the MB γ lobe needs to be reduced in order for this lobe to undergo pruning. As a first experiment, I have used the calcium-modulated photoactivable ratiometric integrator UAS-CaMPARI (Fosque et al., 2015) to quantify calcium levels in γ-KCs during different time point of metamorphosis (Figure 1B). This calcium indicator displays high kinetic properties in calcium binding and sustains irreversible green-to-red fluorescence conversion in high calcium levels and simultaneous experimenter-induced UV illumination (Fosque et al., 2015). I have also contributed in demonstrating the efficiency of transgenic tools UAS-Kir2.1 and UAS-dTrpA1 in suppressing or depolarizing neuronal activity respectively in the MB (Supplementary Figure 2B). In addition, I could also show the excitatory effect of knocking-down the expression of the GABA-B-R1 receptor using an UAS-GABA-B-R1-RNAi construct on γ-KCs (Supplementary Figure 3K).

The experiments displayed in the second manuscript “Visualization of learning-induced synaptic plasticity in output neurons of the *Drosophila* mushroom body γ-lobe” were initiated by Dr. Clare Elizabeth Hancock and in the lab of Prof. Dr. André Fiala, and finished by myself and Stephan Hubertus Deimel. A computational study in

this paper was conducted in collaboration with Prof. Dr. Martin Nawrot and Dr. Vahid Rostami from the University of Cologne-Germany. In this study, I have firstly contributed in generating confocal images of GCaMP3 expression in the MBONs innervating the γ-lobe of the MB (Figure 1D), in addition to statistical quantifications and normalizations for optimizing the computational model shown in Figure 5. The main results that I have generated for this report are the behavioral experiments appearing in Figure 6, where I used the thermo-genetic tool UAS-*Shibire*^{ts} to block synaptic transmission in different MBONs innervating the γ-lobe to evaluate their role in an aversive olfactory conditioning paradigm.

Finally yet importantly, the third manuscript, named “Functional dissection of a neuronal brain circuit mediating higher-order associative learning”, constitutes my main work during my doctoral research. In this manuscript, I aimed to dissect the neuronal circuits underlying higher-order olfactory learning in *Drosophila melanogaster*. First, I started with establishing a new custom-built and automatized apparatus for olfactory conditioning flies (with the help of our workshop and Muhammad Afaque Khan in Arduino programming) (Supplementary Figure 1A-B), to reliably reproduce second-order conditioning, as described by Tabone and de Belle in 2011. In addition, I performed all the necessary control experiments and odor combinations to validate said paradigm (Figure 1B; Supplementary Figure 1C-E). Then, with the occasional help of three Bachelor students, Eva Küsters, Julia Kniep and Marie Eileen Wisenhavern, I proceeded to thermo-genetically manipulate distinct MB-related neuronal populations (shown in confocal exemplary images in Supplementary Figures 1F-G, 2A-B and 3A), using UAS-*Shibire*^{ts} in different training and testing phases of the SOC paradigm (Figure 1E-H; Figure 2; Figure 3) and the FOC paradigm (Supplementary Figure 2C-F and 3B-E). Stephan Hubertus Deimel

imaged “the electric-shock protocol” experiments and where he assessed fluorescence changes in individual DANs (Figure 4A-B) and their innervation compartments in the MB (Figure 4E) in response to electric shocks that I later quantified and statistically analyzed. He used the pre-synaptic indication UAS-Syp-GCaMP3 (Figure 4A), the neurotransmitter release sensor UAS-Syp-pHTomato (Figure 4B) and the green fluorescent cAMP indicator UAS-GFlamp1 (Figure 4E). In that same figure, I conducted connectivity-establishing experiments using the UAS-GRASP tool to demonstrate the innervation pattern of these DANs in the MB compartments (Figure 4C) accompanied by a EM connectomics analysis using the Janelia neuPrint database (Clements et al., 2020) (Figure 4D). Shown in figure 5, I have monitored calcium activity at the level of the post-synaptic sites of the aforementioned MBONs pre- and post- to validate the existence of synaptic plasticity after SOC training, along with using other calcium sensors and showing their limitations into answering the key question of this figure (Supplementary Figure 4). Optogenetic activation of candidate MBONs implicated in SOC memory formation using UAS-CsChrimson, with a simultaneous monitoring of the calcium levels of an individual DAN necessary in the SOC paradigm using UAS-GCaMP6f were performed by our collaborator Dr. Suewei Lin and Chen-Han Lin from Academia Sinica in Taipei-Taiwan (Figure 6 A-D). In the last experiment of the manuscript, Yogesh Gadgil added another layer of training to the SOC paradigm by associating the CS2 odor to a novel odor (CS3) and achieved an even more complex behavior, third-order conditioning (TOC) which I statistically analyzed and compiled.

NB: The references at the end of this thesis represent the cited information used in the general introduction and discussion of this study. Every manuscript has its own reference list.

II. Manuscript 1: Neuronal excitability as a regulator of circuit remodeling

Current Biology, accepted January 2023, will be online in February 2023

Authors: Oded Mayseless[1#], Gal Shapira[1,2#], El Yazid Rachad[3], André Fiala[3], Oren Schuldiner[1,2*]

[1] Department of Molecular Cell Biology, Weizmann Institute of Sciences, Rehovot 7610001, Israel

[2] Department of Molecular Neuroscience, Weizmann Institute of Sciences, Rehovot, 7610001, Israel

[3] Molecular Neurobiology of Behavior, University of Göttingen, Göttingen, Lower Saxony, 37077, Germany

[#] Equal contribution

***** Corresponding author: oren.schuldiner@weizmann.ac.il

Summary

Postnatal remodeling of neuronal connectivity shapes mature nervous systems [1–3]. Pruning of exuberant connections involves cell autonomous and non-cell autonomous mechanisms, such as neuronal activity. Indeed, experience-dependent competition sculpts various excitatory neuronal circuits [4–9]. Moreover, activity has been shown to regulate growth cone motility, and stability of neurites and synaptic connections [10–14]. However, whether inhibitory activity influences remodeling of neuronal connectivity or how activity influences remodeling in systems in which competition is not clearly apparent, is not fully understood. Here we use the *Drosophila* mushroom body (MB) as a model to examine the role of neuronal activity in developmental axon pruning of γ-Kenyon cells. The MB is a neuronal structure in insects, implicated in associative learning and memory [15,16], which receives mostly olfactory input from the antennal lobe [17,18]. The MB circuit includes intrinsic neurons, called Kenyon cells (KCs), which receive inhibitory input from the GABAergic anterior paired lateral neuron (APL) among other inputs. The γ-KCs undergo stereotypic, steroid-hormone dependent remodeling [19,20] that involves pruning of larval neurites followed by regrowth to form adult connections (Figure 1A [21]). We demonstrate that silencing neuronal activity is required for γ-KC pruning. Furthermore, we show that this is mechanistically achieved by cell autonomous expression of the inward rectifying potassium channel (irk1) combined with inhibition by APL neuron activity likely via GABA-B-R1 signaling. These results support the Hebbian-like rule ‘use it or lose it’, where inhibition can destabilize connectivity and promote pruning while excitability stabilizes existing connections.

Keywords:

Neuronal remodeling, γ-KCs, neuronal activity, inhibition, Hebbian plasticity, APL, GABA, Mushroom Body, pruning, plasticity

Results and discussion

Calcium levels in γ-KCs are dynamic upon transition into metamorphosis

Studies from several neural systems have demonstrated that neuronal activity and Ca^{2+} signaling play a vital role in the coordination and control of neuronal remodeling [13,14,22–26]. We therefore set out to examine the calcium (Ca^{2+}) dynamics, as a proxy for neuronal activity, during remodeling of MB γ-KCs (Figure 1A, [20]). The broad term "neuronal activity" refers to several physiological parameters, such as membrane depolarization and neurotransmitter release. It is very well-established that Ca^{2+} dynamics closely match the dynamics of membrane depolarization [27]. CaMPARI is an engineered ratiometric fluorescent protein, which undergoes efficient and irreversible green-to-red conversion only when elevated Ca^{2+} and experimenter-controlled illumination coincide [28,29]. Thus, CaMPARI offers the possibility to image Ca^{2+} dynamics over relatively long periods, and to compare activity levels between developmental stages. We thus examined relative Ca^{2+} levels in γ-KCs from early 3rd instar larvae (L3), up to 6 hours after puparium formation (APF), a time-frame that includes the onset of remodeling. We observed a significant decline in relative Ca^{2+} levels at 0h APF as compared to larval stages (Figure 1B – 0h APF). Subsequently, and to our surprise, Ca^{2+} levels increased at 3h APF and reached elevated levels compared to larval stages (Figure 1B – 6h APF). These results demonstrate that γ-KC Ca^{2+} levels are highly dynamic during the transition from larva to pupa, even in the presumed absence of external inputs.

Chronic activation of γ-KCs during key stages of remodeling inhibits pruning

Change in intracellular Ca^{2+} levels may reflect developmental regulation of Ca^{2+} channels or changes in membrane potential leading to activation of voltage gated Ca^{2+} channels. To examine whether neuronal activity regulates γ-KCs pruning, we manipulated their activity via genetically encoded transgenes [30] and examined the effect on their pruning. Chronically hyperpolarizing γ-KCs, by expressing the inward rectifying K^+ channel Kir2.1 [31] did not affect pruning (Figure 1C-D, all panels quantified in I and S1F, see S1A-E for ranking examples). Additionally, inhibiting neurotransmission, by expressing tetanus toxin light chain (TNT) throughout metamorphosis in γ-KCs, did not affect pruning (Figure 1E). In contrast, chronically

activating γ-KCs by expressing the thermo-sensing cation dTrpA1 channel [32], resulted in a dramatic inhibition of pruning at the permissive 29ºC as compared to the restrictive 22ºC [33] (Figure 1F compared to G). These data suggest that chronic activation of γ-KCs inhibits their pruning. The accumulating literature highlights 3/6h APF as the initiation time for dendrite and axon fragmentation, respectively [21]. Therefore, we took advantage of the temperature sensitivity of the dTrpA1 channel to induce neuronal activation during different stages of development. Interestingly, raising flies in 29ºC (resulting in the opening of the dTrpA1 channel) for the duration of their larval life, and transferring them to 22ºC at 0h APF did not inhibit pruning of γ-KCs. In contrast, transferring flies to 29ºC from 0 to 6h APF significantly inhibited pruning (Figure 1H).

To verify that chronic opening of dTrpA1 induces chronic activation of γ-KCs, we used CaMPARI to examine the Ca^{2+} levels of pupal γ-KCs expressing dTrpA1. As expected, Ca^{2+} levels were significantly elevated upon dTrpA1 expression (Figure S1G-H). Moreover, we wanted to make sure that the ectopic vertical axons seen in the dTrpA1 activated γ-KCs are indeed due to inhibition of pruning rather than exuberant growth or aberrant regrowth. For this purpose, we examined γ-KC morphology at L3 larva, before pruning, and at 24hAPF, after pruning and before developmental regrowth [34]. Indeed, larval MB was indistinguishable from WT, and 24h APF brains contained ectopic γ-KC axons in the vertical lobe, confirming that the vertical neurites observed at the adult stage are a result of pruning inhibition (Figure S1I-L). Together, these results suggest that activation of γ-KCs and elevated Ca^{2+} levels at the onset of metamorphosis are sufficient to inhibit pruning, implying that hyperpolarization of γ-KCs at 0h APF might be required for their pruning.

Reduction of γ-KC activity is required for pruning

Opening Trp channels induces nonspecific ion influx [35]. This can lead to multiple effects including Ca^{2+} influx, which can induce multiple signaling pathways, influx of other cations such as Na^{+} which would induce membranal depolarization, opening of voltage gated Ca^{2+} channels, and lead to subsequent neurotransmitter release. To better understand the nature of the dTrpA1 induced inhibition of pruning, we co-expressed dTrpA1 either with mammalian Kir2.1, or with Tetanus toxin light chain (TNT). Co-expression of Kir2.1 on top of dTrpA1 expression should induce an

influx of K^+ ions, which would counteract the dTrpA1 mediated influence on membranal depolarization and evoked release of neurotransmitters. In contrast, TNT blocks chemical synaptic transmission by cleaving n-Syb (which is expressed in γ-KCs at the onset of metamorphosis [36]) thus preventing fusion of synaptic vesicles with the synaptic membrane. Co-expression of dTrpA1 together with TNT should therefore suppress neurotransmitter release but not membrane depolarization.

Interestingly, while co-expression of either Kir2.1 or TNT suppressed the dTrpA1-induced pruning defect to a significant degree, suppression by Kir2.1 was significantly more penetrant (Figure 2A-C, quantified in D and in S2A). Importantly, as expected, Kir2.1 expression suppressed the elevation in Ca^{2+} levels caused by dTrpA1 opening (Figure S2B). These results suggest that the primary effect of dTrpA1 opening, in the context of γ-KC pruning, is the depolarization of γ-KC membranes rather than the secretion of neurotransmitters or nonspecific Ca^{2+} influx; yet it does not completely rule out non-cell autonomous influence. Taken together, these results indicate that reduction in Ca^{2+} levels which is indicative of γ-KC hyperpolarization is required for the initiation of their pruning.

To identify potential cell-autonomous mechanisms through which γ-KCs could hyperpolarize, we examined their developmental transcriptional landscape [36]. Interestingly, we identified *inwardly rectifying potassium channel 1* (*irk1*) as specifically upregulated in γ-KCs at the onset of metamorphosis (Figure 2E). Irk channels can increase inward flux of K^+ ions thereby maintain K^+ homeostasis, and control of resting membrane potential [37]. In accordance with a possible role of *irk1* channels in reducing γ-KCs excitability, perturbing their expression using RNAi or tissue-specific (ts)CRISPR [38] inhibited γ-KCs pruning (Figure 2F-H quantified in I).

These results demonstrate that cell-autonomous expression of *Irk1* is required for γ-KC pruning. Moreover, these support the idea where reduced neuronal activity is required for γ-KC pruning. An interesting avenue for future studies would be to understand the developmental regulation of *irk1* expression and function, and whether it could be influenced by neuronal activity.

APL activity is required for efficient γ-KC pruning

While *Irk1* expression is required for γ-KC pruning, the pruning defect caused by its perturbation is much milder than that induced by chronic activation of γ-KCs

(via TrpA1-Figure 1F). Moreover, the suppression of dTrpA1 pruning defect by TNT co-expression (Figure 2A-C) suggest an involvement of a feedback mechanism involving synaptic transmission. Therefore, we set out to examine whether non cell-autonomous neural inhibition was also involved. The sole inhibitory input to γ-KCs before metamorphosis is considered to be the GABAergic APL neuron [39]. Moreover, we have recently shown that APL remodeling is coordinated with that of γ-KCs [22]. Therefore, we hypothesized that APL neuronal activity, possibly via secretion of GABA is a prime suspect to relay feedback inhibitory signals to γ-KCs.

To test the role of APL activity in γ-KC pruning, we silenced the APL by expressing Kir2.1 and examined the concurrent effects on γ-KCs. Due to the stochastic nature of the APLi driver [40], we could analyze brains in which the APL is labeled and manipulated only in one brain hemisphere, while the second hemisphere remains unperturbed. Indeed, hemispheres in which the APL neuron expressed Kir2.1 displayed a mild, yet significant γ-KC pruning defect compared to control hemispheres (Figure 3A-C quantified in J). In addition, silencing APL neurotransmitter secretion by expressing TNT within the APL also inhibited γ-KC pruning (Figure 3D-F). Interestingly, expressing TNT in the APL throughout development also induced blebbing of the APL neurites in some of the brains (Figure S2C-E red arrows). Chronic expression of TNT has been known to modulate inflammatory cytokines [41], but whether or how this is related to γ-KC development remains to be investigated. These results therefore suggest that APL activity is required for effective γ-KC pruning. Consistent with our hypothesis that the APL confers a hyperpolarizing effect that promotes pruning in γ-KCs, silencing APL neuronal activity should result in increased excitability of the γ-KCs. To explore this potential epistasis, and to test whether the increased excitability of γ-KCs is the cause for their defective pruning, we simultaneously expressed Kir2.1 in the APL and also in the γ-KCs. Indeed, this suppressed the APL-Kir2.1 driven pruning defect (Figure 3G-I).

Next, we asked whether increasing APL activity is sufficient to induce early or more extensive pruning. Expressing dTrpA1 in APL neurons and activating them by rearing the flies in 29ºC from 0h APF up to 18h APF, did not result in any change in the rate or extent of pruning of γ-KCs, as measured at the peak of remodeling (Figure S2F-H, quantified in I). Taken together, these results suggest APL activity is required, but not

sufficient, to promote efficient axon pruning. However, whether hyperactivation of the APL neuron promotes a strong inhibition of γ-KCs and thus directly promotes pruning remains to be further investigated.

GABA-B-R1 is expressed in γ-KCs, modulates Ca^{2+} levels and is required for γ-KC pruning

GABA exerts its inhibitory function by binding to two types of receptors, the ionotropic GABA-A receptor, and the metabotropic (G protein-coupled) GABA-B receptor [42–44]. The ionotropic GABA-A receptors have been shown to be excitatory during early pupal development and only become inhibitory during late development due to reversal of the chloride potential [45]. The activation of the metabotropic GABA-B receptors is not directly affected by developmental changes in chloride reversal potential [46]. Upon activation, metabotropic GABA-B receptors modulate synaptic transmission by regulating Ca^{2+} and K^{+} currents. However, as these are G-protein coupled receptors their response may activate numerous downstream signaling cascades [47,48]. The *Drosophila* GABA-A receptor, *rdl*, is expressed in γ-KCs at larval stages, however its transcriptional level sharply decreases just prior to pruning in WT animals (Figure S3A[36]). While this suggests that *rdl* is not likely involved in γ-KC pruning we have not ruled out its potential role. Three GABA-B receptors have been identified in *Drosophila*, dGABA-B-R1 and dGABA-B-R2, homologous to their mammalian counterparts, and an insect specific dGABA-B-R3. dGABA-B-R1 and R2 form heterodimers, while only the dGABA-B-R1 binds to GABA [49]. To examine whether GABA-B receptors are involved in γ-KC remodeling we followed the expression of GABA-B-R1 using a protein-GFP fusion (GABA-B-R1^{GFP}) generated by means of Minos Mediated Integration Cassette (MiMIC[50,51]). Interestingly, we detected GABA-B-R1^{GFP} in the MB calyx, the dendritic region of the KCs, before, during, and after metamorphosis (Figure S3B-D). To verify that the GABA-B-R1 mimic line is specifically expressed in the KC calyx and to determine the cellular source of GABA-B-R1, we knocked down GABA-B-R1 by RNAi driven by the strong pan-KC OK107-Gal4. Indeed, GABA-B-R1^{GFP} expression in the calyx was dramatically reduced, thus confirming the specificity of the RNAi, the GABA-B-R1^{GFP} reporter, and the fact that γ-KCs are the primary source of GABA-B-R1 in this brain region at the larval stage (Figure S3E-F). To examine if GABA-B-R1 can regulate γ-

KC activity at pupal stages we examined relative Ca^{2+} levels in WT and GABA-B-R1 KD brains using CaMPARI. As expected, knocking down GABA-B-R1 in γ-KCs induced a significant rise in Ca^{2+} levels as compared to WT brains (Figure S3K). These results suggest that GABA-B-R1 signaling, influences Ca^{2+} levels in γ-KCs prior to pruning and could potentially inhibit neuronal activity. Indeed, in accordance with a possible requirement of neuronal inhibition as a permissive step for γ-KC pruning, GABA-B-R1 KD in all KCs using RNAi (driven by OK107-Gal4), or knocking it out in γ-KCs using tsCRISPR (by R71G10-Gal4-driven Cas9), both resulted in mild pruning defects (Figure S3G-I quantified in J). Overall, these results suggest that GABA-B-R1 expression and possible activation, results in inhibiting γ-KC neuronal activity prior to pruning. However, the precise mechanism by which GABA-B-R1 promotes pruning, and specifically whether it functions directly by modulating Ca^{2+} levels, or alternatively via second-messenger cascades remains to be further investigated.

Irk1 and GABA-B-R1 are synergistically required for γ-KC pruning

The mild nature of the pruning defects induced by Irk1 or GABA-B-R1 knockdown, compared to the dTrpA1-induced pruning defect, could suggest that both processes work in parallel to inhibit neuronal activity in γ-KCs prior to pruning. We therefore perturbed both genes in parallel. While the single gene perturbation of either irk1 or GABA-B-R1 resulted, as expected, in mild to moderate pruning defects (Figure S3, 4A-C), the combined perturbation of both resulted in a significant phenotype exacerbation (Figure 4D, quantified in 4E). In this experiment, automatic macro-based quantification, which is limited and error-prone, was not able to highlight this exacerbation (data not shown). For that reason, three additional independent individuals have ranked the images again, as shown in S4A-C. A complete comparison of all four ranking quantifications is provided in Table S1, but importantly, in all cases, the pruning defects in the GABA-B-R1/irk1 double perturbation was found to be significantly more severe than in the single perturbations. Taken together, these data suggest that irk1 and GABA-B-R1 may work in concert to inhibit γ-KCs neuronal activity at the onset of metamorphosis prior to pruning.

Neuronal activity has been shown to play a major role in remodeling of excitatory circuits, often via competition that is derived from experience-dependent or

intrinsically generated activity waves [5,52–54]. Here we demonstrate that silencing neuronal activity is a prerequisite also in the context of stereotypic remodeling where no competition is likely to play a role. Overall, we suggest that active KC post-synapses are stabilized, and that destabilization in the course of pruning requires silencing of neuronal activity.

Previously, Kanamori and colleagues have nicely demonstrated that transient compartmentalized Ca^{2+} influx through voltage gated Ca^{2+} channels activate Ca^{2+} dependent proteases to allow for the normal progression of pruning in class IV dendritic arborization (C4da) neurons [26]. In contrast, and more similar to our study, Duch and Mentel previously demonstrated that stimulating the mesothoracic motor-neuron 5 (MN5) in *Manduca sexta,* resulted in axonal overgrowth [14] and slowing of dendritic regression and synapse elimination which stereotypically occur during metamorphosis and result in remodeling of the neuromuscular circuit [13]. Thus, while hyperpolarizing C4da neurons inhibited their pruning, it seems that hyperpolarization is required for γ-KC pruning and for the regression of MN-5 dendrites. Taken together, these differences highlight the context dependent nature of Ca^{2+} signaling, and highlight the need for more mechanistic studies. Interestingly, it has been demonstrated that the ENaC (endothelial sodium channel) Pickpocket 26 (Ppk26), is actively degraded in C4da neurons [55], suggesting that C4da actively reduce their excitability prior to pruning. Thus, the precise roles of excitability and Ca^{2+} levels during remodeling of axons and dendrites need to be further clarified, in multiple cellular settings.

The current concept of neuronal activity-mediated plasticity is focused on the plasticity of excitatory connections and is generalized as 'use it or lose it'. This is commonly interpreted such that connections with stimulated (or correlated) inputs grow stronger, while connections with inactive (or uncorrelated) inputs grow weaker. This process is based on mechanisms underlying Hebbian plasticity [54]. Hensch and colleagues have formulated a compelling hypothesis which incorporates inhibition during the process of activity mediated structural remodeling [53,56,57]. In this model, laterail inhibition modulates Hebbian-type plasticity by enhancing the correlative activities of adjacent cortical neurons and producing anti-correlative activities in distal cells. Their model suggests that incorporation of GABAergic inhibition, downstream of retinal input, can provide a scaffold for the mature circuit. Interestingly, our findings

that persistent γ-KC synapses inhibit APL pruning [22], and that APL activity is necessary for γ-KC pruning, are consistent with this model. As such, in a similar manner to the visual system of mammals, GABAergic feedback of the MB is required to destabilize KC (and one could speculate - to decorrelate) activity and thus promote their remodeling.

Acknowledgements

We thank C. Potter, GM. Rubin, the Kyoto (DGRC) and Bloomington Stock Centers for reagents; H. Meltzer, for graphical illustrations, discussions, and critical reading, and other members of the Schuldiner lab, especially I. Alyagor, N. Kollet, S. Yaniv, and V. Berkun, for discussions, critical readings of the manuscript and overall support and assistance during the different working stages. We thank R. Rotkopf for assistance with statistical analyses. This work was supported by Volkswagen Stiftung (joint Lower Saxony – Israel) grant #A112379 to A.F. and O.S., the Israel Science Foundation (ISF) grant #1100/16 to O.S., the German Research Foundation (FOR 2705) to A.F. and O.S., by European Research Council (ERC) advanced grant #101054886 “NeuRemodelBehavior’’ to OS, and an EMBO short term fellowship #382-2016 to O.M. O.S is an incumbent of the Prof. Erwin Netter Professorial Chair of Cell Biology.

Author contributions

O.M. designed, performed, and analyzed experiments, wrote the manuscript and procured funding; R.E.Y. and G.S. performed and analyzed experiments; G.S. additionally was instrumental in coordinating and performing experiments as well as manuscript modifications during the revision; A.F. designed CaMPARI experiments, assisted in data interpretation and analysis, critically read and discussed the manuscript, and procured funding; O.S. designed and analyzed experiments, wrote the manuscript, and procured funding.

Declaration of Interests

The authors declare no competing interests.

Figure 1

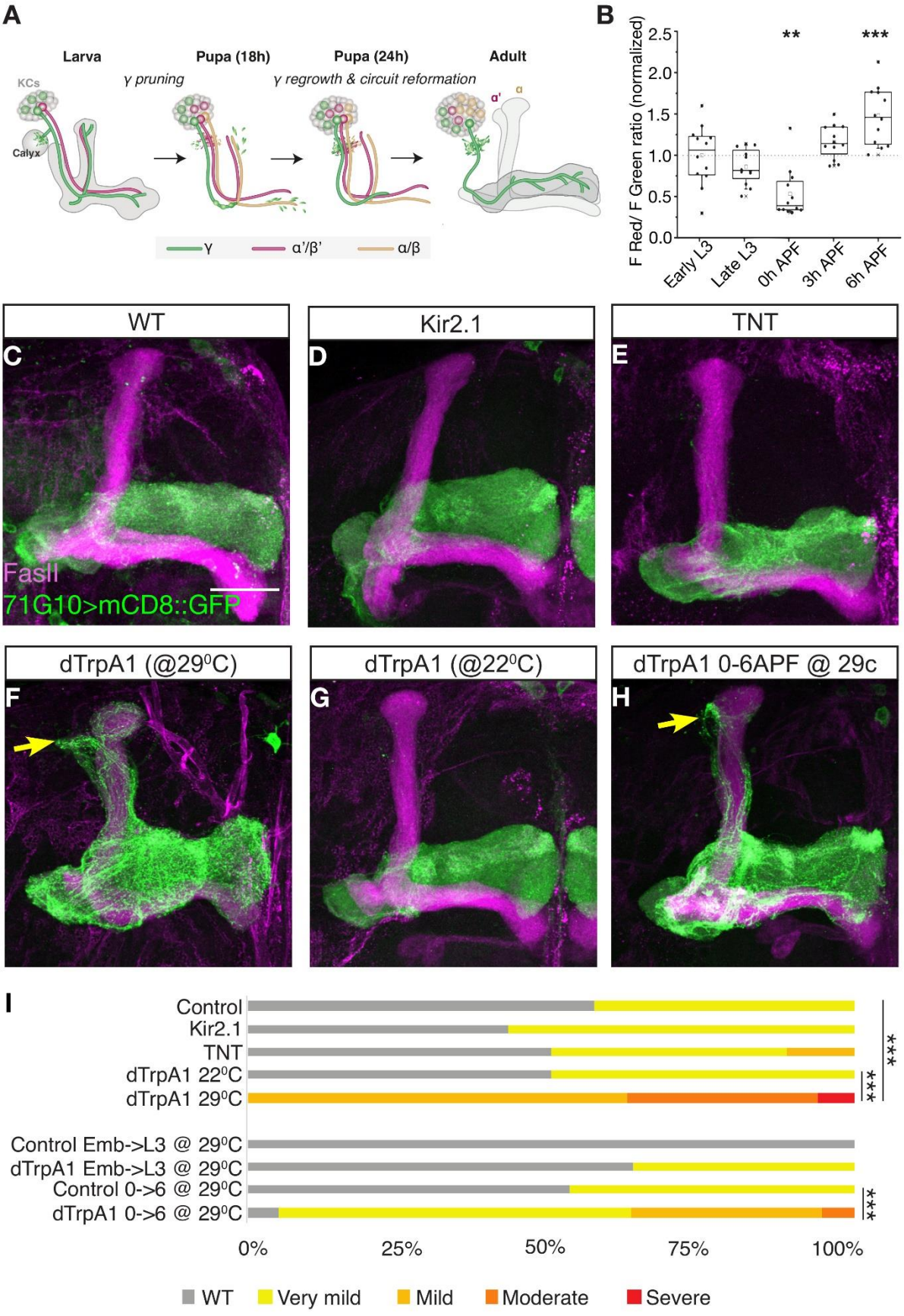
A
Larva
Pupa (18h)
Pupa (24h)
Adult
γ pruning
γ regrowth & circuit reformation
KCs
Calyx
α'
α
γ
α'/β'
α/β
B
F Red/ F Green ratio (normalized)
2.5
2.0
1.5
1.0
0.5
0.0
**
***
Early L3
Late L3
0h APF
3h APF
6h APF
WT
Kir2.1
TNT
C
D
E
FasII
71G10>mCD8::GFP
dTrpA1 (@29⁰C)
dTrpA1 (@22⁰C)
dTrpA1 0-6APF @ 29c
F
G
H
I
Control
Kir2.1
TNT
dTrpA1 22⁰C
dTrpA1 29⁰C
Control Emb->L3 @ 29⁰C
dTrpA1 Emb->L3 @ 29⁰C
Control 0->6 @ 29⁰C
dTrpA1 0->6 @ 29⁰C
***
***
***
0%
25%
50%
75%
100%
WT
Very mild
Mild
Moderate
Severe

Figure 1: Chronic activation of γ-KCs during early pupal stages inhibits pruning

(A) Cartoon illustration depicting developmental remodeling of γ-KCs. Larval γ-KCs send dendrites to the MB calyx and a bifurcated axon which forms the MB lobes. During metamorphosis γ-KC dendrites and axons prune up to a set point, and later regrow to form adult specific connections.

(B) Red to green fluorescence ratio of CaMPARI2^{L398T} driven under the control of the GMR71G10-Gal4 driver at the indicated times, normalized to the mean value of early 3rd instar larvae (early L3). The Shapiro-Wilk test was performed to reject normal distribution. Statistical significance from baseline was calculated using one-sample Wilcoxon signed rank test with Bonferroni correction and is, ** $p=0.0024$ for 0h APF and *** $p<0.001$ for 6h APF. Box plots indicate median values (lines), mean values (open squares), inter-quartile ranges (boxes), 10/90 percentiles (whiskers) and individual data points (black dots).

(C-H) Confocal Z projections of adult brains immunostained with anti-FasII (magenta) and expressing (C) mCD8::GFP (green) under the control of GMR71G10-Gal4, or additionally expressing (D) Kir2.1, (E) TNT, or (F-H) dTRPA1 and grown at different temperatures (F) 29ºC (G) 22ºC (H) 29ºC from 0-6h APF. Arrows indicate unpruned axons.

(I) Ranking score quantification of pruning defect severity, as exemplified in Figure S1A-E. Statistical significance calculated using a Mann Whitney U test and is $p<0.001$ for dTrpA1 at 29ºC (F, n=16) vs trpA1 at 22ºC (G, n=6); $p<0.001$ for dTrpA1 at 29ºC (F, n=16) vs control (C, n=14); and $p=0.00047$ for pupa raised at 29ºC from 0-6h APF with dtrpA1 (H, n=19) vs the same treatment for controls lacking dTrpA1 (not shown, n=17).

Scale bar indicates 30µm.

See also Figure S1.

Figure 2

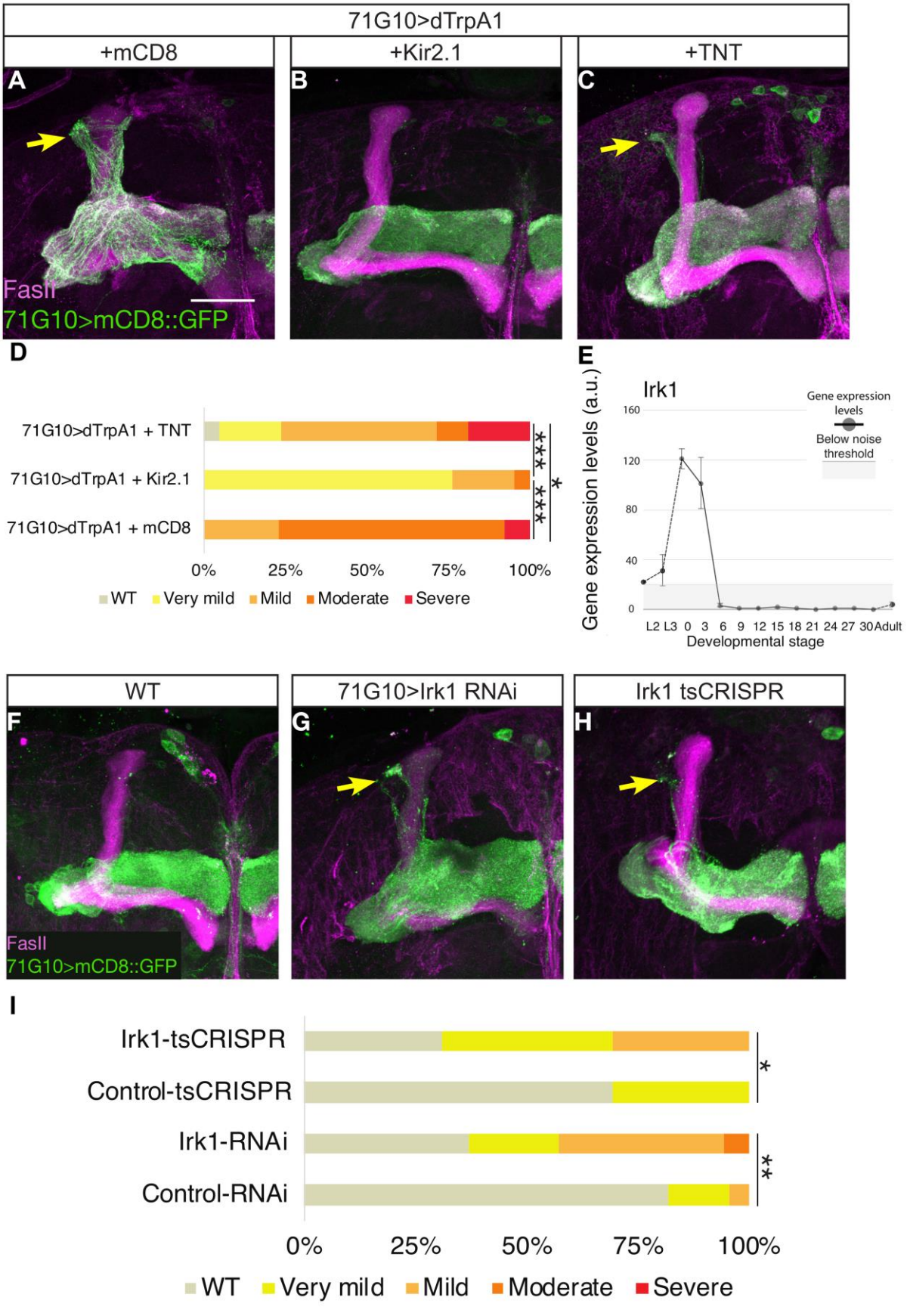
71G10>dTrpA1
+mCD8
+Kir2.1
+TNT
A
B
C
FasII
71G10>mCD8::GFP
D
71G10>dTrpA1 + TNT
71G10>dTrpA1 + Kir2.1
71G10>dTrpA1 + mCD8
***
***
*
0%
25%
50%
75%
100%
WT
Very mild
Mild
Moderate
Severe
E
Irk1
Gene expression levels
Below noise threshold
Gene expression levels (a.u.)
160
120
80
40
0
L2 L3 0 3 6 9 12 15 18 21 24 27 30 Adult
Developmental stage
WT
71G10>Irk1 RNAi
Irk1 tsCRISPR
F
G
H
FasII
71G10>mCD8::GFP
I
Irk1-tsCRISPR
Control-tsCRISPR
Irk1-RNAi
Control-RNAi
*
**
0%
25%
50%
75%
100%
WT
Very mild
Mild
Moderate
Severe

Figure 2: Hyperpolarization of γ-KC is required for pruning

(A-C) Confocal Z projections of adult brains reared at 29ºC, immunostained with anti-FasII (magenta) expressing mCD8::GFP and dTRPA1 under the control of GMR71G10-Gal4, additionally expressing (A) an additional copy of mCD8::GFP, (B) Kir2.1, or (C) TNT. Arrows indicate unpruned axons.

(D) Ranking of pruning defects in A-C. Statistical significance calculated using Mann-Whitney test, and is p-value =0.03752 for dTrpA1, TNT (C, n=22) vs dTrpA1, mCD8, (A; n=13) and p< 0.001 for dTrpA1, Kir2.1, (B; n=28) vs the control (A).

(E) Expression profile of *Irk1* in γ-KCs throughout development, demonstrating an acute increase in expression levels at the onset of metamorphosis. Extracted from[36], L2-L3 are 2nd and 3rd larval stages, 0-30 are hours APF.

(F-H) Confocal Z projections of brains immunostained with anti FasII (magenta), expressing mCD8::GFP under the control of GMR71G10-Gal4 (F), or additionally expressing UAS-Irk1-RNAi^{HMS02480} (G), or UAS-Cas9.C and U6.2:Irk1-gRNA (H).

(I) Ranking of pruning defects in F-H. Statistical significance calculated using Mann-Whitney test, p-value = 0.00168 for Irk1 RNAi (G; n=22) vs control (F; n=35) and 0.01046 for tsCRISPR (H; n=13) vs control (not shown; n=39). Arrows indicate unpruned axons.

Scale bar indicates 30μm.
See also Figure S2.

Figure 3

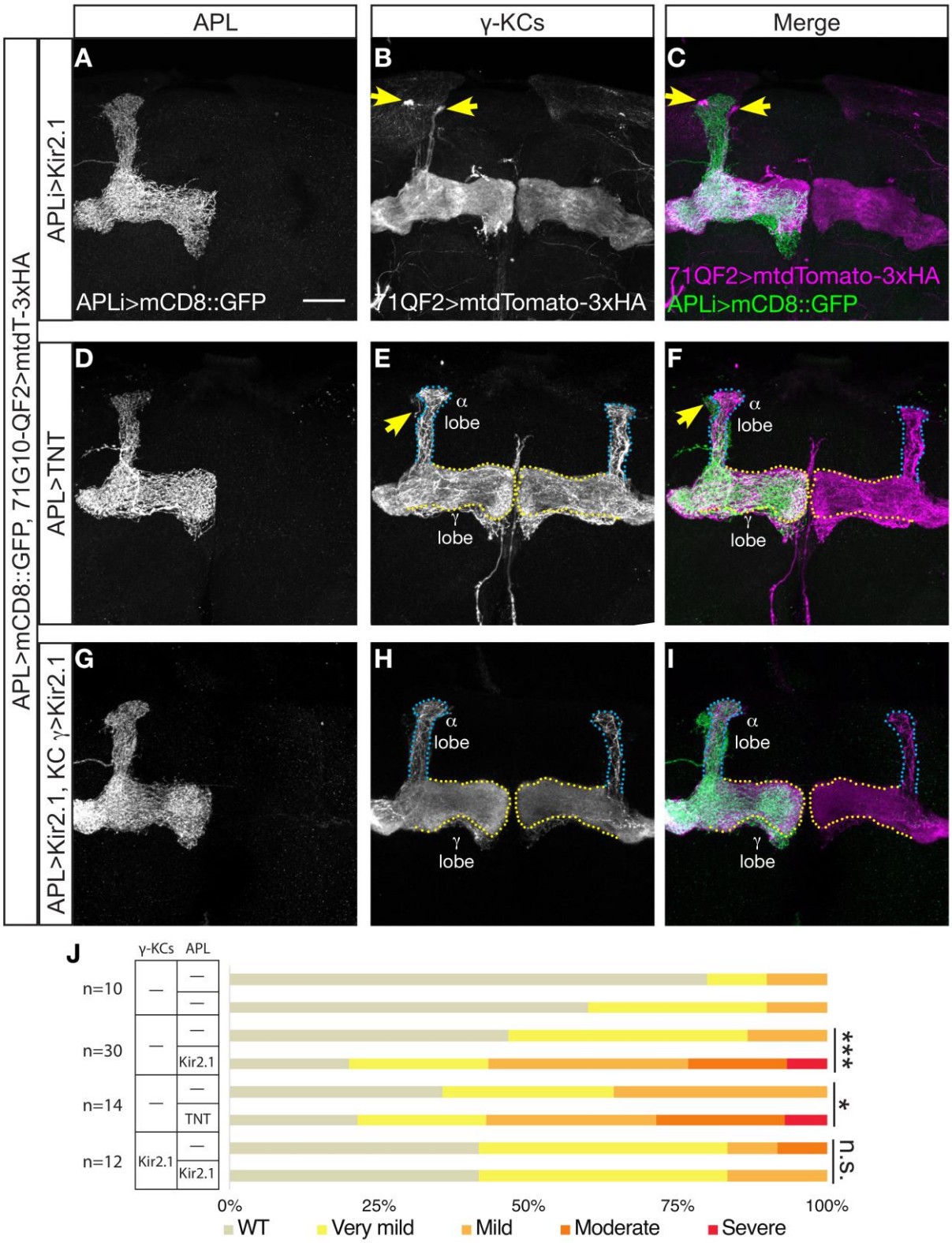
APL
γ-KCs
Merge
APL>mCD8::GFP, 71G10-QF2>mtdT-3xHA
APLi>Kir2.1
APL>TNT
APL>Kir2.1, KC γ>Kir2.1
A
B
C
D
E
F
G
H
I
APLi>mCD8::GFP
71QF2>mtdTomato-3xHA
71QF2>mtdTomato-3xHA
APLi>mCD8::GFP
α lobe
γ lobe
J
γ-KCs
APL
n=10
n=30
n=14
n=12
Kir2.1
TNT
***
*
n.s.
0%
25%
50%
75%
100%
WT
Very mild
Mild
Moderate
Severe

Figure 3: APL activity is required for γ-KCs pruning

(A-I) Confocal Z projections of brains expressing mCD8::GFP under the control APLi-Gal4 (grey in A,D,G and green in C,F,I) and mtdTomato-3xHA under the control of GMR71G10-QF2 (grey in B,E,H and magenta in C,F,I), additionally expressing Kir2.1 under the control of APLi-Gal4 (A-C), TNT under the control of APLi-Gal4 (D-F), or UAS-Kir2.1 under APLi-Gal4, as well as QUAS-Kir2.1 under GMR71G10-QF2 (G-I). Yellow arrows mark unpruned axons. Blue dotted outlines mark leaky expression of GMR71G10-QF2 in α/β KCs, and yellow dotted outlines mark the adult γ lobes. Scale bar indicates 30μm.

(J) Ranking of pruning defects of hemispheres with and without transgene expression in the APL, within the experiments shown in A-I. Statistical significance calculated between hemispheres expressing or not in APL, using paired Wilcoxon signed-rank test with continuity correction, p=0.000133 for APL>Kir2.1, (C; n=31), p= 0.02473 for APL>TNT (F; n= 14), and p= 0.833 for APL>Kir2.1, 71QF2>Kir2.1 (I; n=12).

See also Figure S3.

Figure 4

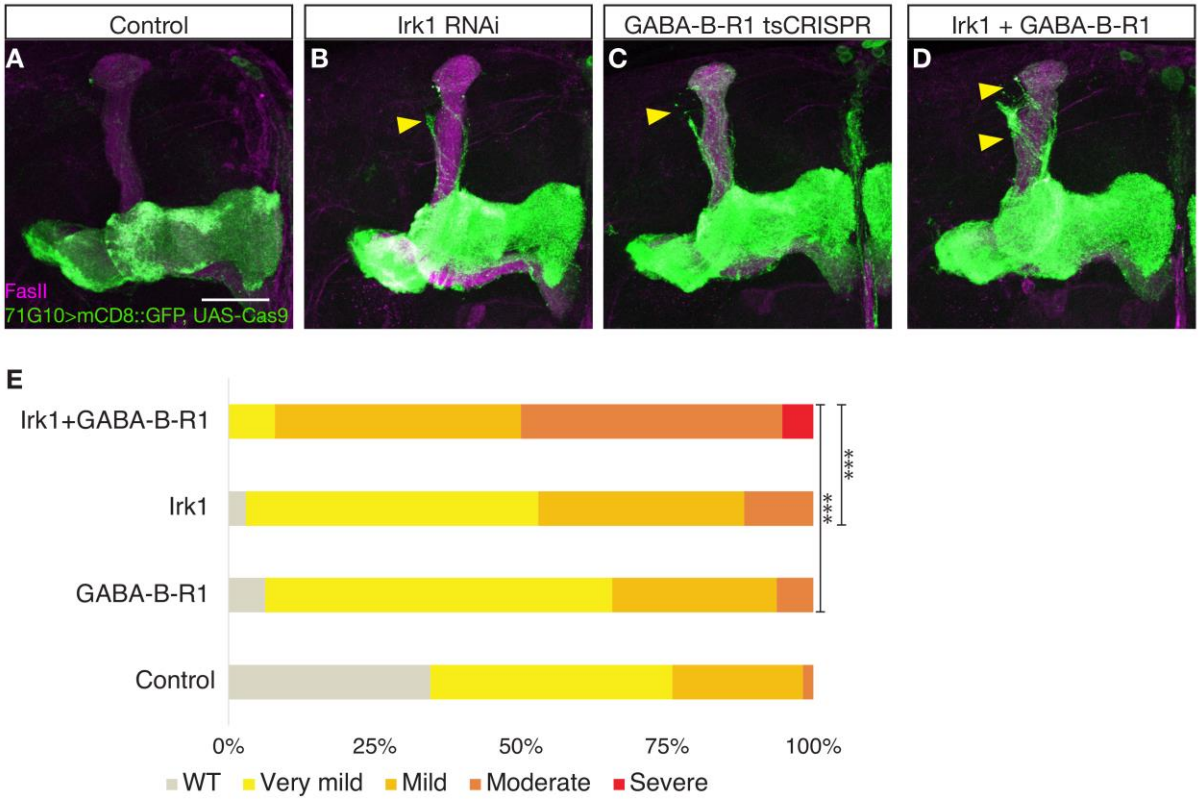

Figure 4: Irk1 and GABA-B-R1 expression are synergistically required for γ-KCs pruning

(A-D) Confocal Z projections of brains immunostained with anti-FasII (magenta), expressing mCD8::GFP and Cas9.C under the control of 2 copies of GMR71G10-Gal4 (A), additionally expressing UAS-Irk1-RNAi^{HMS02480} (B), U6.3:GABA-B-R1 gRNA (C), or both (D). Yellow arrowheads point to unpruned axons. Scale bar indicates 30µm.

(E) Ranking of pruning defect in A-D. Statistical significance between groups was calculated using the Kruskal Wallis H-test with a post-hoc two-tailed Wilcoxon test, and the p-values were adjusted by Bonferroni correction, p-value << 0.001 both for Irk1+GABA-B-R1 (n= 38) vs Irk1 RNAi alone (n= 34), and for Irk1+GABA-B-R1 vs GABA-B-R1 tsCRISPR alone, (n= 32).

See also Figure S4 and Table S1.

Supplementary Figure 1

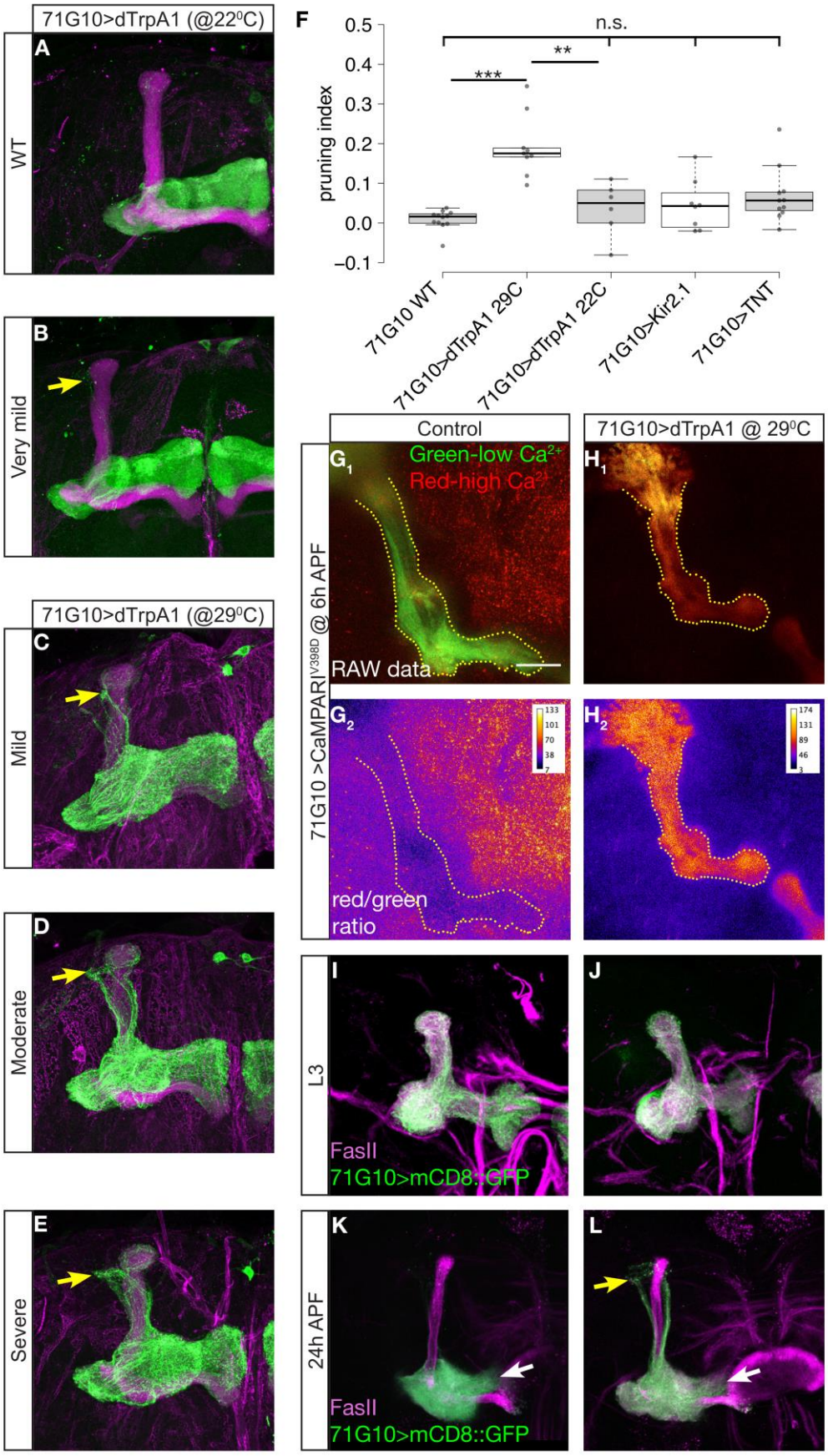

Figure S1: Examples of ranked pruning quantifications and dTrpA1 CaMPARI validation. Related to Figure 1.

(A-E) Examples of the ranking of pruning defect severity in experiments shown in Figure 1. Yellow arrowheads point towards unpruned axons.

(F) Script based quantification of the data in Figure 1 to complement Figure 1I. Statistical significance was calculated with a 2 tailed, 2 sample with equal variance students t-test. P-values are as follows: 71G10 WT Vs 71G10>dTrpA1@29^0C $p<0.001$, 71G10>dTrpA1@29^0C vs 71G10>dTrpA1@22^0C $p=0.0015$.Whiskers represent 1.5 IQR. See more information in the methods section.

(G-H) Confocal Z projections of adult brains reared at 29ºC, expressing CaMPARI^{V398D} (G), or both dTRPA1 and CaMPARI^{V398D} (H), under the control of GMR71G10-Gal4 and exposed to photoconverting light for 15 minutes at 6h APF. (G_1 and H_1) Green indicates low relative Ca^{2+}, while red indicates high relative Ca^{2+}. (G_2 and H_2) ratio of red to green fluorescence. Dotted yellow line outlines MB structure. Scale bar indicates 30µm.

(I-L) Confocal Z projections of either L3(I, J) or 24h APF (K, L) brains reared at 29ºC, either expressing mCD8-GFP (I, K) or mCD8:GFP together with dTrpA1 (J, L) under the control of GMR71G10-Gal4. Yellow arrow indicates unpruned γ-KCs. White arrows indicate regrowing γ-KCs.

Supplementary Figure 2

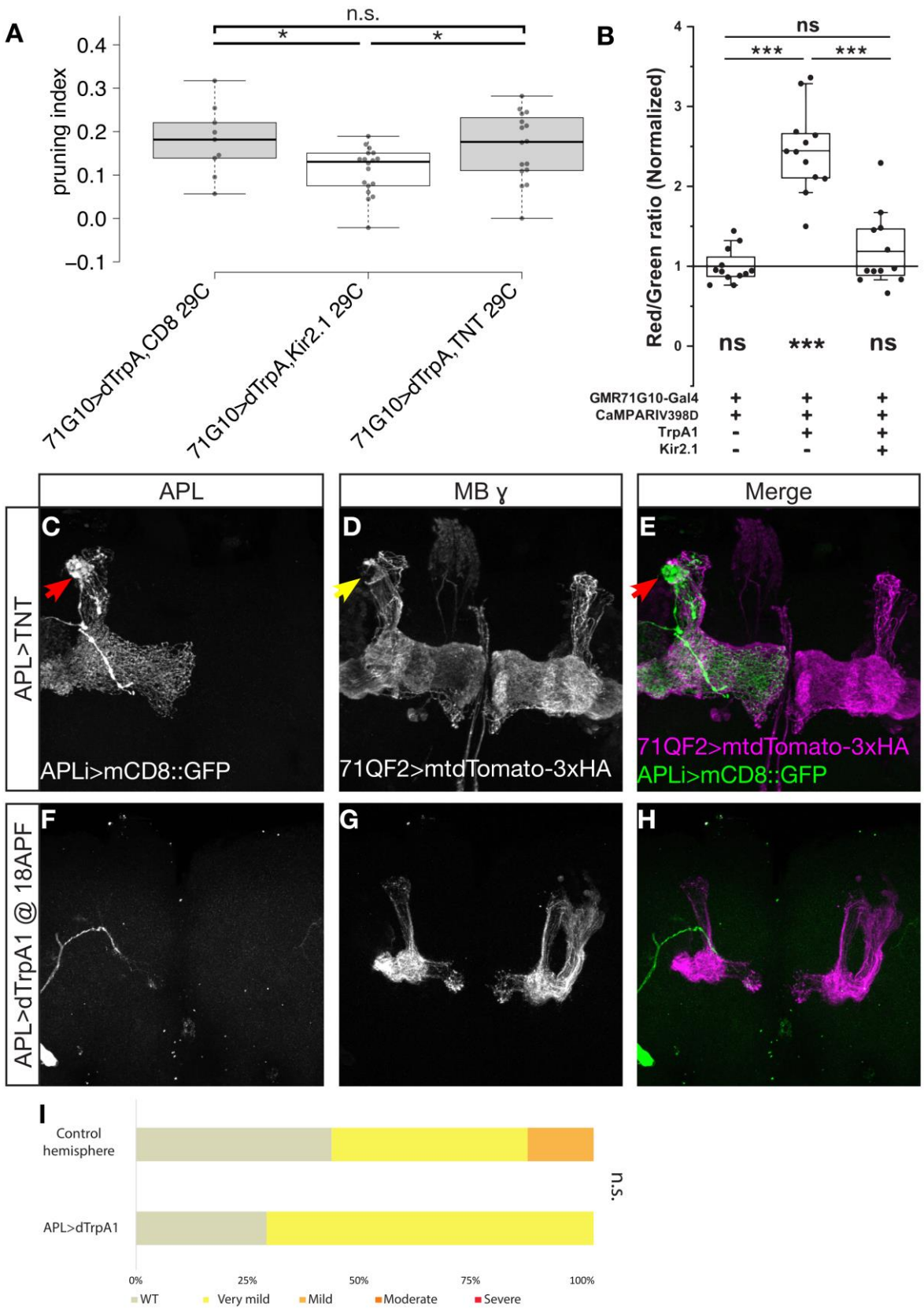

Figure S2: Expression of TNT in APL induces blebbing and activation of the APL is not sufficient to induce KC pruning. Related to Figure 2.

(A) Script based quantification of the data ranked in Figure 2D. Statistical significance was calculated with a 2 tailed, 2 sample with equal variance students t-test. P-values are as follows: 71G10>dTrpA1,mCD8 @29^0C vs 71G10>dTrpA1,Kir2.1 @29^0C p=0.01, 71G10>dTrpA1,Kir2.1 @29^0C Vs 71G10>dTrpA1,TNT @29^0C p=0.022. Whiskers represent 1.5 IQR See more information in the methods section.

(B) Normalized red to green fluorescence ratio of either CaMPARI^{V398D} driven under the control of the R71G10-Gal4 driver, or additionally expressing the indicated transgenes. The Shapiro-Wilk test was performed to confirm normal distribution; A two-tailed one-sample t-test against 1 with Bonferroni correction revealed that dTRPA1 was significantly different from baseline ($p<<0.0001$) but not for dTrpA1+Kir2.1 ($p=0.1926$), as indicated below the box plots. Additionally, statistical significance between groups (above the box plot) was calculated using one-way ANOVA ($p<<0.0001$) with Tukey post-hoc comparisons. Box plots indicate median values (lines), mean values (black squares), inter-quartile ranges (boxes), 10/90 percentiles (whiskers) and individual data points (black dots). All data points are normalized to the mean red/green ratio of 71G10 driving CaMPARI^{V398D} (left box plot).

(C-E) Confocal Z projections of adult brains expressing mCD8::GFP and TNT under the control of APLi-Gal4 (grey in C and green in E) and mtdTomato-3cHA under the control of GMR71G10-QF2 (grey in D and magenta in E). Red arrowheads point to blebbing in the APL, yellow arrowheads point to unpruned γ-KC axons.

(F-H) Confocal Z projections of brains of 18h APF pupa reared in 29^0C from 0hAPF expressing mCD8::GFP and dTrpA1 under the control APLi-Gal4 (grey in F and green in H) and mtdTomato-3xHA under the control of GMR71G10-QF2 (grey in G and magenta in H).

(I) Ranking of pruning defect severity in WT hemispheres (right hemisphere in H) vs hemispheres expressing the dTrpA1 under the control of the APLi driver (H, left hemisphere) grown in 29ºC.

Supplementary Figure 3

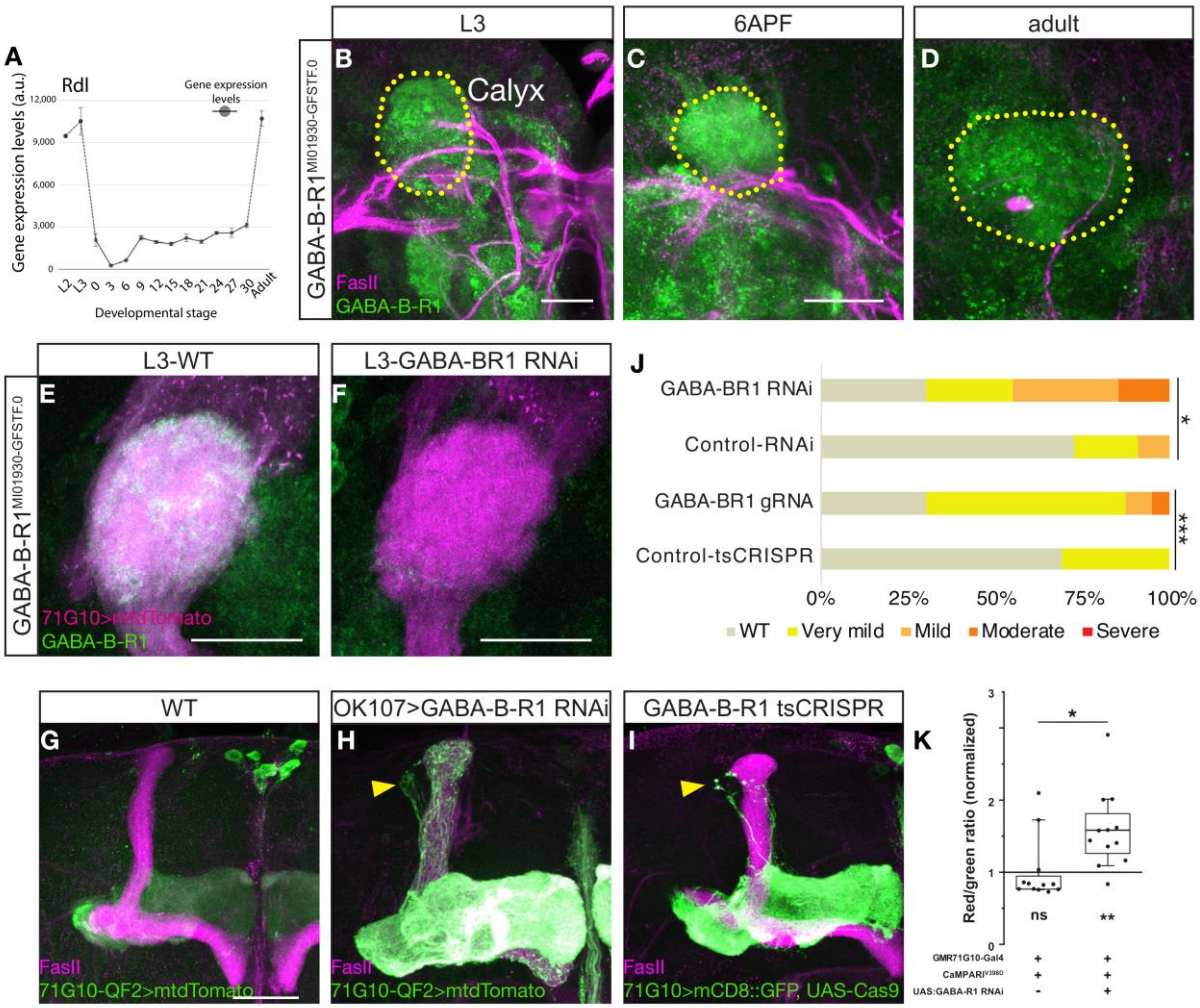

Figure S3: GABA B-R1 expression is required for Kenyon cell pruning. Related to Figure 3.

(A) Expression profile of Rdl in γ-KCs throughout development, showing an acute decrease in expression levels at the onset of metamorphosis. Extracted from (Alyagor et al., 2018), L2-L3 are 2nd and 3rd larval stages, 0-30 are hours APF.

(B-D) Confocal Z projections of L3 (B), 6h APF (C) and adult (D) brains expressing GFP-GABA-B-R1$^{MI01930\text{-}GFSTF.0}$ (green; MiMiC lines from Bellen et al., 2015; Venken et al., 2011), immunostained with anti fasII (magenta).

(E-F) Confocal Z projections of L3 brains expressing GABA-B-R1$^{MI01930\text{-}GFSTF.0}$ and mtdTomato-3xHA under the control of GMR71G10-QF2 (E; magenta) or additionally GABA-B-R1 RNAi^{HMC03388} (F).

(G-I) Confocal Z projections of adult brains immunostained with anti-FasII (magenta) expressing mtdTomato-3xHA under the control of GMR71G10-QF2 (G; green), or additionally expressing GABA-B-R1 RNAi ^{HMC03388} (H) or UAS-Cas9.C and GABA-B-R1 gRNA (I) under the control of OK107-Gal4.

(J) Ranking of pruning defects in (G-I). Statistical significance calculated using Mann-Whitney U test, p-value =.02444 for GABA-BR1 RNAi (I; n= 11) vs control (H; n= 20) and < .00001 for tsCRISPR (J; n=40) vs control (not shown; n= 39).

(K) Normalized red to green fluorescence ratio of either CaMPARI^{V398D} driven under the control of the R71G10-Gal4 driver, or additionally expressing GABA-B-R1 RNAi. The Shapiro-Wilk test was performed to reject normal distribution. A one-sample Wilcoxon signed rank test against 1 with Bonferroni correction revealed that 71G10> CaMPARI^{V398D} + GABA-B-R1 RNAi was significantly different from baseline ($p<0.01$), as indicated below the box plots. Additionally, statistical significance between groups (above the box plot) was calculated using the Mann Whitney U-test. Boxplots indicate median values (lines), mean values (black squares), inter-quartile ranges (boxes), 10/90 percentiles (whiskers) and individual data points (black dots). All data points are normalized to the mean red/green ratio of 71G10 driving CaMPARI^{V398D} alone. Scale bar indicates 30µm.

Supplementary Figure 4

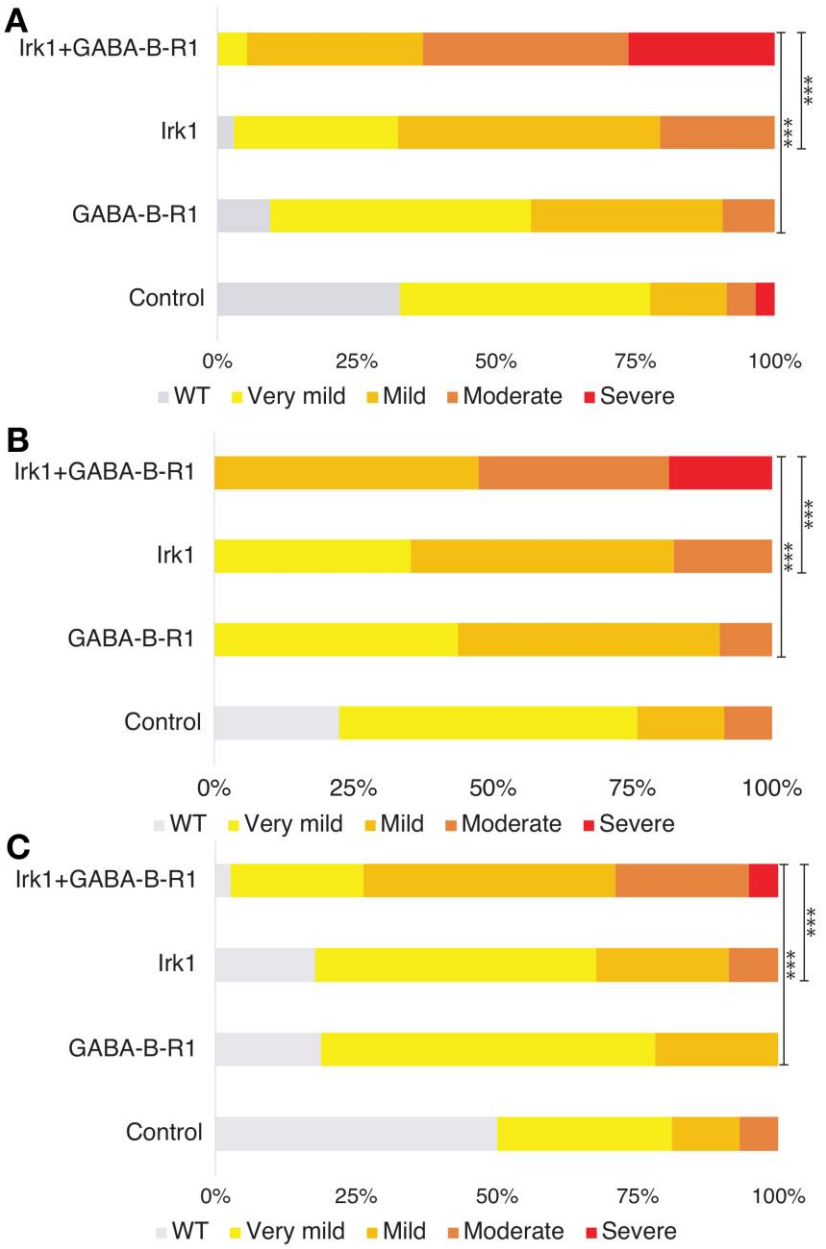

Figure S4: Additional ranking quantification of Irk1 and GABA-B-R1 double knockdown. Related to Figure 4.

(A-C) Independent ranking of the phenotypes shown in Figure 4A-D by three additional unrelated individuals. Statistical significance between groups was calculated using the Kruskal Wallis H-test with a post-hoc two-tailed Wilcoxon test, and the p-values were Bonferroni corrected. For all rankers, p-value << 0.001 for Irk1+GABA-B-R1 (n= 38) vs Irk1 RNAi alone (n= 34), and for Irk1+GABA-B-R1 vs GABA-B-R1 tsCRISPR alone, (n= 32). The complete ranking is shown in Table S1.

Table S1: Blind quantification of four independent individuals. Related to Figure 4/S4. Full genotypes of these flies are:

Control: Two copies of GMR71G10-Gal4 driver, UAS-Cas9. **Irk1**: Two copies of GMR71G10-Gal4 driver, UAS-Cas9, UAS-Irk1-RNAi^{HMS02480}. **GABA-B-R1**: Two copies of GMR71G10-Gal4 driver, UAS-Cas9, GABA-B-R1 gRNA$^{WKO.1-G2}$. **Irk1+GABA-B-R1**: Two copies of GMR71G10-Gal4 driver, UAS-Cas9, UAS-Irk1-RNAi^{HMS02480}, GABA-B-R1 gRNA$^{WKO.1-G2}$.

Genotype	Ranker #1	Ranker #2	Ranker #3	Ranker #4
control	1	2	2	1
control	2	1	1	1
control	1	2	2	1
control	1	1	2	1
control	2	2	2	2
control	1	1	1	1
control	2	1	1	1
control	1	1	1	1
control	1	2	2	1
control	1	2	2	1
control	2	1	1	1
control	2	1	1	1
control	1	2	2	1
control	1	1	2	1
control	1	2	2	2
control	2	1	1	1
control	1	2	2	2
control	1	1	2	1
control	1	2	2	1
control	2	1	1	1
control	3	2	2	2
control	2	2	2	2
control	3	2	2	1
control	2	2	2	2
control	1	1	1	1
control	1	1	2	1
control	4	4	3	2
control	1	1	1	1
control	2	2	2	1
control	2	2	2	1
control	1	1	1	1
control	2	1	2	2
control	2	2	2	2
control	2	2	2	2
control	3	2	2	2
control	1	1	1	1
control	2	2	2	1
control	3	2	2	2
control	2	2	2	1

control	3	3	3	3
control	3	4	4	4
control	2	2	2	2
control	2	3	3	3
control	3	3	3	3
control	3	5	4	4
control	3	3	3	3
control	2	2	3	2
control	2	3	3	2
control	3	3	4	3
control	2	1	2	1
control	3	3	3	3
control	2	2	2	2
control	2	3	3	3
control	3	4	4	4
control	3	5	4	4
control	1	2	2	2
control	1	1	1	1
control	2	2	2	2
Irk1+GABA-B-R1	2	3	3	2
Irk1+GABA-B-R1	3	3	3	2
Irk1+GABA-B-R1	2	3	3	2
Irk1+GABA-B-R1	3	3	3	2
Irk1+GABA-B-R1	3	3	3	2
Irk1+GABA-B-R1	3	4	3	2
Irk1+GABA-B-R1	4	5	4	4
Irk1+GABA-B-R1	3	3	3	3
Irk1+GABA-B-R1	3	3	3	2
Irk1+GABA-B-R1	3	3	3	2
Irk1+GABA-B-R1	4	4	4	3
Irk1+GABA-B-R1	2	2	3	1
Irk1+GABA-B-R1	4	4	4	3
Irk1+GABA-B-R1	3	2	3	2
Irk1+GABA-B-R1	4	5	4	3
Irk1+GABA-B-R1	3	3	3	3
Irk1+GABA-B-R1	4	4	4	3
Irk1+GABA-B-R1	4	5	4	3
Irk1+GABA-B-R1	3	3	4	3
Irk1+GABA-B-R1	4	5	4	4
Irk1+GABA-B-R1	3	4	4	3
Irk1+GABA-B-R1	4	4	3	3
Irk1+GABA-B-R1	4	4	4	4
Irk1+GABA-B-R1	4	4	5	4
Irk1+GABA-B-R1	3	4	5	4
Irk1+GABA-B-R1	4	4	3	3
Irk1+GABA-B-R1	5	5	5	5
Irk1+GABA-B-R1	5	5	5	4
Irk1+GABA-B-R1	3	3	3	3
Irk1+GABA-B-R1	4	5	5	4
Irk1+GABA-B-R1	3	4	3	3
Irk1+GABA-B-R1	4	4	4	3
Irk1+GABA-B-R1	4	4	5	4

Irk1+GABA-B-R1	4	5	5	5
Irk1+GABA-B-R1	4	5	4	4
Irk1+GABA-B-R1	4	5	4	3
Irk1+GABA-B-R1	3	3	3	3
Irk1+GABA-B-R1	3	4	3	3
GABA-B-R1	3	3	3	2
GABA-B-R1	2	2	2	2
GABA-B-R1	1	2	2	1
GABA-B-R1	2	1	2	1
GABA-B-R1	2	2	2	2
GABA-B-R1	3	3	3	2
GABA-B-R1	3	2	2	2
GABA-B-R1	2	2	2	2
GABA-B-R1	2	2	2	2
GABA-B-R1	2	3	2	2
GABA-B-R1	4	4	4	3
GABA-B-R1	2	1	2	1
GABA-B-R1	2	2	3	2
GABA-B-R1	3	3	3	3
GABA-B-R1	2	3	3	3
GABA-B-R1	3	4	3	3
GABA-B-R1	2	3	3	3
GABA-B-R1	1	1	2	1
GABA-B-R1	3	3	3	2
GABA-B-R1	3	3	3	2
GABA-B-R1	3	3	3	2
GABA-B-R1	2	2	2	1
GABA-B-R1	2	2	3	2
GABA-B-R1	2	2	2	1
GABA-B-R1	4	4	4	3
GABA-B-R1	2	2	2	2
GABA-B-R1	2	2	3	2
GABA-B-R1	2	2	3	2
GABA-B-R1	2	3	3	2
GABA-B-R1	2	2	2	2
GABA-B-R1	2	2	3	2
GABA-B-R1	3	3	4	3
irk1	3	4	3	2
irk1	2	2	3	2
irk1	3	3	3	2
irk1	3	2	3	2
irk1	3	2	2	1
irk1	1	2	2	1
irk1	2	2	2	2
irk1	3	3	2	2
irk1	2	3	2	1
irk1	4	3	3	3
irk1	2	1	2	1
irk1	2	3	3	2
irk1	4	3	3	3
irk1	4	4	3	2
irk1	2	2	2	1

irk1	4	4	4	4
irk1	3	3	3	3
irk1	2	3	4	3
irk1	3	4	3	3
irk1	3	3	4	3
irk1	3	4	4	4
irk1	3	4	4	3
irk1	2	3	3	2
irk1	2	2	2	2
irk1	3	4	4	4
irk1	2	3	3	2
irk1	2	2	2	2
irk1	2	3	3	2
irk1	2	3	3	2
irk1	2	2	2	2
irk1	2	2	2	1
irk1	2	3	3	2
irk1	2	3	2	2
irk1	3	3	3	3

STAR methods:

KEY RESOURCE TABLE

REAGENT or RESOURCE	SOURCE	IDENTIFIER
Antibodies		
Chicken anti GFP 1:500	AVES	GFP-1020 AB_10000240
Mouse monoclonal anti FasII 1:25	Developmental Studies Hybridoma Bank (DSHB)	1D4 AB_528235
Rat monoclonal anti HA 1:250	Sigma Aldrich	11867423001 AB_10094468
FITC Goat anti chicken 1:300	Invitrogen	A-16055 AB_2534728
Alexa fluor 647 Goat anti rat 1:300	Invitrogen	A-21247 AB_141778
Alexa fluor 647 goat anti mouse 1:300	Invitrogen	A-32728 AB_2633277
Experimental Models: Organisms/Strains		
D. melanogaster: w[*]; P{y[+t7.7] w[+mC]=10XUAS-IVS-mCD8:GFP}attP2	Gift from GM Rubin	N/A
D. melanogaster: w[*]; P{y[+t7.7] w[+mC]=10XUAS-IVS-mCD8:GFP}attP40	Bloomington drosophila stock center (BDSC)	BDSC: 32185; FlyBase: FBst0032185
D. melanogaster: NP2631-Gal4, GH146-flp/CyO ; Mkrs,Sb/Tm6,Hu,Tb	Bloomington drosophila stock center (BDSC)	BDSC: 32186; FlyBase: FBst0032186
D. melanogaster: TubP,FRT,Gal80,FRT,UAS-mCD8:GFP/CyO ; Mkrs,Sb/Tm6,Hu,Tb	Gift from AC Lin[40]	N/A
D. melanogaster: GMR71G10-QF2^{Hack}	Bloomington drosophila stock center (BDSC)	BDSC: 6872; FlyBase: FBst0006872
D. melanogaster: UAS-TNT		
D. melanogaster: OK107-Gal4	Bloomington drosophila stock center (BDSC)	BDSC: 854; FlyBase: FBti0004170
D. melanogaster: QUAS-mtdTomato-3xHA	Bloomington drosophila stock center (BDSC)	BDSC: 30005; FlyBase: FBti0129951
D. melanogaster: GMR71G10-Gal4	Bloomington drosophila stock center (BDSC)	BDSC: 39604; FlyBase: FBti0137964
D. melanogaster: UAS-TNT (w[*]; P{w[+mC]=UAS-TeTxLC.tnt}R3)	Bloomington drosophila stock center (BDSC)	BDSC: 28997; FlyBase: FBti0038570
D. melanogaster: UAS-Kir2.1 (w[*]; P{w[+mC]=UAS-Hsap\KCNJ2.EGFP}7)	Bloomington drosophila stock center (BDSC)	BDSC: 6595; FlyBase: FBti0017552
D. melanogaster: QUAS-Kir2.1	Bloomington drosophila stock center (BDSC)	BDSC: 91802
D. melanogaster: UAS-dTrpA1	Bloomington drosophila stock center (BDSC)	BDSC: 26264; FlyBase: FBti0114502
D. melanogaster: UAS-Irk1-RNAi^{HMS02480}	Bloomington drosophila stock	BDSC: 42644; FlyBase:

	center (BDSC)	FBti0151128
D. melanogaster: UAS-GABA-B-R1-RNAi^{HMC03388}	Bloomington drosophila stock center (BDSC)	BDSC: 51817; FlyBase: FBti0157782
D. melanogaster: w[1118]; P{y[+t7.7] w[+mC]=UAS-Cas9.C}attP2	Bloomington drosophila stock center (BDSC)	BDSC: 54595; FlyBase: FBti0159186
D. melanogaster: GABA-B-R1 gRNA (y[1]; M{v[+t1.8]=WKO.1-G2}ZH-86Fb)	Bloomington drosophila stock center (BDSC)	BDSC: 83036; FlyBase: FBti0205338
D. melanogaster: Irk1 gRNA (y[1] v[1]; P{y[+t7.7] v[+t1.8]=U6.2-Irk1.dgRNA}attP40)	Bloomington drosophila stock center (BDSC)	BDSC: 92531; FlyBase: FBti0215651
D. melanogaster: w[*]; P{y[+t7.7] w[+mC]=UAS-CaMPARI.V398D}attP40	Bloomington drosophila stock center (BDSC)	BDSC: 58762; FlyBase: FBti0166951
D. melanogaster: w[1118] P{y[+t7.7] w[+mC]=UAS-CaMPARI2.L398T}su(Hw)attP8	Bloomington drosophila stock center (BDSC)	BDSC: 78320; FlyBase: FBti0199492
D. melanogaster: y[1] w[67c23]; Mi{PT-GFSTF.0}GABA-B-R1[MI01930-GFSTF.0]	Bloomington drosophila stock center (BDSC)	BDSC: 60522; FlyBase: FBti0178464
Software and Algorithms		
FIJI	Image J	https://imagej.net/Fiji/Downloads
Other		
Zeiss LSM 710 and 800 confocal microscope		
40x 1.3 NA oil immersion lens	Zeiss	
TCS SP8 confocal microscope	Leica	

RESOURCE AVAILABILITY

Lead contact

Further information and requests for resources and reagents should be directed to and will be fulfilled by the Lead Contact, Oren Schuldiner (oren.schuldiner@weizmann.ac.il)

Materials availability

This study did not generate new unique reagents.

Data and code availability

- Data reported in this paper will be shared by the lead contact upon request
- This paper does not report original code.
- Any additional information required to reanalyze the data reported in this paper is available from the lead contact upon request.

EXPERIMENTAL MODEL

Drosophila melanogaster rearing and strains

All fly strains were reared under standard laboratory conditions at 25°C (unless stated otherwise) on molasses containing food. Males and females were chosen at random. Developmental stage is referred to in the relevant places while adult refers to 3-5 days post eclosion.

APLi lines: NP2631-Gal4, GH146-flp/CyO; Sb/Tm3,Ser and TubP,FRT,Gal80,FRT,UAS-mCD8:GFP/CyO; Sb/Tm3,Ser, were generated and kindly provided by Dr. Gero Miesenböck.

71G10-QF^{Hack} was kindly provided by Dr. Christopher J. Potter.

METHOD DETAILS

Immunostaining

Drosophila brains were dissected in cold ringer solution, fixed using 4% paraformaldehyde (PFA) for 20 minutes at room temperature (25^{0}C) on a nutator, after which brains were washed several times in PBT (phosphate buffer supplemented with 0.3% triton-x) blocked using heat inactivated goat serum and subjected to primary antibody staining overnight at 4^{0}C, followed by three washes with PBT, then staining with secondary antibodies for 2 hours at RT, secondary antibodies were quickly washed with PBT and then washed again 3 times.

Imaging and image processing

All stained brains were mounted on Slowfade (Invitrogen) and imaged on Zeiss LSM 710 or 800 confocal microscopes using 40x 1.3 NA oil immersion lens. Images were processed with ImageJ (NIH).

Manual ranking/script-based quantifications

Ranking was performed on maximum Z-projections by one or more independent scorers in a double-blind manner with similar significance scores. The results of one scorer are shown for simplicity. Examples of rank severity score are shown in Figure S1(A-E).

Script based quantifications were done in a similar manner as in Ref[36]. Briefly, using a custom FIJI script, the thickest part of the dorsal α lobe was semi-automatically identified based on FasII staining, and the fluorescence of the GFP positive neurons γ-KCs surrounding it (up to ±10µm radius from the α lobe, excluding the α lobe itself and therefore expected to be unpruned γ-KCs) was automatically measured and normalized as compared to the average fluorescence measured in the MB branching point.

Larval staging

Late vs early 3rd instar (L3) larval stage was set by rearing larvae on fly food with added red food coloring. Early L3 larvae displayed a colored gut, while late L3 larvae had no coloration.

CaMPARI photoconversion and imaging

Drosophila of the appropriate genotype were collected at the marked developmental stage; Early L3 (wandering stage with coloration in gut), Late L3 (wandering stage with no gut coloration), 0h APF (white pupa), 3h APF, and 6h APF. Larvae/pupae were illuminated using a UV illumination table (395nm) for 15 minutes, directly dissected in ice cold Ca^{2+} free Ringers solution, and immediately mounted on an aluminum foil wrapped microscope slide for imaging using a 20x Objective with 2.5 Zoom on an SP8 Leica confocal microscope.

Hybrid detector 1, between 510nm and 545nm; and Hybrid detector 2, between 568nm and far red (maximum), averaging 2 iterations per line.

Two different wavelength lasers were used: 488nm (10% intensity) and 561nm (10% intensity) scanned simultaneously. It was confirmed beforehand that there was no “spill-over” between detection channels.

ImageJ was used to measure the fluorescence in the acquired images in selected ROIs, which had background subtracted using an identical ROI measuring background intensity. Red/Green fluorescence was normalised to the mean of the first time-window (divided every measurement by the mean of the first group).

QUANTIFICATION AND STATISTICAL ANALYSIS

In all cases, *** represent a p-value lower than 0.001; ** represent a p-value lower than 0.01 and * represents a p-value lower than 0.05. Statistical tests were run using R-Studio or OriginPro 8.5G. specific p-values and sample sizes and testes are indicated in the relevant figure legend and in text.

For all script based quantifications significance was quantified with a 2 tailed, 2 sample with equal variance students t-test. P-values are as follows; Figure S1F; 71G10 WT Vs 71G10>dTrpA1@29^0C $p<0.001$, 71G10>dTrpA1@29^0C vs 71G10>dTrpA1@22^0C $p=0.0015$. Figure S2A; 71G10>dTrpA1,mCD8 @29^0C vs

71G10>dTrpA1,Kir2.1 @29^{0}C p=0.01, 71G10>dTrpA1,Kir2.1 @29^{0}C Vs 71G10>dTrpA1,TNT @29^{0}C p=0.022. Figure S4A; Cas9_cntrl Vs Irk1_KD p<0.001, GABS_BR1 KD Vs double KD P=0.0001.

References:

1. Luo, L., and O'Leary, D.D.M. (2005). Axon retraction and degeneration in development and disease. Annual review of neuroscience *28*, 127–156. 10.1146/annurev.neuro.28.061604.135632.
2. Schuldiner, O., and Yaron, A. (2014). Mechanisms of developmental neurite pruning. Cellular and molecular life sciences : CMLS. 10.1007/s00018-014-1729-6.
3. Akin, O., and Zipursky, S.L. (2020). Activity regulates brain development in the fly. Current Opinion in Genetics and Development *65*, 8–13. 10.1016/j.gde.2020.04.005.
4. Johnson-Venkatesh, E.M., Khan, M.N., Murphy, G.G., Sutton, M.A., and Umemori, H. (2015). Excitability governs neural development in a hippocampal region specific manner. Development, 3879–3891. 10.1242/dev.121202.
5. Katz, L., and Shatz, C. (1996). Synaptic Activity and the Construction of Cortical Circuits. Science *274*, 1133–1138. 10.1126/science.274.5290.1133
6. Hashimoto, K., Ichikawa, R., Kitamura, K., Watanabe, M., and Kano, M. (2009). Translocation of a "Winner" Climbing Fiber to the Purkinje Cell Dendrite and Subsequent Elimination of "Losers" from the Soma in Developing Cerebellum. Neuron *63*, 106–118. 10.1016/j.neuron.2009.06.008.
7. Chung, W.-S., and Barres, B.A. (2009). Selective Remodeling: Refining Neural Connectivity at the Neuromuscular Junction. PLOS Biology *7*, e1000185. 10.1371/JOURNAL.PBIO.1000185.
8. Walsh, M.K., and Lichtman, J.W. (2003). In Vivo Time-Lapse Imaging of Synaptic Takeover Associated with Naturally Occurring Synapse Elimination. Neuron *37*, 67–73. 10.1016/S0896-6273(02)01142-X.
9. Tapia, J.C., Wylie, J.D., Kasthuri, N., Hayworth, K.J., Schalek, R., Berger, D.R., Guatimosim, C., Seung, H.S., and Lichtman, J.W. (2012). Pervasive Synaptic Branch Removal in the Mammalian Neuromuscular System at Birth. Neuron *74*, 816–829. 10.1016/j.neuron.2012.04.017.
10. White, C.K., Zweerink, H.J., Ralph, S.J., Harvey, J.D., Bellamy, A.R., Cohan, C.S., and KATERt, S.B. (1986). Suppression of Neurite Elongation and Growth Cone Motility by Electrical Activity. Science *232*, 1638–1640. 10.1126/SCIENCE.3715470.
11. O'Rourke, N.A., Cline, H.T., and Fraser, S.E. (1994). Rapid remodeling of retinal arbors in the tectum with and without blockade of synaptic transmission. Neuron *12*, 921–934. 10.1016/0896-6273(94)90343-3.
12. Lom, B., and Cohen-Cory, S. (1999). Brain-Derived Neurotrophic Factor Differentially Regulates Retinal Ganglion Cell Dendritic and Axonal Arborization In Vivo. Journal of Neuroscience *19*, 9928–9938. 10.1523/JNEUROSCI.19-22-09928.1999.
13. Duch, C., and Mentel, T. (2004). Activity Affects Dendritic Shape and Synapse Elimination during Steroid Controlled Dendritic Retraction in Manduca sexta. Journal of Neuroscience *24*, 9826–9837. 10.1523/JNEUROSCI.3189-04.2004.
14. Duch, C., and Mentel, T. (2003). Stage-specific activity patterns affect motoneuron axonal retraction and outgrowth during the metamorphosis of Manduca sexta. European Journal of Neuroscience *17*, 945–962. 10.1046/J.1460-9568.2003.02523.X.
15. Heisenberg, M., Borst, A., Wagner, S., and Byers, D. (1985). Drosophila Mushroom Body Mutants are Deficient in Olfactory Learning. Journal of Neurogenetics *2*, 1–30. 10.3109/01677068509100140.

16. Bilz, F., Geurten, B.R.H., Hancock, C.E., Widmann, A., and Fiala, A. (2020). Visualization of a Distributed Synaptic Memory Code in the Drosophila Brain. Neuron *106*, 963-976.e4. 10.1016/J.NEURON.2020.03.010.
17. Zheng, Z., Lauritzen, J.S., Perlman, E., Robinson, C.G., Nichols, M., Milkie, D., Torrens, O., Price, J., Fisher, C.B., Sharifi, N., et al. (2018). A Complete Electron Microscopy Volume of the Brain of Adult Drosophila melanogaster. Cell *174*, 730-743.e22. 10.1016/j.cell.2018.06.019.
18. Takemura, S., Aso, Y., Hige, T., Wong, A., Lu, Z., Xu, C.S., Rivlin, P.K., Hess, H., Zhao, T., Parag, T., et al. (2017). A connectome of a learning and memory center in the adult Drosophila brain. eLife *6*. 10.7554/elife.26975.
19. Lee, T., and Luo, L. (1999). Mosaic analysis with a repressible cell marker for studies of gene function in neuronal morphogenesis. Neuron *22*, 451–461. 10.1016/s0896-6273(00)80701-1
20. Lee, T., Marticke, S., Sung, C., Robinow, S., and Luo, L. (2000). Cell-autonomous requirement of the USP/EcR-B ecdysone receptor for mushroom body neuronal remodeling in Drosophila. Neuron *28*, 807–818. 10.1016/s0896-6273(00)00155-0
21. Watts, R.J., Hoopfer, E.D., and Luo, L. (2003). Axon pruning during Drosophila metamorphosis: evidence for local degeneration and requirement of the ubiquitin-proteasome system. Neuron *38*, 871–885. 10.1016/s0896-6273(03)00295-2
22. Mayseless, O., Berns, D.S., Yu, X.M., Riemensperger, T., Fiala, A., and Schuldiner, O. (2018). Developmental Coordination during Olfactory Circuit Remodeling in Drosophila. Neuron, 1–12. 10.1016/j.neuron.2018.07.050.
23. Kano, M., Watanabe, T., Uesaka, N., and Watanabe, M. (2018). Multiple Phases of Climbing Fiber Synapse Elimination in the Developing Cerebellum. Cerebellum *17*, 722–734. 10.1007/s12311-018-0964-z.
24. Golovin, R.M., Vest, J., Vita, D.J., and Broadie, K. (2019). Activity-dependent remodeling of Drosophila olfactory sensory neuron brain innervation during an early-life critical period. Journal of Neuroscience *39*, 2995–3012. 10.1523/JNEUROSCI.2223-18.2019.
25. Qiu, Q., Wu, Y., Ma, L., Ramalingam, V., and Yu, C.R. (2020). Acquisition of Innate Odor Preference Depends on Spontaneous and Experiential Activities During Critical Period. bioRxiv, 2020.01.28.923722. 10.1101/2020.01.28.923722.
26. Kanamori, T., Kanai, M.I., Dairyo, Y., Yasunaga, K., Morikawa, R.K., and Emoto, K. (2013). Compartmentalized calcium transients trigger dendrite pruning in Drosophila sensory neurons. Science (New York, N.Y.) *340*, 1475–1478. 10.1126/science.1234879.
27. Berridge, M.J. (1998). Neuronal calcium signaling. Neuron *21*, 13–26. 10.1016/0166-2236(87)90099-3.
28. Fosque, B.F., Sun, Y., Dana, H., Yang, C., Ohyama, T., Tadross, M.R., Patel, R., Zlatic, M., Kim, D.S., Ahrens, M.B., et al. (2015). Neural circuits. Labeling of active neural circuits in vivo with designed calcium integrators. Science (New York, N.Y.) *347*, 755–760. 10.1126/science.1260922.
29. Moeyaert, B., Holt, G., Madangopal, R., Perez-Alvarez, A., Fearey, B.C., Trojanowski, N.F., Ledderose, J., Zolnik, T.A., Das, A., Patel, D., et al. (2018). Improved methods for marking active neuron populations. Nature Communications *9*. 10.1038/s41467-018-06935-2.
30. Venken, K.J.T.J.T., Simpson, J.H.H., and Bellen, H.J.J. (2011). Genetic manipulation of genes and cells in the nervous system of the fruit fly. Neuron *72*, 202–230. 10.1016/j.neuron.2011.09.021.

31. Baines, R.A., Uhler, J.P., Thompson, a, Sweeney, S.T., and Bate, M. (2001). Altered electrical properties in Drosophila neurons developing without synaptic transmission. The Journal of neuroscience : the official journal of the Society for Neuroscience *21*, 1523–1531. 10.1523/jneurosci.21-05-01523.2001
32. Rosenzweig, M., Brennan, K.M., Tayler, T.D., Phelps, P.O., Patapoutian, A., and Garrity, P.A. (2005). The Drosophila ortholog of vertebrate TRPA1 regulates thermotaxis. Genes & development *19*, 419–424. 10.1101/gad.1278205.
33. Hamada, F.N., Rosenzweig, M., Kang, K., Pulver, S.R., Ghezzi, A., Jegla, T.J., and Garrity, P.A. (2008). An internal thermal sensor controlling temperature preference in Drosophila. Nature *454*, 217–220. 10.1038/nature07001.
34. Rabinovich, D., Yaniv, S.P., Alyagor, I., and Schuldiner, O. (2016). Nitric Oxide as a Switching Mechanism between Axon Degeneration and Regrowth during Developmental Remodeling. Cell *164*, 170–182. 10.1016/j.cell.2015.11.047.
35. Bevan, S., and Szolcsányi, J. (1990). Sensory neuron-specific actions of capsaicin: mechanisms and applications. Trends in Pharmacological Sciences *11*, 331–333. 10.1016/0165-6147(90)90237-3.
36. Alyagor, I., Berkun, V., Keren-Shaul, H., Marmor-Kollet, N., David, E., Mayseless, O., Issman-Zecharya, N., Amit, I., and Schuldiner, O. (2018). Combining Developmental and Perturbation-Seq Uncovers Transcriptional Modules Orchestrating Neuronal Remodeling. Developmental Cell *47*, 38-52.e6. 10.1016/j.devcel.2018.09.013.
37. Döring, F., Wischmeyer, E., Kühnlein, R.P., Jäckle, H., and Karschin, A. (2002). Inwardly Rectifying K + (Kir) Channels in Drosophila. Journal of Biological Chemistry *277*, 25554–25561. 10.1074/jbc.M202385200.
38. Meltzer, H., Marom, E., Alyagor, I., Mayseless, O., Berkun, V., Segal-Gilboa, N., Unger, T., Luginbuhl, D., and Schuldiner, O. (2019). Tissue-specific (ts)CRISPR as an efficient strategy for in vivo screening in Drosophila. *10*. 10.1038/s41467-019-10140-0.
39. Masuda-Nakagawa, L.M., Ito, K., Awasaki, T., and O'Kane, C.J. (2014). A single GABAergic neuron mediates feedback of odor-evoked signals in the mushroom body of larval Drosophila. Frontiers in neural circuits *8*, 35. 10.3389/fncir.2014.00035.
40. Lin, A.C., Bygrave, A.M., de Calignon, A., Lee, T., and Miesenböck, G. (2014). Sparse, decorrelated odor coding in the mushroom body enhances learned odor discrimination. Nature neuroscience *17*, 559–568. 10.1038/nn.3660.
41. Yan, B.C., Park, J.H., Kim, I.H., Shin, B.N., Ahn, J.H., Yoo, K.Y., Lee, D.S., Kim, M.J., Kang, I.J., and Won, M.H. (2012). Chronological changes in inflammatory cytokines immunoreactivities in the mouse hippocampus after systemic administration of high dosage of tetanus toxin. Experimental Brain Research *223*, 271–280. 10.1007/S00221-012-3257-7.
42. Janigro, D., and Schwartzkroin, P.A. (1988). Effects of GABA and baclofen on pyramidal cells in the developing rabbit hippocampus: an "in vitro" study. Brain research *469*, 171–184. 10.3389/neuro.02.013.2009.
43. Gahwiler, B.H., and Brown, D.A. (1985). GABAB-receptor-activated K+ current in voltage-clamped CA3 pyramidal cells in hippocampal cultures. Proceedings of the National Academy of Sciences *82*, 1558–1562. 10.1073/pnas.82.5.1558.
44. Menon-Johansson, A.S., Berrow, N., and Dolphin, A.C. (1993). G(o) transduces GABAB-receptor modulation of N-type calcium channels in cultured dorsal root ganglion neurons. Pflugers Archiv : European journal of physiology *425*, 335–343. 10.1007/BF00374184.

45. Ryglewski, S., Vonhoff, F., Scheckel, K., and Duch, C. (2017). Intra-neuronal Competition for Synaptic Partners Conserves the Amount of Dendritic Building Material. Neuron *93*, 632-645.e6. 10.1016/j.neuron.2016.12.043.
46. Cherubini, E., Gaiarsa, J.L., and Ben-Ari, Y. (1991). GABA: an excitatory transmitter in early postnatal life. Trends in neurosciences *14*, 515–519. 10.1016/0166-2236(91)90003-D.
47. Couve, A., Moss, S.J., and Pangalos, M.N. (2000). GABAB Receptors: A New Paradigm in G Protein Signaling. Molecular and Cellular Neuroscience *16*, 296–312. 10.1006/MCNE.2000.0908.
48. Bettler, B., Kaupmann, K., Mosbacher, J., and Gassmann, M. (2004). Molecular structure and physiological functions of GABAB receptors. Physiological Reviews *84*, 835–867. 10.1152/PHYSREV.00036.2003
49. Mezler, M., Müller, T., and Raming, K. (2001). Cloning and functional expression of GABAB receptors from Drosophila. European Journal of Neuroscience *13*, 477–486. 10.1046/j.1460-9568.2001.01410.x.
50. Venken, K.J.T., Schulze, K.L., Haelterman, N.A., Pan, H., He, Y., Evans-Holm, M., Carlson, J.W., Levis, R.W., Spradling, A.C., Hoskins, R.A., et al. (2011). MiMIC: a highly versatile transposon insertion resource for engineering Drosophila melanogaster genes. Nature methods *8*, 737–743. 10.1038/nmeth.1662.
51. Bellen, H.J., Campbell, M.E., Hoskins, R.A., Venken, K.J., Chen, K., Busby, T., Schulze, K.L., Booth, B.W., Evans-Holm, M., Spradling, A.C., et al. (2015). A library of MiMICs allows tagging of genes and reversible, spatial and temporal knockdown of proteins in Drosophila. eLife *4*, 1–28. 10.7554/elife.05338.
52. Wong, R.O.L., Meister, M., and Shatz, C.J. (1993). Transient period of correlated bursting activity during development of the mammalian retina. Neuron *11*, 923–938. 10.1016/0896-6273(93)90122-8.
53. Hensch, T.K. (2005). Critical period plasticity in local cortical circuits. Nature Reviews Neuroscience *6*, 877–888. 10.1038/nrn1787.
54. Hebb, D. (1949). The Organization of Behavior. A Neuropsychological Theory (Wiley).
55. Krämer, R., Rode, S., and Rumpf, S. (2019). Rab11 is required for neurite pruning and developmental membrane protein degradation in Drosophila sensory neurons. Developmental Biology. 10.1016/j.ydbio.2019.03.003.
56. Hensch, T.K., and Fagiolini, M. (2005). Excitatory–inhibitory balance and critical period plasticity in developing visual cortex. In Progress in Brain Research, pp. 115–124. 10.1016/S0079-6123(04)47009-5.
57. Ferster, D. (2004). NEUROSCIENCE: Blocking Plasticity in the Visual Cortex. Science *303*, 1619–1621. 10.1126/science.1096224.

III. Manuscript 2: Visualization of learning-induced synaptic plasticity in output neurons of the *Drosophila* mushroom body γ-lobe

Scientific Reports, June 2022

Authors: Clare E. Hancock[1], Vahid Rostami[2], El Yazid Rachad[1], Stephan H. Deimel[1], Martin P. Nawrot[2], and André Fiala[1,*].

[1] Molecular Neurobiology of Behavior, University of Göttingen, Göttingen, Lower Saxony, 37077, Germany

[2] Computational Systems Neuroscience, University of Cologne, Cologne, Northrhine-Westfalia, 50931, Germany

* Corresponding author: afiala@gwdg.de

scientific reports

Check for updates

OPEN

Visualization of learning-induced synaptic plasticity in output neurons of the *Drosophila* mushroom body γ-lobe

Clare E. Hancock[1], Vahid Rostami[2], El Yazid Rachad[1], Stephan H. Deimel[1], Martin P. Nawrot[2] & André Fiala[1]✉

By learning, through experience, which stimuli coincide with dangers, it is possible to predict outcomes and act pre-emptively to ensure survival. In insects, this process is localized to the mushroom body (MB), the circuitry of which facilitates the coincident detection of sensory stimuli and punishing or rewarding cues and, downstream, the execution of appropriate learned behaviors. Here, we focused our attention on the mushroom body output neurons (MBONs) of the γ-lobes that act as downstream synaptic partners of the MB γ-Kenyon cells (KCs) to ask how the output of the MB γ-lobe is shaped by olfactory associative conditioning, distinguishing this from non-associative stimulus exposure effects, and without the influence of downstream modulation. This was achieved by employing a subcellularly localized calcium sensor to specifically monitor activity at MBON postsynaptic sites. Therein, we identified a robust associative modulation within only one MBON postsynaptic compartment (MBON-γ1pedc > α/β), which displayed a suppressed postsynaptic response to an aversively paired odor. While this MBON did not undergo non-associative modulation, the reverse was true across the remainder of the γ-lobe, where general odor-evoked adaptation was observed, but no conditioned odor-specific modulation. In conclusion, associative synaptic plasticity underlying aversive olfactory learning is localized to one distinct synaptic γKC-to-γMBON connection.

Deciphering how and where in neuronal brain circuits learned information is acquired and stored, i.e., distributed across many neurons or localized to specific synapses, is a central topic in neuroscience. The fruit fly, *Drosophila melanogaster*, has proven to be a valuable model organism for testing hypotheses in this area of research. Indeed, despite their relatively modest brain size compared with mammals, fruit flies are able to perform a variety of complex learning tasks. This includes classical, Pavlovian-style conditioning[1] in which an odor (conditioned stimulus, CS) is associated with an appetitive or aversive unconditioned stimulus (US)[2,3]. Such associative learning forms the basis of the current study. In *Drosophila*, the mushroom bodies of the central brain have been identified as the site of the neural plasticity that facilitates this learning process[4,5]. More specifically, the γ-lobes of the mushroom bodies are required for the acquisition process and the formation of a short-term memory directly after training[6–8]. Consequently, not only have intrinsic mushroom body neurons (Kenyon cells, KCs) been identified as essential for associative learning, but so too have their extrinsic, axonal up- and downstream synaptic partners. Ensembles of KCs encode different odor stimuli selectively, as sparsely distributed neuronal activity[9–12]. Assigning behavior-instructive values to these odor representations through learning is mediated by axonal upstream US-encoding dopaminergic neurons (DANs) and downstream action-inducing mushroom body output neurons (MBONs)[13–16]. Whereas the former signal the presence of the US at the time of conditioning[15,16], the latter have been identified as key players in the guiding of approach towards or repulsion away from the learned odor[13]. With distinct populations of MBONs signalling positive or negative valence[13], current models postulate that the coincident activity of the odor-coding KCs and antagonistically acting (i.e. rewarding or punishing) US-coding DANs leads to a shift in the relative activation of the respective antagonistically acting MBONs[17,18]. This implies that the balanced activity of populations of MBONs ultimately represent the behavior-instructive 'readout' of the memory trace. Coupled with findings that learning leads to a synaptically localized

[1]Molecular Neurobiology of Behavior, Johann-Friedrich-Blumenbach-Institute of Zoology and Anthropology, University of Göttingen, Julia-Lermontowa-Weg 3, 37077 Göttingen, Germany. [2]Computational Systems Neuroscience, Institute of Zoology, University of Cologne, Zülpicherstraße 47b, 50674 Cologne, Germany. ✉email: afiala@biologie.uni-goettingen.de

modulation of KC activity[11], and that specifically the synaptic output from the KCs is required for short-term memory recall but not its acquisition[19,20], the KC-to-MBON presynapses have emerged as the site of plasticity mediating this type of learning[14,17,21,22]. However, determining which exact synapses become modified through the coincidence between the CS and US (i.e., the 'memory trace' in a strict sense) has been difficult because electrophysiological or functional imaging approaches typically monitor a neuron's activity in its entirety, including all excitatory, inhibitory, and modulatory inputs. In this study, we address this issue directly by targeting the genetically encoded calcium indicator GCaMP to the MBON postsynapse, via fusion to the postsynaptic density protein *d*Homer[23] (Fig. 1). Therefore, the relative changes in fluorescence that we quantify here are reflective of changes in calcium influx directly at the postsynapse, and less so of the integrated calcium signal across the larger dendritic arborizations that lacks the precision required to address our question. Using this more precise tool we were able to ask, for the first time at this level, whether associative plasticity is distributed across different KC-to-MBON synapses along the γ-KC axons or, alternatively, whether it is confined to particular axonal compartments. We found that differential aversive olfactory conditioning led to an odor-specific, associative modulation of a single MBON postsynapse innervating the γ1 compartment. All other MBONs (innervating the γ2-5 compartments) showed non-associative, adaptive plasticity. Therefore, we here confine the associative short-term memory trace to one synapse type along a distinct axonal compartment of the mushroom body. We test this both computationally using a machine learning approach as well as experimentally by identifying the potential downstream consequences of specific, localized plasticity within the MB circuit.

Methods

Fly strains. Flies were reared on standard cornmeal food medium at 25 °C and 60% relative humidity with a 12:12 h light/dark cycle. Split-gal4 driver lines used to drive expression in MBONs were obtained from the Bloomington Drosophila Stock Centre: MB112C (BDSC #68263, MBON-γ1pedc > α/β (one neuron per hemisphere)), MB077B (BDSC #68283, MBON-γ2α'2 (two neurons per hemisphere)), MB083C (BDSC #68287, MBON-γ3 and MBON-γ3β'1 (one neuron each per hemisphere)), MB298B (BDSC #68309, MBON-γ4 > γ1γ2 (one per hemisphere)), MB210B (BDSC #68272, MBON-γ5β'2a, MBON-β'2mp (one neuron each per hemisphere)). UAS-GCaMP3[24] and UAS-GCaMP6f[25] flies were also obtained from Bloomington Drosophila Stock Centre (BDSC #32236 and #52869, respectively). UAS-dHomerGCaMP3 flies were generated by Pech et al.[23].

For behavioral experiments using temperature-sensitive UAS-Shibirets to block synaptic output from MBONs, the same split-gal4 driver lines as above were crossed together with UAS-Shibirets or w1118 (both obtained from Bloomington Drosophila Stock Centre, BDSC #5811 and #5905, respectively). The resulting offspring were reared at 18 °C and 60% relative humidity.

Immunohistochemistry. Flies were cold anaesthetized on ice for 5 min before being moved to a dissection dish and fixed with insect pins. Brains were extracted in Ringer's solution (5 mM KCl, 130 nM NaCl, 2 mM $MgCl_2$, 2 mM $CaCl_2$, 5 mM Hepes, 36 mM sucrose, pH 7.3) by removing the head capsule and detaching the brain from the ventral nerve cord. Brains were then fixed in 4% paraformaldehyde at room temperature for 45 min, and then washed three times in PBS with 0.6% Triton-X before being incubated for 2 h at room temperature in blocking solution containing 2% bovine serum albumin. To amplify GCaMP signal, brains were incubated with anti-GFP primary antibody (rabbit anti-GFP, Invitrogen A6455) at a concentration of 1:2000. Additionally, an anti-discs large (DLG) primary antibody (mouse anti-DLG, Developmental Studies Hybridoma Bank 4F3) was used at a concentration of 1:200 to visualize brain structures. Brains were incubated in primary antibody solution for 1 day at 4 °C, and washed again three times in PBS with Triton-X before incubation in secondary antibody. Secondary antibodies anti-rabbit AlexaFluor488 and anti-mouse AlexaFluor633 were used, both at a concentration of 1:300, for 1 day at 4 °C. Brains were washed again three times in PBS with Triton-X, and then mounted in VectaShield for confocal scanning.

In vivo calcium imaging. Female flies aged between 3 and 8 days after eclosion were prepared and imaged as described by Hancock et al.[26]. Flies were cold anaesthetized on ice for no more than 5 min, placed in a custom-built chamber, and fixed in place using clear adhesive tape. A small window was cut in the tape and the head was glued in position using blue, light-curing glue. The head cuticle was then removed in a drop of Ringer's solution using a fine-bladed knife and forceps, and excess tissue was carefully removed to expose the brain for imaging. Prepared flies were then placed downstream of a custom-built odor delivery device under a Zeiss 7MP microscope equipped with a Ti–Sapphire laser (Coherent) and a Plan-Apochromat 20× water immersion objective (NA = 1). An excitation wavelength of 920 nm was used. Image acquisition was controlled using Zeiss Zen (2011 SP4) software. Images were captured at a framerate of 4 Hz and with a frame size of 512 × 512 pixels. Simultaneous odor delivery and image acquisition was controlled via a custom written LabView program (National Instruments). Three odors were used in all experiments, as follows: 4-methylcyclohexanol (MCH), 3-Octanol (3-Oct), and 1-Octen-3-ol (1-Oct), at concentrations of 1:750, 1:500, and 1:400, respectively, in mineral oil.

To induce and monitor the effects of aversive olfactory conditioning, a three-stage imaging protocol was used. First, flies were sequentially presented with the three odorants and changes in fluorescence were monitored. Second, the flies were exposed to one of three conditioning protocols. This second step immediately followed the first (i.e., within 60 s). Third, the flies were again presented with the three odorants and their responses were measured (see also the schematic illustration in Fig. 3). This final imaging step was carried out 3–4 min following the end of the respective conditioning protocol. The three conditioning protocols were as follows: classical aversive associative conditioning ('paired'), in which one odor (the CS+, either MCH or 3-Oct) was presented for 60 s while a pulsing electric shock was delivered to the legs and thorax of the fly (twelve 90 V shocks over 60 s, each lasting 1.25 s), followed by a 60 s break, and then a 60 s presentation of a second odor (the CS−, either

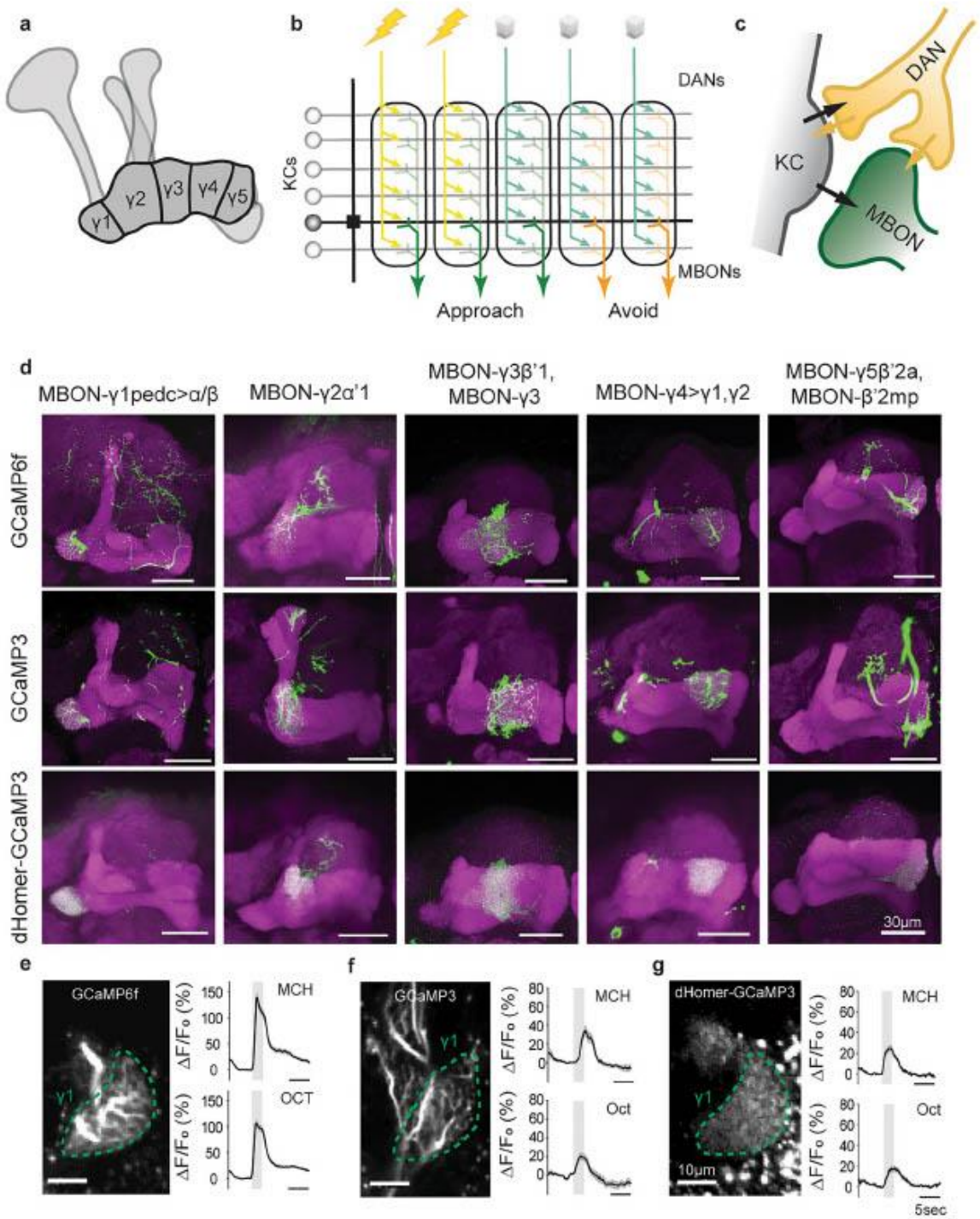

Figure 1. Visualization of postsynaptic calcium in the mushroom body output neurons. (a) Mushroom body structure and compartmentalization of the γ-lobe. (b) Functional compartmentalization of the γ-lobe, indicating the connectivity between odor-encoding Kenyon cells (KCs), punishminent- or reward-signaling dopaminergic neurons (DANs) and behavior-instructive mushroom body oitput neurons (MBONs). (c) Putative connectivity within the Kenyon cell (KC)-dopaminergic neuron (DAN)-mushroom body output neuron (MBON) microcircuit in the γ-lobe. (d) Representative confocal images showing the expression pattern of cytosolic sensors GCaMP6f and GCaMP3, and postsynaptically localized homer-GCaMP across the MBONs of the γ-lobe. (e–g) Examples of functional imaging recordings using cytosolic GCaMP6f and GCaMP3 and postsynaptically localized homer-GCaMP. Line graphs show mean $\Delta F/F_0$ values and SEM. Grey bars indicate the odor presentation period for the odorants 4-methylcyclohexanol (MCH) and 3-octanol (OCT). For GCaMP6f, n = 119 flies, for GCaMP3, n = 12 flies, for homer-GCaMP, n = 30 flies.

MCH or 3-Oct) without the electric shock; an 'odor only' control, in which the same procedure was presented with the omission of the electric shock; or a 'shock only' control, in which only the electric shock stimulus was delivered, with no odors. In the first and third stages (the 'pre-training' and 'post-training' imaging steps), all odor presentations had a duration of 2.5 s and were separated by an interval of approximately 40 s. For each MBON type and for each conditioning protocol, 10 individual flies were measured. In rare cases that strong, clear movement artefacts were identified in recordings, flies were removed from analysis.

Images were processed using ImageJ/Fiji (National Institutes of Health, NIH). Any small movements were corrected using the TurboReg plugin[27]. Regions of interest (ROIs) were drawn manually to encompass the entire dendritic compartment for each MBON. The fluorescent intensity throughout the recording period was then extracted from these ROIs and used to calculate the normalized relative change in fluorescence over time ($\Delta F/F_0$) for each recording. For all measurements, F_0 was calculated as the average fluorescence intensity over the 2 s preceding odor delivery, and ΔF was calculated by subtracting this value at each time point. In order to statistically compare responses and provide input for the population decoding analysis below, each response was quantified as the area under the curve (AUC) of each $\Delta F/F_0$ time series. The AUC was derived from the 5 s after odor onset. Due to large variability in odor responses between MCH and 3-Octanol, AUC values were normalized before being used in the population decoding analysis, below (within each experimental group, all responses to each odor were normalized to the mean pre-training response to that odor).

Population decoding. We devised a supervised machine learning approach with the goal to predict punishment (CS+) vs. no punishment (CS–) from the single trial neural population activity across all five distinct MBON types during the post-training phase of the aversive conditioning protocol (Fig. 5a). This amounts to a binary classification task based on a five-dimensional feature vector for which we devised a support vector machine (SVM).

Because functional imaging could only be performed in a single type of MBON in each individual animal, we had no access to the simultaneous population activity across the five MBON types in the same animal. Per individual and in the post-training phase we are left with two single-trial calcium traces obtained during a single CS+ and a single CS– presentation. For each of the five MBON types we have recordings from nine or ten animals. Thus, we have in total for each MBON type nine or ten per-animal samples (50 samples in total, Fig. 5a) where each consist of one CS+ and one CS– trial. To this end, we used the AUC as normalized time-integrated signal as described above.

For training and testing a single SVM model we proceeded as follows. We randomly drew one sample from each MBON type to define the test set (Fig. 5a). This defines a non-simultaneously recorded pseudo population[28] of all five MBONs consisting of the population responses to CS+ and CS– (i.e., two vectors that contain five AUC values). The remaining 45 samples (nine per MBON type) represent the training set. For training, we performed 1000 repeated drawings with replacement to obtain a new training sample, i.e. a pseudo population across the five MBON types as illustrated in Fig. 5a. Each sample provided a single feature vector for the class CS+ and a single feature vector for the class CS–. After training a single SVM model with the 2000 feature vectors we tested the model with the two feature vectors of the test set. We denote a correct classification with 1 and an incorrect classification with 0. The possible outcomes for the single model are thus [1, 1], [1, 0], [0, 1] or [0, 0], from which we can compute the single model accuracy as 0%, 50% or 100% with a random chance level of 50%. We repeated the complete procedure for 100 independent models, each defined by the random combination of five samples that constructed the pseudo population of the test set. Across 100 models we then computed the average accuracy in percentage of correct binary classification.

We performed three controls. For each we repeated the same approach as outlined above to obtain mean accuracy and standard error of the mean (Fig. 5b). We first classified single-trial odor responses in the pre-training phase (Fig. 5b). Each single odor response to either MCH or 3-OCT was labeled as CS+ or CS– according to its assigned label during the later training phase. The expected classification accuracy is thus at chance level (50%) before training. We next tested classification during the post-training phase after 'odor only' presentation (omission of shock) and during the post-training phase after 'shock only' presentation (omission of odor). For both control conditions we created two classes *A* and *B* through random assignment of odors to those labels. We again expect an average accuracy at chance level (50%).

To assess the importance of each individual MBON type for the classification, we repeated the classification approach as explained above by excluding each MBON type one by one from the feature space combination of the four remaining MBON types.

All analysis has been carried out with Python and the implementation of SVM in the Scikit-learn package[29].

Classical aversive associative conditioning. To examine the behavioral effects of blocking synaptic output from MBONs during aversive associative conditioning, flies were trained and tested in a custom-built conditioning apparatus. All experiments were carried out at a humidity of 65–85% and either at permissive temperature (22–25 °C) or restrictive temperature (30–32 °C) for control experiments and experiments in which synaptic output was blocked by *Shibire*[ts], respectively.

For the training phase, approximately 30 flies aged between 3 and 7 days were placed into tubes lined with copper wire and connected to an air flow. Flies were conditioned according to the same procedure as the "paired" group described above. Briefly, flies were first presented with an odor (that becomes the CS+ odor) together with a pulsing 90 V electric shock for 60 s. This was followed by a 60 s break before a second odor was presented alone for 60 s (becoming the CS– odor). As in previous experiments, flies were trained reciprocally using the odorants 4-methylcyclohexanol and 3-Octanol. Timely delivery of electric shocks and odor stimuli throughout was controlled by custom-written software.

For the testing phase, flies were transferred from the training tubes to the testing arena. This arena comprised multiple lanes, with each being loaded with one of the groups of approximately 30 flies from the training tubes. Flies were initially held in a central carrier before being released into the lanes, into which the CS+ and CS− odors were presented from opposite sides. The flies were allowed two minutes to distribute between the two sides of the arena before a picture was captured using a camera mounted above the arena that would be used to quantify the distribution of the flies between CS+ and CS−.

To analyze whether flies exhibit a learned avoidance of the punishment-coupled CS+ odor, the number of flies on each side of each lane was counted. Preference indices were calculated independently for reciprocally trained groups (by subtraction of flies that chose CS− from those that chose CS+, divided by total number of flies), before being averaged to generate a learning index. Raw data were processed with OriginPro.

Statistical analyses. Odor-induced calcium dynamics throughout are presented as line graphs, with lines representing mean $\Delta F/F_0$ values over time, and shaded areas representing the standard error of the mean (SEM). To quantify and compare responses, the integrated AUC for each $\Delta F/F_0$ time series was calculated over the 5 s after odor onset. Tests for significant changes in pre-to-post training AUC were carried out using Wilcoxon signed rank tests.

For behavioral experiments (Fig. 6), tests for statistical differences between groups was performed using a one-way ANOVA with a Tukey post-hoc test. A Bonferroni-corrected two-tailed one-sample t-test was also performed on each group to test for differences from 0.

Results

Visualization of postsynaptic calcium in mushroom body output neurons. Acquisition and formation of an associative short-term memory is localized to the KC presynapses of the γ-lobe of the MB[6–8]. Thus, when looking for a readout of the synaptic plasticity underlying this form of memory, we focused on the population of compartment-specific MBONs that lie directly downstream of the γ-type KCs. These neurons each receive synaptic input from KCs in their respective compartment, the weight of which is modulated by input from DANs and comprises the canonical site of learning-induced plasticity within this circuit (Fig. 1a–c)[14,17,21]. In addition, MBONs receive direct modulatory input from DANs as well (Fig. 1c). Therefore, we utilized a postsynaptically localized tool, *d*Homer-fused GCaMP3[23], that allowed for the monitoring of odor-evoked activity precisely at the site of MBON input. To first verify the localization of *d*Homer-GCaMP to the postsynaptic compartments of the MBONs, we removed the brains of flies expressing this construct in individual MBONs of the mushroom body γ-lobe and subjected them to immunohistochemistry and confocal microscopy. When compared to the most often used cytosolic GCaMP6f and the original cytosolic form of GCaMP3, *d*Homer-GCaMP results in a spatially restricted, overall more punctuated fluorescence that is localized primarily in the dendritic compartments of neurons (Fig. 1d). This difference was also observed when neurons were visualized in vivo using two-photon microscopy (Fig. 1e,f), with the large neurites that predominate the GCaMP6f and GCaMP3 fluorescence being absent in *d*Homer-GCaMP-expressing flies (the γ1 compartment innervation by MBON-γ1pedc > α/β is shown here as an example). To further verify that the latter can also be used to detect postsynaptic odor-evoked activity in MBONs, flies were presented with MCH and 3-Oct and changes in fluorescence were quantified (Fig. 1e–g). Indeed, as has been previously documented[25], odor responses monitored using both cytosolic GCaMP3 and *d*Homer-GCaMP were lower in magnitude observed using GCaMP6f., although both give rise to clear robust odor-evoked changes in fluorescence that can reliably be detected and analyzed. With this, we validate *d*Homer-GCaMP as a viable tool for studying localized odor representations at the level of the MBON postsynapse.

γ-Lobe MBONs receive heterogeneous odor-evoked inputs. Congruent with their receipt of inputs from large populations of KCs, previous studies have shown that MBONs innervating the MB lobes have broad odor response profiles[30]. In this vein, we first sought to analyze the postsynaptic responsiveness of our γ-MBONs of interest to the experimental odors, MCH and 3-Oct. To do so, we carried out in vivo functional imaging of individual female flies expressing *d*Homer-GCaMP in each of the MBONs and quantified the odor-evoked changes in postsynaptic calcium (Fig. 2; individual and mean response traces shown in Supplementary Fig. 1).

This analysis revealed that, indeed, in the case of the MBONs innervating the γ1, γ3, and γ4 compartments, robust responses to both odors were observable in the majority of flies measured (Fig. 2a,c,d). Surprisingly, the γ2-innervating MBON (γ2α′1) only responded to 3-Oct in a small number of flies, in contrast to MCH (Fig. 2b). It has previously been reported that the dendritic arbors of MBONs in the γ5 compartment (MBON-γ5β′2a, MBON-β′2mp) show little or no response to olfactory stimuli[31]. We also observed this result, with responses being detected in only ~ 17% of flies measured (Fig. 2e, Supplementary Fig. 1). Differences in the magnitude of responses are also notable, with those measured at the MBON-γ3/MBON-γ3β′1 postsynapse sometimes being 4–5 × greater than those measured in, for example, MBON-γ1pedc > α/β. These differences in magnitude were also be observed between odors within animals, with MCH eliciting stronger responses than 3-Oct in most cases. These findings indicate that, first, olfactory responses between the γ-lobe MBONs and, thus, the efficiency of KC-to-MBON connections in different γ-lobe compartments, are not homogenous. Second, within MBON types, responses to different odors are not homogenous across individuals. Therefore, we confirm that the neurons in this MBON population possess distinct and individualized odor response properties that could indeed influence and/or result from individual experience such as olfactory learning, as already reported using a cytosolic calcium sensor[30].

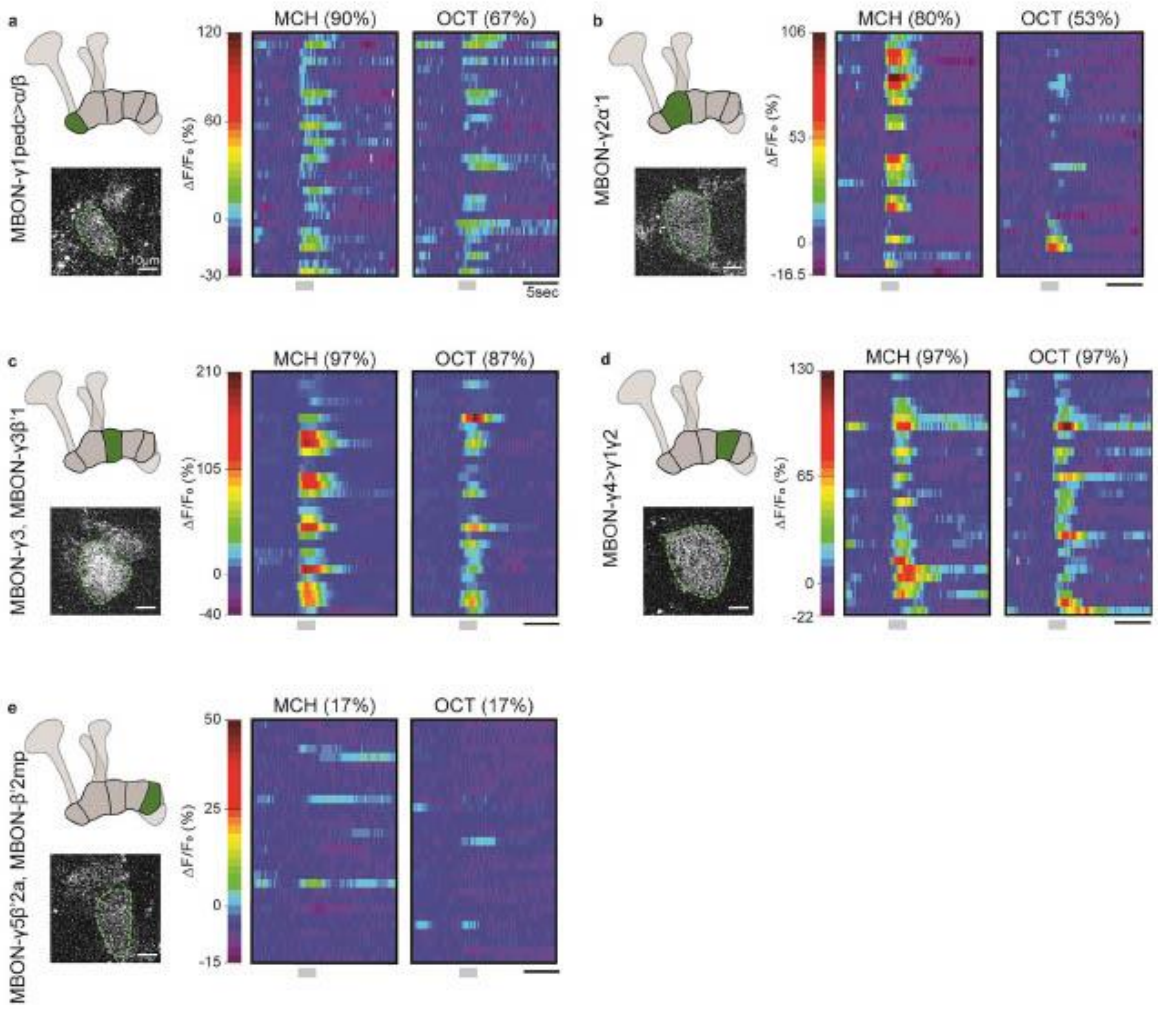

Figure 2. Odor-evoked responses at the MBON postsynapse. Heatmaps show false-color coded $\Delta F/F_0$ values over time, measured in each of the γ-lobe MBONs ((**a**) MBON-γ1pedc > α/β; (**b**) MBON-γ2α'1; (**c**) MBON-γ3 and MBON-γ3β'1; (**d**) MBON-γ4> γ1γ2; (**e**) MBON-γ5β'2a and MBON-β'2mp). Each row corresponds to a recording of an individual neuron in an individual fly in response to a single odor presentation. Values above heatmaps show the percentage of flies that showed a response to that odor in each MBON. Grey bars indicate the odor delivery period. For (**a**, **c**–**e**), n = 29; for (**b**), n = 30. Schematic diagrams and single frame in vivo functional imaging examples on the left show the dendritic region of each MBON that was imaged. The green dotted line shows the region that was quantified.

Associative conditioning gives rise to compartment-specific plasticity. To investigate if and how these odor representations are influenced by associative learning, we subjected the same flies expressing *d*Homer-GCaMP in the γ-lobe MBONs to an aversive conditioning protocol under the microscope and monitored odor-evoked postsynaptic calcium. Flies were placed in a custom-built imaging chamber in which they could be exposed to both odor and electric shock stimuli during functional imaging, allowing for the visualization of odor-evoked postsynaptic activity before and after an aversive training in which flies learned to associate a given odor with punishment[26].

Based on the hypothesis that the combinatorial activity of the γ-lobe MBONs holds behavior-instructive information about learned odor valence, we first hypothesized that aversive associative conditioning would lead to bidirectional modulation of MBONs such that approach-mediating MBONs would be suppressed in response to the aversively paired odor and avoidance-mediating MBONs would be potentiated. Indeed, such effects have been reported when measuring with cytosolic calcium indicators or using electrophysiology[22,31–34]. In the following sections, however, we demonstrate that modulation directly at the MBON postsynapse is a highly specialized occurrence, localized to a singular compartment of the γ-lobe.

Pairing of an odor with electric shock led to a significant reduction in the postsynaptic calcium response elicited by the trained odor (CS+) in MBON-γ1pedc>α/β (Wilcoxon signed rank test, Z = 2.01399, p = 0.03906) (Fig. 3c, left). This is consistent with the identification of this neuron in the signaling of positive stimulus valence[13]. Neither the CS– odor (that was explicitly not paired with electric shock) nor the control odor (1-Oct) elicited statistically significant changes in response after conditioning (CS–: Wilcoxon signed rank test, Z = 0, p = 1; control odor: Wilcoxon signed rank test, Z = 0.82929, p = 0.42578) (Fig. 3c, center and right). This was also the case in the control groups for odor presentation, but without any electric shock ('CS only' control; Fig. 3d). This finding demonstrates association-specific modulation of the odor-driven inputs to MBON-γ1pedc>α/β, dependent on CS-US contiguity. Interestingly, the stimulation with electric shock, but without any odor presentation ('US only control'; Fig. 3e) induced a slight, but not statistically significant increase in MBON-γ1pedc>α/β response at the given sample size. However, when data for both odorants that were also used for associative training, MCH and 3-Oct, were pooled, a statistically significant increase was detected (Supplementary Fig. 3) (Wilcoxon signed rank test, Z = – 2.55729; p = 0.00831). This illustrates that the postsynaptic calcium response in this particular MBON can be bidirectionally modulated; it decreases in response to an odor associated with punishment, and it increases in response to an odor if the punishment does not occur in temporal coincidence with it. Moreover, the enhancement of odor response in this approach-mediating MBON may form part of the physiological basis for the previously described reduction in odor avoidance after electric shock punishment[35].

Conversely, no association-induced changes were observable in MBONs of the remaining γ-lobe compartments (Fig. 4). Rather, a strong decrease in odor-evoked calcium activity occurred between the pre- and post-training odor response measurements in MBONs innervating the γ3 and γ4 compartments, but both to the CS+ and CS– odor (Fig. 4a,c,e,g). The γ5-innervating MBONs represent an exception in that, in most cases, they showed no responses to odors throughout experiments (Fig. 4g). In MBONs innervating the γ2 compartment, this effect was not statistically significant, perhaps because of relatively weak odor-evoked calcium activity before training in this group of animals (Fig. 4a). The relatively high variability in odor-evoked calcium activity across individuals is in accordance with previous reports that suggest highly individualized, perhaps experience-dependent responsiveness in MBONs innervating the lobes[30]. Flies that received the 'odor only' control procedure also displayed strong reductions in responses (Fig. 4b,d,f). Strikingly, the previously high amplitude responses in the γ3-innverating MBON are almost entirely lost through either of these protocols (Fig. 4c,d). We also observed that, although CS+ and CS– -evoked responses underwent similar degrees of adaptation, the γ4-innervating MBON showed statistically weaker depression in response to the "mock CS+" odor in the odor only control condition (Fig. 4e,f). In most cases, this adaptation is not odor-identity specific and is generalized to the third odor, 1-Oct, that is not presented during training (Supplementary Fig. 2). We conclude that this adaptation is likely caused by the prolonged odor exposure that occurs during both the conditioned (paired) and the 'odor only' control protocols, as adaptation is much weaker in flies that received the 'shock only' control procedure (Supplementary Fig. 3).

These results go beyond confirmation that the MBONs of the γ-lobe show differential naïve odor responses[30], and that the manner in which those odor responses are modulated by dopamine is diverse across different MBONs[36]. Our data indicate that experience-dependent changes in odor-evoked, postsynaptic calcium activity occur in γ1–γ4 MBONs. However, a differential modulation resulting from CS-US coincidence is restricted to the γ1 compartment. Therefore, the synaptic DAN-KC-MBON microcircuitry that mediates the CS-US association process during aversive olfactory conditioning (i.e., the memory trace in a strict sense) is confined to a single γ-lobe compartment and not distributed across different compartments.

MBON responses are indicative of whether an odor has been aversively trained or not. Given this finding, we sought to test in an unbiased manner whether these observed changes in postsynaptic calcium responses are actually indicative of whether the odor-evoked calcium transients have been aversively trained or not. To do so, we applied a machine learning approach, and used pseudo-populations of γ1–γ5 MBON responses to train a classifier. Over multiple training sessions, the classifier was provided with the pre- or post-training odor responses of such pseudo populations of γ-lobe MBONs and was then asked to predict whether the response was from one of two conditions, CS+ or CS– (Fig. 5a). On average, the conditioned odor (CS+) was distinguished with significantly greater accuracy than any other condition (one sample Wilcoxon sign rank test against level of chance (50%), Z = 16.78943, p = 0) (Fig. 5b). Indeed, all other experimental conditions (pre-training, 'odor only,' or 'shock only' conditions), resulted in an approximate 50% success rate (one sample Wilcoxon sign rank test against level of chance (50%), pre-training: Z = 1.7353, p = 0.08269, 'odor only' control: Z = 0.19191, p = 0.84782, 'shock only' control: Z = 1.15577, p = 0.24778) (Fig. 5b), indicating that the odor representations that we observed at the MBON postsynapse are in fact indicators of whether the odor has been trained as aversive or not. We then compared the accuracy with which the classifier could distinguish between CS– and CS+ odors after training in a situation in which one of the five γ-lobe MBON types was removed from the training data sets. Only removing the MBON innervating the γ1 compartment decreased the accuracy of differentiating CS+ from CS– to the level of chance (Fig. 5c) (one sample Wilcoxon signed rank test against level of chance (50%), Z = 1.77029, p = 0.07668). Excluding any other MBON type did not significantly affect the accuracy of discriminability (Fig. 5c) (one sample Wilcoxon signed rank test against level of chance (50%), γ2 excluded: Z = 16.39812, p = 0, γ3 excluded: Z = 9.87016, p = 0, γ4 excluded: Z = 10.72866, p = 0, γ5 excluded: Z = 13.54734, p = 0), in line with our previously drawn conclusion that γ2–γ5 MBON odor responses are not indicative of associative conditioning induced plasticity (despite the slight differentiation in the γ4 MBON between real and "mock" CS+, Fig. 4e,f). This corroborates the finding of the γ1 compartment as the primary site of differential synaptic plasticity underlying aversive discrimination learning.

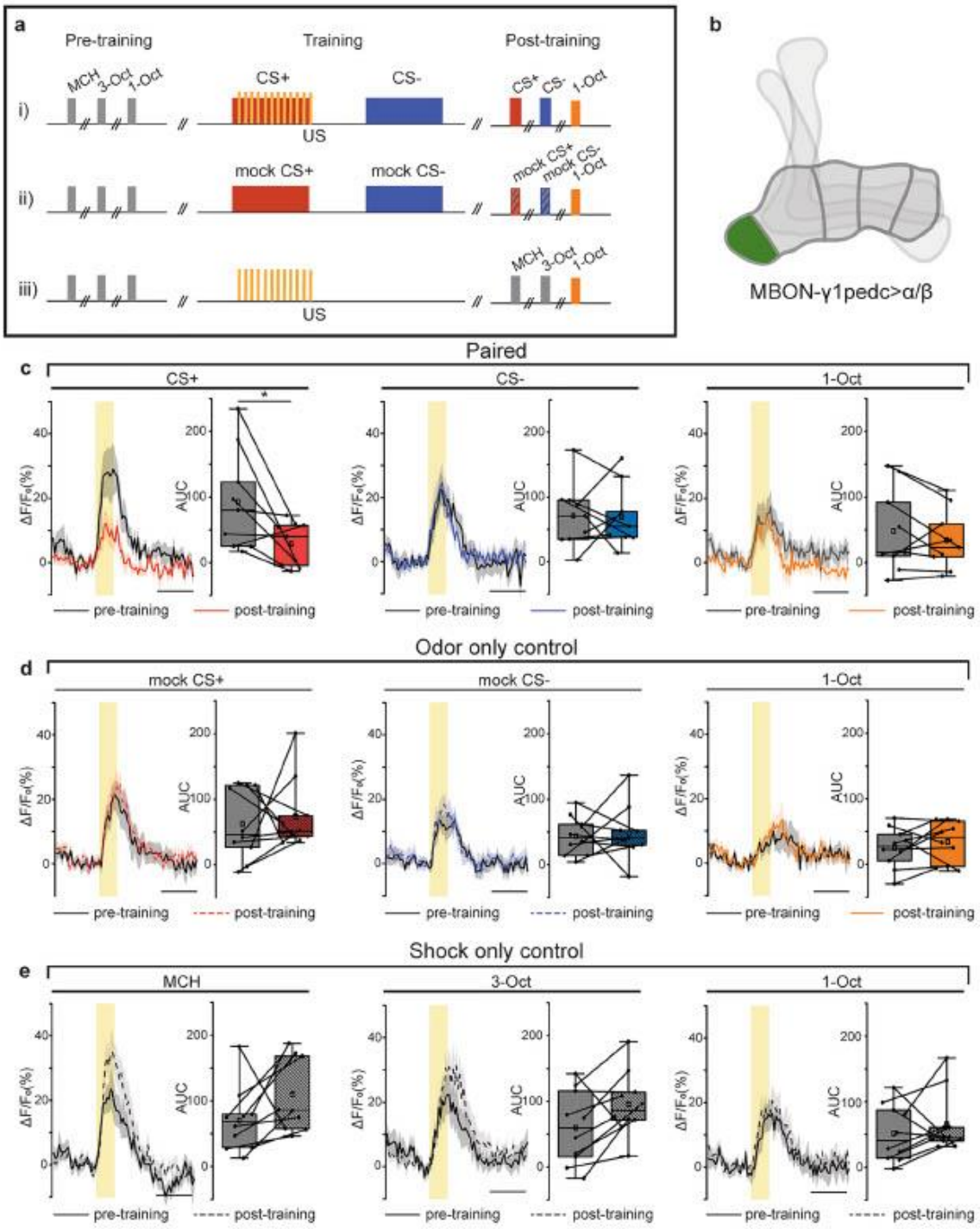

Synaptic output from MBON-γ1pedc>α/β and MBON-γ5β′2/MBON-β′2mp instruct behavioral distinction of punished odors. We have provided evidence so far that aversive associative conditioning leads to localized, specific plasticity within a single postsynaptic compartment of the γ-lobe and that this provides a sufficient basis for the distinction of an odor that is predictive of punishment from one that is not. Unclear thus far, however, is if and how this highly localized plasticity relates to behavioral action. Based on recent evidence[13,32,33] we hypothesize that the CS+-specific reduction in odor-evoked input to the γ1 MBON may

◂**Figure 3.** Induction and visualization of learning-induced plasticity at the MBON-γ1pedc>α/β postsynapse. (**a**) Imaging procedures used to probe the effects of associative conditioning on MBON odor responses. Flies were exposed to one of three protocols: (1) aversive associative conditioning; (2) 'odor only' control; or (3) 'shock only' control. Before and after the training procedure, three odors were presented and MBON postsynaptic calcium was monitored using homer-GCaMP. (**b**) Schematic highlighting the γ1 compartment in which MBON-γ1pedc>α/β postsynaptic sites were imaged. (**c–e**) MBON-γ1pedc>α/β odor responses measured before (pre-training) and after (post-training) one of the three training protocols. Lines indicate means, and shaded areas represent SEMs. The black line in each case represents the pre-training response. Post-training responses are shown in color, dependent on condition. The yellow box indicates the period of odor presentation. The area under the curve (AUC) was calculated over the 5 s after odor onset, and pre- to post-training differences were tested using Wilcoxon signed rank tests (*$p < 0.05$). Boxes represent 25% and 75% quartiles, squares indicate means, and horizontal lines indicate medians. Whiskers show minimum and maximum values. For the paired group (**c**), n = 9 flies. For both control groups (**d**, **e**), n = 10 flies.

lead to a disinhibition of its downstream partners that also instruct behavior, meaning that although the plasticity underlying learned avoidance is restricted to a single compartment, its downstream effects are more broad.

To assess this theory, we blocked the synaptic output from each of the γ-lobe MBONs using temperature-sensitive shibire^{ts} and tested the flies' ability to distinguish between an odor that was aversively conditioned (paired with electric shock punishment, CS+ odor) and one that was not (CS– odor)(Fig. 6). Blockage of synaptic output from the γ1 MBON led to a complete absence of conditioned odor preference (Fig. 6b; Bonferroni corrected two-tailed one-sample t-test against test mean of 0, $p = 0.3318$ [Bonferroni adjusted $\alpha = 0.0083$). This was not the case for the respective genetic controls or flies trained and tested at permissive temperature. This corroborates previous studies that showed the same effect[13,32], as well as supporting the indispensability of the γ1 MBON in odor-electric shock conditioning that we concluded from our functional imaging data.

Further mirroring our previous findings, we observed no effect on learning performance when blocking synaptic output from MBONs innervating the γ2, γ3, or γ4 compartments (Fig. 6c–e). The implications of these data are twofold: first, the negligible role of these MBONs in the distinction between odors that are and are not aversively conditioned is consistent between physiological recordings and behavioral observations. Second, associative conditioning-induced modulation of the γ2, γ3, and γ4-innverating MBONs downstream of the KC-to-MBON synapse (e.g., via MBON-to-MBON or DAN-to-MBON connections) is also unlikely. We therefore conclude that, while we do not exclude their importance in other experience-dependent or associative learning tasks, these MBON types play a negligible role in the form of associative conditioning investigated here.

Crucially, we did find that blocking synaptic output from the most distal MBONs of the γ-lobe (innervating γ5 and β′2) caused an inability of flies to distinguish between CS+ and CS– odors when tested for preference (Fig. 6f; two-tailed one-sample t-test against 0, $p = 0.031$ [Bonferroni adjusted $\alpha = 0.0125$]). This was not the case for the respective genetic controls or flies trained and tested at permissive temperature. This means that, despite there being no observed plasticity in odor-evoked activity at the postsynaptic sites of these MBONs, they do play a vital role behaviorally. As described above, we suggest that the positioning of these neurons downstream of the γ1 MBON is crucial to this role. The MBONs innervating the γ1 compartment and γ5/β′2 have been shown to convey opposite valences (positive and negative, respectively)[13], and thus present a logical circuit-level mechanism for the balancing between promotion of approach and promotion of avoidance in response to a conditioned odor. The balance point depends on the strength of KC-to-MBON input in the γ1 compartment and subsequent inhibition exerted by the γ1-innervating MBON on the γ5-innervating MBONs, with both factors determined by the relative (plastic) odor-evoked activity at the γ1 postsynapse.

Discussion

Determining the substrate mediating the acquisition and storage of learned information through the properties of single neurons, their synapses, and the neural circuits the neurons are part of is a key challenge in neuroscience. Here, we do not define the term 'memory trace' as all potential physiological changes within neurons, synapses, and the entire neuronal circuits that accompany or result from the learning process. Considering that plastic changes in synaptic transmission are the principal substrate underlying learning and memory formation[37–39], we define a memory trace as those synaptic changes that are required and sufficient to induce the learned response[38,40]. In the case of classical conditioning, these synaptic changes must be the site of CS-US integration. Decades of research have established that (a) axonal KC presynapses are required for associative odor learning and short-term memory formation[19,20,40], and (b) γ-lobe KCs are required in particular[6–8]. The criterion of sufficiency is difficult to address because the stochastic and sparsely distributed nature of odor representations across all KCs precludes any artificial activation of a selected KC and subsequent test of whether an odor stimulus has been learned. However, artificial activation of defined KCs in coincidence with electric shocks has been used to show that a particular KC activity pattern can be trained, and its subsequent activation causes an aversive behavioral response[41]. In addition, plasticity in γ-lobe KCs resulting from associative learning has been clearly demonstrated[11,42].

However, genetic manipulation of neurons (e.g., using transgenes to depolarize or hyperpolarize neuronal membranes or to block synaptic transmission) inevitably affects entire cells; the question of which dendritic or axonal part of a neuron is required or sufficient for mediating learning remains unanswered using such approaches in isolation. This is of importance because the functional compartmentalization of KC axons, with each compartment being innervated by distinct subsets of DANs mediating reward or punishment, and MBONs inducing different behavioral actions, suggests that entire neurons are not the functional units representing the

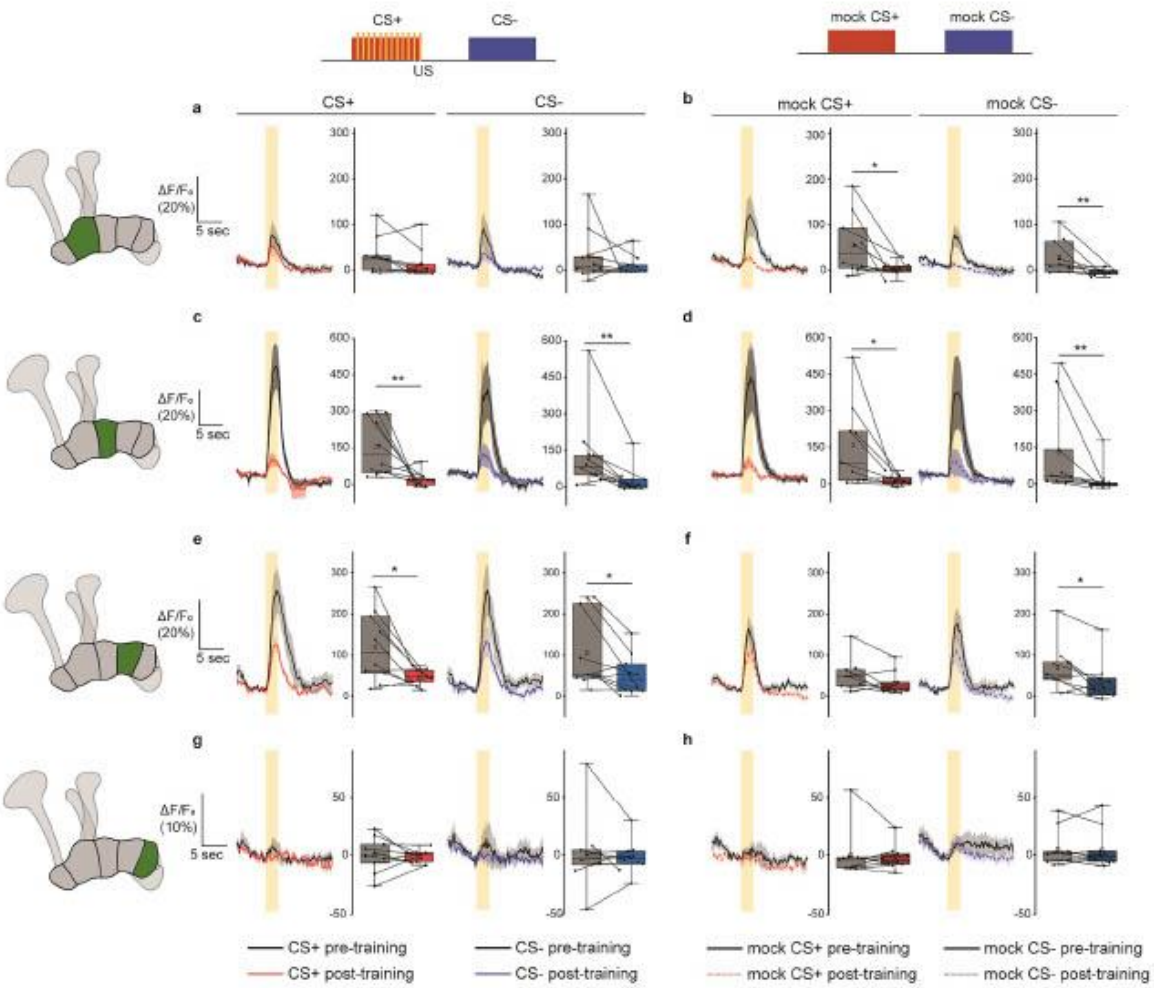

Figure 4. Non-associative plasticity at MBON postsynapses in γ2, 3, and 4 compartments. Odor responses before and after either aversive associative conditioning (**a**, **c**, **e**, **g**) or a control protocol (**b**, **d**, **f**, **h**) in which the unconditioned stimulus was omitted (training protocols, top). In each case, pre-training responses are depicted in black (line graphs) or gray (box plots), and post-training responses are shown in color, dependent on condition. The yellow bar represents the odor presentation period. The area under the curve (AUC) was calculated over the 5 s following odor onset. Boxes represent 25% and 75% quartiles, squares indicate means, and horizontal lines indicate medians. Whiskers show minimum and maximum values. Pre- to post-training effects were tested using Wilcoxon signed rank tests (*$p < 0.05$; **$p < 0.01$). For (**a–c**, **e**, **g**, **h**), n = 10 flies; for (**d**) and (**f**), n = 9 flies.

substrate of memory traces (such as 'engram cells'). Rather, subcellular partitions of neurons, in this case partitions of axons spanning a compartment, represent independently modulated functional units[11].

Previous functional imaging and electrophysiological studies recording from neurons in their entirety (i.e., measurements at the soma level), have also reported bidirectional modulation of MBONs as a result of associative olfactory conditioning[22,31,32,34]. We conclude from our data that plasticity in these neurons arises downstream of the KC-to-MBON synapse via previously identified feedforward and feedback loops that exist in the MB circuit. For example, it was shown that plasticity in the specific KC > MBON-γ1pedc > α/β connection does not remain confined to the γ1 compartment, but causes subsequent downstream changes in MBONβ′2mp and MBONγ5β′2a as well via a feedforward inhibition loop[33]. Our behavioral data support the presence and potential significance of such a circuit motif (Fig. 6). As a consequence, flies in which output from either the γ1 or γ5 MBONs is blocked not only during learning, but importantly in the choice situation during retrieval, are unable to correctly prefer the CS− odor over the shock-associated CS+ odor, which confirms previous reports[31]. Note that in Fig. 3 we show that association-driven suppression of γ1 MBON odor responses is specific to only the CS+ and not the CS− odor, while in Fig. 6 MBON output is blocked in the presence of both thus disrupting their distinction in the choice assay. It is of course important to note here that although the vast majority of inputs to MBONs arise from KCs,

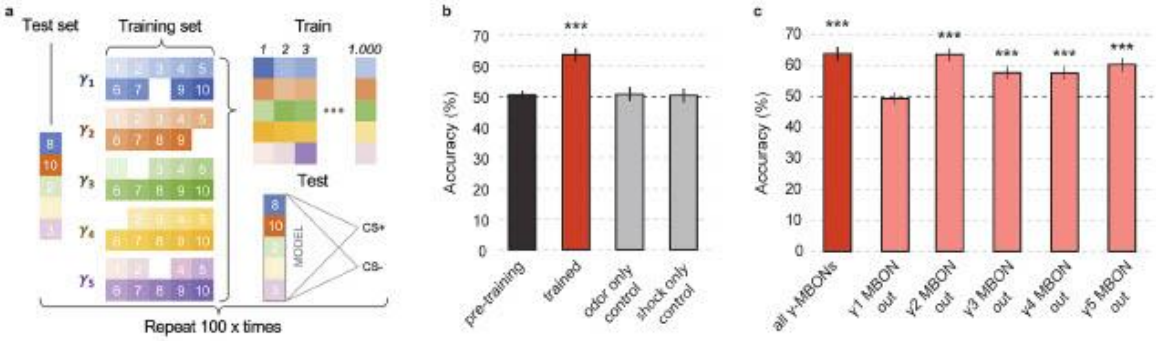

Figure 5. A supervised classifier can distinguish a conditioned from unconditioned odor when γ1-MBON is taken into account. (**a**) Each MBON type (γ1–γ5) was imaged in a group of animals. From this data set we constructed a pseudo-population of non-simultaneously imaged neurons by randomly drawing one individual animal per MBON type. This defined the test set. All remaining sample established the training set. During training, repeated random drawing with replacement allowed to generate independent training samples. Each sample consisted of two single population responses to the presentation of the CS+ odor and to the CS– odor, respectively. After training the SVM model with 1000 such random samples the model was subjected to the previously unseen test set, which again consisted of a single CS+ and a single CS– population response vector. We trained 100 independent models and computed the average accuracy across 100 × 2 classification results. (**b**) Accuracy before and after classical conditioning ('pretraining' and 'trained') or randomly assigned designations of odor A and B to be differentiated in control conditions ('odor only' control and 'shock only' control). (**c**) Accuracy after classical conditioning if all γ-lobe MBONs are included, or if one MBON type is removed from the training and test data sets. Bars represent means ± SEM across 100 models. Significant difference from level of chance (50%) determined by one sample Wilcoxon signed rank test (***$p < 0.0001$).

MBONs receive inputs at various dendritic regions from diverse cell types (including DANs and other MBONs). Our approach to confine the measurement to MBON postsynapses might therefore contribute to distinguishing the primary effects of the CS-US association (i.e., the 'memory trace') and subsequent downstream effects that result from it[43]. Indeed, we showcase here the importance of this more precise approach, demonstrating that by looking only at whole cell activity or at crude behavioral output one is at risk of overlooking the true locale and mechanism of the underlying physiology. Importantly, we also used odor stimuli and electric shocks as unconditioned stimuli, as they are typically applied in behavioral learning experiments; this approach is in contrast to optogenetic stimulation of selected DANs[22,36] that may or may not reflect real sensory stimulation.

Our results directly support recent computational model studies. A circuit model by Springer and Nawrot[18] assumed downregulation of the synaptic input from KCs to MBON-γ1pedc > α/β through a plasticity mechanism that requires pairing of the CS+ odor stimulus with neuromodulatory input from the aversive US-signaling PPL1-γ1pedc DAN. This simulation showed a significant reduction in MBON-γ1pedc > α/β synaptic input and avoidance behavior after a single pairing, as confirmed in our experiments (Fig. 3). In this model, feedforward inhibition from MBON-γ1pedc > α/β to MBON-γ5β′2a and feedback excitation to dopaminergic neurons establishes a prediction-error mechanism that supports the saturation of the behavioral learning curve and enables extinction learning. Similarly, a recent model by Bennet et al.[44] assumed the explicit downregulation of the synaptic weight between KCs and an unspecified approach-mediating MBON to implement aversive conditioning and reward prediction through positive MBON-DAN feedback. In fact, recent advances in connectomics have revealed the presence of numerous, multilayered feedback motifs in and around the MB that are implicated in learning and memory formation (see[45–47]). Of course, our data do not rule out the possibility for associative learning-induced modulation of other MBONs in other forms of learning, e.g., over longer time periods, conditioning of different valences such as reward, or context. For example, it is well-established that long-term memory formation requires KCs of the vertical α/α′-lobes[48]. It must be pointed out that our data refer only to the acquisition process and short-term memory formation of aversive olfactory learning.

The broad and generalized suppression of odor responses in all more distal MBON postsynapses indicates that they, unlike MBON-γ1pedc > α/β, possess properties more tuned to signaling non-associative events, such as adaptation resulting from prolonged odor stimulation. This distinction is apparent when comparing postsynaptic responses in flies that received only prolonged odor presentation and those that received that prolonged stimulation together with punishment, with only the γ1-innervating MBON showing a specific depression in response to the punished odor whereas a generalized adaption predominated all other MBON post-training responses. Two key observations indicate that the non-associative changes manifested principally as strong reductions in odor-evoked postsynaptic calcium responses in post-training recordings in the majority of MBONs (namely: MBON-γ2α′1, MBON-γ3 and MBON-γ3β′1, and MBON-γ4 > γ1γ2; see Fig. 4) are likely demonstrative of an intrinsic adaptive property of these MBONs, rather than merely sensory adaptation. First, the observed adaptations are not odor specific, but instead are generalized across all odors (Fig. 4, Supplementary Fig. 2). Second, adaptation in the upstream olfactory pathway would theoretically lead to adapation across all MBONs, which we do not observe (MBON-γ1pedc > α/β displayed no adaptation in any context; Fig. 3). This further highlights

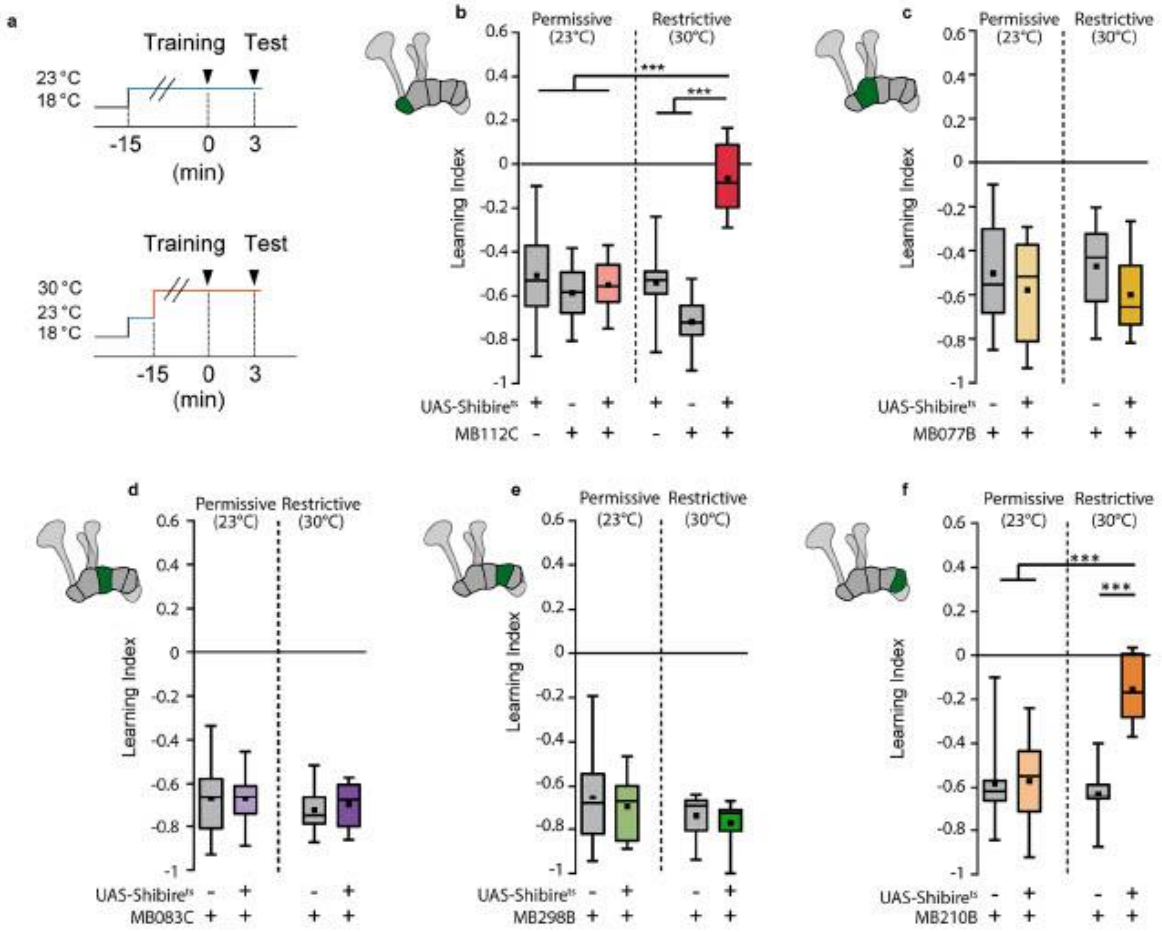

Figure 6. MBONs innervating the γ1 and γ5 mushroom body compartments are required for conditioned odor avoidance. (**a**) Training and test procedures. Training refers to aversive associative conditioning procedure schematized in Fig. 3. Temperature-sensitive shibire expression was used to block synaptic vesicle exocytosis. Upper panel shows the control condition in which training and test were carried out at permissive temperature. Lower panel shows experimental procedure in which training and test were carried out at restrictive temperature. (**b–f**) Box plots showing learning indices when blocking synaptic output from different MBON types ((**b**) MBON-γ1pedc > α/β; (**c**) MBON-γ2α′2; (**d**) MBON-γ3, MBON-γ3β′1; (**e**) MBON-γ4 > γ1γ2; (**f**) MBON-γ5β′2a, MBON-β′2mp). Boxes represent 25% and 75% quartiles, squares indicate means, and horizontal lines indicate medians. Whiskers show minimum and maximum values. For all groups, n = 8. Difference between groups were tested using one-way ANOVA with Tukey post-hoc tests.

MBON-γ1pedc > α/β as functionally distinct from the remaining γ-lobe MBONs investigated here. The non-associative effects observed here are yet to be included in future computational circuit models of the fly MB. At the population level of KCs, synaptic plasticity induced by associative olfactory learning causes decorrelation of odor-evoked calcium influx at axonal synaptic boutons, and across the axonal compartments γ2–γ5[11]; axonal KC boutons in the γ1 compartment could not be recorded due to technical limitations, which leaves open the question of whether axonal boutons in this compartment similarly change their correlated activity. However, the fact that differential training affects odor coding across KC populations differentially implies that the learned change in odor-coding of mushroom body circuit and the learned behavior-instructive properties of the MBON signals are two distinct aspects of associative learning that can be experimentally dissociated.

Data availability

The datasets generated during and analyzed during the current study are available in the "Research Data Platform of the DFG Research Unit FOR 2705" repository, http://hdl.handle.net/21.11124/For2705_000095.

Received: 25 January 2022; Accepted: 7 June 2022
Published online: 21 June 2022

References

1. Pavlov, I. P. *Conditioned reflexes: an investigation of the physiological activity of the cerebral cortex*. (Oxford Univ. Press, 1927).
2. Tempel, B. L., Bonini, N., Dawson, D. R. & Quinn, W. G. Reward learning in normal and mutant Drosophila. *Proc. Natl. Acad. Sci. U. S. A.* 80, 1482–1486 (1983).
3. Tully, T. & Quinn, W. G. Classical conditioning and retention in normal and mutant Drosophila melanogaster. *J. Comp. Physiol. A* 157, 263–277 (1985).
4. de Belle, J. S. & Heisenberg, M. Associative odor learning in Drosophila abolished by chemical ablation of mushroom bodies. *Science* 263, 692–695 (1994).
5. Heisenberg, M., Borst, A., Wagner, S. & Byers, D. Drosophila mushroom body mutants are deficient in olfactory learning. *J. Neurogenet.* 2, 1–30 (1985).
6. Zars, T., Fischer, M., Schulz, R. & Heisenberg, M. Localization of a short-term memory in Drosophila. *Science* 288, 672–675 (2000).
7. Blum, A. L., Li, W., Cressy, M. & Dubnau, J. Short-and long-term memory in Drosophila require cAMP signaling in distinct neuron types. *Curr. Biol.* 19, 1341–1350 (2009).
8. Qin, H. *et al.* Gamma neurons mediate dopaminergic input during aversive olfactory memory formation in drosophila. *Curr. Biol.* 22, 608–614 (2012).
9. Perez-Orive, J. *et al.* Oscillations and sparsening of odor representations in the mushroom body. *Science* 297, 359–365 (2002).
10. Honegger, K. S., Campbell, R. A. & Turner, G. C. Cellular-resolution population imaging reveals robust sparse coding in the Drosophila mushroom body. *J. Neurosci.* 31, 11772–11785 (2011).
11. Bilz, F., Geurten, B. R. H., Hancock, C. E., Widmann, A. & Fiala, A. Visualization of a distributed synaptic memory code in the Drosophila brain. *Neuron* 106, 963-976.e4 (2020).
12. Betkiewicz, R., Lindner, B. & Nawrot, M. P. Circuit and cellular mechanisms facilitate the transformation from dense to sparse coding in the insect olfactory system. *eNeuro* 7, (2020).
13. Aso, Y. *et al.* Mushroom body output neurons encode valence and guide memory-based action selection in Drosophila. *Elife* 3, e04580 (2014).
14. Aso, Y. *et al.* The neuronal architecture of the mushroom body provides a logic for associative learning. *Elife* 3, e04577 (2014).
15. Riemensperger, T., Völler, T., Stock, P., Buchner, E. & Fiala, A. Punishment prediction by dopaminergic neurons in Drosophila. *Curr. Biol.* 15, 1953–1960 (2005).
16. Cohn, R., Morantte, I. & Ruta, V. Coordinated and compartmentalized neuromodulation shapes sensory processing in Drosophila. *Cell* 163, 1742–1755 (2015).
17. Heisenberg, M. Mushroom body memoir: From maps to models. *Nat. Rev. Neurosci.* 4, 266–275 (2003).
18. Springer, M. & Nawrot, M. P. A mechanistic model for reward prediction and extinction learning in the fruit fly. *eNeuro* 8, ENEURO.0549-20.2021 (2021).
19. Dubnau, J., Grady, L., Kitamoto, T. & Tully, T. Disruption of neurotransmission in Drosophila mushroom body blocks retrieval but not acquisition of memory. *Nature* 411, 476–480 (2001).
20. McGuire, S. E., Le, P. T., Osborn, A. J., Matsumoto, K. & Davis, R. L. Spatiotemporal rescue of memory dysfunction in Drosophila. *Science* 302, 1765–1768 (2003).
21. Zhang, S. & Roman, G. Presynaptic inhibition of gamma lobe neurons is required for olfactory learning in Drosophila. *Curr. Biol.* 23, 2519–2527 (2013).
22. Hige, T., Aso, Y., Modi, M. N., Rubin, G. M. & Turner, G. C. Heterosynaptic plasticity underlies aversive olfactory learning in Drosophila. *Neuron* 88, 985–998 (2015).
23. Pech, U., Revelo, N. H., Seitz, K. J., Rizzoli, S. O. & Fiala, A. Optical dissection of experience-dependent pre- and postsynaptic plasticity in the Drosophila brain. *Cell Rep.* 10, 2083–2095 (2015).
24. Tian, L. *et al.* Imaging neural activity in worms, flies and mice with improved GCaMP calcium indicators. *Nat. Methods* 6, 875–881 (2009).
25. Chen, T.-W. *et al.* Ultrasensitive fluorescent proteins for imaging neuronal activity. *Nature* 499, 295–300 (2013).
26. Hancock, C. E., Bilz, F. & Fiala, A. In vivo optical calcium imaging of learning-induced synaptic plasticity in Drosophila melanogaster. *J. Vis. Exp.* https://doi.org/10.3791/60288 (2019).
27. Thévenaz, P., Ruttimann, U. E. & Unser, M. A pyramid approach to subpixel registration based on intensity. *IEEE Trans. Image Process. Publ.* 7, 27–41 (1998).
28. Rickert, J., Riehle, A., Aertsen, A., Rotter, S. & Nawrot, M. P. Dynamic encoding of movement direction in motor cortical neurons. *J. Neurosci.* 29, 13870–13882 (2009).
29. Pedregosa, F. *et al.* Scikit-learn: Machine learning in Python. *J. Mach. Learn. Res.* 12, 2825–2830 (2011).
30. Hige, T., Aso, Y., Rubin, G. M. & Turner, G. C. Plasticity-driven individualization of olfactory coding in mushroom body output neurons. *Nature* 526, 258–262 (2015).
31. Perisse, E. *et al.* Aversive learning and appetitive motivation toggle feed-forward inhibition in the Drosophila mushroom body. *Neuron* 90, 1086–1099 (2016).
32. Owald, D. *et al.* Activity of defined mushroom body output neurons underlies learned olfactory behavior in Drosophila. *Neuron* 86, 417–427 (2015).
33. Felsenberg, J. *et al.* Integration of parallel opposing memories underlies memory extinction. *Cell* 175, 709-722 (2018).
34. Berry, J. A., Phan, A. & Davis, R. L. Dopamine neurons mediate learning and forgetting through bidirectional modulation of a memory trace. *Cell Rep.* 25, 651-662 (2018).
35. Préat, T. Decreased odor avoidance after electric shock in Drosophila mutants biases learning and memory tests. *J. Neurosci.* 18, 8534–8538 (1998).
36. Aso, Y. & Rubin, G. M. Dopaminergic neurons write and update memories with cell-type-specific rules. *Elife* 5, e16135 (2016).
37. Magee, J. C. & Grienberger, C. Synaptic plasticity forms and functions. *Annu. Rev. Neurosci.* 43, 95–117 (2020).
38. Martin, S. J., Grimwood, P. D. & Morris, R. G. M. Synaptic plasticity and memory: An evaluation of the hypothesis. *Annu. Rev. Neurosci.* 23, 649–711 (2000).
39. Takeuchi, T., Duszkiewicz, A. J. & Morris, R. G. M. The synaptic plasticity and memory hypothesis: Encoding, storage and persistence. *Philos. Trans. R. Soc. B Biol. Sci.* 369, (2014).
40. Gerber, B., Tanimoto, H. & Heisenberg, M. An engram found? Evaluating the evidence from fruit flies. *Curr. Opin. Neurobiol.* 14, 737–744 (2004).
41. Vasmer, D., Pooryasin, A., Riemensperger, T. & Fiala, A. Induction of aversive learning through thermogenetic activation of Kenyon cell ensembles in Drosophila. *Front. Behav. Neurosci.* 8, (2014).
42. Boto, T., Louis, T., Jindachomthong, K., Jalink, K. & Tomchik, S. M. Dopaminergic modulation of cAMP drives nonlinear plasticity across the Drosophila mushroom body lobes. *Curr. Biol. CB* 24, 822–831 (2014).
43. Fiala, A. & Riemensperger, T. Localization of a memory trace: Aversive associative olfactory learning and short-term memory in Drosophila. In *Learning and Memory: A Comprehensive Reference* Vol. 1 (eds Menzel, R. & Byrne, J. H.) 475–482 (Aacademic Press, Oxford, 2017).
44. Bennett, J. E. M., Philippides, A. & Nowotny, T. Learning with reinforcement prediction errors in a model of the Drosophila mushroom body. *Nat. Commun.* 12, 2569 (2021).

45. Eichler, K. *et al.* The complete connectome of a learning and memory centre in an insect brain. *Nature* 548, 175–182 (2017).
46. Li, F. *et al.* The connectome of the adult Drosophila mushroom body provides insights into function. *Elife* 9, e62576 (2020).
47. Takemura, S. Y. *et al.* A connectome of a learning and memory center in the adult Drosophila brain. *Elife* 6, 1–43 (2017).
48. Pascual, A. & Préat, T. Localization of long-term memory within the Drosophila mushroom body. *Science* 294, 1115–1117 (2001).

Acknowledgements
We are grateful to the Janelia Research Campus and the Bloomington Drosophila stock center for providing *Drosophila* strains. This work was funded by the Deutsche Forschungsgemeinschaft (DFG, German Research Foundation) through the Research Unit "Structure, Plasticity and Behavioral Function of the Drosophila Mushroom Body" (FOR 2705, project no. 365082554) to A.F. and M.N, and through SFB 889/B04 to A.F (project no. 154113120).

Author contributions
C.E.H., E.Y.R., and S.H.D. performed experiments, V.R. and M.P.N. designed and performed computational analysis, A.F. and C.E.H. designed experiments, analyzed data, and wrote the manuscript with the help of all authors.

Funding
Open Access funding enabled and organized by Projekt DEAL.

Competing interests
The authors declare no competing interests.

Additional information
Supplementary Information The online version contains supplementary material available at https://doi.org/10.1038/s41598-022-14413-5.

Correspondence and requests for materials should be addressed to A.F.

Reprints and permissions information is available at www.nature.com/reprints.

Publisher's note Springer Nature remains neutral with regard to jurisdictional claims in published maps and institutional affiliations.

IV. Manuscript 3: Functional dissection of a neuronal brain circuit mediating higher-order associative learning

In preparation

Authors: El Yazid Rachad[1], Stephan H. Deimel[1], Yogesh Gadgil[1], Anna-Maria Jürgensen[2], Magdalena Springer[2], Chen-Han Lin[3], Martin P. Nawrot[2], Suewei Lin[3], and André Fiala[1,*].

[1] Molecular Neurobiology of Behavior, University of Göttingen, Göttingen, Lower Saxony, 37077, Germany

[2] Computational Systems Neuroscience, University of Cologne, Cologne, Northrhine-Westfalia, 50931, Germany

[3] Laboratory of Motivation and Memory, Academia Sinica, Taipei, Nangkang, Taiwan.

* Corresponding author: afiala@gwdg.de

Summary

A cardinal feature of many species' brains is the ability to form associative chains through learning. In simple forms of associative learning, sensory stimuli coinciding with experienced reward or a punishment become attractive or repulsive. However, stimuli previously learned as attractive or repulsive can also become reinforcers themselves, with the ability to be associated with further sensory stimuli again. If this process is consecutively repeated, it leads to higher-order associations. Here, we use aversive odor conditioning in *Drosophila* to functionally dissect the architecture of neuronal networks underlying higher-order associative learning. We show that the responsible neuronal circuit, located in the mushroom bodies of the brain, is characterized by parallel processing of odor information, and by recurrent excitatory and inhibitory feedback loops that enable odors to gain control over the dopaminergic valence-signaling system. Together, our findings establish a paradigmatic framework of a neuronal circuit diagram enabling the acquisition of associative chains.

Keywords

Associative learning, higher-order conditioning, mushroom body, *Drosophila melanogaster*, neuronal circuit dissection, learning and memory, insect brain, odor coding, dopamine, neuronal networks.

Introduction

Detecting and learning associations between events in the world is arguably a cardinal feature of the brains of many species. In its most simplistic form, a stimulus that temporally coincides with a positive or negative outcome is learned as pleasant or unpleasant. The undoubtedly most famous example for this principle is that of Pavlov's dogs, which learned salivating in response to a conditioned tone that predicted a meaty taste reward (Pavlov, 1927). However, animals and humans rarely learn to predict outcomes through regularly encountering rewards or punishments directly. Rather, complex steps and chains of multiple associations occur, without the necessity of receiving reward or punishment each time. Already Pavlov has observed that his dogs could further associate the conditioned tone with a black square, a finding he termed second-order conditioning (Pavlov, 1927). Thereby, a learned stimulus that has acquired relevance can be associated with a second-order stimulus, and this stimulus again with a third-order stimulus, and so on and so forth. In sum, higher-order conditioning involves the chain-like, multistep, consecutive learning of causal links between stimuli and events that enables one to create novel inferences. Importantly, it differs from first-order classical conditioning in that the reinforcing "teaching" signal does not innately carry a positive or negative valence, but has acquired its reinforcing valence through previous experience. This is a key aspect of what brains constantly accomplish.

The charm of analyzing higher-order associations particularly through employing a second-order learning regime is that it can be studied in the laboratory under strictly controlled conditions, allowing for a clear determination what is actually associated and when. Moreover, the rules by which higher-order conditioning is accomplished can be generalized across animal species because it constitutes a widespread

phenomenon that occurs throughout the animal kingdom. Second-order conditioning has been observed not only in humans (Craddock et al., 2018; Lee et al., 2021) or rodents (Rizley and Rescorla, 1972; Gostolupce et al., 2021), but also in mollusks (Hawkins et al., 1998; Loy et al., 2006) or insects, like honeybees (Bitterman et al., 1983; Hussaini et al., 2007) and fruit flies (Brembs and Heisenberg, 2001; Tabone and de Belle, 2011).

Despite of the obvious fundamentality of this brain function, the underpinning neuronal circuits and their modes of operation remain elusive as of yet. Whereas brain regions have been identified that are implicated in higher-order associative learning in various species and behavioral paradigms (reviewed by Holmes et al., 2022), e.g., the basolateral amygdala or the hippocampus in rats (e.g., Gilboa et al., 2014; Gostolupce et al., 2021), precise circuit diagrams that explain how exactly memory traces in terms of changes in synaptic connectivity occur, are lacking. In recent years, substantial advances have been achieved in generating methods to express transgenes designed for the functional analysis of neuronal circuits, which is possible in transgenic organisms such as mice, zebrafish or C. elegans (Luo et al., 2018). The fruit fly *Drosophila melanogaster*, with its uniquely ample genetic toolbox (Venken et al., 2011), is particularly suitable for dissecting neuronal circuits underlying learning and memory formation. With ~ 100.000 neurons, its brain is, on the one hand, numerically much simpler than that of vertebrates with its millions of neurons. On the other hand, insects like fruit flies display an enormously rich behavioral repertoire that allows for a functional comparison with mammals. One aspect of this richness is a complex learning behavior. In *Drosophila*, higher-order conditioning has been investigated using several approaches and behavioral paradigms. A recent study has used simulated olfactory reward learning of second-

order to identify dopaminergic neurons and neuronal feedback loops that might be implicated in modifying odor representations through odor-odor associations (Yamada et al., 2023). On the contrary, aversive second-order learning has been observed in behavior using the flight simulator using visual stimuli as conditioned stimuli (Brembs and Heisenberg, 2001), and in a T-maze situation using olfactory stimuli (Tabone and de Belle, 2011), but without any attempts to identify the underpinning neuronal substrates. Here, we have adopted the latter paradigm as the basis for our work. We have chosen this learning paradigm because the neuronal architecture enabling simple aversive olfactory first-order conditioning has been characterized to a high degree (Busto et al., 2010; Fiala and Riemensperger, 2017; Boto et al., 2020). This enables us to directly address the question in which aspects the neuronal circuits mediating simple classical conditioning differ from and/or overlap with those enabling higher-order associative learning.

The most simplistic form of Pavlovian learning relies on the detection of odor stimuli that flies perceive by olfactory sensory neurons located on the third antennal segments and maxillary palps that target the glomeruli of the antennal lobes (Vosshall and Stocker, 2007). Second-order olfactory projection neurons convey the odor information to the lateral horn and the calyx of the mushroom body (Marin et al., 2002; Wong et al., 2002), similar to the vertebrates' mitral/tufted cells. Here, olfactory projection neurons synapse onto intrinsic mushroom body neurons (Kenyon cells) that encode odor identity as sparsely distributed activity: only a small fraction of neurons respond selectively to a given odor (Turner et al., 2008; Honegger et al., 2011; Bilz et al., 2020), similar to the situation in the anterior piriform cortex (Stettler and Axel, 2009). The parallel arranged axons of Kenyon cells collectively form the mushroom body lobes. The axons from α/β and α'/β' Kenyon cells bifurcate and

constitute the α-, β-, α'- and β' lobes; the γ Kenyon cells' axons do not bifurcate and give rise to the γ lobes. It is the Kenyon cell axons where the coincidence between odor signal and punishment signal occurs (Heisenberg, 2003; Fiala and Riemensperger, 2017) (Figure 1A). The reinforcing valence as the "teaching" signal is mediated by dopaminergic neurons (DANs) (Riemensperger et al., 2005), similar to the reinforcing function of midbrain dopaminergic neurons in vertebrates (Schultz, 2007). Those dopaminergic neurons that signal punishment originate from protocerebral posterior lateral (PPL) 1 cluster (Riemensperger et al., 2005; Aso et al., 2012) that innervate the mushroom body lobes in spatially restricted areas termed lobe compartments (Aso et al. 2014a). In the course of classical conditioning, coincident activation of Kenyon cells through odor stimulation together with punishment-induced dopamine release causes presynaptic depression of synapse between Kenyon cells and mushroom body output neurons (MBONs) (Hige et al., 2015a) that ultimately instruct the animals approach or avoidance behavior (Aso et al., 2014b). Whereas accumulating evidence over the last decades have corroborated this concept, it remains unknown how higher-order associative chains might be formed. First, it is not clear whether the reinforcing dopaminergic neurons that innately respond to punishments or rewards mediate the valence of learned reinforcers. Second, the exact location of odor representations within lobe compartments that become modified in the course of higher-order learning is unclear. Third, the synaptic changes that mediate the learned change in behavior, i.e., the engram in a strict sense, is unknown. Here, we report our endeavor to answering these questions with the goal to characterize the neuronal circuit mediating the formation of associative chains as a paradigmatic case.

Results

To confirm *Drosophila's* ability for higher-order associative odor learning according to Tabone and deBelle (2011), we designed a computer-controlled training apparatus (Figure S1A, B) to subject wild-type flies to an aversive second-order conditioning regime (Figure 1B). In a first training phase, an odor (conditioned stimulus +; CS1) was temporally paired with a series of pulsed, punishing electric shocks (unconditioned stimulus; US). A different odor (CS-) was presented without electric shocks. In a second training phase, a novel odor CS2 was then temporally paired with pulsed presentations of the previously conditioned odor CS1. In a subsequent T-maze test situation, the behavioral response to the odor CS2 trained in second-order was tested against the CS-. A robust and statistically significant avoidance of the odor trained in second-order was confirmed (Figure 1B). Control experiments, in which either the temporal coincidence of CS+ and US was dissolved in the first, but not second, training phase ("unpaired-paired"), or in which the two odors in the second training phase were presented with a temporal gap, did not result in any learning (Figure 1B). These commonly used control experiments (Rescorla et al., 1980) indeed demonstrate that the temporal coincidence of trained stimuli in the two training phases causes the learned avoidance (Tabone and de Belle, 2011). Moreover, these experiments confirm that the learned avoidance was not based on a potential attractiveness of the CS- acquired during the first training phase, a phenomenon known as "condition inhibition" that can occur in flies (Barth et al., 2014). Three different chemical compounds (3-octanol, 4-methylcyclohexanol and benzaldehyde) were used as odorants, and their concentrations were carefully chosen such that their innate repulsive valences were balanced (Figure S1C). All three odorants were used either as CS1, CS2 or CS-, and flies could achieve

second-order conditioning in all odorant combinations, independent of their chemical identity (Figure S1D). Second-order conditioning resulted in slightly weaker learning index than simple first-order conditioning (Figure S1E). It is well-established that in *Drosophila* olfactory memories become generally weaker with progressing time from the training (Margulies et al., 2005). Therefore, we wondered whether the lower learning indices might result from the longer-lasting training procedure when compared with the commonly used first-order conditioning regime and subsequent short-term memory test that lasts only several minutes (Tully and Quinn, 1985). In fact, when a regular simple first-order conditioning procedure was conducted, but the second training phase was replaced by a temporal gap, the first-order memory score was significantly reduced when compared to a memory test directly three minutes after training. This memory score was only slightly, but not significantly, higher than that induced by second-order conditioning (Figure S1E). Therefore, the lower memory score induced by second-order conditioning can be attributed, at least partially, to the longer-lasting training procedure that requires a maintained storage of the memory acquired during the first training phase.

After having confirmed that aversive olfactory second-order conditioning can be robustly reproduced in our hands, we tested which neuronal circuits mediate this form of learning. It appeared plausible that the circuits required for it are localized in the mushroom body circuitry; however, a formal demonstration was unsettled. Therefore, we ectopically expressed in Kenyon cells the dominant negative and temperature-sensitive dynamin mutant shibire^{ts}, which is widely used to reversibly block synaptic transmission by shifting the animals to a restrictive temperature (Kitamoto, 2001; 2002; Figure 1C). The reversible property of this tool makes it possible to block synaptic transmission in defined neurons selectively during the first training phase,

the second training phase or the test situation (Figure 1D). As a first step, synaptic output was blocked in all intrinsic mushroom body cells (Kenyon cells) using a novel MB247-Gal4 line, kindly provided by Betty Hong, that targets Kenyon cells of all lobes (Figure S1F, G). When Kenyon cell output was blocked only during the first, but not during the subsequent second training phase, memory scores were unaffected (Figure 1E). On the contrary, when synaptic output was blocked only during memory retrieval during the test phase, no significant learned avoidance was observed any more (Fig. 1E). This is in accordance with well-established findings that learning induced by odor-shock association relies on modifications of Kenyon cell presynapses (Hige et al., 2015a); Kenyon cell output is required for the retrieval of first-order associative short-term memory, but not for its acquisition (Dubnau et al., 2001; McGuire et al., 2001; Schwaerzel et al., 2002). However, and interestingly, we found that blocking synaptic output from Kenyon cells during the second training phase does disrupt learning and memory formation (Figure 1E). This leads to the conclusion that synaptic output from Kenyon cells is required to initiate learning of higher order, either in brain regions different from the mushroom body, or within the mushroom body circuit through feedback loops. To refine the potential mushroom body output that is actually required, we expressed shibire^{ts} in the three Kenyon cell populations that constitute either α/β-lobes, α'/β'-lobes or γ-lobes using specific Gal4-driver lines (Figure 1F-H). Blocking synaptic output from γ-lobe Kenyon cells resulted in the same effect as blocking all Kenyon cells (Figure 1F), with a requirement of synaptic transmission during the second training phase and the memory test. This is in accordance with the concept that regular first-order odor-shock learning and subsequent short-term memory retrieval is localized to synaptic changes in the γ-lobes (Zars et al., 2000; Qin et al., 2012), and here in particular in the γ1

compartment (Hancock et al., 2022). Surprisingly, synaptic output from α'/β'-lobe Kenyon cells turned out to be required as well, but only during the second training phase in which the conditioned odor is temporally paired with the novel odor; output during the test phase was not necessary (Figure 1G). On the contrary, synaptic transmission from α/β-lobe Kenyon cells was completely dispensable for second-order conditioning at any phase (Figure 1H).

After having revealed that two mushroom body output pathways both are required in parallel for enabling second-order conditioning, we asked which exact mushroom body output neurons (MBONs) would mediate this. Using very specific split-Gal4 lines (Aso et al., 2014; Figure S2A, B) we expressed shibire^{ts} in each MBON type that targets a specific compartment of the γ-lobes (Figure 2 A-E) or α'/β'-lobes (Figure 2F-J). We found that synaptic transmission from only one MBON receiving input from the γ-lobe Kenyon cells is required during the second-order training phase and the memory retrieval test (Figure 2A), namely MBON-γ1pedc>α/β (also known as MBON11 or MB-MVP2). Synaptic output from all other MBONs receiving input in the γ2 to γ5 compartments are dispensable for this specific task (Figure 2B-E). When the MBONs innervating the α'/β'-lobes were tested, we found that, again, synaptic output from only one MBON was required for this learning task, and only during the second training phase in which the already conditioned odor CS1 is paired with the novel odor CS2 (Figure 2F-J). This MBON targets the α'2 compartment (also known as MBON-α'2, MBON13, or MB-V4) (Figure 2G). No functional role had been described for this neuron so far. We wondered whether it is indeed second-order associative learning for which MBON-α'2 is required or, alternatively, whether it is necessary for maintaining learned information during the relatively long-lasting training procedure. After all, the second-order training protocol with its three blocks of

CS1-US associations during the first training phase, and again three blocks of CS2-CS1 associations during the second training phase, before a test for memory recall can be conducted. The resulting memory might, therefore, not only be based on neuronal mechanisms of short-term memory formation, but also include already middle-term memory phases. These different memory phases do not only differ in molecular mechanisms (Margulies et al., 2005), but also in individual mushroom body extrinsic neurons (Dubnau and Chiang, 2013) or even mushroom body lobes that are involved (Yang et al., 2016). Therefore, we tested whether the requirement of MBON-α'2 might depend on the time of training and test. We used shibire^{ts} expression in either of the two MBONs involved in second-order learning, i.e., MBON-γ1pedc>α/β and MBON-α'2, and blocked their output during a regular first-order odor-shock learning and subsequent test for short-term memory three minutes after the training (Figure S2C). As reported already previously (Hancock et al., 2022), synaptic transmission from MBON-γ1pedc>α/β and MBONs γ5β'2a-β'2mp is required for memory recall (Figure S2E), the latter presumably through disinhibition by MBON-γ1pedc>α/β (Hancock et al., 2022). Synaptic output from MBON-α'2 is not required. We compared this result with a first-order conditioning protocol in which the CS-US association was repeated in three blocks, equivalent to the second-order training protocol, and in which a temporal gap after the training was introduced that lasted as long as the second-order training phase did (Figure S2D). It turned out that MBON-γ1pedc>α/β is required for the recall of this memory again, and output from MBON-α'2 was still not required (Figure S2F). In conclusion, so far we did not find evidence that the requirement of MBON-α'2 for second-order conditioning might be due to a potential role in memory consolidation.

Associative learning depends on at least three types of signals or neuronal representations. One type of signal must encode the conditioned odor stimuli, and this is accomplished in *Drosophila* by the array of Kenyon cells. The learned, conditioned response must be signaled through neurons that instruct behavior-modulating circuits, and this is achieved in *Drosophila* through distinct MBONs (Aso et al., 2014b). The third signal conveys the reinforcing valence, in this case a punishment; in *Drosophila*, electric shock punishment during aversive conditioning is mediated by dopamine-releasing neurons (Riemensperger et al., 2005). To address the question which dopaminergic neurons mediate the reinforcing information in second-order conditioning, we first used two Gal4-driver lines that target the two main populations of dopaminergic neurons in the *Drosophila* brain, i.e., mainly the PPL cluster of neurons and mainly the PAM cluster of neurons (Pech et al., 2013). When synaptic output was blocked through shibire^{ts} expression, we found that only dopaminergic neurons of the PPL cluster are required for inducing learning, both during the first and the second conditioning phase, but not during memory retrieval in the test phase (Figure 3B). Synaptic output from dopaminergic neurons of the PAM cluster is dispensable for any phase of aversive second-order conditioning (Figure 3C). We then employed again highly specific split-Gal4 driver lines (Aso et al., 2014a; Figure S3A) to test in a refined way which exact PPL1 cluster neurons innervating the γ-lobes and α'-lobes are necessary for second-order conditioning. During the first conditioning phase, in which the CS1 odor is associated with the electric shock, dopamine release from neurons innervating the γ1 compartment (PPL1-γ1pedc DAN, PPL101 or MB-MP1) are necessary; blocking their output decreases the memory score significantly, but interestingly not completely (Figure 3D). The same is true for dopaminergic neurons innervating the γ2 compartment that, at the same time, also

innervates the α'1 compartment (PPL1-γ2α′1 DAN, PPL103 or MB-MV1) (Figure 3E). Blocking synaptic output from this dopaminergic neuron during the first conditioning phase resulted also in a statistically significant, but not complete, reduction in second-order learning (Figure 3E). Apparently, PPL1-γ1pedc and PPL1-γ2α′1 DANs both are required, but not completely sufficient, to mediate the electric shock information during the first training phase for subsequent second-order learning. Importantly, in the second training phase, in which CS1 and CS2 are associated, only PPL1-γ1pedc DAN is required (Figure 3D). Synaptic output from all other dopaminergic neurons is dispensable (Figure 3E-G). The identity of the dopaminergic neurons that mediate the reinforcing properties of the punishment are equivalent for the odor-shock association in regular first-order conditioning and in the first training phase of the second-order conditioning protocol. In both cases, PPL1-γ1pedc and PPL1-γ2α′1 DANs are required (Figure S3 B-E). This is independent of the duration of the training protocol, although the contribution of PPL1-γ2α′1 DAN is smaller in the longer-lasting learning and memory protocol (Figure S3 B-E).

We had now the puzzling situation that mushroom body inputs and outputs that are required for second-order conditioning differ in their specific compartments. For the γ1 compartment, the situation is logical: Both dopaminergic input and output through its concomitant MBON are required, the valence signaling dopamine release during the two training phases, the behavior-instructive MBON during the memory retrieval. However, for the γ2 compartment, the dopaminergic input is required only during the first conditioning phase (Figure 3E), but not its concomitant MBON-γ2α'1 (also known as MBON12) (Figure 2B). Moreover, for the α'2 compartment, the respective MBON is required only during the second conditioning phase (Figure 2G), but not its concomitant dopaminergic input neuron (Figure 3F). To solve this conundrum, we

first wanted to confirm which of the dopaminergic neurons under investigation could actually signal electric shock information. To this end, we employed *in vivo* two-photon imaging and a combination of a presynaptically localized green fluorescent calcium (Ca^{2+}) sensor (Synaptophysin-GCamP) and a red fluorescent pH-sensitive sensor localized to the lumen of synaptic vesicles (Synaptophysin-pHTomato) to monitor synaptic exocytosis (Pech et al., 2015). These experiments revealed that both PPL1-γ1pedc and PPL1-γ2α′1 DANs respond reliably and strongly to the pulses of electric shocks (Figure 4A, B). On the contrary, dopaminergic neurons innervating the α'2 compartment (PPL1-α′2α2 DAN, PPL105 or MB-V1) did not show any response to the electric shocks, similarly to the PAM cluster dopaminergic neuron that innervates the γ5 compartment (PAM-γ5 DAN, PAM01 or MB-M1) (Figure 4A, B), which we have used as a negative control due to its role in mediating reward signals (Yamagata et al., 2015). Because MBON α'2 is required during the second training phase, during which the novel odor CS2 is associated with the previously trained odor CS1, we concluded that this compartment should encode and store information about the "punished" odor CS1 to be able to further transmit information about it. Conclusively, it should receive a so far unknown input "teaching" signal of the punishment. To clarify whether such a functional connection exists, we asked whether the two dopaminergic neurons that clearly respond to electric shocks (Figure 4A, B) and that are required for second-order conditioning (Figure 3D, E), might contact the α'2 compartment as well. Indeed, splitGFP-reconstitution across synaptic partners (GRASP) (Feinberg et al., 2008) revealed that PPL1-γ2α′1 DAN innervates also small fraction of the α'2 compartment (Figure 4Ci). The PPL1-γ1pedc or the PAM-γ5 DANs used as a negative control do not deviate in their innervation from their concomitant compartment they have been assigned to (Figure 4C). To confirm

this finding, we made use of the electron microscopy-based connectome (Scheffer et al., 2020) and its web-based user interface NeuPrint to reconstruct the morphology of the PPL1-γ2α′1 DAN (Figure 4Cii). This neuron innervates the MB lobes very densely in the adjacent γ2 and α'1 compartments. However, if one compares the exact areas of innervation with the dendritic tree of the reconstructed MBON-α'2 (Figure 4Cii), one can identify a small region of overlap at the posterior end of the α'2 lobe (Figure 4Ciii). A quantification of identified synaptic connections corroborates this finding: The Kenyon cells' synapses within the α'2 compartment target of course predominantly MBON-α'2; but in addition, reciprocal synaptic connections exist between these Kenyon cells and the PPL1-γ2α'1 DAN. Very few reciprocal synaptic connections were also identified between PPL1-γ2α'1 DAN and MBON-α'2 (Figure 4Civ). In conclusion, the connectome database confirms a synaptic connectivity of the PPL1-γ2α'1 DAN with the α'2 compartment at the level of Kenyon cells and, to a small degree, also at the level of the respective MBON. That is, the γ1 compartment receives punishment information through its concomitant PPL1-γ1pedc DAN, and the α'2 compartment through the PPL1-γ2α'1 DAN. However, the effects that these two independent dopaminergic signals on the two distinct and separated populations of Kenyon cell axon compartments had remained to be clarified. Of course, we reasoned that a reinforcing, punishment-mediating "teaching" signal through dopaminergic neurons, might cause synaptic plasticity in Kenyon cell-to-MBON connections. In order to determine whether such learning-induced plasticity exists, we conducted functional optical Ca^{2+} imaging experiments. Individual flies with their head capsule opened and brain-exposed were positioned under a two-photon microscope and subjected to stimulation with odors stimuli and punitive electric shocks (Figure 5A). Equivalent to the conditioning procedure in freely behaving flies,

animals underwent an associative second-order conditioning regime. Control animals were subjected to conditioning protocols in which the stimuli were presented in temporal separation either in the first training phase (unpaired-paired) or in the second training phase (paired-unpaired) (Figure 5B), equivalent to the behavioral experiments (Figure 1B). The fast responsive Ca^{2+} sensor GCamP6f (Chen et al., 2013) was expressed in MBON-α'2 using MB018B-Gal4, and odor-evoked neuronal activity was monitored in the dendritic arborizations innervating the respective lobe compartment. The odorants 4-methyl cyclohexanol and 3-octanol were use in a balanced manner as CS1 and CS-, benzaldehyde served as CS2. Odor stimulations evoked a clear and robust Ca^{2+} influx, detectable as transient increase in fluorescence (Figure 5C). After the two training phases, the response intensity as determined by the integral value of the Ca^{2+} transient (area under curve) was significantly increased, but only for the odor that served as CS1, i.e., that was paired with the electric shock punishment (Figure 5D). No significant change in odor responsivity was detected for the CS- and the CS2. Accordingly, this potentiation was detectable also in the paired-unpaired control, but not in unpaired-paired control flies. This confirms a potentiating effect due to the specific odor-shock coincidence. Unfortunately, the spatially more restricted fluorescence sensor dHomer-GCaMP3 that is targeted specifically to the postsynaptic density (Pech et al., 2015) could not be used in this neuron because odor-evoked Ca^{2+} influx was not detectable (Figure S4). In contrast, dHomer-GCamP3 reliably reported odor-evoked Ca^{2+} signal in MBON-γ1pedc>α/β (Figure 5E, Figure S4). The reason for this discrepancy is not entirely clear. It might be speculated that in MBON-γ1pedc>α/β acetylcholine receptors might have a higher Ca^{2+} conductivity than those expressed by MBON-α'2. However, dHomer-GCaMP3 was used to determine potential plastic effects in

MBON-γ1pedc>α/β dendritic tree. Here, after training a strong depression of odor-evoked Ca^{2+} signals was observed for the CS1 (Figure 5F), as previously reported (Hancock et al., 2022). Interestingly, the depression occurred also after second-order training for the CS2, and this depression was dependent on the temporal pairing of CS1 and US during the first training phase, and of CS2 and CS1 during the second training phase (Figure 5F). In conclusion, we determine two memory traces manifested in oppositional changes in the activity of two different MBONs. MBON-α'2 that is required only during the second-order training phase (Figure 2G) shows potentiated activity, but only as a result of odor-shock-training for the CS1, not as a result of second-order training. By contrast, MBON-γ1pedc>α/β whose output is required for both training phases (Figure 2A) shows a depression for both the CS1 and the CS. The first finding indicates that during odor-shock association the odor representation for the CS1 is modified as "relevant" such that in a subsequent training phase a CS2-CS1 association can take place. The latter finding demonstrates that the synaptic depression, which is typically induced by an innate reinforcer such as punitive electric shocks (Hige et al. 2015a; Hancock et al., 2022) can be induced by a learned odor as reinforcement as well. This in turn implies that the learned odor representation can take control over the reinforcing dopamine system, i.e., PPL1-γ1pedc DAN.

To test this concept more directly, we asked what effects do the activities of the inhibitory, GABAergic MBON-γ1pedc>α/β, and the excitatory, cholinergic MBON-α'2 actually have on PPL1-γ1pedc DAN, either via mono- or polysynaptic connections. The red-sifted, light-sensitive channelrhodopsin variant CS-Chrimson (Klapoetke et al., 2014) was used to optogenetically drive the excitation of both MBONs. Simultaneously, the activity of PPL1-γ1pedc DAN was monitored under a two-photon

microscope using the Ca^{2+} sensor GCaMP6m (Chen et al., 2013). In comparison with a control that carried only the UAS construct, clear effects were observed: MBON-α'2 induced an increase in activity of the PPL1-γ1pedc DAN. On the contrary, MBON-γ1pedc>α/β inhibited it, in accordance with previous reports (Aso et al., 2014a; Ueoka et al., 2017). This finding leads to a circuit model that encompasses two feedback loops, one that inhibits the reinforcing PPL1-γ1pedc DAN, and one that activates it. During the first training phase, the electric shock activates both PPL1-γ1pedc and PPL1-γ2 α'1 DAN. The coincidently induced odor representations in terms of in Kenyon cells-to-MBON synapses are potentiated in the α'2 compartment, and depressed in the γ1 compartment (Figure 6E). This enables the trained odor CS1 in the second training phase to drive the PPL1-γ1pedc DAN through an activation by the potentiated and excitatory MBON-α'2, and by the depressed and thereby disinhibiting MBON-γ1pedc>α/β. Through the coincident activation of the CS2 with the CS1-induced dopamine release, the Kenyon cell-to-MBON-γ1pedc>α/β synapses become inhibited as well. The memory readout, i.e., avoidance of the learned odor through higher-order conditioning, relies on the inhibition of the approach-inducing MBON-γ1pedc>α/β (Figure 6E). The multiple target brain regions of this neuron, such as the crepine or the superior medial protocerebrum might act as pre-motor centers to guide learned avoidance behavior.

As consistent as the experimental data and this circuit model are, we felt that in order to make the claim that flies can truly form associative chains, a demonstration of higher-order learning beyond second-order conditioning was needed. Therefore, we tested whether associative learning can be extended by at least one more chain link, i.e., third-order conditioning. Indeed, pairing of an odor with an electric shock punishment, subsequent second-order conditioning of a novel odor with the trained

one, and a third-order conditioning training of a further novel odor with the previously trained odor as a reinforcer leads to a clear and statistically significant learned avoidance in wildtype flies (Figure 7). The required control experiments show that, in each training phase, the temporal coincidence between the conditioned stimuli and their respective reinforcements is necessary to induce this type of higher-order learning, which excludes potential non-associative effects or conditioned inhibition of the CS-. In sum, flies can learn associative chains, and the neuronal circuit that we have characterized is suitable for mediating it.

Discussion

Numerous theoretical, computational and artificial neuronal models of associative learning and of varying complexity are able to carry out second-order conditioning tasks (e.g., Sanchez et al., 2010). Several computational models have also been created based on the *Drosophila* mushroom body circuitry (Faghihi et al., 2017; Springer et al., 2021; Bennett et al., 2021; Zhao et al., 2021). Obviously, empirical data are useful to evaluate which aspects of theoretical models actually fit biological reality. Here, we have uncovered a neuronal circuit that underlies higher-order associative learning in *Drosophila*, which shows several novel aspects.

The first, unexpected aspect of the discovered neuronal circuit is the separation of the reinforcement signal into two additive dopamine “channels”, i.e., the punishment-activated PPL1-γ1pedc and the PPL1-γ2α’1 DANs. One potential reason for this separation might rely on the difference in learning-induced plasticity in the neuronal response of the two dopaminergic neurons. Theoretical models of predictive learning dictate that the responsiveness of the reinforcing neuron to the unconditioned stimulus, in our case the electric shock, changes in the course of CS-US

associations. There is no empiric evidence for prediction error coding in dopaminergic neurons in *Drosophila* (Riemensperger et al., 2005; Dylla et al., 2017) as it is, for example, the case in midbrain dopaminergic neurons of monkeys (Schultz et al., 1997). In the case of reward prediction error coding in monkeys, the reinforcing neurons cease responding to the unconditioned stimulus once it is already predicted by the learned conditioned stimulus. However, in flies reinforcing neurons start responding stronger or longer to the conditioned stimulus in addition to their response to electric shocks (Riemensperger et al., 2005; Dylla et al., 2017), and this plasticity can be attributed solely to the PPL1-γ1pedc DAN, not to the PPL1-γ2α'1 DAN (Vrontou et al., 2021). In this context, it is important to consider that in a second training phase of SOC the trained stimulus CS1 is presented without electric shock, which potentially leads to extinction. Consequently, the odorant presented as CS2 simultaneously with the CS1 might, in the beginning of the training phase, be learned as second-order predictor for the punishment, which is in Pavlovian terms a conditioned excitation. With ongoing training, the CS1 might become subject to extinction, which would render the CS2 a predictor of the omission of a punishment, which is in Pavlovian terms a conditioned inhibition. In fact, conditioned inhibition has been demonstrated in flies (Barth et al., 2014). Recurrent feedback loops from MBONs to DANs that involve an adjustment of reward-mediating dopaminergic neurons have been proposed to explain extinction of an aversive conditioned stimulus in flies (Felsenberg et al., 2017; Felsenberg et al., 2018). Given the complex learning-dependent modification of the responsiveness of PPL1-γ1pedc DAN, an independent, stable, unmodified responsiveness to the unconditioned stimulus in PPL1-γ2α'1 DAN could help to associate novel, unpredicted conditioned stimuli independent of a previous learning history. In fact, it has been proposed that the US-

like, reinforcing properties of an acquired conditioned stimulus should be independent of the original reinforcement by the innate unconditioned stimulus to avoid constant conditioned inhibition (Miller et al., 1995). This concept would be in agreement of a proposed role of MBON-α'2 in mediating surprisingly (i.e., unpredicted) occurring reconsolidating aversive shock signals (Felsenberg et al., 2017), because these MBONs receive input from PPL1-γ2α'1 DANs.

A second unexpected finding refers to the across-compartment signaling of dopaminergic neurons. We find that the PPL1-γ2α'1 DAN is not entirely restricted in its innervation to the two mushroom body lobe compartments to which it has been assigned, i.e., the γ2 and the α'1 compartment. The concept of lobe compartments as completely independently acting functional units appears to be less strict.

A third unexpected finding is the discovery of both a learning-induced synaptic depression (in the Kenyon cell-to-MBON-γ1pedc>α/β compartment) and a learning-induced synaptic potentiation (in the Kenyon cell-to-MBON-α'2 compartment). How could that be potentially mediated? A differential involvement of various dopaminergic neurons in different temporal learning regimes (i.e., "learning rules") have been described (Aso and Rubin, 2019), which ultimately leads to highly individualized response patterns across individual animals and across MBONs (Hige et al., 2015b). Antagonistic synaptic depression and potentiation has been described for temporally different CS-US contingencies. It is well-established that CS-US paring with an odor preceding a punishing reinforcer leads to conditioned avoidance (forward conditioning); by contrast, US-CS paring with the punishment preceding Temporally precise optogenetic activation of punishing dopaminergic neurons lead to antagonistic synaptic plasticity (Handler et al., 2019). Synaptic depression was mediated by DopR1 dopamine receptors, whereas synaptic potentiation involved

DopR2 dopamine receptors (Handler et al., 2019). It might be interesting to test in the future whether the different directions of plasticity observed here in the γ1 and the α'2 compartments might be based on a differential receptor expression as well.

The differential signs of plasticity correspond to the effects that the two MBONs involved in second-order conditioning exert on the PPL1-γ1pedc DAN, i.e., inhibitory and excitatory. This architecture of potentiating an excitatory connection while depressing an inhibitory connection (disinhibition) might serve a stabilizing function. Potentiating an excitatory input might rapidly increase the response of the postsynaptic reinforcing neurons, while a graded inhibition/disinhibition balance might keep the system within an appropriate working range. Optogenetically induced inhibition of the MBON-γ1pedc>α/β in coincidence with an odor stimulus has been reported to result in an aversive memory for that odor (König et al., 2019), which corroborates our findings in that its inhibition is not only required for second-order conditioning, but also sufficient. It will be interesting to see in the future whether optogenetic activation of the MBON-α'2 suffices as well for inducing a reinforcement signal. Overall, the characterization of the neuronal circuit underlying higher-order associative learning beyond computational modeling, i.e., in the "real world" and in a paradigmatic model system such as the fruit fly brain, might be helpful for our conceptual understanding of the acquisition of associative chains in general.

Acknowledgements

We are grateful to Betty Hong for proving a novel MB247-Gal4 strain, to the Janelia Research Campus and their FlyLight Project for providing numerous fly strains, to Amrita Paul Nishu, Eva Küsters, Marie Eileen Wiesenhavern and Julia Kniep for help with experiments, to Jan Hoffmann and Tobias Mühmer for constructing electronic

devices, to Muhammad Afaque Khan for help with programming, and to Sabyasachi Chakrabarty for assistance with data analysis. This work was funded by the German Research Council (DFG) through the Research Unit FOR 2705 “Dissection of a Brain Circuit: Structure, Plasticity and Behavioral Function of the *Drosophila* Mushroom Body” (project number 365082554) to AF and MN.

Author contributions

A.F. conceptualized and supervised the entire project. E.Y.R., S.H.D., Y.G., and C.H.L. designed and performed experiments, and analyzed data. A.M.J., M.S. and M.P.N. designed and performed a computational analysis. M.P.N. and S.L. supervised parts of the project. A.F. and E.Y.R. wrote the manuscript.

Figure 1

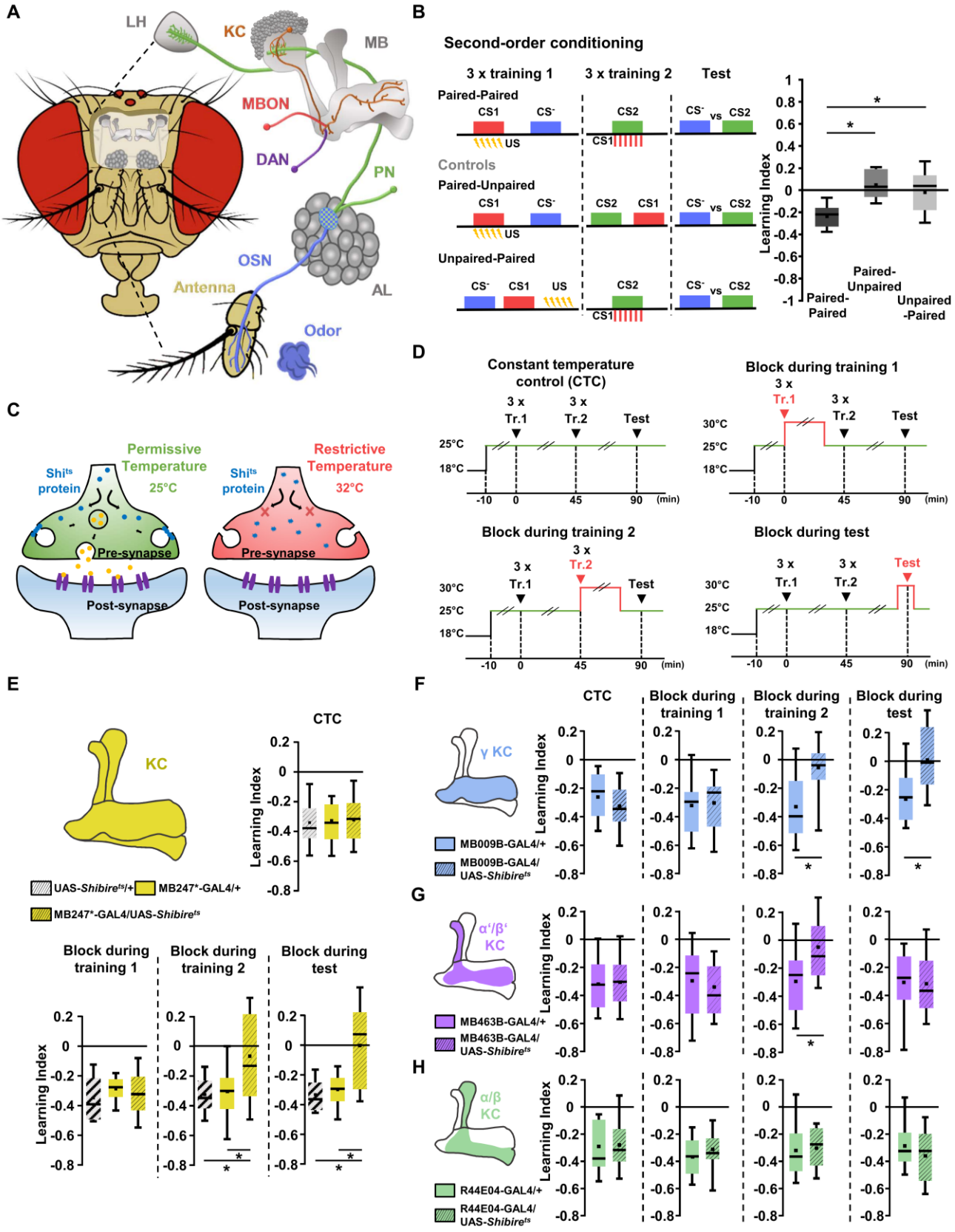
A
LH
KC
MB
MBON
DAN
PN
OSN
Antenna
AL
Odor
B
Second-order conditioning
3 x training 1
3 x training 2
Test
Paired-Paired
Controls
Paired-Unpaired
Unpaired-Paired
Learning Index
Paired-Paired
Paired-Unpaired
Unpaired-Paired
C
Permissive Temperature
25°C
Restrictive Temperature
32°C
Shi^ts protein
Pre-synapse
Post-synapse
D
Constant temperature control (CTC)
Block during training 1
Block during training 2
Block during test
3 x Tr.1
3 x Tr.2
Test
25°C
30°C
18°C
(min)
E
KC
CTC
Learning Index
UAS-Shibire^ts/+
MB247*-GAL4/+
MB247*-GAL4/UAS-Shibire^ts
Block during training 1
Block during training 2
Block during test
F
γ KC
MB009B-GAL4/+
MB009B-GAL4/ UAS-Shibire^ts
G
α'/β' KC
MB463B-GAL4/+
MB463B-GAL4/ UAS-Shibire^ts
H
α/β KC
R44E04-GAL4/+
R44E04-GAL4/ UAS-Shibire^ts

Figure 1: The mushroom body Kenyon cells are necessary for aversive second-order learning establishment

(A) Representation of the olfactory system of *Drosophila melanogaster*.

(B) Left: Schematic timeline of the second-order conditioning (SOC) paradigm with the unpaired controls. Rectangles represent the conditioned stimuli (red for CS1, blue for CS^-, and green for CS2), the sequence of aligned lightning bolts represents the electric shocks (unconditioned stimulus), and the dashed red boxes represent the pulses of the CS1 acting as reinforcement in the second training phase.
Right: Box plots show learning indices after second-order learning and the unpairing controls. The Shapiro-Wilk test was performed to confirm normal distribution. Statistical significance from baseline (0) was calculated using One-Sample T-tests with Bonferroni correction (see Table S1 in supplementary material and methods). For all groups, $n = 24$. Differences between groups were tested using one-way ANOVA with Tukey post-hoc tests. Box plots represent inter-quartile ranges (25% and 75%), squares indicate means, horizontal lines indicate medians, and whiskers show 10/90 values.

(C) Simplified sketch of spatio-temporal blocking of neurotransmission using the temperature sensitive mutation of *shibire*.

(D) Timeline representation of the protocols for selective thermo-genetic manipulation using $shibire^{ts}$ of distinct neuronal populations of the mushroom body circuitry during the different phases of first-order training, second order training or in the test phase.

(E) Upper left: a schematic depiction of the MB was highlighted along with color-coded boxes to indicate the used genotypes (empty boxes for genetic controls and striped boxes for experimental groups).
Upper right and bottom: Box plots represent learning indices after second-order learning while blocking, or not, the output from KCs in different training and test phases. The Shapiro-Wilk test was performed to confirm normal distribution. Statistical significance from baseline (0) was calculated using One-Sample T-tests with Bonferroni correction (see Table S1 in supplementary material and methods). For all groups, $n = 16$. Differences between groups were tested using one-way ANOVA with Tukey post-hoc tests. Box plots represent inter-quartile ranges (25%

and 75%), squares indicate means, horizontal lines indicate medians, and whiskers show 10/90 values.

(F-H) Left: schematic drawings of the different MB lobes were highlighted along with color-coded boxes to indicate the used genotypes (empty boxes for genetic controls and striped boxes for experimental groups).
Right: Box plots represent learning indices after SOC while blocking, or not, the individual output from γ-lobe (F), α‘/β‘-lobe (G), or α/β-lobe KCs (H) in different training and test phases. The Shapiro-Wilk test was performed to confirm normal distribution. Statistical significance from baseline (0) was calculated using One-Sample T-tests with Bonferroni correction (see Table S1 in supplementary material and methods). For all groups, n = 16. Differences between groups were tested using Two-Sample T-test with Welch correction. Box plots represent inter-quartile ranges (25% and 75%), squares indicate means, horizontal lines indicate medians, and whiskers show 10/90 values.

Figure 2

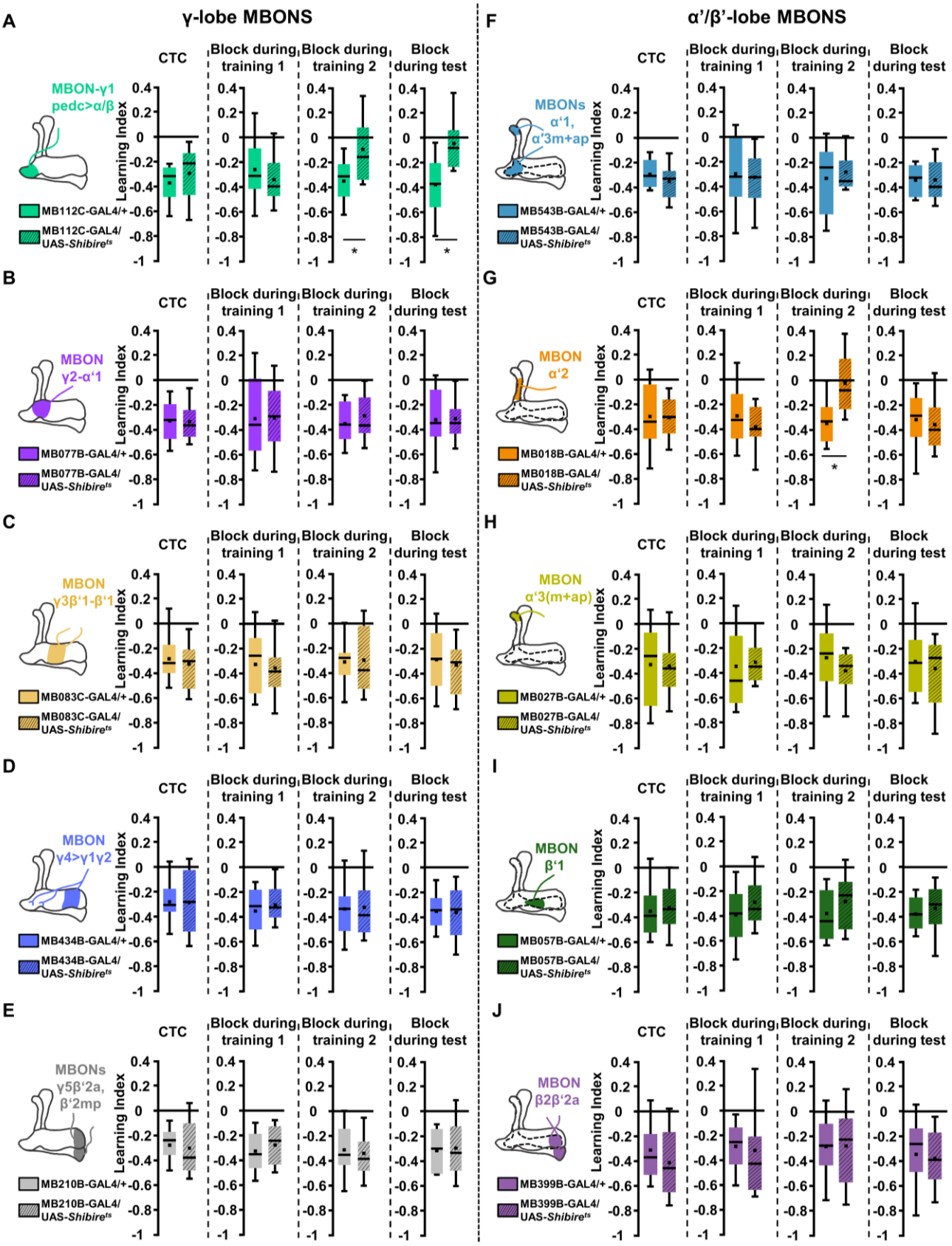
γ-lobe MBONS
α'/β'-lobe MBONS
A
B
C
D
E
F
G
H
I
J
CTC
Block during training 1
Block during training 2
Block during test
Learning Index
MBON-γ1 pedc>α/β
MB112C-GAL4/+
MB112C-GAL4/ UAS-Shibirets
MBON γ2-α'1
MB077B-GAL4/+
MB077B-GAL4/ UAS-Shibirets
MBON γ3β'1-β'1
MB083C-GAL4/+
MB083C-GAL4/ UAS-Shibirets
MBON γ4>γ1γ2
MB434B-GAL4/+
MB434B-GAL4/ UAS-Shibirets
MBONs γ5β'2a, β'2mp
MB210B-GAL4/+
MB210B-GAL4/ UAS-Shibirets
MBONs α'1, α'3m+ap
MB543B-GAL4/+
MB543B-GAL4/ UAS-Shibirets
MBON α'2
MB018B-GAL4/+
MB018B-GAL4/ UAS-Shibirets
MBON α'3(m+ap)
MB027B-GAL4/+
MB027B-GAL4/ UAS-Shibirets
MBON β'1
MB057B-GAL4/+
MB057B-GAL4/ UAS-Shibirets
MBON β2β'2a
MB399B-GAL4/+
MB399B-GAL4/ UAS-Shibirets

Figure 2: A screen through output neurons of the MB γ and α‘/β‘-lobes unveils an important role of neurotransmission from two distinct MBONs innervating the γ1 and α‘2 compartments in shaping second-order learning.

(A-J) Left: illustrations of the different MBONs and the MB compartment that they innervates were emphasized along with color-coded boxes to indicate the used genotypes (empty boxes for genetic controls and striped boxes for experimental groups).

Right: Box plots show learning indices after SOC while blocking, or not, the individual output from all MBONs innervating the different compartment of the MB γ-lobe (A-E) and α‘/β‘-lobe (F-J) in different training and test phases. The Shapiro-Wilk test was performed to confirm normal distribution. Statistical significance from baseline (0) was calculated using One-Sample T-tests with Bonferroni correction (see Table S1 in supplementary material and methods). For all groups, $n = 16$. Differences between groups were tested using Two-Sample T-test with Welch correction. Box plots represent inter-quartile ranges (25% and 75%), squares indicate means, horizontal lines indicate medians, and whiskers show 10/90 values.

Figure 3

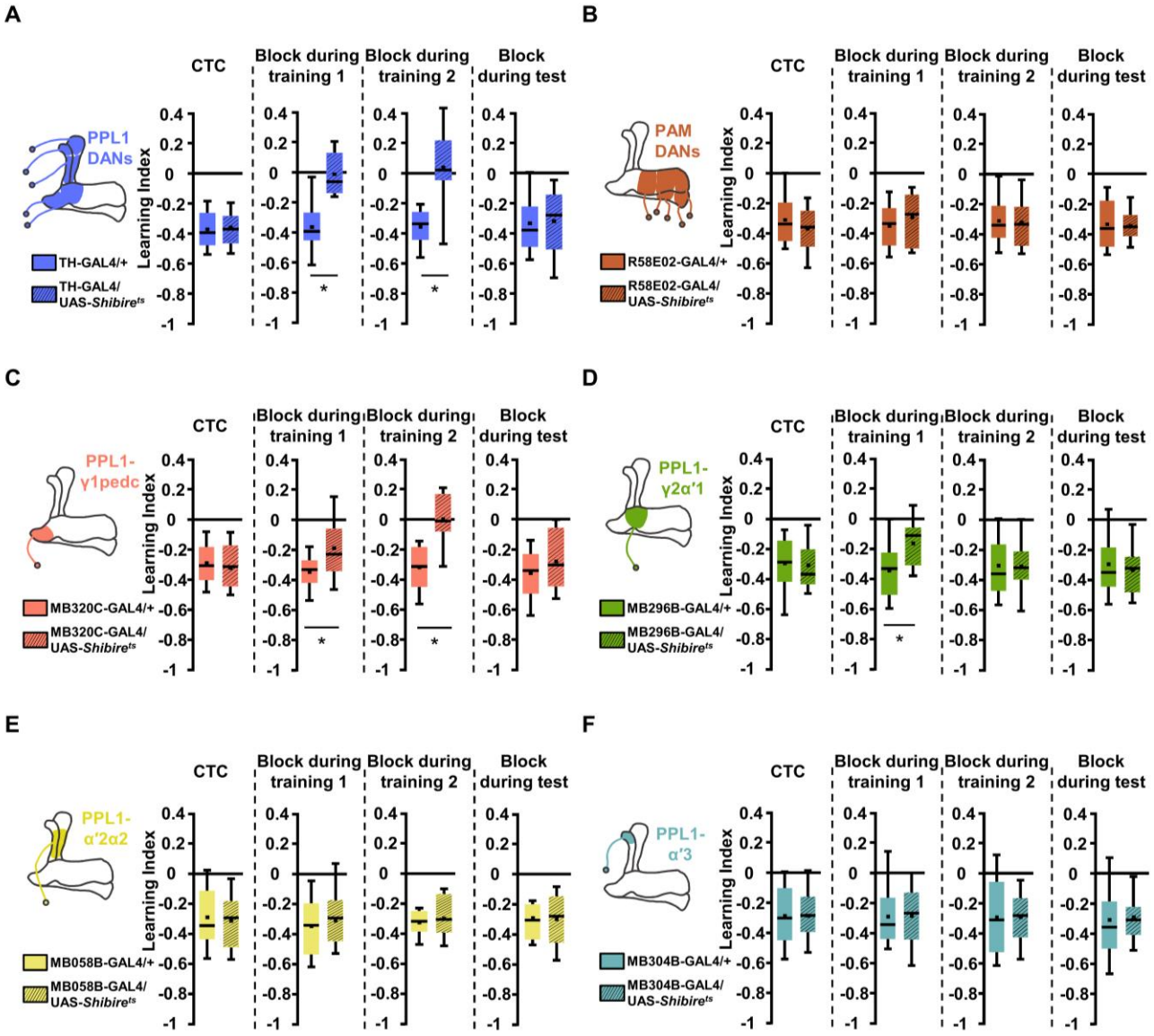
A
B
C
D
E
F
CTC
Block during training 1
Block during training 2
Block during test
Learning Index
PPL1 DANs
TH-GAL4/+
TH-GAL4/ UAS-Shibirets
PAM DANs
R58E02-GAL4/+
R58E02-GAL4/ UAS-Shibirets
PPL1-γ1pedc
MB320C-GAL4/+
MB320C-GAL4/ UAS-Shibirets
PPL1-γ2α'1
MB296B-GAL4/+
MB296B-GAL4/ UAS-Shibirets
PPL1-α'2α2
MB058B-GAL4/+
MB058B-GAL4/ UAS-Shibirets
PPL1-α'3
MB304B-GAL4/+
MB304B-GAL4/ UAS-Shibirets

Figure 3: Modulation from MB intrinsic neurons DANs is required in second-order memory establishment

(B-G) Left: Drawings represent the different DANs and the MB compartment that they innervates were highlighted and color-coded along with boxes indicating the used genotypes (empty boxes for genetic controls and striped boxes for experimental groups).

Right: Box plots represent performance indices after SOC while blocking, or not, neurotransmission of all punishing PPL1 (A) or rewarding PAM (B) DANs, together with individual PPL1 DANs innervating the different compartment of the MB (C-E) in different training and test phases. The Shapiro-Wilk test was performed to confirm normal distribution. Statistical significance from baseline (0) was calculated using One-Sample T-tests with Bonferroni correction (see Table S1 in supplementary material and methods). For all groups, $n = 16$. Differences between groups were tested using Two-Sample T-test with Welch correction. Box plots represent inter-quartile ranges (25% and 75%), squares indicate means, horizontal lines indicate medians, and whiskers show 10/90 values.

Figure 4

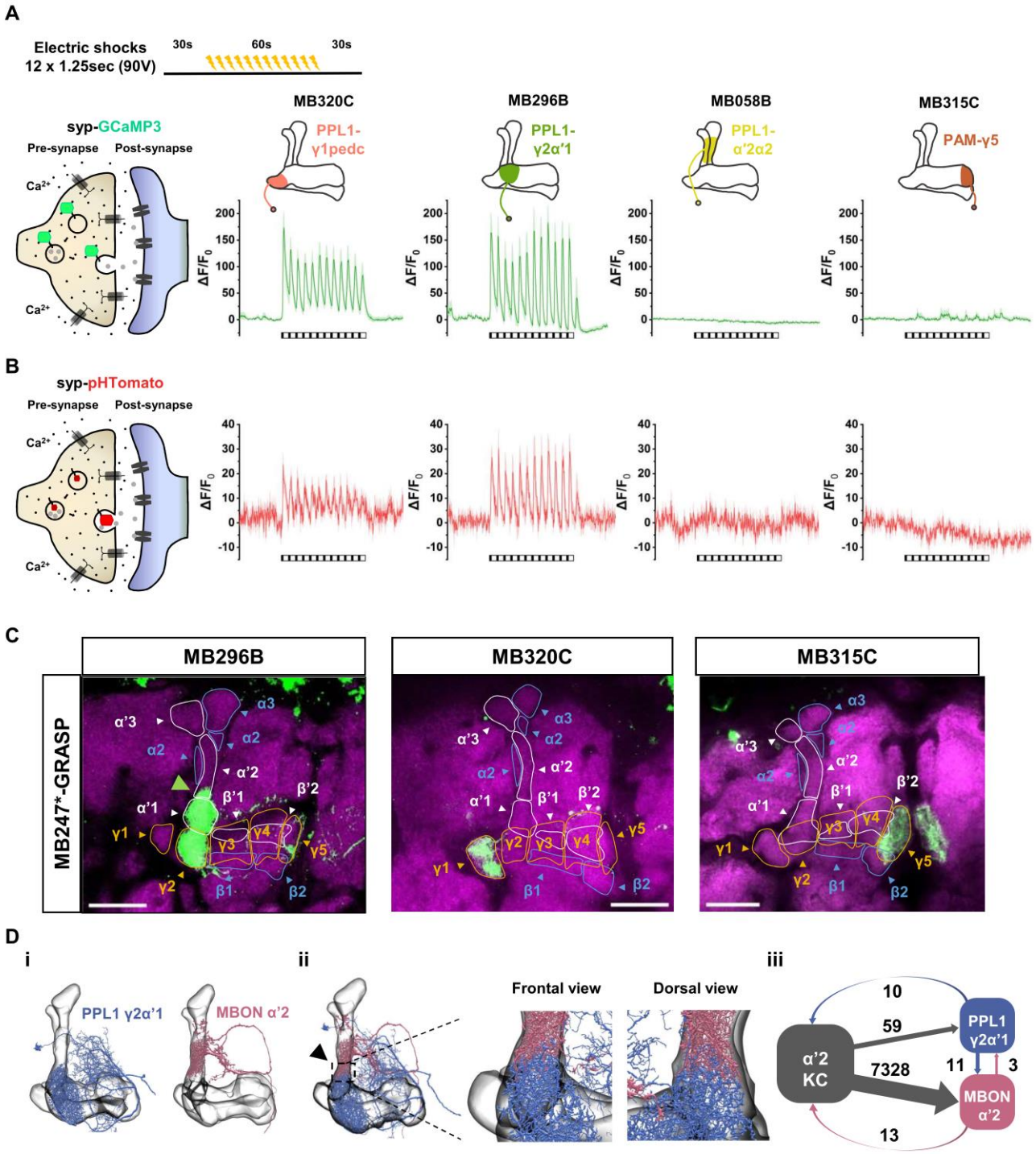
A
Electric shocks
12 x 1.25sec (90V)
30s
60s
30s
syp-GCaMP3
Pre-synapse
Post-synapse
Ca2+
Ca2+
MB320C
PPL1-γ1pedc
MB296B
PPL1-γ2α'1
MB058B
PPL1-α'2α2
MB315C
PAM-γ5
ΔF/F0
B
syp-pHTomato
Pre-synapse
Post-synapse
Ca2+
Ca2+
ΔF/F0
C
MB296B
MB320C
MB315C
MB247*-GRASP
α3
α'3
α2
α'2
β'1
β'2
α'1
γ1
γ2
γ3
γ4
γ5
β1
β2
D
i
PPL1 γ2α'1
MBON α'2
ii
Frontal view
Dorsal view
iii
10
59
7328
11
3
13
α'2 KC
PPL1 γ2α'1
MBON α'2

Figure 4: Collateral arborizations from γ2-α‘1 DAN leak to the α‘2 compartment of the KC and modulates it

(A) Upper left: Timeline scheme represents the shock-only imaging protocol where flies were imaged and simultaneously subjected to (90V x 12 pulses of 1.25 seconds every 5 seconds for 60 sec).
Left: Simplified illustration describes the pre-synaptic calcium indicator syp-GCaMP3 (fused to C-terminus of rat Synaptophysin).
Right: Shock-induced fluorescence changes of syp-GCaMP3 in individual PPL1-DANs (electric pulses are represented by horizontal rectangle with dashed black lines). For all groups, n = 8.

(B) Left: Simplified drawing shows the neurotransmitter release indicator syp-pHTomato in the lumen of synaptic vesicles (fused to the first intravesicular domain of rat Synaptophysin).
Right: Shock-induced fluorescence changes of syp-pHTomato in individual PPL1-DANs (electric pulses are represented by horizontal rectangle with dashed black lines). For all groups, n = 8.

(C) Representative confocal images showing the expression PPL1-γ1pedc (MB320C), PPL1-γ2α‘1 (MB296B), PAM-γ5 (MB315C) DANs in their MB compartments using of MB247-GRASP. The reconstituted split-GFP is shown in green and N-Cadherin in magenta to visualize the brain structures. Scale bars indicate 30 µm.

(D) (i-iii) Reconstruction and synaptic quantification of α‘2 compartment of the MB, PPL1-γ2α‘1 DAN and MBON-α‘2 using the neuPrint: Analysis Tools for EM Connectomics by Janelia (PPL1-γ2α‘1 DAN: id #5813022424 and MBON-α‘2: id #1139667240).

Figure 5

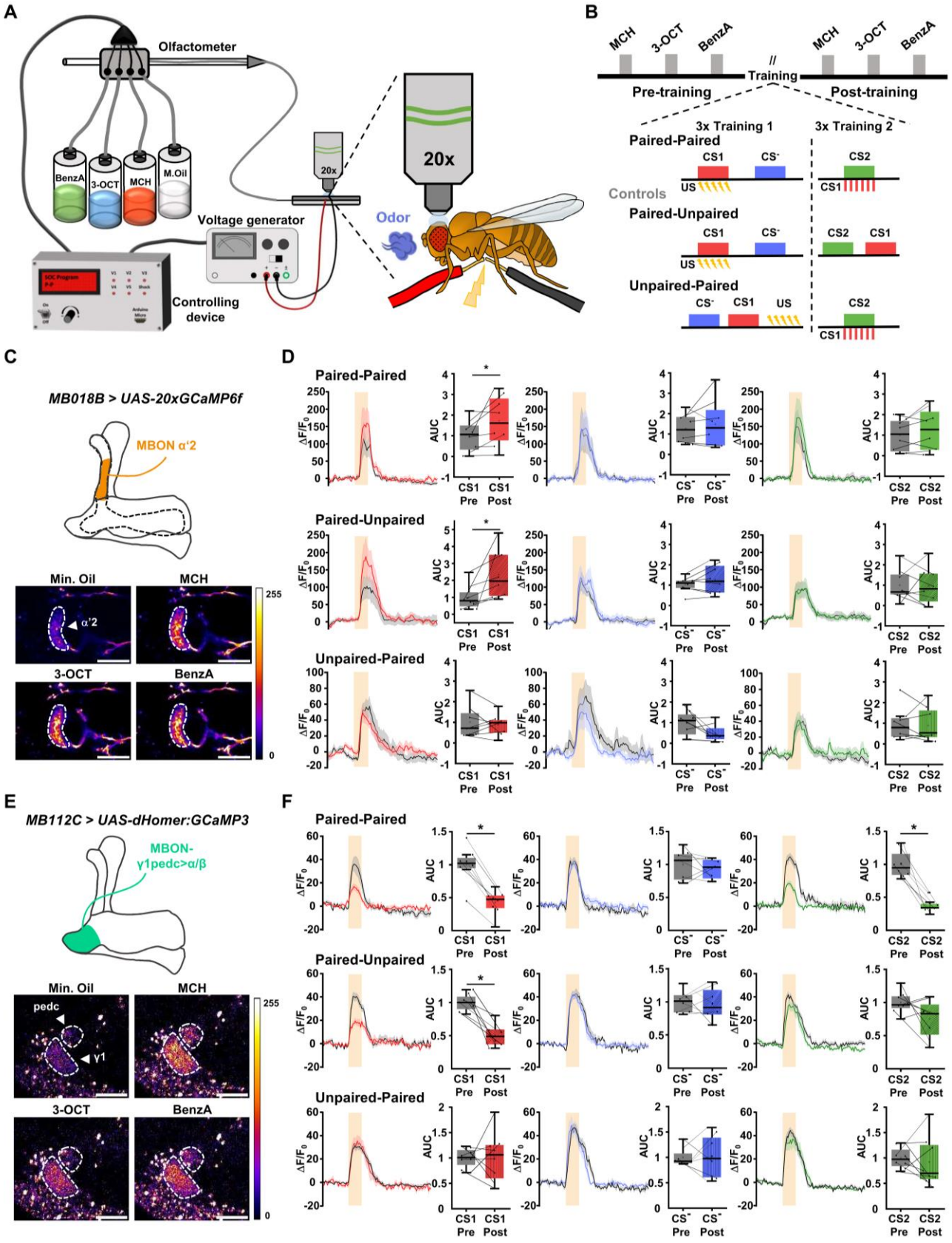
A
Olfactometer
BenzA
3-OCT
MCH
M.Oil
Voltage generator
Controlling device
20x
Odor
B
MCH
3-OCT
BenzA
Training
Pre-training
Post-training
3x Training 1
3x Training 2
Paired-Paired
Controls
Paired-Unpaired
Unpaired-Paired
CS1
CS-
CS2
US
C
MB018B > UAS-20xGCaMP6f
MBON α'2
Min. Oil
MCH
3-OCT
BenzA
α'2
255
0
D
Paired-Paired
Paired-Unpaired
Unpaired-Paired
ΔF/F0
AUC
CS1 Pre
CS1 Post
CS- Pre
CS- Post
CS2 Pre
CS2 Post
E
MB112C > UAS-dHomer:GCaMP3
MBON-γ1pedc>α/β
pedc
γ1
F

Figure 5: Functional imaging of the post-synaptic changes in the mushroom body output after SOC training

(A) Left: Drawing shows the custom-built set-up for imaging SOC using a two-photon microscope.
Right: Cartoon illustration demonstrating odors and electric shocks being presented to a dissected fly head connected to the microscope's objective with with a Ringer's solution drop.

(B) Timeline of the imaging protocol of the SOC paradigm. The same training paradigm along with the two controls as described in Figure 1B were used in this experiment. Each experiment was preceded (pre-training) and followed (post-training) by a sequence of the three used odorants that were imaged to assess the baseline odor-evoked activity in each region.

(C&E) Top: Schematic drawing that highlights the two regions of interest that were imaged at their post-synaptic sites (MBON-γ1pedc>α/β and MBON-α'2).
Bottom: Pseudo-colored example images show the odor-evoked reaction of post-synaptic region of the MBON-γ1pedc>α/β (D) or MBON-α'2 (F) to the used odorants and mineral oil. Scale bars indicate 10 µm.

(D&F) MBON-α'2 (D) and MBON-γ1pedc>α/β (F) odor-evoked calcium responses measured before (pre-training) and after (post-training) SOC, using respectively GCaMP6f and d-Homer-GCaMP, in the three training protocols ("Paired-Paired", "Paired-Unpaired" and "Unpaired-Paired"). Lines indicate the mean calcium traces, and shaded areas represent SEMs. The black line in each graph represents the pre-training response and the colored lines represent the post-training responses per condition. The shaded orange rectangles indicate the total duration of odor presentations (3 seconds). Box plots represent areas under the curve (AUC) of the pre- and post-training calcium traces. The Shapiro-Wilk test was performed to confirm normal distribution. For all groups, $n = 8$. Differences between groups were tested using Paired-Sample T-test. Box plots represent inter-quartile ranges (25% and 75%), squares indicate means, horizontal lines indicate medians, and whiskers show 10/90 values. Diagonally striped boxes represent the AUC of post-training responses in the "Paired-Unpaired" protocol and the vertically striped boxes are for the AUC of post-training responses in the "Unpaired-Paired" protocol.

Figure 6

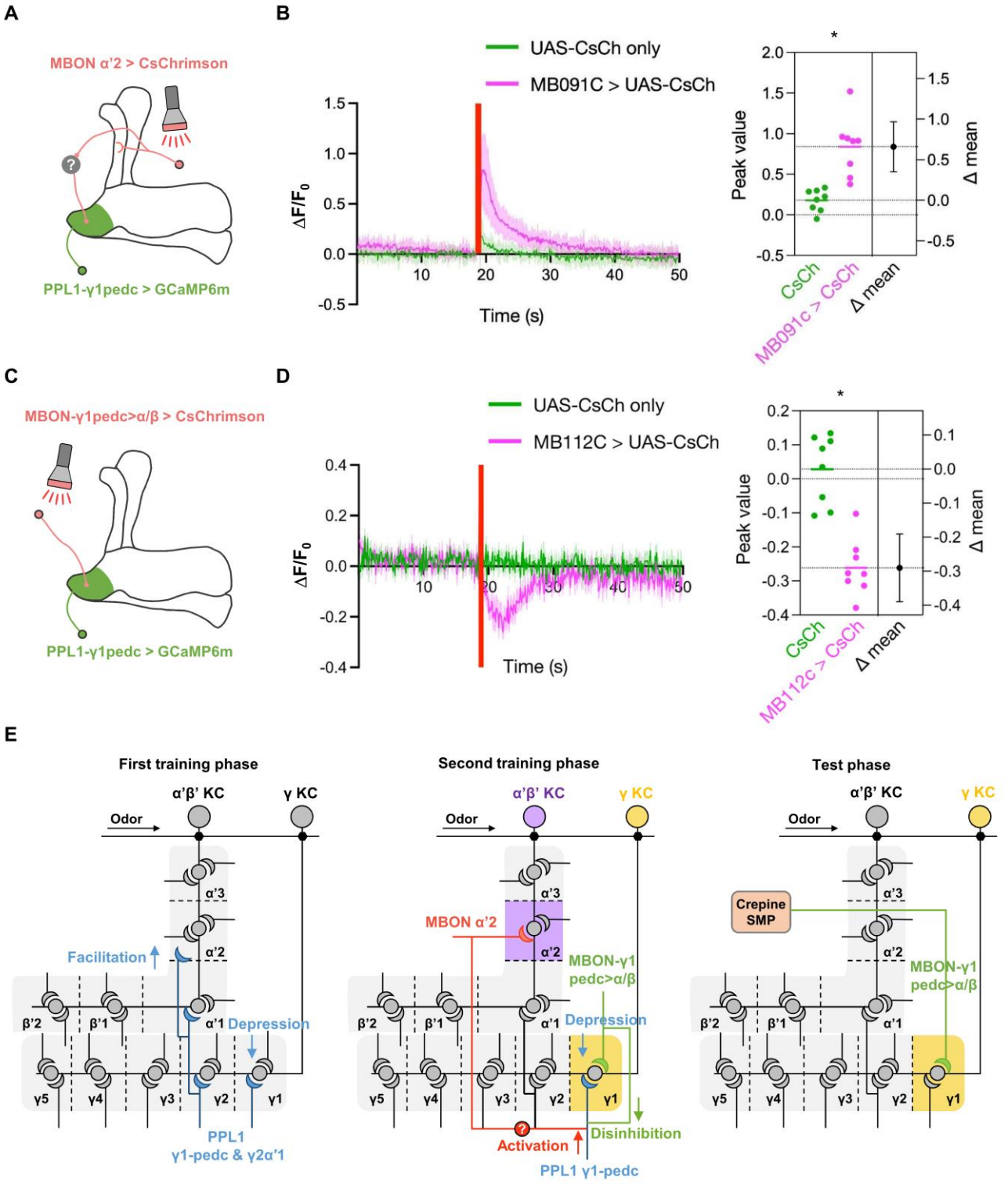
A
MBON α'2 > CsChrimson
PPL1-γ1pedc > GCaMP6m
B
UAS-CsCh only
MB091C > UAS-CsCh
ΔF/F0
Time (s)
Peak value
Δ mean
CsCh
MB091c > CsCh
C
MBON-γ1pedc>α/β > CsChrimson
PPL1-γ1pedc > GCaMP6m
D
UAS-CsCh only
MB112C > UAS-CsCh
ΔF/F0
Time (s)
Peak value
Δ mean
CsCh
MB112c > CsCh
E
First training phase
α'β' KC
γ KC
Odor
α'3
α'2
Facilitation
β'2
β'1
α'1
Depression
γ5
γ4
γ3
γ2
γ1
PPL1
γ1-pedc & γ2α'1
Second training phase
α'β' KC
γ KC
Odor
α'3
MBON α'2
α'2
MBON-γ1
pedc>α/β
β'2
β'1
α'1
Depression
γ5
γ4
γ3
γ2
γ1
Activation
Disinhibition
PPL1 γ1-pedc
Test phase
α'β' KC
γ KC
Odor
Crepine
SMP
α'3
α'2
MBON-γ1
pedc>α/β
β'2
β'1
α'1
γ5
γ4
γ3
γ2
γ1

Figure 6: Activity dependent bidirectional feedback from MBON-γ1pedc>α/β and MBON-α‘2 onto PPL1-γ1pedc DAN is responsible for aversive SOC

(A&C) Schematic illustration demonstrates optogenetic activation of MBON-α‘2 (A) or MBON-γ1pedc>α/β (C) using CsChrimson and simultaneously monitoring the calcium activity by expressing GCaMP6m in the PPL1-γ1pedc DAN using the LexA-LexAOp system.

(B&D) Left: GCaMP6m signals in PPL-γ1pedc DAN in response to the optogenetic activation of MBON-α‘2 (B) and MBON-γ1pedc>α/β (D). TH-LexA was used to drive LexAop-GCaMP6m expression in all PPL1 DANs. MB091C and MB112C were used to drive UAS-CsChrimson (CsCh) expression respectively in MBON-α‘2 (B) and MBON-γ1pedc>α/β (D) (magenta trace). A train of 20 red light pulses lasting for 0.5 s activated the MBONs and is indicated by the red vertical bar. GCaMP6m signals in the UAS-CsCh only control brains are also shown (green trace).
Right: Comparison is shown between the maximum values of the evoked responses in the UAS-CsCh-only (green) and MB091C (B) or MB112C (D) > UAS-CsCh (magenta) groups. This estimation plot displays peak values in the left column and the mean difference with the 95% confidence interval in the right column. For all groups, n = 8. The Shapiro-Wilk test was performed to confirm normal distribution. Since equal variance was not assumed, the light-evoked responses in the two groups were compared using an Unpaired Two-Sample T-test with Welch’s correction.

(E) Circuit diagram representing MB neuronal circuits underlying the first training (left), the second training (middle), and the test phases (right) of the SOC paradigm.

Figure 7

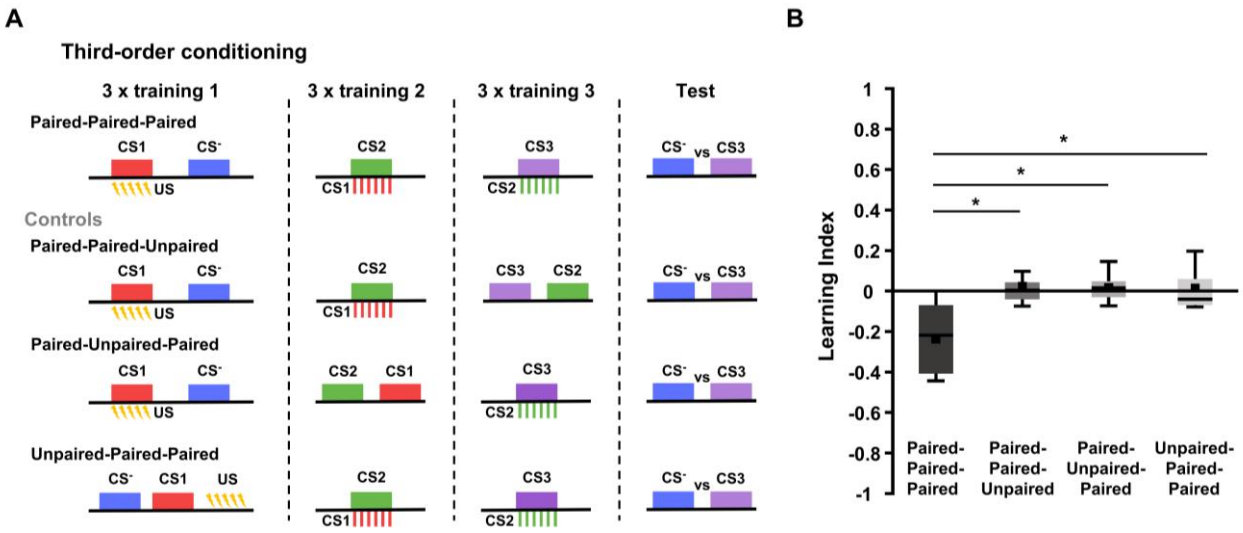

Figure 7: Higher-order associative chains in *Drosophila melanogaster*

(A) Schematic timeline of the third-order conditioning (TOC) paradigm together with the unpaired controls. Rectangles represent the conditioned stimuli (red for CS1, blue for CS^-, green for CS2, and purple for CS3), the sequence of aligned lightning bolts represents the electric shocks (unconditioned stimulus), and the dashed red and green boxes represent the pulses of the CS1 and CS2 respectively acting as reinforcements in the second and third training phases.

(B) Box plots showing learning indices after TOC and unpairing the reinforcement from the stimuli during the three training phases (unpaired controls). The Shapiro-Wilk test was performed to reject normal distribution. Statistical significance from baseline (0) was calculated using Wilcoxon One-Sample Signed-Rank test with Bonferroni correction (see Table S1 in supplementary material and methods). For all groups, $n = 8$. Differences between groups were tested using a Kruskal-Wallis ANOVA with Dunn's post-hoc tests. Box plots represent inter-quartile ranges (25% and 75%), squares indicate means, horizontal lines indicate medians, and whiskers show 10/90 values.

Supplementary Figure 1

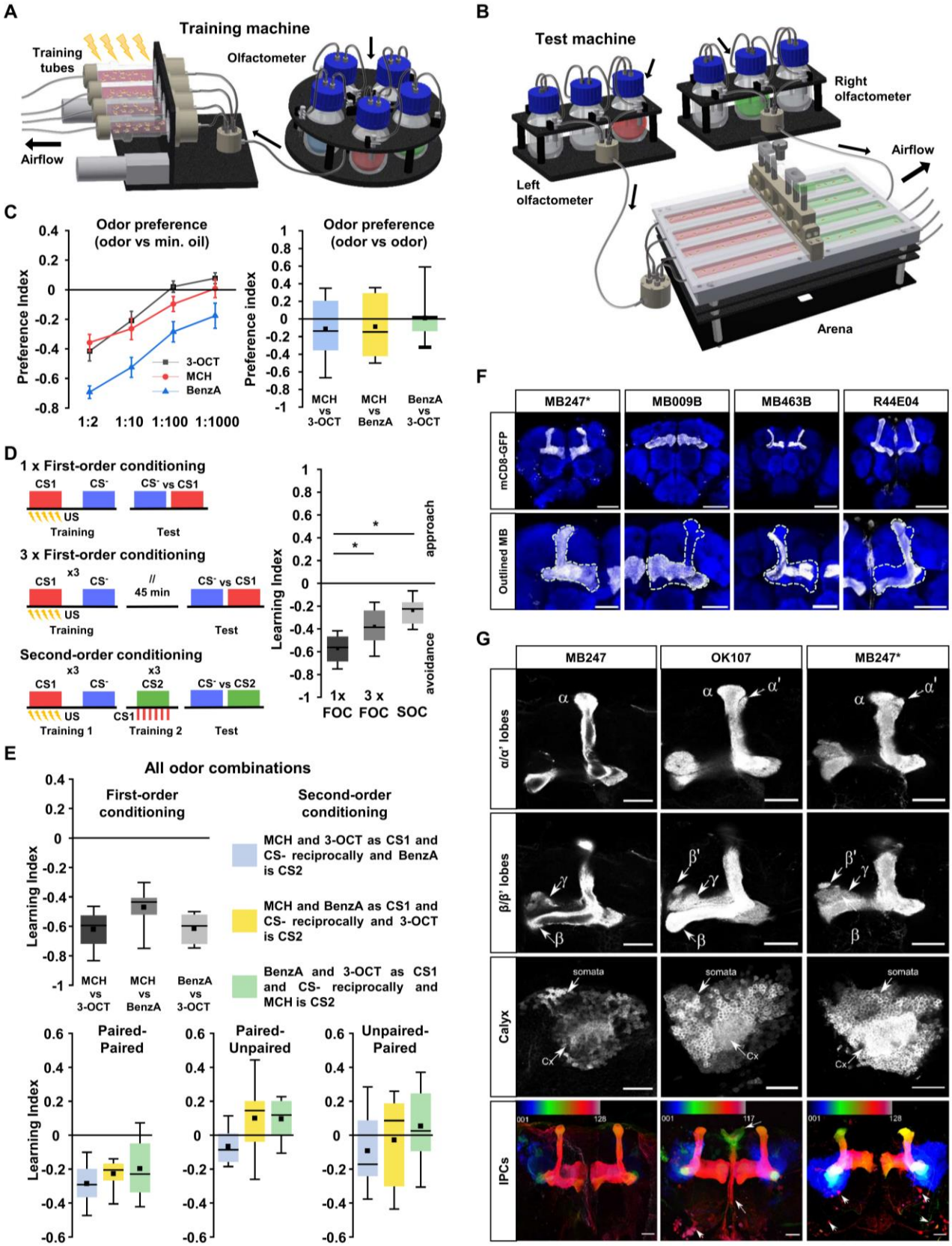

Supplementary Figure 1: Establishing a new custom-built automatized apparatus for higher-order olfactory conditioning in *Drosophila* and introducing a new MB pan neuronal driver line

(A) Training machine composed of four double-wired copper electric tubes that can be connected to a voltage generator and an olfactometer with different odor bottles. An Arduino programmed custom-built device controls shock and odor automatically by providing precise input to the voltage generator and the valves of the olfactometer.

(B) Test machine comprises an arena that contains a central carrier where the flies are loaded, four lanes to test the same groups that were trained all at once and infrared LEDs under these lanes for video acquisition, along with two olfactometers connected to both sides of said arena. The test procedure is filmed using a high-speed camera (Basler GigE camera acA 1300 – 60gc / CS – mount) with an objective (Lens Kowa 4.4-11mm zoom lens) that is equipped with an IR filter. A second custom-built controlling device provides input to the arena and the olfactometers.

(C) Left: An odor concentration gradient (1:2, 1:10, 1:100 and 1:1000) was performed to assess the naïve level of aversion that each odor evoke in the flies. The odors were presented against mineral oil and the side bias was accounted for.
Right: odor concentrations that evoke a similar naïve odor aversion were tested in all combination to verify the odor balance. The Shapiro-Wilk test was performed to confirm normal distribution. Statistical significance from baseline (0) was calculated using One-Sample T-tests with Bonferroni correction. For all groups, $n = 8$. Differences between groups were tested using one-way ANOVA with Tukey post-hoc tests. Box plots represent inter-quartile ranges (25% and 75%), squares indicate means, horizontal lines indicate medians, and whiskers show 10/90 values.

(D) Left: Timeline representation of the three used paradigms (1x FOC, 3x FOC and SOC). Rectangles represent the conditioned stimuli (red for CS1, blue for CS^-, and green for CS2), the sequence of aligned lightning bolts represents the electric shocks (unconditioned stimulus), and the dashed red boxes represent the pulses of the CS1 acting as reinforcement in the second training phase of SOC.
Right: Box plots showing learning indices after either one trial of FOC, 3 trials of FOC with a 45 minute gap between the training and testing or SOC. The Shapiro-Wilk test was performed to confirm normal distribution. Statistical significance from baseline

(0) was calculated using One-Sample T-tests with Bonferroni correction (see Table S1 in supplementary material and methods). For all groups, $n = 24$. Differences between groups were tested using one-way ANOVA with Tukey post-hoc tests. Box plots represent inter-quartile ranges (25% and 75%), squares indicate means, horizontal lines indicate medians, and whiskers show 10/90 values.

(E) All possible odor combinations were tested for the FOC and SOC paradigms and show no significant difference in their assignment to neither CS1 and CS- or CS2 conditions. The Shapiro-Wilk test was performed to confirm normal distribution. Statistical significance from baseline (0) was calculated using One-Sample T-tests with Bonferroni correction. For all groups, $n = 8$. Differences between groups were tested using one-way ANOVA with Tukey post-hoc tests. Box plots represent inter-quartile ranges (25% and 75%), squares indicate means, horizontal lines indicate medians, and whiskers show 10/90 values.

(F) Example confocal images showing the expression pattern of the GAL4 driver lines used in the behavioral study in Figure 1E-H by crossing these drivers to membrane bound mCD8::GFP. The GFP signal is shown in gray and discs large (DLG) in blue to visualize the brain structures. Scale bars in the upper images indicate 100 µm, and the bars in the outlined pictures on the bottom represent 30 µm.

(G) One focal plane images showing the vertical and horizontal lobes, and the calyx of the MB demonstrate that the new MB247*-GAL4 driver line targets the prime lobes in its expression pattern as opposed to the old MB247-GAL4 line. In addition, color-coded Z-projections show the absence of the insulin-producing cells (IPCs) in the MB247*-GAL4 in contrast to the OK107-GAL line. Scale bars represent 30 µm.

Supplementary Figure 2

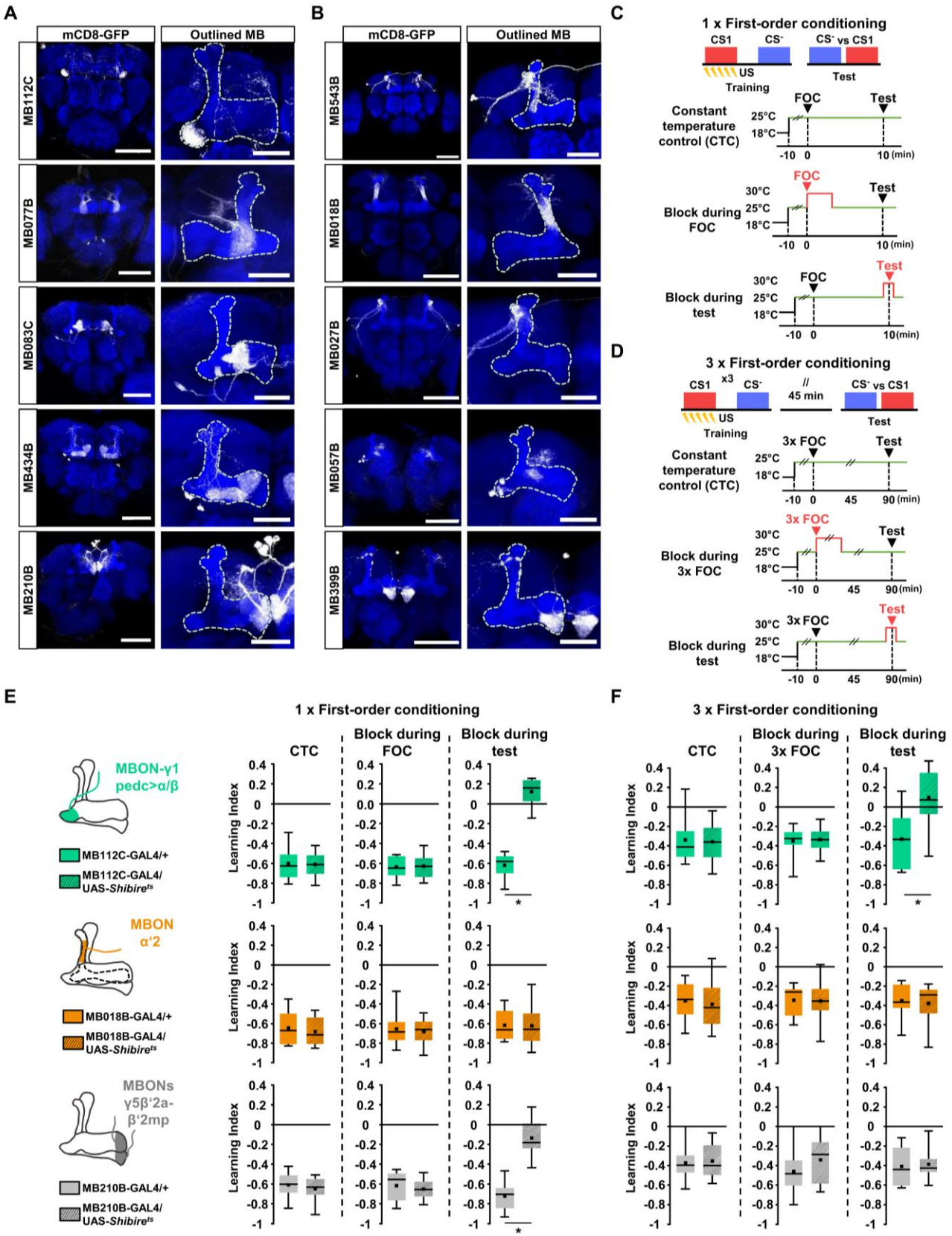

Supplementary Figure 2: Behavioral dissection of MBONs underlying FOC

(A-B) Representative confocal images showing the expression pattern of the GAL4 driver lines used in the behavioral study in Figure 2 by crossing these drivers to membrane bound mCD8::GFP. GFP signal is shown in gray and discs large (DLG) in blue to visualize the brain structures. Scale bars in the upper images indicate 100 µm, and the bars in the outlined pictures on the bottom represent 30 µm.

(C-D) Top: timeline scheme for showing the experimental design of the one trial FOC (C) and three trials of FOC (D) paradigms.
Bottom: Timeline schemes depicting the experimental procedure for selective thermo-genetic manipulation using *shibire*^{ts} of distinct MBONs during the different training and test phases of one trial FOC (C) and three trials FOC (D).

(E-F) Left (E): schematic illustrations of the different MBONs were highlighted along with the compartment they innervate; in addition to color-coded boxes to indicate the used genotypes (empty boxes for genetic controls and striped boxes for experimental groups).
Right (E) and (F): Box plots show learning indices after SOC while blocking, or not, the individual transmission from MBON-γ1pedc>α/β (top), MBON-α‘2 (middle) or MBON-γ5β‘2a-β‘2mp (bottom) MBONs. The Shapiro-Wilk test was performed to confirm normal distribution. Statistical significance from baseline (0) was calculated using One-Sample T-tests with Bonferroni correction (see Table S1 in supplementary material and methods). For all groups, n = 8. Differences between groups were tested using Two-Sample T-test with Welch correction. Box plots represent inter-quartile ranges (25% and 75%), squares indicate means, horizontal lines indicate medians, and whiskers show 10/90 values.

Supplementary Figure 3

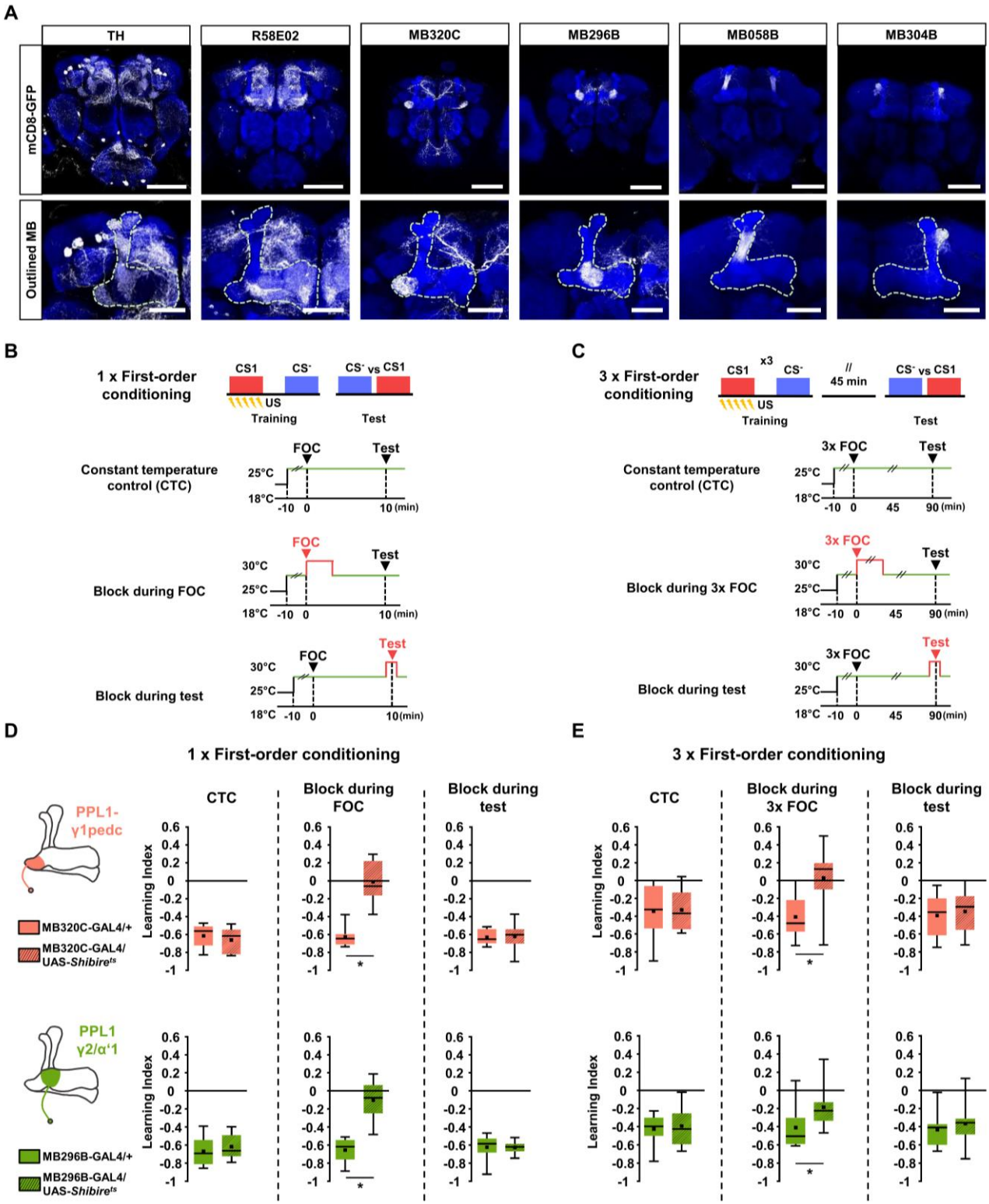

Supplementary Figure 3: Behavioral dissection of the DANs underlying FOC

(A) Representative confocal images showing the expression pattern of the GAL4 driver lines used in the behavioral study in Figure 3 by crossing these drivers to mCD8::GFP. GFP signal is shown in gray and DLG in blue to visualize the brain structures. Scale bars in the upper images indicate 100 µm, and the bars in the outlined pictures on the bottom represent 30 µm.

(B-C) Top, Timeline depiction shows the experimental design of the one trial FOC (B) and three trials of FOC (C) paradigms.
Bottom: Experimental procedures for selective thermo-genetic manipulation using *shibire*^{ts} of PPL1-γ1pedc and PPL1-γ2α‘1 DANs during the different training and test phases of one trial FOC (B) and three trials FOC (C).

(D&E) Left (D): Highlight drawings of the two DANs and the MB compartment that they project to along with color-coded boxes to indicate the used genotypes (empty boxes for genetic controls and striped boxes for experimental groups).
Right (D) and (E): Box plots represent performance indices after SOC while blocking, or not, the individual neurotransmission from PPL1-γ1pedc (top) and PPL1-γ2α‘1 (bottom) DANs. The Shapiro-Wilk test was performed to confirm normal distribution. Statistical significance from baseline (0) was calculated using One-Sample T-tests with Bonferroni correction (see Table S1 in supplementary material and methods). For all groups, n = 8. Differences between groups were tested using Two-Sample T-test with Welch correction. Box plots represent inter-quartile ranges (25% and 75%), squares indicate means, horizontal lines indicate medians, and whiskers show 10/90 values.

Supplementary Figure 4

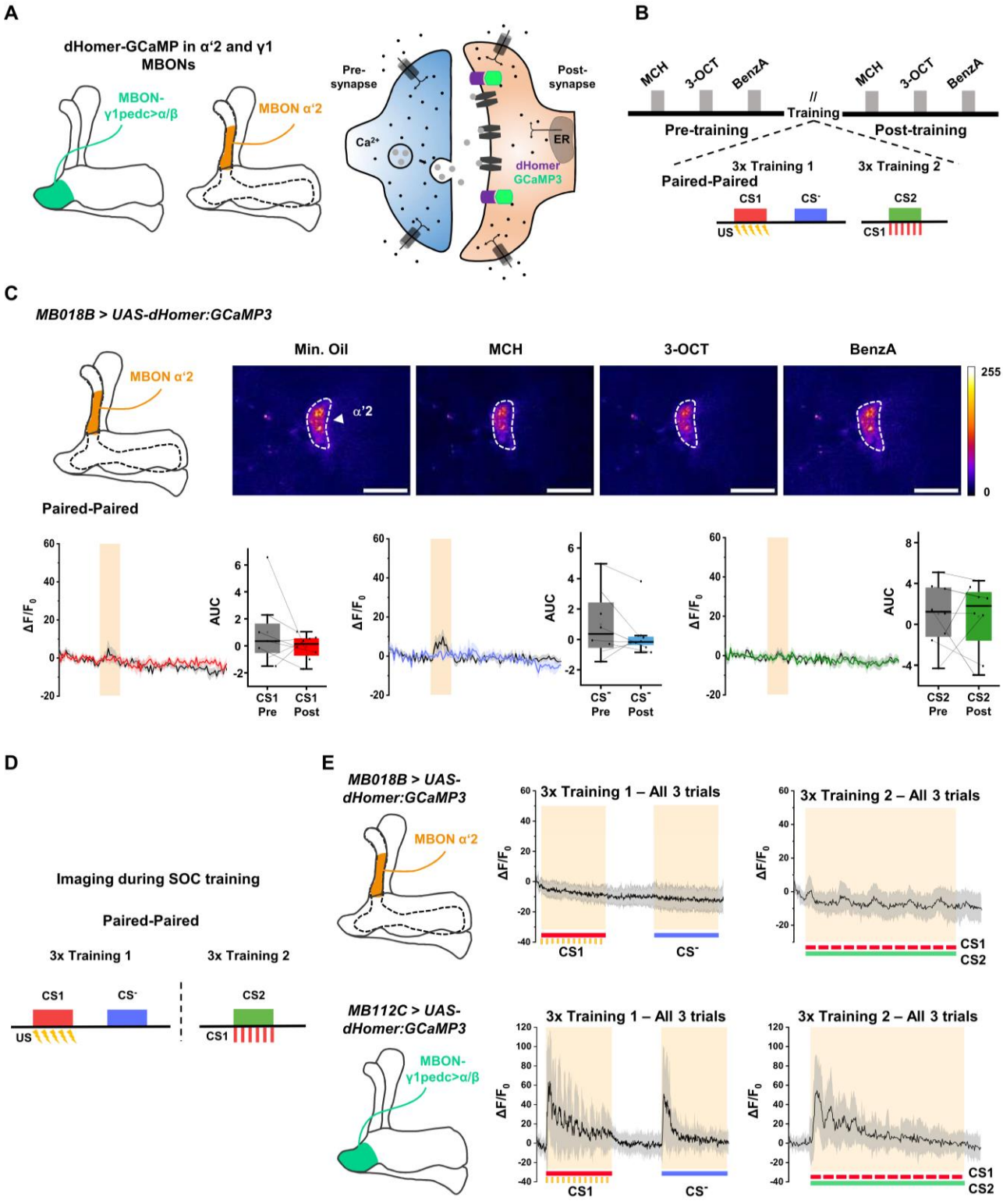

Supplementary Figure 4: Functional imaging of the post-synaptic changes in the mushroom body output after SOC training

(A) Left: Schematic drawing that highlights the two regions of interest that were imaged at post-synaptic sites of MBON-γ1pedc>α/β and MBON-α‘2.
Right: Simplified illustration describes the post-synaptic calcium indicator dHomer-GCaMP3 (fused to C-terminus of *dHomer*).

(B) Timeline for imaging pre- and post-training calcium traces in the SOC paradigm (“Paired-Paired” protocol only).

(C) Top left: Illustration emphasizes the post-synaptic sites of MBON-α‘2.
Top right: Pseudo-colored images exemplify odor-evoked reactions of post-synaptic region MBON-α‘2 to the used odorants and mineral oil. Scale bars indicate 10 µm.

Bottom: Odor-evoked calcium responses in post-synaptic sites of MBON-α‘2 measured before (pre-training) and after (post-training) the SOC paradigm. Lines indicate the mean calcium traces, and shaded areas represent SEMs. The black line in each graph represents the pre-training response and the colored lines represent the post-training responses per condition. The shaded orange rectangles indicate the total duration of odor presentations (3 seconds). Box plots represent areas under the curve (AUC) of the pre- and post-training calcium traces. The Shapiro-Wilk test was performed to confirm normal distribution. For all groups, $n = 8$. Differences between groups were tested using Paired-Sample T-test. Box plots represent inter-quartile ranges (25% and 75%), squares indicate means, horizontal lines indicate medians, and whiskers show 10/90 values.

(D) Timeline for imaging all the training phases (3x training 1 and 3x training 2) of the SOC paradigm (“Paired-Paired” protocol only).

(E) Post-synaptic MBON-α‘2 (top) MBON-γ1pedc>α/β (bottom) odor-evoked calcium responses during the training phases of the “Paired-Paired” protocol of SOC. Black lines in each trace indicate the mean calcium traces, and shaded areas represent SEMs. The shaded orange rectangles indicate the total duration of either the whole CS1, CS^- in the first training phases, or simultaneous CS1 and CS2 presentation in the second training phases. Under each graph of the first training phases, red elongated bars represent the conditioned stimuli CS1, the blue ones represent CS^-,

and the sequence of aligned yellow rectangles are 12 pulses of electric shocks (unconditioned stimulus). Under the graphs of the second training phases, the dashed red boxes represent the pulses of the CS1 acting as reinforcement in the second training phase and the long green bar is the CS2.

STAR METHODS

Key resources table

REAGENT OR RESOURCE	SOURCE	IDENTIFIER
Antibodies		
Mouse anti-discs large (DLG)	Developmental Studies Hybridoma Bank	Cat#4F3; RRID: AB_528203
Rabbit anti-GFP	Invitrogen	Cat#A-6455; RRID: AB_221570
Mouse anti-IgG (AlexaFluor 633)	Invitrogen	Cat#A-21050; RRID: AB_2535718
Rabbit anti-IgG (AlexaFluor 488)	Invitrogen	Cat#A-11034; RRID: AB_2576217
Rat anti-Cadherin, DN- (extracellular domain)	Developmental Studies Hybridoma Bank	Cat# DN-Ex #8; RRID: AB_528121
Mouse monoclonal anti-green fluorescent protein (GFP) – clone GFP-20	Sigma-Aldrich	Cat#G6539
Chemicals, peptides, and recombinant proteins		
Triton™ X-100	Sigma-Aldrich	Cat# X100; CAS: 9036-19-5
Bovine Serum Albumin (BSA)	Carl Roth GmbH + Co. KG	Cat#0163; CAS: 90604-29-8
Normal goat serum (NGS)	Invitrogen - Thermo Fisher Scientific	Cat#31873; RRID AB_2532167
Paraformaldehyde (PFA)	Carl Roth GmbH + Co. KG	Cat#0335; CAS: 30525-89-4
Mineral Oil	Sigma-Aldrich	Cat#M8410; CAS: 8042-47-5
4-Methycyclohexanol	Sigma-Aldrich	Cat#153095; CAS: 589-91-3

3-Octanol	Sigma-Aldrich	Cat#218405; CAS: 589-98-0
Benzaldehyde	Sigma-Aldrich	Cat#12010; CAS: 100-52-7
	Sigma-Aldrich	Cat#109584; CAS: 628-63-7
VECTASHIELD® Antifade Mounting Medium	Vector Laboratories Inc	Cat#H-1000; CAS: Trade Secret
All-trans-retinal	Sigma, MO, USA	Cat# R2500; CAS: 116-31-4
Experimental models: organisms/strains		
D. melanogaster: Canton-S	Bloomington Drosophila Stock Center; Lindsley and Grell, 1968	BDSC: 64349 ; FlyBase: FBst0064349
D. melanogaster: w[1118]	Bloomington Drosophila Stock Center; Hoskins et al., 2001	BDSC: 6326 ; FlyBase: FBst0006326
D. melanogaster: UAS-Shibire^{ts}	Bloomington Drosophila Stock Center; Kasuya et al., 2009	BDSC: 44222 ; FlyBase: FBst0044222
D. melanogaster: MB247BH-GAL4	This study	Generated by Elizabeth J. Hong. (The Hong lab) California Institute of Technology. Department of Biology and Bioengineering. 1200 E. California Blvd M/C 216-76. Pasadena, CA 91125
D. melanogaster: MB009B-splitGAL4	Bloomington Drosophila Stock Center; Aso et al., 2014a	BDSC: 68292 ; FlyBase: FBst0068292

D. melanogaster: MB463B-splitGAL4	Bloomington Drosophila Stock Center; Aso et al., 2014a	BDSC: 68370 ; FlyBase: FBst0068370
D. melanogaster: R44E04-GAL4	Bloomington Drosophila Stock Center; Jenett et al., 2012	BDSC: 50210 ; FlyBase: FBst0050210
D. melanogaster: TH-GAL4	Bloomington Drosophila Stock Center, Riemensperger et al., 2013	BDSC: 8848 ; FlyBase: FBst0008848
D. melanogaster: R58E02-GAL4	Bloomington Drosophila Stock Center; Jenett et al., 2012	BDSC: 41347 ; FlyBase: FBst0041347
D. melanogaster: MB320C-splitGAL4	Bloomington Drosophila Stock Center; Aso and Rubin, 2016	BDSC: 68253 ; FlyBase: FBst0068253
D. melanogaster: MB296B-splitGAL4	Bloomington Drosophila Stock Center; Aso et al., 2014a	BDSC: 68308 ; FlyBase: FBst0068308
D. melanogaster: MB058B-splitGAL4	Bloomington Drosophila Stock Center; Aso et al., 2014a	BDSC: 68278 ; FlyBase: FBst0068278
D. melanogaster: MB304B-splitGAL4	Bloomington Drosophila Stock Center; Aso et al., 2014a	BDSC: 68367 ; FlyBase: FBst0068367

D. melanogaster: MB112C-splitGAL4	Bloomington Drosophila Stock Center; Aso et al., 2014a	BDSC: 68263 ; FlyBase: FBst0068263
D. melanogaster: MB077B-splitGAL4	Bloomington Drosophila Stock Center; Aso et al., 2014a	BDSC: 68283 ; FlyBase: FBst0068283
D. melanogaster: MB083C-splitGAL4	Bloomington Drosophila Stock Center; Aso et al., 2014a	BDSC: 68287 ; FlyBase: FBst0068287
D. melanogaster: MB434B-splitGAL4	Bloomington Drosophila Stock Center; Aso et al., 2014a	BDSC: 68325 ; FlyBase: FBst0068325
D. melanogaster: MB210B-splitGAL4	Bloomington Drosophila Stock Center; Aso et al., 2014a	BDSC: 68272 ; FlyBase: FBst0068272
D. melanogaster: MB027B-splitGAL4	Bloomington Drosophila Stock Center; Aso et al., 2014a	BDSC: 68301 ; FlyBase: FBst0068301
D. melanogaster: MB018B-splitGAL4	Bloomington Drosophila Stock Center; Aso et al., 2014a	BDSC: 68296 ; FlyBase: FBst0068296
D. melanogaster: MB543B-splitGAL4	Bloomington Drosophila Stock Center; Aso et al., 2014a	BDSC: 68335 ; FlyBase: FBst0068335

D. melanogaster: MB057B-splitGAL4	Bloomington Drosophila Stock Center; Aso et al., 2014a	BDSC: 68277; FlyBase: FBst0068277
D. melanogaster: MB399B-splitGAL4	Bloomington Drosophila Stock Center; Aso et al., 2014a	BDSC: 68369; FlyBase: FBst0068369
D. melanogaster: MB091C-SplitGal4	Aso et al., 2014a, Gift from Aso, Y	N/A
D. melanogaster: 5HT1B-GAL4	Bloomington Drosophila Stock Center; Ries et al., 2017	BDSC: 27637; FlyBase: FBst0027637
D. melanogaster: UAS-dhomer-GCaMP3	Pech et al., 2015	N/A
D. melanogaster: UAS-GCaMP6f	Bloomington Drosophila Stock Center; Dana et al., 2019	BDSC: 52869; FlyBase: FBst0052869
D. melanogaster: 20XUAS-CsChrimson-mCherry (VK00005)	Bloomington Drosophila Stock Center; Jovanic et al. 2016, Gift from Jayaraman, V	BDSC: 82180; FlyBase: FBst0082180
D. melanogaster: 13XLexAop2-IVS-GCaMP6m-p10 (attp1)	Bloomington Drosophila Stock Center; Strother et al., 2017	BDSC: 44275; FlyBase: FBst0044275
D. melanogaster: TH-LexA (2rd)	Berry et al., 2015, Gift from Davis, R	N/A

D. melanogaster: UAS-mCD8::GFP, UAS-n-syb::GFP	Riemensperger et al., 2013	N/A
D. melanogaster: UAS:sypGCaMP3; syp3xpHTomato	Pech et al., 2015	N/A
D. melanogaster: GRASP recombination: Mb247-GFP11; UAS-GFP1-10	Pech et al., 2013	N/A
Software and algorithms		
ImageJ	N/A	https://imagej.nih.gov/ij/
Zen 2011 SP4 (black edition)	Carl Zeiss AG	https://www.micro-shop.zeiss.com/de/de/softwarefinder/software-categories/zen-black/
Leica Application Suite X (LASX; software)	Leica Microsystems GmbH	https://www.leica-microsystems.com/products/microscope-software/p/leica-las-x-ls/
Ethovision XT15	Noldus	https://www.noldus.com/ethovision-xt
Pylon Viewer 64-Bit	Basler AG	https://www.baslerweb.com/en/downloads/software-downloads/
OriginPro 2020	OriginLab Corp.	https://www.originlab.com/index.aspx?go=Products/Origin
GraphPad Prism 9	GraphPad Software, San Diego, California USA	https://www.graphpad.com
Arduino	Arduino	https://www.arduino.cc

Other		
Two-photon microscope	Carl Zeiss AG	LSM 7MP
Two-photon microscope	Carl Zeiss AG	LSM880
Chameleon laser	Coherent Inc.	Chameleon Ultra Ti:Sapphire Laser
Ti-Sapphire laser	Spectra-Physics, CA, USA	Mai Tai HP 1040S
Water Immersion Objective W Plan-Apochromat 20x	Carl Zeiss AG	Cat# 421452-9800-000
High-power LED driver	Doric Lens	N/A
Confocal laser scanning microscope	Leica Microsystems GmbH	SP8 LIGHTNING confocal microscope
Microscope slides	Carl Roth GmbH + Co. KG	Cat#0656
Blue light curing glue	NorDenta - Kent Dental	Cat#953683
Blue light lamp (Starlight pro)	Mectron Deutschland GmbH	Cat#05100083
Fine forceps - mirror finish	Fine Science Tools GmbH	Cat#11412-11
Surgical scalpel blade no.11	Swann-Morton	Cat#0303
Surgical scalpel handle no. 7	Swann-Morton	Cat#0907
Insect Minutien pins	Fine Science Tools GmbH	Cat#26002-10
Blade holders & breakers - Concave-convex jaws	Fine Science Tools GmbH	Cat#10053-09
Microknife	Fine Science Tools GmbH	Cat#10315-12

RESOURCE AVAILABILITY

Lead contact

Further information and requests for resources and reagents should be directed to the lead contact, André Fiala (afiala@gwdg.de).

Materials availability

All reagents, strains and experimental apparatus' design generated in this study are available from the lead contact.

Data and code availability

- **Data:** All data, raw and processed, will be deposited at FOR2705 database with a "DOI" and will be publicly available as of the date of publication.
- **Code:** All original code will be available as a ".txt" document in the same deposited "DOI".

EXPERIMENTAL MODEL AND SUBJECT DETAILS

Drosophila strains and genotypes

Flies were reared on standard cornmeal food medium in incubators maintained at 25˚C and 60% relative humidity with a 12hr/12hr light/dark cycle. The lines that were used throughout this study are: For the behavioral study, wild-type Canton S flies were used to establish the learning paradigm. In addition, different specific GAL4 driver lines were crossed to the UAS-*Shibire*^{ts} (BDSC #44222) and to W[1118] (BDSC #6326) flies to obtain the experimental lines in the filial generations. The following driver lines were used: Mushroom body: All KC (MB247*-GAL4/CyO, generated by Elizabeth Hong and published in this study), α/β KC (R44E04-GAL4, BDSC #50210), α'/β' KC (MB463B, BDSC #30829), and γ KC (MB009B, BDSC #68292). Split-GAL4 driver lines used to drive expression in MBONs were obtained from the Bloomington Drosophila Stock Centre: MBON-γ1pedc>α/β (MB112C, BDSC #68263), MBON-γ2α'1 (MB077B, BDSC #68283), MBON-γ3 and MBON-γ3β'1 (MB083C, BDSC #68287), MBON-γ4>γ1γ2 (MB434B, BDSC #68325), MBON-

γ5β’2a, MBON-β’2mp (MB210B, BDSC #68272), MBON-α’1 (MB543B, BDSC #68335), MBON-α’2 (MB018B, BDSC #68296), MBON-α’3ap and MBON-α’3m (MB027B, BDSC #68301), MBON-β’1 (MB057B, BDSC #68301), and MBON-β2β’2a (MB399B, BDSC #68369). PPL1 cluster: All PPL1-DANs (TH-GAL4, BDSC #8848), PPL1-γ1pedc (MB320C, BDSC #68253), PPL1-γ2α’1 (MB296B, BDSC #68308), PPL1- α’2α2 (MB058B, BDSC #68278), and PPL1- α’3 (MB304B, BDSC #68367). PAM cluster: All PAM-DANs (R58E02-GAL4, BDSC #41347). The resulting offspring was reared at 18°C and 60% relative humidity.

For two-photon imaging, the reporter lines that were used to evaluate pre- and post-calcium activity and during SOC training are UAS-dHomerGCaMP3 (self-generated by Pech et al., 2015) and UAS-GCaMP6f (BDSC #52869) crossed to MB112C (MBON-γ1pedc>α/β) and MB018B (MBON-α’2). For the electric shock imaging protocol syp-GCaMP3;syp3x-pHTomato (self-generated by Pech et al., 2015) was crossed to MB320C (PPL1-γ1pedc), MB296B (PPL1-γ2α’1), MB058B (PPL1- α’2α2) and MB315C (PPL1-γ5, BDSC #68316).

For optogenetic activation and simultaneous optical imaging, 20XUAS-CsChrimson-mCherry (Jovanic et al., 2016) and 13XLexAop2-IVS-GCaMP6m-p10 (Strother et al., 2017) were crossed to MB091C (MBON-α’2), MB112C (MBON-γ1pedc>α/β) and TH-LexA (Berry et al., 2015).

For confocal imaging of the IHC, GAL4 driver lines were crossed to UAS-mCD8:GFP-nsyb:GFP (self-generated by Riemensperger et al., 2013) and GRASP recombination: Mb247-GFP11; UAS-GFPb1-10 (Pech et al., 2013)

METHOD DETAILS

Aversive olfactory conditioning

The flies were trained and tested in a custom-built conditioning apparatus (Suppl. Figure 1A-B). All experiments were performed at a humidity of 65-85% and a temperature of either 22-25°C for normal conditions or 29-30°C for *Shibire*^{ts} restrictive conditions. To achieve this, two separate setups were designated in different boxes to maintain the desired temperature. Each setup contains of a training and a testing apparatus. For the training phase, the flies were placed in double-wired

copper electric tubes that are connected to a voltage generator and a vacuum. A custom-built and Arduino programed shock/odor-delivery controlling device connects and provides input to the different components of the machine (see Arduino code for training and testing machine). The input from this device procures a precise and automatic spatiotemporal modulation to the voltage generator and the valves of the olfactometer. To present the odors in the training tubes, air flows through the odor bottles at a rate of 0.20 – 0.25 LPM.

For first-order conditioning (FOC), around 30 flies with the age of 3 to 7days were loaded into four separate training tubes that were trained and then tested. During training, the flies in received the shock and the odors according to the classical conditioning paradigm described by Tully and Quinn (Tully and Quinn, 1985). CS1 was presented for 60s together with 12 x 1.25-sec pulses of 90V shocks every 5 sec, followed by 60 sec of blank odor, and then finally CS^- is introduced in the tubes for 60 sec. Reciprocal training was accounted for.

For second-order conditioning experiments, the flies received the shock and the odors according to the protocol as described by Tabone and de Belle (Tabone, C.J., & de Belle, J.S., 2011). The second-order conditioning paradigm (SOC) is comprised of three phases: a first training phase, a second training phase, and testing (Figure 1B). The reinforcer and the stimuli are paired in the standard second-order conditioning paradigm, also referred to as “Paired-Paired” (Figure 1B). In the first training phase, 3 to 7 days old flies were placed into the double-wired copper electric tubes that are connected to electric wires and the vacuum. During training, they were first exposed to a blank odor (mineral oil) for 90 sec. Next, CS1 was presented for 60 sec together with 12 x 1.25-sec pulses of 90V shocks every 5 sec, followed by another 45 sec of the blank odor. In the end, CS^- is presented in the tubes for 60 sec. This training cycle was repeated three times with 10 min intervals in between. In the second training phase, the flies receive another presentation of a blank odor for 90 sec followed by 7 sec of CS2. For the next 60 sec, CS2 was dispensed in a continuous airflow paired with 12 x 4 sec pulses of CS1 alternating with the blank odor every 5 sec. The blank odor was then presented alone for 45 sec to flush any odor contamination during this phase. This cycle was also repeated three times with 10 min intervals.

Control experiments were conducted such as the reinforcer and the stimuli were either unpaired during the first or the second training phases. The first control experiment “Paired-Unpaired” (Figure 1B) consisted of unpairing the CS1 and CS2 odors during the second training phase, which resulted in 60 sec of CS2 presented alone, followed by 45 sec of blank odor, then 60 sec of CS1. In the second control experiment “Unpaired-Paired (Figure 1B), the electric shocks and the CS1 odor are presented separately during the first training phase (60 sec of CS^-, followed by 45 sec of blank and 60 sec of CS1, then another 45 sec blank followed by 12 x 1.25-sec pulses of 90V shocks every 5 sec).

Third-order conditioning (TOC) experiments consisted of adding one more training phase (training phase 3) to the SOC paradigm. In this phase, a blank odor was presented for 90 sec followed by 7 sec of CS2, then followed by a continuous airflow of CS3 paired with 12 x 4 sec pulses of CS2 alternating with the blank odor every 5 seconds. Control experiments were conducted where the reinforcer and the stimulus were unpaired during the first, second or third training phases (Figure 7A-B).

For the testing phase of FOC, SOC and TOC, the flies were transferred after the training from the electric tubes to the central carrier of the testing arena. Composed of four lanes, this arena matches the training tubes in number. A second controlling device is connected to the testing arena along with its respective olfactometers (one for each side) so that according to the program, the two selected odors are presented from either the left or the right side of said arena. The air pressure was maintained the same in comparison to the training tubes (0.20 – 0.25 LPM). When the lever of the central carrier is pushed down, the flies have two minutes to choose one of the two sides of the arena. This phase is recorded by a high-speed camera (Basler GigE camera acA 1300 – 60gc / CS – mount) with an objective (Lens Kowa 4.4-11mm zoom lens) that is equipped with an IR filter. During the testing phase, multiple IR-LED bulbs are switched on from under the arena for video acquisition.

We used four different odorants, Benzaldehyde (BenzA) (1:100), 3-Octanol (3-OCT) (1:10), 4-Methylcyclohexanol (MCH) (1:10) and Pentyl acetate (PA). While MCH and 3-OCT were reciprocally used as CS1 and CS^- to account for odor bias, BenzA remained as CS2 and PA as CS3 in all experiments. Control experiments demonstrate that all other possible odor combinations show no significant difference

(Suppl. Figure 1E). The positions of the odors in the testing phase were also reversed to account for the side bias by switching the odor presentations from the left and right olfactometer.

In vivo functional imaging

Fly brains were prepared for *in vivo* imaging as described in Hancock et al., 2019 and 2020 and this procedure was used in all imaging experiments performed with the two-photon microscope. Single flies were cold anesthetized by putting them on a previously cooled down steel plate on ice. Once immobilized, the fly was then moved to a custom-built chamber (Figure 6B), in which the head was placed on a small pedestal to ensure the contact with the tape. A small window was carefully cut into the tape to exposing the head capsule while the antennae and the thorax remain covered. Moreover, the head was hindered from further movement by applying UV-hardening glue around the sides of the cut window and setting it with a special UV-emitting lamp to limit movement of the sample, and thus disrupting the imaging experiments. The head capsule is then covered with 2-3 drops of RT Ringer's solution to ensure physiological conditions during the dissection and avoiding dryness of the brain. A micro-blade was lastly used to open the head capsule by making a first incision into the ocelli, followed by two perpendicular cuts along the left and right sides of the of the head capsule. After removing the cuticle and the excess fat tissue with fine forceps, Ringer solution was refreshed and the chamber was then allocated to the mechanical stage of the microscope to start image acquisition.

Prepared flies were then placed under the microscope's objective and connected to a custom-built odor delivery device (Figure 6B). An excitation wavelength of 920 nm (for homer-GCaMP3, GCaMP6f and G-Flamp1) and 950nm (for syp-GCaMP3 and syp-pHTomato) were used for image acquisition which is controlled using Zeiss Zen (2011 SP4 black edition) software. Images were captured at a framerate of 4 Hz and with a frame size of 512x512 pixels. Simultaneous odor delivery, shock pulses and image acquisition were controlled via a custom-built controlling device (Figure 6B). Three odorants were used in all experiments, as follows: 4-methylcyclohexanol (MCH), 3-Octanol (3-Oct), and Benzaldehyde (BA), at concentrations of 1:10, 1:10, and 1:100, respectively, and were diluted in mineral oil.

To monitor the effects of second-order conditioning, a three-step imaging protocol was used. First, flies were sequentially presented with the three odors to assess the naïve odor-evoked responses by monitoring the changes in fluorescence (pre-training). The second step immediately followed the first and consisted of exposing the flies to any of the three SOC protocols (Paired-Paired, Paired-Unpaired and Unpaired-Paired). Third, the flies were again presented with the three odorants and their responses were measured (post-training) (Figure 6C). This final imaging step was carried out 3-4 min after the end of the respective conditioning protocol. In the first and third steps, all odor presentations lasted of 3 sec and were separated by an interval of approximately 40 sec.

For the shock imaging protocol (Figure 4A, B and D), image acquisition started 30 seconds before the first electric pulsation. The imaged shock protocol consisted of 90V x 12 pulses of 1.25 seconds presented every 5 seconds for a total duration of one minute, followed by 30 seconds of imaging post the shock protocol.

Optogenetic stimulation and calcium imaging

1-3-day-old flies were fed with regular fly food containing 0.4 mM all-trans-retinal for 48-72 hours in dark at 23 °C and 60% humidity. The fly brain was then dissected in imaging buffer (103 mM NaCl, 3 mM KCl, 26 mM NaHCO3, 1 mM NaH2PO4, 1.5 mM CaCl2, 4 mM MgCl2, 8 mM trehalose, 10 mM glucose, 5mM TES, osmolarity 275 mOsm, pH 7.3) and placed in a recording chamber (PH-5 & RC-20, Wanner Instrument). The brain was perfused with imaging buffer mixed with 95% O2 and 5% CO2 for 5 minutes before being imaged under a two-photon microscope with a 20x water-immersion objective lens (Zeiss LSM880). The fluorescence signal of GCamp6m expressed in γ1-projecting DANs was excited by a 910 nm two-photon laser (Spectra-Physics, CA, USA; Mai Tai HP 1040S). The GCaMP6m signals were captured at 9.63 frames per second with 80 x 100 pixels resolution. Each brain was recorded twice, 500 frames each, and the interval between the two recordings was 10 seconds. During each recording, the baseline GCaMP6m signals were collected for 20 seconds (~185 frames), followed by the stimulation of CsChrimson expressing MBONs with a 633 mm LED light for 0.5 seconds (40 Hz, 20 pulses with a 25 ms pulse duration). The GCaMP6m signals from the two recordings were averaged to generate a mean signal trace for subsequent data analyses.

Immunohistochemistry

Flies first had to be immobilized by placing them on ice in empty vials for about five minutes. A single fly was then fixed on a dissection plate dorsal side down with two pins placed into the thorax and then covered with Ringer's solution. Brains were extracted in Ringer's solution (5 mM KCl, 130 nM NaCl, 2 mM MgCl2, 2 mM CaCl2, 5 mM Hepes, 36 mM sucrose, pH 7.3) by swiftly removing the proboscis and detaching the brain from the head capsule. Brains were then fixed in 4% paraformaldehyde at room temperature for 45 min, and then washed three times for 30 min each in PBS with 0.6% Triton-X. Brains were then incubated at 4°C overnight in blocking solution containing 2% bovine serum albumin and 2% normal goat serum. Subsequently, brains were incubated with anti-GFP primary antibody (rabbit anti-GFP, Invitrogen A6455) at a concentration of 1:2000 and, an anti-discs large (DLG) primary antibody (mouse anti-DLG, Developmental Studies Hybridoma Bank 4F3) was used at a concentration of 1:200 to visualize brain structures. For the GRASP experiments, anti-splitGFP (mouse monoclonal anti-green fluorescent protein (GFP) – clone GFP-20, Sigma-Aldrich G6539) was used at a concentration of 1:2000, and anti-Cadherin (Rat anti-Cadherin DN-extracellular domain, Developmental Studies Hybridoma Bank DN-Ex #8) at a concentration of 1:50 was used for background staining. Brains were incubated in primary antibody solution for 1 day at 4°C, and washed again three times in PBS with Triton-X before incubation in secondary antibody. Secondary antibodies anti-rabbit AlexaFluor488, anti-mouse Alexa633 and anti-rat Alexa633 were used, both at a concentration of 1:300, for 1 day at 4°C. Brains were washed again three times in PBS with Triton-X, and then mounted in VectaShield for confocal scanning.

Confocal microscopy

A Leica SP8 line scanning confocal microscope was used to image the stained brains. An argon laser of a wavelength of 488 nm and HeNe-laser 633nm were used to excite the corresponding secondary antibodies. Scanning and image acquisition were performed using Leica LSAX software. Laser intensity and hybrid detector gains were optimized to ensure minimal noise and bleaching. The brains were then scanned using a 20x objective and 1024x1024 resolutions with a 2 frame averaging, and Z-Stacks were acquired as LIF files for processing.

Reconstruction with neuPrint database

Reconstruction and synaptic quantification of the connectivity of γ2-α‘1 DAN and α‘2 MBON in the α‘2 compartment of the MB was performed using the neuPrint database: Analysis Tools for EM Connectomics by Janelia (link in key resource table). The identification numbers for the two used neurons are γ2-α‘1 DAN (id #5813022424) and α‘2 MBON (id #1139667240). The reconstruction images were obtained in “Skeleton view” mode along with allowing only the MB lobes to show using the scroll bar and selecting the regions of interest. The synaptic connectivity quantification was gained by adding input/output from α‘2 compartment of the MB by allowing all brain regions and selecting a‘2(R) in the scroll down menu “Output brain regions” of “Find neurons”.

QUANTIFICATION AND STATISTICAL ANALYSIS

Two-photon images processing

Images were processed using ImageJ (https://imagej.nih.gov/ij/). Small movements on the X and Y axes were corrected using the TurboReg plugin (Thévenaz et al., 1998). The desired structures of the mushroom body were manually drawn to encircle the entire dendritic arborization and thus highlighting the regions of interest (ROIs). The fluorescent intensity throughout the recording period was then multi-measured from these ROIs and used to calculate the normalized relative change in fluorescence over time (ΔF/F0) for each recording. This normalized relative fluorescence was calculated by obtaining the average fluorescence intensity over the 2 sec preceding odor delivery (baseline or F0), and ΔF was calculated by subtracting this value at each time point of the measurement. In order to statistically compare responses pre- and post-training, the area under the curve (AUC) of each ΔF/F0 of these responses was quantified. The AUC was integrated from the odor onset to 2 seconds after its offset. Before pooling the data together by arranging them in their respective CS1, CS^- or CS2 slot, the large variability in odor responses between the odors was accounted for, and AUC values were normalized within each experimental group (all responses to each odor were normalized to the mean pre-training response to that odor).

Statistical analyses consisted of comparing Pre and Post values using a Paired Sample T-test.

Behavioral statistical analysis

To analyze the flies' learned behavior, an end-point calculation at the end of the two-minute time window of the testing phase. Flies were counted on each lane for both sides of the testing arena. Preference index 1 was calculated (PI_1) according to equation (1), wherein **A** stands for the number of flies that chose the CS1 odor (for classical conditioning) or CS2 (for SOC), and **B** represents the amount of flies that chose the CS^- odor. The performance index 2 (PI_2) corresponds to the reciprocal training and was similarly calculated.

$$PI_1 = \frac{A - B}{A + B} \qquad (1)$$

As stated in equation (2), the mean value of the performance indices was then calculated to obtain the flies' learning index (LI).

$$LI = \frac{PI_1 + PI_2}{2} \qquad (2)$$

The analysis of the raw data was performed with OriginPro2020. First, a Shapiro-Wilk test was performed to verify the normal distribution of the groups. If the groups exhibit a normal distribution, a Two-Tailed One-Sample T-test was performed with a Bonferroni correction to test the hypothesis of means against 0, and Two-Tailed Two-sample T-test was performed to test the difference in between the experimental and genetic control group. A One-Way ANOVA with a Tukey Post-hoc test was used for 3 or more group comparisons. If the groups do not follow a normal distribution, a Wilcoxon Signed-Rank test with a Bonferroni correction was performed to test the hypothesis of medians against 0 and Mann–Whitney U tests were executed to assess the difference between the groups. A Kruskal-Wallis ANOVA with a Dunn's post hoc comparison test was carried out to test the difference between 3 or more groups.

Confocal images processing

All confocal image processing was conducted using ImageJ (NIH). The stacks were separated by channel; the slices of interest in the Z-Stack were transformed into a

single Z-projection for each channel and the brightness and contrast adjusted to minimize background noise. The two channels were then merged to obtain an overlay picture showing the structures of interest. For the GRASP experiments, the stacks stained with the brain structure antibody (N-cadherin) were meticulously screened to draw the different compartments of the mushroom body.

Table S1: Statistical tests

<table>
<tr><th colspan="2">Figure</th><th>Normality test (Shapiro-Wilk test)</th><th>Hypothesis testing for mean/median (Two-tailed)</th><th>Group comparison</th></tr>
<tr><td colspan="2" rowspan="3">Figure 1B</td><td>“Paired-Paired” P-P: normally distributed p=0.97281</td><td>One-Sample T-test with Bonferroni Correction: ***p= 1.07044E-8</td><td rowspan="3">One-Way Anova: F= 18.89581; ***p= 2.85601E-7

Post-hoc Tukey test:
P-P vs P-U
***p= 4.7605E-7
P-P vs U-P
***p= 5.08075E-5
P-U vs U-P
p= 0.45672</td></tr>
<tr><td>“Paired-Unpaired” P-U: normally distributed p=0.19891</td><td>One-Sample T-test with Bonferroni Correction: p= 0.07725</td></tr>
<tr><td>“Unpaired-Paired” U-P: normally distributed p=0.72573</td><td>One-Sample T-test with Bonferroni Correction: p= 0.96889</td></tr>
<tr><td rowspan="4">Figure 1E</td><td rowspan="3">CTC</td><td>“UAS-Shibire^{ts}”: normally distributed p= 0.41281</td><td>One-Sample T-test with Bonferroni Correction: ***p= 2.15027E-6</td><td rowspan="3">One-Way Anova: F= 0.04418; p= 0.95682

Post-hoc Tukey test:
UAS vs GAL4
p= 0.97336
GAL4 vs GAL4/UAS
p= 0.99794
UAS vs GAL4/UAS
p= 0.95701</td></tr>
<tr><td>“MB247*-GAL4”: normally distributed p= 0.39404</td><td>One-Sample T-test with Bonferroni Correction: ***p= 1.8163E-6</td></tr>
<tr><td>“MB247*-GAL4/ UAS-Shibire^{ts}”: normally distributed p=0.96753</td><td>One-Sample T-test with Bonferroni Correction: ***p= 2.76644E-6</td></tr>
<tr><td>Block during training 1</td><td>“UAS-Shibire^{ts}”: normally distributed p= 0.15424</td><td>One-Sample T-test with Bonferroni Correction: ***p= 1.26551E-7</td><td>One-Way Anova: F= 0.67485; p= 0.51431</td></tr>
</table>

		"MB247*-GAL4": normally distributed p= 0.55743	One-Sample T-test with Bonferroni Correction: ***p= 2.71721E-9	Post-hoc Tukey test: **UAS** vs **GAL4** p= 0.48189 **GAL4** vs **GAL4/UAS** p= 0.82852 **UAS** vs **GAL4/UAS** p= 0.83347
		"MB247*-GAL4/ UAS-*Shibire^{ts}*": normally distributed p= 0.49006	One-Sample T-test with Bonferroni Correction: ***p= 3.09328E-6	
	Block during training 2	**"UAS-*Shibire^{ts}*"**: normally distributed p= 0.83625	One-Sample T-test with Bonferroni Correction: ***p= 4.3062E-7	One-Way Anova: F= 4.92477; *p= 0.01164 Post-hoc Tukey test: **UAS** vs **GAL4** p= 0.9611 **GAL4** vs **GAL4/UAS** *p= 0.03516 **UAS** vs **GAL4/UAS** *p= 0.01807
		"MB247*-GAL4": normally distributed p= 0.95463	One-Sample T-test with Bonferroni Correction: ***p= 2.66076E-5	
		"MB247*-GAL4/ UAS-*Shibire^{ts}*": normally distributed p= 0.32868	One-Sample T-test with Bonferroni Correction: p= 0.371	
	Block during test	**"UAS-*Shibire^{ts}*"**: normally distributed p= 0.29898	One-Sample T-test with Bonferroni Correction: ***p= 3.0819E-9	One-Way Anova: F= 14.15951; ***p= 1.69788E-5 Post-hoc Tukey test: **UAS** vs **GAL4** p= 0.86507 **GAL4** vs **GAL4/UAS** ***p= 2.38835E-4 **UAS** vs **GAL4/UAS** ***p= 4.52632E-5
		"MB247*-GAL4": normally distributed p= 0.99806	One-Sample T-test with Bonferroni Correction: ***p= 1.38481E-7	
		"MB247*-GAL4/ UAS-*Shibire^{ts}*": normally distributed p= 0.51439	One-Sample T-test with Bonferroni Correction: p= 0.96362	
Figure 1F	CTC	**"MB009B-GAL4"**: normally distributed p= 0.70968	One-Sample T-test with Bonferroni Correction: ***p= 5.39047E-5	Two-Sample T-test with Welch's correction: p= 0.16289
		"MB009B-GAL4/ UAS-*Shibire^{ts}*": normally distributed p= 0.89864	One-Sample T-test with Bonferroni Correction: ***p= 2.94298E-6	

	Block during training 1	**"MB009B-GAL4"**: normally distributed p= 0.24819	One-Sample T-test with Bonferroni Correction: ***p= 5.02409E-5	Two-Sample T-test with Welch's correction: p= 0.82987
		"MB009B-GAL4/ UAS-*Shibire^{ts}*": normally distributed p= 0.24331	One-Sample T-test with Bonferroni Correction: ***p= 3.90766E-5	
	Block during training 2	**"MB009B-GAL4"**: normally distributed p= 0.12001	One-Sample T-test with Bonferroni Correction: ***p= 7.63844E-5	Two-Sample T-test with Welch's correction: **p= 0.0027
		"MB009B-GAL4/ UAS-*Shibire^{ts}*": normally distributed p= 0.34953	One-Sample T-test with Bonferroni Correction: p= 0.31401	
	Block during test	**"MB009B-GAL4"**: normally distributed p= 0.50711	One-Sample T-test with Bonferroni Correction: **p= 8.95789E-4	Two-Sample T-test with Welch's correction: **p= 0.00201
		"MB009B-GAL4/ UAS-*Shibire^{ts}*": normally distributed p= 0.6704	One-Sample T-test with Bonferroni Correction: p= 0.57717	
Figure 1G	CTC	**"MB463B-GAL4"**: normally distributed p= 0.91101	One-Sample T-test with Bonferroni Correction: ***p= 5.33536E-5	Two-Sample T-test with Welch's correction: p= 0.87681
		"MB463B-GAL4/ UAS-*Shibire^{ts}*": normally distributed p= 0.96496	One-Sample T-test with Bonferroni Correction: ***p= 1.00908E-4	
	Block during training 1	**"MB463B-GAL4"**: normally distributed p= 0.30475	One-Sample T-test with Bonferroni Correction: **p= 0.00146	Two-Sample T-test with Welch's correction: p= 0.46946

		“MB463B-GAL4/ UAS-*Shibire^{ts}*”: normally distributed p= 0.74635	One-Sample T-test with Bonferroni Correction: ***p= 3.73765E-5	
	Block during training 2	**“MB463B-GAL4”**: normally distributed p= 0.62125	One-Sample T-test with Bonferroni Correction: ***p= 2.8392E-4	Two-Sample T-test with Welch’s correction: *p= 0.01476
		“MB463B-GAL4/ UAS-*Shibire^{ts}*”: normally distributed p= 0.55424	One-Sample T-test with Bonferroni Correction: p= 0.44028	
	Block during test	**“MB463B-GAL4”**: normally distributed p= 0.21476	One-Sample T-test with Bonferroni Correction: ***p= 2.43255E-4	Two-Sample T-test with Welch’s correction: p= 0.90324
		“MB463B-GAL4/ UAS-*Shibire^{ts}*”: normally distributed p= 0.29333	One-Sample T-test with Bonferroni Correction: ***p= 1.30669E-4	
Figure 1H	CTC	**“R44E04-GAL4”**: normally distributed p= 0.0609	One-Sample T-test with Bonferroni Correction: ***p= 9.21551E-5	Two-Sample T-test with Welch’s correction: p= 0.88497
		“R44E04-GAL4/ UAS-*Shibire^{ts}*”: normally distributed p= 0.43065	One-Sample T-test with Bonferroni Correction: ***p= 5.24131E-5	
	Block during training 1	**“R44E04-GAL4”**: normally distributed p= 0.50844	One-Sample T-test with Bonferroni Correction: ***p= 3.92706E-8	Two-Sample T-test with Welch’s correction: p= 0.39868
		“R44E04-GAL4/ UAS-*Shibire^{ts}*”: normally distributed p= 0.21523	One-Sample T-test with Bonferroni Correction: ***p= 3.90024E-5	

	Block during training 2	**"R44E04-GAL4"**: normally distributed p= 0.50818	One-Sample T-test with Bonferroni Correction: ***p= 4.86022E-5	Two-Sample T-test with Welch's correction: p= 0.80448
		"R44E04-GAL4/ UAS-*Shibire^{ts}*": normally distributed p= 0.12811	One-Sample T-test with Bonferroni Correction: ***p= 1.23929E-6	
	Block during test	**"R44E04-GAL4"**: normally distributed p= 0.14745	One-Sample T-test with Bonferroni Correction: ***p= 2.72247E-5	Two-Sample T-test with Welch's correction: p= 0.3211
		"R44E04-GAL4/ UAS-*Shibire^{ts}*": normally distributed p= 0.37352	One-Sample T-test with Bonferroni Correction: ***p= 6.33373E-6	
Figure 2A	CTC	**"MB112C-GAL4"**: normally distributed p= 0.07389	One-Sample T-test with Bonferroni Correction: ***p= 2.46864E-7	Two-Sample T-test with Welch's correction: p= 0.3004
		"MB112C-GAL4/ UAS-*Shibire^{ts}*": normally distributed p= 0.36275	One-Sample T-test with Bonferroni Correction: ***p= 1.8366E-4	
	Block during training 1	**"MB112C-GAL4"**: normally distributed p= 0.7902	One-Sample T-test with Bonferroni Correction: **p= 0.00343	Two-Sample T-test with Welch's correction: p= 0.3468
		"MB112C-GAL4/ UAS-*Shibire^{ts}*": normally distributed p= 0.37879	One-Sample T-test with Bonferroni Correction: ***p= 1.3363E-5	
	Block during training 2	**"MB112C-GAL4"**: normally distributed p= 0.39476	One-Sample T-test with Bonferroni Correction: ***p= 1.8496E-6	Two-Sample T-test with Welch's correction: **p= 0.00361

		"MB112C-GAL4/ UAS-*Shibire^{ts}": normally distributed p= 0.1533	One-Sample T-test with Bonferroni Correction: p= 0.13671	
	Block during test	**"MB112C-GAL4"**: normally distributed p= 0.69004	One-Sample T-test with Bonferroni Correction: ***p= 1.40513E-4	Two-Sample T-test with Welch's correction: ***p= 8.51576E-4
		"MB112C-GAL4/ UAS-*Shibire^{ts}": normally distributed p= 0.08358	One-Sample T-test with Bonferroni Correction: p= 0.78144	
Figure 2B	CTC	**"MB077B-GAL4"**: normally distributed p= 0.99757	One-Sample T-test with Bonferroni Correction: ***p= 8.05653E-6	Two-Sample T-test with Welch's correction: p=0.92408
		"MB077B-GAL4/ UAS-*Shibire^{ts}": normally distributed p= 0.639	One-Sample T-test with Bonferroni Correction: ***p= 1.55151E-6	
	Block during training 1	**"MB077B-GAL4"**: normally distributed p= 0.12704	One-Sample T-test with Bonferroni Correction: **p= 0.00297	Two-Sample T-test with Welch's correction: p=0.96159
		"MB077B-GAL4/ UAS-*Shibire^{ts}": normally distributed p= 0.55719	One-Sample T-test with Bonferroni Correction: **p= 0.00122	
	Block during training 2	**"MB077B-GAL4"**: normally distributed p= 0.80297	One-Sample T-test with Bonferroni Correction: ***p= 5.79521E-6	Two-Sample T-test with Welch's correction: p=0.38909
		"MB077B-GAL4/ UAS-*Shibire^{ts}": normally distributed p= 0.37126	One-Sample T-test with Bonferroni Correction: ***p= 4.74408E-5	

	Block during test	**"MB077B-GAL4"**: normally distributed p= 0.47166	One-Sample T-test with Bonferroni Correction: ***p= 4.67139E-4	Two-Sample T-test with Welch's correction: p=0.91401
		"MB077B-GAL4/ UAS-*Shibire^{ts}*": normally distributed p= 0.22166	One-Sample T-test with Bonferroni Correction: ***p= 6.48041E-5	
Figure 2C	CTC	**"MB083C-GAL4"**: normally distributed p= 0.58553	One-Sample T-test with Bonferroni Correction: ***p= 2.04648E-4	Two-Sample T-test with Welch's correction: p=0.62564
		"MB083C-GAL4/ UAS-*Shibire^{ts}*": normally distributed p=0.84374	One-Sample T-test with Bonferroni Correction: ***p= 1.74166E-4	
	Block during training 1	**"MB083C-GAL4"**: normally distributed p=0.58699	One-Sample T-test with Bonferroni Correction: ***p= 4.11555E-4	Two-Sample T-test with Welch's correction: p=0.76917
		"MB083C-GAL4/ UAS-*Shibire^{ts}*": normally distributed p=0.27062	One-Sample T-test with Bonferroni Correction: ***p= 1.74166E-4	
	Block during training 2	**"MB083C-GAL4"**: normally distributed p=0.64889	One-Sample T-test with Bonferroni Correction: ***p= 1.20149E-4	Two-Sample T-test with Welch's correction: p=0.8796
		"MB083C-GAL4/ UAS-*Shibire^{ts}*": normally distributed p=0.40229	One-Sample T-test with Bonferroni Correction: **p= 0.0014	
	Block during test	**"MB083C-GAL4"**: normally distributed p=0.66596	One-Sample T-test with Bonferroni Correction: **p= 6.24557E-4	Two-Sample T-test with Welch's correction: p=0.67417

		"MB083C-GAL4/ UAS-*Shibire^{ts}*": normally distributed p=0.05951	One-Sample T-test with Bonferroni Correction: **p= 5.28717E-4	
Figure 2D	CTC	**"MB434B-GAL4"**: normally distributed p=0.69124	One-Sample T-test with Bonferroni Correction: ***p= 3.1313E-5	Two-Sample T-test with Welch's correction: p=0.94376
		"MB434B-GAL4/ UAS-*Shibire^{ts}*": normally distributed p=0.17427	One-Sample T-test with Bonferroni Correction: **p= 5.65172E-4	
	Block during training 1	**"MB434B-GAL4"**: normally distributed p=0.95664	One-Sample T-test with Bonferroni Correction: ***p= 1.60439E-5	Two-Sample T-test with Welch's correction: p=0.5408
		"MB434B-GAL4/ UAS-*Shibire^{ts}*": normally distributed p=0.63775	One-Sample T-test with Bonferroni Correction: ***p= 8.00173E-5	
	Block during training 2	**"MB434B-GAL4"**: normally distributed p=0.44264	One-Sample T-test with Bonferroni Correction: ***p= 6.62098E-5	Two-Sample T-test with Welch's correction: p=0.90464
		"MB434B-GAL4/ UAS-*Shibire^{ts}*": normally distributed p=0.63775	One-Sample T-test with Bonferroni Correction: ***p= 3.05786E-4	
	Block during test	**"MB434B-GAL4"**: normally distributed p=0.90508	One-Sample T-test with Bonferroni Correction: ***p= 3.68813E-7	Two-Sample T-test with Welch's correction: p=0.88951
		"MB434B-GAL4/ UAS-*Shibire^{ts}*": normally distributed p=0.65685	One-Sample T-test with Bonferroni Correction: ***p= 1.41904E-5	

Figure 2E	CTC	**"MB210B-GAL4"**: normally distributed p=0.09436	One-Sample T-test with Bonferroni Correction: ***p= 3.96476E-5	Two-Sample T-test with Welch's correction: p=0.74983
		"MB210B-GAL4/ UAS-*Shibire^{ts}*": normally distributed p=0.06129	One-Sample T-test with Bonferroni Correction: ***p= 8.8193E-5	
	Block during training 1	**"MB210B-GAL4"**: normally distributed p=0.62216	One-Sample T-test with Bonferroni Correction: ***p= 1.43089E-6	Two-Sample T-test with Welch's correction: p=0.43881
		"MB210B-GAL4/ UAS-*Shibire^{ts}*": normally distributed p=0.27041	One-Sample T-test with Bonferroni Correction: ***p= 1.87287E-5	
	Block during training 2	**"MB210B-GAL4"**: normally distributed p=0.7107	One-Sample T-test with Bonferroni Correction: ***p= 5.53459E-5	Two-Sample T-test with Welch's correction: p=0.71
		"MB210B-GAL4/ UAS-*Shibire^{ts}*": normally distributed p=0.59609	One-Sample T-test with Bonferroni Correction: ***p= 7.63362E-6	
	Block during test	**"MB210B-GAL4"**: normally distributed p=0.05767	One-Sample T-test with Bonferroni Correction: ***p= 3.67926E-6	Two-Sample T-test with Welch's correction: p=0.79649
		"MB210B-GAL4/ UAS-*Shibire^{ts}*": normally distributed p=0.94161	One-Sample T-test with Bonferroni Correction: ***p= 2.88426E-4	
Figure 2F	CTC	**"MB543B-GAL4"**: normally distributed p= 0.36498	One-Sample T-test with Bonferroni Correction: ***p= 1.62379E-7	Two-Sample T-test with Welch's correction: p= 0.25989

		"MB543B-GAL4/ UAS-*Shibire^{ts}": normally distributed p= 0.46511	One-Sample T-test with Bonferroni Correction: ***p= 2.15213E-7	
	Block during training 1	**"MB543B-GAL4"**: normally distributed p= 0.10576	One-Sample T-test with Bonferroni Correction: **p= 0.00243	Two-Sample T-test with Welch's correction: p= 0.78573
		"MB543B-GAL4/ UAS-*Shibire^{ts}": normally distributed p= 0.80993	One-Sample T-test with Bonferroni Correction: ***p= 1.77282E-4	
	Block during training 2	**"MB543B-GAL4"**: normally distributed p= 0.10164	One-Sample T-test with Bonferroni Correction: ***p= 4.1806E-4	Two-Sample T-test with Welch's correction: p= 0.56722
		"MB543B-GAL4/ UAS-*Shibire^{ts}": normally distributed p= 0.14151	One-Sample T-test with Bonferroni Correction: ***p= 2.06329E-5	
	Block during test	**"MB543B-GAL4"**: normally distributed p= 0.05097	One-Sample T-test with Bonferroni Correction: ***p= 2.70757E-4	Two-Sample T-test with Welch's correction: p= 0.99428
		"MB543B-GAL4/ UAS-*Shibire^{ts}": normally distributed p= 0.33115	One-Sample T-test with Bonferroni Correction: ***p= 1.19058E-6	
Figure 2G	CTC	**"MB018B-GAL4"**: normally distributed p= 0.65671	One-Sample T-test with Bonferroni Correction: **p= 6.26164E-4	Two-Sample T-test with Welch's correction: p= 0.93562
		"MB018B-GAL4/ UAS-*Shibire^{ts}": normally distributed p= 0.49664	One-Sample T-test with Bonferroni Correction: ***p= 8.09686E-5	

	Block during training 1	**"MB018B-GAL4"**: normally distributed p= 0.63244	One-Sample T-test with Bonferroni Correction: ***p= 2.39469E-4	Two-Sample T-test with Welch's correction: p= 0.27619
		"MB018B-GAL4/ UAS-*Shibire^{ts}*": normally distributed p= 0.68436	One-Sample T-test with Bonferroni Correction: ***p= 3.16339E-6	
	Block during training 2	**"MB018B-GAL4"**: normally distributed p= 0.94592	One-Sample T-test with Bonferroni Correction: ***p= 2.23845E-5	Two-Sample T-test with Welch's correction: **p= 0.00105
		"MB018B-GAL4/ UAS-*Shibire^{ts}*": normally distributed p= 0.06053	One-Sample T-test with Bonferroni Correction: p= 0.88015	
	Block during test	**"MB018B-GAL4"**: normally distributed p= 0.28398	One-Sample T-test with Bonferroni Correction: ***p= 2.00481E-4	Two-Sample T-test with Welch's correction: p= 0.65988
		"MB018B-GAL4/ UAS-*Shibire^{ts}*": normally distributed p= 0.53703	One-Sample T-test with Bonferroni Correction: ***p= 2.4387E-5	
Figure 2H	CTC	**"MB027B-GAL4"**: normally distributed p= 0.41193	One-Sample T-test with Bonferroni Correction: **p= 0.00161	Two-Sample T-test with Welch's correction: p= 0.91354
		"MB027B-GAL4/ UAS-*Shibire^{ts}*": normally distributed p= 0.51933	One-Sample T-test with Bonferroni Correction: ***p= 5.81884E-5	
	Block during training 1	**"MB027B-GAL4"**: normally distributed p= 0.2371	One-Sample T-test with Bonferroni Correction: **p= 0.00316	Two-Sample T-test with Welch's correction: p= 0.7767

		"MB027B-GAL4/ UAS-*Shibire^{ts}": normally distributed p= 0.28022	One-Sample T-test with Bonferroni Correction: ***p= 9.16684E-5	
	Block during training 2	**"MB027B-GAL4"**: normally distributed p= 0.98227	One-Sample T-test with Bonferroni Correction: **p= 0.00295	Two-Sample T-test with Welch's correction: p= 0.25609
		"MB027B-GAL4/ UAS-*Shibire^{ts}": normally distributed p= 0.30121	One-Sample T-test with Bonferroni Correction: ***p= 1.00379E-6	
	Block during test	**"MB027B-GAL4"**: normally distributed p= 0.60084	One-Sample T-test with Bonferroni Correction: **p= 5.29724E-4	Two-Sample T-test with Welch's correction: p= 0.61268
		"MB027B-GAL4/ UAS-*Shibire^{ts}": normally distributed p= 0.26898	One-Sample T-test with Bonferroni Correction: **p= 7.53086E-4	
Figure 2I	CTC	**"MB057B-GAL4"**: normally distributed p= 0.59155	One-Sample T-test with Bonferroni Correction: ***p= 3.46171E-5	Two-Sample T-test with Welch's correction: p= 0.73429
		"MB057B-GAL4/ UAS-*Shibire^{ts}": normally distributed p= 0.95998	One-Sample T-test with Bonferroni Correction: ***p= 3.33952E-5	
	Block during training 1	**"MB057B-GAL4"**: normally distributed p= 0.9723	One-Sample T-test with Bonferroni Correction: ***p= 1.19795E-5	Two-Sample T-test with Welch's correction: p= 0.23706
		"MB057B-GAL4/ UAS-*Shibire^{ts}": normally distributed p= 0.60831	One-Sample T-test with Bonferroni Correction: **p= 5.75767E-4	

	Block during training 2	**"MB057B-GAL4"**: normally distributed p= 0.72174	One-Sample T-test with Bonferroni Correction: ***p= 4.10076E-5	Two-Sample T-test with Welch's correction: p= 0.29568
		"MB057B-GAL4/ UAS-*Shibire^{ts}*": normally distributed p= 0.86812	One-Sample T-test with Bonferroni Correction: **p= 5.75767E-4	
	Block during test	**"MB057B-GAL4"**: normally distributed p= 0.98237	One-Sample T-test with Bonferroni Correction: ***p= 1.3395E-7	Two-Sample T-test with Welch's correction: p= 0.52003
		"MB057B-GAL4/ UAS-*Shibire^{ts}*": normally distributed p= 0.70963	One-Sample T-test with Bonferroni Correction: ***p= 4.03732E-5	
Figure 2J	CTC	**"MB399B-GAL4"**: normally distributed p= 0.3723	One-Sample T-test with Bonferroni Correction: ***p= 2.66838E-4	Two-Sample T-test with Welch's correction: p= 0.3282
		"MB399B-GAL4/ UAS-*Shibire^{ts}*": normally distributed p= 0.34541	One-Sample T-test with Bonferroni Correction: ***p= 7.4196E-5	
	Block during training 1	**"MB399B-GAL4"**: normally distributed p= 0.91995	One-Sample T-test with Bonferroni Correction: ***p= 1.6738E-4	Two-Sample T-test with Welch's correction: p= 0.61232
		"MB399B-GAL4/ UAS-*Shibire^{ts}*": normally distributed p= 0.05615	One-Sample T-test with Bonferroni Correction: **p= 0.00126	
	Block during training 2	**"MB399B-GAL4"**: normally distributed p= 0.7954	One-Sample T-test with Bonferroni Correction: **p= 0.00122	Two-Sample T-test with Welch's correction: p= 0.96658

		"MB399B-GAL4/ UAS-*Shibire^{ts}*": normally distributed p= 0.69167	One-Sample T-test with Bonferroni Correction: **p= 0.00613	
	Block during test	**"MB399B-GAL4"**: normally distributed p= 0.46731	One-Sample T-test with Bonferroni Correction: ***p= 8.32226E-4	Two-Sample T-test with Welch's correction: p= 0.74639
		"MB399B-GAL4/ UAS-*Shibire^{ts}*": normally distributed p= 0.50376	One-Sample T-test with Bonferroni Correction: ***p= 1.35637E-5	
Figure 3A	CTC	**"TH-GAL4"**: normally distributed p=0.24822	One-Sample T-test with Bonferroni Correction: ***p=9.71045E-9	Two-Sample T-test with Welch's correction: p=0.78532
		"TH-GAL4/ UAS-*Shibire^{ts}*": normally distributed p=0.48713	One-Sample T-test with Bonferroni Correction: ***p=1.39337E-8	
	Block during training 1	**"TH-GAL4"**: normally distributed p=0.72306	One-Sample T-test with Bonferroni Correction: ***p=3.1517E-6	Two-Sample T-test with Welch's correction: ***p= 9.77434E-6
		"TH-GAL4/ UAS-*Shibire^{ts}*": normally distributed p=0.46243	One-Sample T-test with Bonferroni Correction: p=0.87697	
	Block during training 2	**"TH-GAL4"**: normally distributed p=0.78861	One-Sample T-test with Bonferroni Correction: ***p=3.10429E-8	Two-Sample T-test with Welch's correction: ***p= 9.71407E-5
		"TH-GAL4/ UAS-*Shibire^{ts}*": normally distributed p= 0.35852	One-Sample T-test with Bonferroni Correction: p= 0.69617	
	Block during test	**"TH-GAL4"**: normally distributed p=0.26275	One-Sample T-test with Bonferroni Correction: ***p=6.07523E-6	Two-Sample T-test with Welch's correction: p= 0.87072

		"TH-GAL4/ UAS-*Shibire^{ts}*": normally distributed p=0.90566	One-Sample T-test with Bonferroni Correction: ***p=1.56607E-4	
Figure 3B	CTC	**"R58E02-GAL4"**: normally distributed p=0.13479	One-Sample T-test with Bonferroni Correction: ***p=2.33276E-6	Two-Sample T-test with Welch's correction: p= 0.33459
		"R58E02-GAL4/ UAS-*Shibire^{ts}*": normally distributed p=0.62826	One-Sample T-test with Bonferroni Correction: ***p=4.72624E-7	
	Block during training 1	**"R58E02-GAL4"**: normally distributed p=0.47987	One-Sample T-test with Bonferroni Correction: ***p=2.07247E-7	Two-Sample T-test with Welch's correction: p= 0.33709
		"R58E02-GAL4/ UAS-*Shibire^{ts}*": normally distributed p= 0.06261	One-Sample T-test with Bonferroni Correction: ***p= 6.24009E-6	
	Block during training 2	**"R58E02-GAL4"**: normally distributed p=0.99142	One-Sample T-test with Bonferroni Correction: ***p=9.25273E-6	Two-Sample T-test with Welch's correction: p= 0.89889
		"R58E02-GAL4/ UAS-*Shibire^{ts}*": normally distributed p=0.55887	One-Sample T-test with Bonferroni Correction: ***p=3.82448E-6	
	Block during test	**"R58E02-GAL4"**: normally distributed p=0.29512	One-Sample T-test with Bonferroni Correction: ***p=2.1924E-6	Two-Sample T-test with Welch's correction: p= 0.85683
		"R58E02-GAL4/ UAS-*Shibire^{ts}*": normally distributed p=0.97878	One-Sample T-test with Bonferroni Correction: ***p=2.52034E-9	

Figure 3C	CTC	**"MB320C-GAL4"**: normally distributed p=0.92394	One-Sample T-test with Bonferroni Correction: ***p=5.7839E-6	Two-Sample T-test with Welch's correction: p= 0.67689
		"MB320C-GAL4/ UAS-*Shibire^{ts}*": normally distributed p= 0.75306	One-Sample T-test with Bonferroni Correction: ***p= 1.97415E-6	
	Block during training 1	**"MB320C-GAL4"**: normally distributed p= 0.92696	One-Sample T-test with Bonferroni Correction: ***p= 5.55592E-8	Two-Sample T-test with Welch's correction: *p= 0.02675
		"MB320C-GAL4/ UAS-*Shibire^{ts}*": normally distributed p= 0.47381	One-Sample T-test with Bonferroni Correction: **p= 0.00539	
	Block during training 2	**"MB320C-GAL4"**: normally distributed p= 0.89834	One-Sample T-test with Bonferroni Correction: ***p= 5.03728E-6	Two-Sample T-test with Welch's correction: ***p= 7.45925E-5
		"MB320C-GAL4/ UAS-*Shibire^{ts}*": normally distributed p= 0.14694	One-Sample T-test with Bonferroni Correction: p= 0.62606	
	Block during test	**"MB320C-GAL4"**: normally distributed p= 0.85965	One-Sample T-test with Bonferroni Correction: ***p= 1.80928E-6	Two-Sample T-test with Welch's correction: p= 0.29169
		"MB320C-GAL4/ UAS-*Shibire^{ts}*": normally distributed p= 0.36231	One-Sample T-test with Bonferroni Correction: ***p= 7.37688E-5	
Figure 3D	CTC	**"MB296B-GAL4"**: normally distributed p= 0.88478	One-Sample T-test with Bonferroni Correction: ***p= 1.62091E-5	Two-Sample T-test with Welch's correction: p= 0.83979

		"MB296B-GAL4/ UAS-*Shibire^{ts}": normally distributed p= 0.09651	One-Sample T-test with Bonferroni Correction: ***p= 1.26966E-6	
	Block during training 1	**"MB296B-GAL4"**: normally distributed p= 0.91725	One-Sample T-test with Bonferroni Correction: ***p= 1.91131E-5	Two-Sample T-test with Welch's correction: *p= 0.03061
		"MB296B-GAL4/ UAS-*Shibire^{ts}": normally distributed p= 0.80028	One-Sample T-test with Bonferroni Correction: **p= 0.00918	
	Block during training 2	**"MB296B-GAL4"**: normally distributed p= 0.30442	One-Sample T-test with Bonferroni Correction: ***p= 2.65866E-5	Two-Sample T-test with Welch's correction: p= 0.94672
		"MB296B-GAL4/ UAS-*Shibire^{ts}": normally distributed p= 0.68291	One-Sample T-test with Bonferroni Correction: ***p= 1.35106E-5	
	Block during test	**"MB296B-GAL4"**: normally distributed p= 0.15288	One-Sample T-test with Bonferroni Correction: ***p= 8.27333E-5	Two-Sample T-test with Welch's correction: p= 0.65428
		"MB296B-GAL4/ UAS-*Shibire^{ts}": normally distributed p= 0.22906	One-Sample T-test with Bonferroni Correction: ***p= 2.66108E-6	
Figure 3E	CTC	**"MB058B-GAL4"**: normally distributed p= 0.57268	One-Sample T-test with Bonferroni Correction: ***p= 7.87259E-5	Two-Sample T-test with Welch's correction: p= 0.77088
		"MB058B-GAL4/ UAS-*Shibire^{ts}": normally distributed p= 0.48991	One-Sample T-test with Bonferroni Correction: ***p= 9.87769E-5	

	Block during training 1	**"MB058B-GAL4"**: normally distributed p= 0.96651	One-Sample T-test with Bonferroni Correction: ***p= 2.23005E-5	Two-Sample T-test with Welch's correction: p= 0.64445
		"MB058B-GAL4/ UAS-*Shibire^{ts}*": normally distributed p= 0.80529	One-Sample T-test with Bonferroni Correction: ***p= 7.55129E-5	
	Block during training 2	**"MB058B-GAL4"**: normally distributed p= 0.66809	One-Sample T-test with Bonferroni Correction: ***p= 1.82769E-9	Two-Sample T-test with Welch's correction: p= 0.4977
		"MB058B-GAL4/ UAS-*Shibire^{ts}*": normally distributed p= 0.22744	One-Sample T-test with Bonferroni Correction: ***p= 4.24872E-6	
	Block during test	**"MB058B-GAL4"**: normally distributed p= 0.10546	One-Sample T-test with Bonferroni Correction: ***p= 5.56796E-6	Two-Sample T-test with Welch's correction: p= 0.88733
		"MB058B-GAL4/ UAS-*Shibire^{ts}*": normally distributed p= 0.30829	One-Sample T-test with Bonferroni Correction: ***p= 9.43277E-6	
Figure 3F	CTC	**"MB304B-GAL4"**: normally distributed p= 0.68795	One-Sample T-test with Bonferroni Correction: **p= 0.00133	Two-Sample T-test with Welch's correction: p= 0.9851
		"MB304B-GAL4/ UAS-*Shibire^{ts}*": normally distributed p= 0.34716	One-Sample T-test with Bonferroni Correction: ***p= 8.76527E-5	
	Block during training 1	**"MB304B-GAL4"**: normally distributed p= 0.23476	One-Sample T-test with Bonferroni Correction: ***p= 2.19664E-4	Two-Sample T-test with Welch's correction: p= 0.9669

		"MB304B-GAL4/ UAS-*Shibire^{ts}": normally distributed p= 0.73575	One-Sample T-test with Bonferroni Correction: ***p= 1.97473E-4	
	Block during training 2	**"MB304B-GAL4"**: normally distributed p= 0.95662	One-Sample T-test with Bonferroni Correction: **p= 0.00271	Two-Sample T-test with Welch's correction: p= 0.99163
		"MB304B-GAL4/ UAS-*Shibire^{ts}": normally distributed p= 0.98675	One-Sample T-test with Bonferroni Correction: ***p= 4.00183E-5	
	Block during test	**"MB304B-GAL4"**: normally distributed p= 0.59637	One-Sample T-test with Bonferroni Correction: **p= 6.67108E-4	Two-Sample T-test with Welch's correction: p= 0.85417
		"MB304B-GAL4/ UAS-*Shibire^{ts}": normally distributed p= 0.0722	One-Sample T-test with Bonferroni Correction: ***p= 2.27799E-4	
Figure 6B		**"CSCh"**: normally distributed p=0.6051		Two-tailed Unpaired T-test with Welch's correction: ***p=0.0009
		"MB091C > CsCh": normally distributed p=0.3469		
Figure 6D		**"CSCh"**: normally distributed p=0.1093		Two-tailed Unpaired T-test with Welch's correction: ***p<0.0001
		"MB112C > CsCh": normally distributed p=0.7207		
Figure 5F	Paired-Paired	**"CS1 Pre"**: normally distributed p= 0.23397		Two-Tailed Paired-Sample T-test: **Pre** vs **Post** ***p= 1.59115E-5
		"CS1 Post": normally distributed p= 0.47725		
		"CS$^-$ Pre": normally distributed p= 0.29163		Two-Tailed Paired-Sample T-test: **Pre** vs **Post** p= 0.4888
		"CS$^-$ Post": normally distributed p= 0.21333		

		“CS2 Pre”: normally distributed p= 0.11469	Two-Tailed Paired-Sample T-test: **Pre** vs **Post** ***p= 9.179E-5
		“CS2 Post”: normally distributed p= 0.21979	
	Paired-Unpaired	**“CS1 Pre”**: normally distributed p= 0.81547	Two-Tailed Paired-Sample T-test: **Pre** vs **Post** ***p= 1.82703E-4
		“CS1 Post”: normally distributed p= 0.47219	
		“CS- Pre”: normally distributed p= 0.55068	Two-Tailed Paired-Sample T-test: **Pre** vs **Post** p= 0.7569
		“CS- Post”: normally distributed p=0.49613	
		“CS2 Pre”: normally distributed p=0.91325	Two-Tailed Paired-Sample T-test: **Pre** vs **Post** p= 0.10688
		“CS2 Post”: normally distributed p=0.3871	
	Unpaired-Paired	**“CS1 Pre”**: normally distributed p= 0.49092	Two-Tailed Paired-Sample T-test: **Pre** vs **Post** p= 0.93047
		“CS1 Post”: normally distributed p= 0.71326	
		“CS- Pre”: normally distributed p= 0.0946	Two-Tailed Paired-Sample T-test: **Pre** vs **Post** p= 0.95701
		“CS- Post”: normally distributed p= 0.34086	
		“CS2 Pre”: normally distributed p= 0.42989	Two-Tailed Paired-Sample T-test: **Pre** vs **Post** p= 0.66974
		“CS2 Post”: normally distributed p= 0.16898	
Figure 5D	Paired-Paired	**“CS1 Pre”**: normally distributed p= 0.87222	Two-Tailed Paired-Sample T-test: **Pre** vs **Post** *p= 0.04007
		“CS1 Post”: normally distributed p= 0.57235	
		“CS- Pre”: normally distributed p= 0.15633	Two-Tailed Paired-Sample T-test: **Pre** vs **Post** p= 0.43132
		“CS- Post”: normally distributed p= 0.25895	
		“CS2 Pre”: normally distributed p= 0.21859	Two-Tailed Paired-Sample T-test: **Pre** vs **Post** p= 0.18478
		“CS2 Post”: normally distributed p= 0.29652	
	Paired-Unpaired	**“CS1 Pre”**: normally distributed p= 0.12089	Two-Tailed Paired-Sample T-test: **Pre** vs **Post** *p= 0.02849
		“CS1 Post”: normally distributed p= 0.25453	
		“CS- Pre”: normally distributed p= 0.58046	Two-Tailed Paired-Sample T-test: **Pre**

		"CS⁻ Post": normally distributed p= 0.36		vs **Post** p= 0.17612
		"CS2 Pre": normally distributed p= 0.32809		Two-Tailed Paired-Sample T-test: **Pre** vs **Post** p= 0.90867
		"CS2 Post": normally distributed p= 0.63367		
	Unpaired-Paired	**"CS1 Pre"**: normally distributed p= 0.06281		Two-Tailed Paired-Sample T-test: **Pre** vs **Post** p= 0.59083
		"CS1 Post": normally distributed p= 0.82976		
		"CS⁻ Pre": normally distributed p= 0.62572		Two-Tailed Paired-Sample T-test: **Pre** vs **Post** p= 0.05939
		"CS⁻ Post": normally distributed p= 0.13634		
		"CS2 Pre": normally distributed p= 0.14752		Two-Tailed Paired-Sample T-test: **Pre** vs **Post** p= 0.82582
		"CS2 Post": normally distributed p= 0.17802		
Figure 7B		"**Paired-Paired-Paired**" **P-P-P**: normally distributed p= 0.75531	One-Sample Wilcoxon Signed Rank test with Bonferroni correction: ***p= 2.44141E-4	Kruskal-Wallis Anova: Chi square= 19.95796; ***p= 1.73182E-4 Post-hoc Dunn's test: **P-P-P** vs **P-P-U** **p= 0.00166 **P-P-P** vs **P-U-P** ***p= 4.69173E-4 **P-P-P** vs **U-P-P** **p= 0.00825 **P-P-U** vs **P-U-P** p= 1 **P-P-U** vs **U-P-P** p= 1 **P-U-P** vs **U-P-P** p= 1
		"**Paired-Paired-Unpaired**" **P-P-U**: Not normally distributed ***p= 7.03394E-5	One-Sample Wilcoxon Signed Rank test with Bonferroni correction: p= 0.97797	
		"**Paired-Unpaired-Paired**" **P-U-P**: normally distributed p= 0.45329	One-Sample Wilcoxon Signed Rank test with Bonferroni correction: p= 0.4212	
		"**Unpaired-Paired-Paired**" **U-P-P**: Not normally distributed **p= 0.00613	One-Sample Wilcoxon Signed Rank test with Bonferroni correction: p= 0.78195	
Suppl.Figure 1C (Box plots)		"**MCH vs 3-OCT**": normally distributed p= 0.84295	One-Sample T-test with Bonferroni Correction: p= 0.38787	One-Way Anova: F= 0.33403; p= 0.71977 Post-hoc Tukey

		“**MCH vs BenzA**”: normally distributed p= 0.06791	One-Sample T-test with Bonferroni Correction: p= 0.47477	test: **MCH vs 3-OCT** vs **MCH vs BenzA** p= 0.99648 **MCH vs 3-OCT** vs **BenzA vs 3-OCT** p= 0.74022 **MCH vs BenzA** vs **BenzA vs 3-OCT** p= 0.78631
		“**BenzA vs 3-OCT**”: normally distributed p= 0.05777	One-Sample T-test with Bonferroni Correction: p= 0.91103	
Suppl. Figure 1D		“**FOC**”: normally distributed p= 0.7987	One-Sample T-test with Bonferroni Correction: ***p= 1.44741E-15	One-Way Anova: F= 29.37658; ***p= 5.89484E-10 Post-hoc Tukey test: **FOC** vs **3x FOC** ***p= 1.85544E-4 **FOC** vs **SOC** ***p= 0 **3x FOC** vs **SOC** **p= 0.00273
		“**3x FOC**”: normally distributed p= 0.95668	One-Sample T-test with Bonferroni Correction: ***p= 3.93192E-10	
		“**SOC**”: normally distributed p= 0.97281	One-Sample T-test with Bonferroni Correction: ***p= 1.07044E-8	
Suppl. Figure1 1E	First-order condition.	“**MCH vs 3-OCT**”: normally distributed p= 0.91558	One-Sample T-test with Bonferroni Correction: ***p= 1.50467E-5	One-Way Anova: F= 2.79163; p= 0.08412 Post-hoc Tukey test: **MCH vs 3-OCT** vs **MCH vs BenzA** 0.15215 **MCH vs 3-OCT** vs **BenzA vs 3-OCT** p= 0.97888 **MCH vs BenzA** vs **BenzA vs 3-OCT** p= 0.10628
		“**MCH vs BenzA**”: normally distributed p= 0.21914	One-Sample T-test with Bonferroni Correction: ***p= 2.37049E-5	
		“**BenzA vs 3-OCT**”: normally distributed p= 0.19936	One-Sample T-test with Bonferroni Correction: ***p= 5.41069E-7	
	Second-order Condition. (Paired-Paired)	“**Combi.1 (blue)**”: normally distributed p= 0.87733	One-Sample T-test with Bonferroni Correction: ***p= 2.8546E-4	One-Way Anova: F= 1.99852; p= 0.1605 Post-hoc Tukey

		“**Combi.2 (yellow)**”: normally distributed p= 0.17612	One-Sample T-test with Bonferroni Correction: ***p= 1.53619E-4	test: **Combi.1 (blue)** vs **Combi.2 (yellow)** p= 0.61764 **Combi.1 (blue)** vs **Combi.3 (green)** p= 0.13731 **Combi.2 (yellow)** vs **Combi.3 (green)** p= 0.55355
		“**Combi.3 (green)**”: normally distributed p= 0.92956	One-Sample T-test with Bonferroni Correction: *p= 0.01802	
	Second-order Condition. (Paired-Unpaired)	“**Combi.1 (blue)**”: normally distributed p= 0.34899	One-Sample T-test with Bonferroni Correction: p= 0.40619	One-Way Anova: F= 3.02175; p= 0.07025 Post-hoc Tukey test: **Combi.1 (blue)** vs **Combi.2 (yellow)** p= 0.07641 **Combi.1 (blue)** vs **Combi.3 (green)** p= 0.16791 **Combi.2 (yellow)** vs **Combi.3 (green)** p= 0.9057
		“**Combi.2 (yellow)**”: normally distributed p= 0.34588	One-Sample T-test with Bonferroni Correction: p= 0.0818	
		“**Combi.3 (green)**”: normally distributed p= 0.46395	One-Sample T-test with Bonferroni Correction: p= 0.05927	
	Second-order Condition. (Unpaired-Paired)	“**Combi.1 (blue)**”: normally distributed p= 0.2777	One-Sample T-test with Bonferroni Correction: p= 0.47274	One-Way Anova: F= 0.39625; p= 0.67776 Post-hoc Tukey test: **Combi.1 (blue)** vs **Combi.2 (yellow)** p= 0.96652 **Combi.1 (blue)** vs **Combi.3 (green)** p= 0.66789 **Combi.2 (yellow)** vs **Combi.3 (green)** p= 0.81311
		“**Combi.2 (yellow)**”: normally distributed p= 0.20822	One-Sample T-test with Bonferroni Correction: p= 0.87267	
		“**Combi.3 (green)**”: normally distributed p= 0.77742	One-Sample T-test with Bonferroni Correction: p= 0.54015	
Suppl. Figure 2E 1x FOC (γ1-	CTC	**“MB112C-GAL4”**: normally distributed p= 0.4294	One-Sample T-test with Bonferroni Correction: ***p= 2.4158E-5	Two-Sample T-test with Welch’s correction: p=0.91359

pedc MBON)		**"MB112C-GAL4/ UAS-*Shibire^{ts}"**: normally distributed p= 0.99408	One-Sample T-test with Bonferroni Correction: ***p= 2.93421E-6	
	Block during FOC	**"MB112C-GAL4"**: normally distributed p= 0.25908	One-Sample T-test with Bonferroni Correction: ***p= 1.12593E-6	Two-Sample T-test with Welch's correction: p=0.87605
		"MB112C-GAL4/ UAS-*Shibire^{ts}": normally distributed p= 0.81427	One-Sample T-test with Bonferroni Correction: ***p= 2.64977E-6	
	Block during test	**"MB112C-GAL4"**: normally distributed p= 0.19218	One-Sample T-test with Bonferroni Correction: ***p= 3.34563E-6	Two-Sample T-test with Welch's correction: ***p=3.54065E-8
		"MB112C-GAL4/ UAS-*Shibire^{ts}": normally distributed p= 0.22103	One-Sample T-test with Bonferroni Correction: *p= 0.04752	
Suppl. Figure 2E 1x FOC (α'2 MBON)	CTC	**"MB018B-GAL4"**: normally distributed p=0.23704	One-Sample T-test with Bonferroni Correction: ***p= 2.1975E-5	Two-Sample T-test with Welch's correction: p=0.66724
		"MB018B-GAL4/ UAS-*Shibire^{ts}": normally distributed p=0.25804	One-Sample T-test with Bonferroni Correction: p= 4.72062E-6	
	Block during FOC	**"MB018B-GAL4"**: normally distributed p=0.27591	One-Sample T-test with Bonferroni Correction: ***p= 2.05885E-5	Two-Sample T-test with Welch's correction: p=0.73903
		"MB018B-GAL4/ UAS-*Shibire^{ts}": normally distributed p=0.85975	One-Sample T-test with Bonferroni Correction: ***p= 2.91382E-6	

	Block during test	**"MB018B-GAL4"**: normally distributed p=0.14204	One-Sample T-test with Bonferroni Correction: ***p= 1.64212E-5	Two-Sample T-test with Welch's correction: p=0.95566
		"MB018B-GAL4/ UAS-*Shibire^{ts}*": normally distributed p=0.57807	One-Sample T-test with Bonferroni Correction: ***p= 1.14833E-4	
Suppl. Figure 2E 1x FOC (γ5β'2a-β'2mp MBON)	CTC	**"MB210B-GAL4"**: normally distributed p=0.96298	One-Sample T-test with Bonferroni Correction: ***p= 2.59554E-6	Two-Sample T-test with Welch's correction: p=0.43702
		"MB210B-GAL4/ UAS-*Shibire^{ts}*": normally distributed p=0.42075	One-Sample T-test with Bonferroni Correction: ***p= 1.99784E-6	
	Block during FOC	**"MB210B-GAL4"**: normally distributed p=0.31555	One-Sample T-test with Bonferroni Correction: ***p= 9.17378E-6	Two-Sample T-test with Welch's correction: p=0.6052
		"MB210B-GAL4/ UAS-*Shibire^{ts}*": normally distributed p=0.22127	One-Sample T-test with Bonferroni Correction: ***p= 1.03626E-6	
	Block during test	**"MB210B-GAL4"**: normally distributed p=0.92533	One-Sample T-test with Bonferroni Correction: ***p= 2.07205E-6	Two-Sample T-test with Welch's correction: ***p=2.2694E-5
		"MB210B-GAL4/ UAS-*Shibire^{ts}*": normally distributed p=0.92041	One-Sample T-test with Bonferroni Correction: p= 0.0979	
Suppl. Figure 2F 3x FOC (γ1-pedc MBON)	CTC	**"MB112C-GAL4"**: normally distributed p= 0.11294	One-Sample T-test with Bonferroni Correction: **p= 0.00618	Two-Sample T-test with Welch's correction: p=0.865

		"MB112C-GAL4/ UAS-*Shibire^{ts}*": normally distributed p= 0.87808	One-Sample T-test with Bonferroni Correction: **p= 0.00197	
	Block during 3x FOC	**"MB112C-GAL4"**: normally distributed p= 0.09462	One-Sample T-test with Bonferroni Correction: **p= 5.23965E-4	Two-Sample T-test with Welch's correction: p=0.82853
		"MB112C-GAL4/ UAS-*Shibire^{ts}*": normally distributed p= 0.55205	One-Sample T-test with Bonferroni Correction: ***p= 2.4382E-4	
	Block during test	**"MB112C-GAL4"**: normally distributed p= 0.44701	One-Sample T-test with Bonferroni Correction: *p= 0.01996	Two-Sample T-test with Welch's correction: *p=0.01755
		"MB112C-GAL4/ UAS-*Shibire^{ts}*": normally distributed p= 0.61509	One-Sample T-test with Bonferroni Correction: p= 0.43034	
Suppl. Figure 2F 3x FOC (α'2 MBON)	CTC	**"MB018B-GAL4"**: normally distributed p=0.38952	One-Sample T-test with Bonferroni Correction: **p= 0.00239	Two-Sample T-test with Welch's correction: p=0.77087
		"MB018B-GAL4/ UAS-*Shibire^{ts}*": normally distributed p=0.67001	One-Sample T-test with Bonferroni Correction: *p= 0.00516	
	Block during 3x FOC	**"MB018B-GAL4"**: normally distributed p=0.10872	One-Sample T-test with Bonferroni Correction: **p= 6.10084E-4	Two-Sample T-test with Welch's correction: p=0.94475
		"MB018B-GAL4/ UAS-*Shibire^{ts}*": normally distributed p=0.83714	One-Sample T-test with Bonferroni Correction: **p= 0.00347	

	Block during test	**"MB018B-GAL4"**: normally distributed p=0.32969	One-Sample T-test with Bonferroni Correction: **p= 0.00104	Two-Sample T-test with Welch's correction: p=0.77705
		"MB018B-GAL4/ UAS-*Shibire^{ts}*": normally distributed p=0.07214	One-Sample T-test with Bonferroni Correction: **p= 0.00164	
Suppl. Figure 2F 3x FOC (γ5β'2a-β'2mp MBON)	CTC	**"MB210B-GAL4"**: normally distributed p=0.64772	One-Sample T-test with Bonferroni Correction: **p= 9.56738E-4	Two-Sample T-test with Welch's correction: p=0.86542
		"MB210B-GAL4/ UAS-*Shibire^{ts}*": normally distributed p=0.28886	One-Sample T-test with Bonferroni Correction: **p= 0.00131	
	Block during 3x FOC	**"MB210B-GAL4"**: normally distributed p=0.67396	One-Sample T-test with Bonferroni Correction: **p= 0.00113	Two-Sample T-test with Welch's correction: p=0.36139
		"MB210B-GAL4/ UAS-*Shibire^{ts}*": normally distributed p=0.48693	One-Sample T-test with Bonferroni Correction: **p= 0.00619	
	Block during test	**"MB210B-GAL4"**: normally distributed p=0.24118	One-Sample T-test with Bonferroni Correction: **p= 7.81159E-4	Two-Sample T-test with Welch's correction: p=0.82153
		"MB210B-GAL4/ UAS-*Shibire^{ts}*": normally distributed p=0.21422	One-Sample T-test with Bonferroni Correction: ***p= 3.00631E-4	
Suppl. Figure 3D 1x FOC (γ1DAN)	CTC	**"MB320C-GAL4"**: normally distributed p= 0.17866	One-Sample T-test with Bonferroni Correction: ***p= 3.11943E-6	Two-Sample T-test with Welch's correction: p= 0.51335

		“MB320C-GAL4/ UAS-*Shibire^{ts}*”: normally distributed p= 0.17225	One-Sample T-test with Bonferroni Correction: ***p= 3.48891E-6	
	Block during FOC	**“MB320C-GAL4”**: normally distributed p= 0.10339	One-Sample T-test with Bonferroni Correction: ***p= 1.53685E-6	Two-Sample T-test with Welch’s correction: ***p= 8.20829E-5
		“MB320C-GAL4/ UAS-*Shibire^{ts}*”: normally distributed p= 0.50533	One-Sample T-test with Bonferroni Correction: p= 0.8332	
	Block during test	**“MB320C-GAL4”**: normally distributed p= 0.29351	One-Sample T-test with Bonferroni Correction: ***p= 2.27689E-7	Two-Sample T-test with Welch’s correction: p= 0.95403
		“MB320C-GAL4/ UAS-*Shibire^{ts}*”: normally distributed p= 0.9403	One-Sample T-test with Bonferroni Correction: ***p= 9.23225E-6	
Suppl. Figure 3D 1x FOC (γ2/α‘1 DAN)	CTC	**“MB296B-GAL4”**: normally distributed p=0.41662	One-Sample T-test with Bonferroni Correction: ***p=9.18885E-6	Two-Sample T-test with Welch’s correction: p= 0.45869
		“MB296B-GAL4/ UAS-*Shibire^{ts}*”: normally distributed p=0.62658	One-Sample T-test with Bonferroni Correction: ***p=3.40096E-6	
	Block during FOC	**“MB296B-GAL4”**: normally distributed p=0.26063	One-Sample T-test with Bonferroni Correction: ***p=3.09122E-6	Two-Sample T-test with Welch’s correction: ***p= 9.12234E-5
		“MB296B-GAL4/ UAS-*Shibire^{ts}*”: normally distributed p=0.69077	One-Sample T-test with Bonferroni Correction: p=0.24088	

	Block during test	**"MB296B-GAL4"**: normally distributed p=0.29803	One-Sample T-test with Bonferroni Correction: ***p=3.91844E-6	Two-Sample T-test with Welch's correction: p= 0.98984
		"MB296B-GAL4/ UAS-*Shibire^{ts}*": normally distributed p=0.98935	One-Sample T-test with Bonferroni Correction: ***p=7.61172E-8	
Suppl. Figure 3E 3x FOC (γ1 DAN)	CTC	**"MB320C-GAL4"**: normally distributed p=0.50777	One-Sample T-test with Bonferroni Correction: *p=0.01598	Two-Sample T-test with Welch's correction: p=0.92636
		"MB320C-GAL4/ UAS-*Shibire^{ts}*": normally distributed p=0.41065	One-Sample T-test with Bonferroni Correction: *p=0.00542	
	Block during 3x FOC	**"MB320C-GAL4"**: normally distributed p=0.43383	One-Sample T-test with Bonferroni Correction: **p=0.00253	Two-Sample T-test with Welch's correction: **p=0.0148
		"MB320C-GAL4/ UAS-*Shibire^{ts}*": normally distributed p=0.23623	One-Sample T-test with Bonferroni Correction: p=0.81098	
	Block during test	**"MB320C-GAL4"**: normally distributed p=0.66956	One-Sample T-test with Bonferroni Correction: **p=0.00231	Two-Sample T-test with Welch's correction: p=0.68907
		"MB320C-GAL4/ UAS-*Shibire^{ts}*": normally distributed p=0.75584	One-Sample T-test with Bonferroni Correction: **p=0.00621	
Suppl. Figure 3E 3x FOC (γ2/α'1 DAN)	CTC	**"MB296B-GAL4"**: normally distributed p=0.24852	One-Sample T-test with Bonferroni Correction: ***p=2.51917E-4	Two-Sample T-test with Welch's correction: p=0.76523

		“MB296B-GAL4/ UAS-*Shibire^{ts}”: normally distributed p=0.65231	One-Sample T-test with Bonferroni Correction: **p=0.00156	
	Block during 3x FOC	**“MB296B-GAL4”**: normally distributed p=0.05212	One-Sample T-test with Bonferroni Correction: **p=0.00222	Two-Sample T-test with Welch’s correction: *p=0.03515
		“MB296B-GAL4/ UAS-*Shibire^{ts}”: normally distributed p=0.15229	One-Sample T-test with Bonferroni Correction: p=0.10976	
	Block during test	**“MB296B-GAL4”**: normally distributed p=0.16926	One-Sample T-test with Bonferroni Correction: **p=5.63551E-4	Two-Sample T-test with Welch’s correction: p=0.57314
		“MB296B-GAL4/ UAS-*Shibire^{ts}”: normally distributed p=0.41493	One-Sample T-test with Bonferroni Correction: **p=0.00496	

References

Aso, Y., & Rubin, G. M. (2016). Dopaminergic neurons write and update memories with cell-type-specific rules. *eLife*, *5*, e16135. https://doi.org/10.7554/eLife.16135

Aso, Y., Hattori, D., Yu, Y., Johnston, R. M., Iyer, N. A., Ngo, T. T., Dionne, H., Abbott, L. F., Axel, R., Tanimoto, H., & Rubin, G. M. (2014a). The neuronal architecture of the mushroom body provides a logic for associative learning. *eLife*, *3*, e04577. https://doi.org/10.7554/eLife.04577

Aso, Y., Herb, A., Ogueta, M., Siwanowicz, I., Templier, T., Friedrich, A. B., Ito, K., Scholz, H., & Tanimoto, H. (2012). Three dopamine pathways induce aversive odor memories with different stability. *PLoS genetics*, *8*(7), e1002768. https://doi.org/10.1371/journal.pgen.1002768

Aso, Y., Sitaraman, D., Ichinose, T., Kaun, K. R., Vogt, K., Belliart-Guérin, G., Plaçais, P. Y., Robie, A. A., Yamagata, N., Schnaitmann, C., Rowell, W. J., Johnston, R. M., Ngo, T. T., Chen, N., Korff, W., Nitabach, M. N., Heberlein, U., Preat, T., Branson, K. M., Tanimoto, H., … Rubin, G. M. (2014b). Mushroom body output neurons encode valence and guide memory-based action selection in Drosophila. *eLife*, *3*, e04580. https://doi.org/10.7554/eLife.04580

Barth, J., Dipt, S., Pech, U., Hermann, M., Riemensperger, T., & Fiala, A. (2014). Differential associative training enhances olfactory acuity in Drosophila melanogaster. *The Journal of neuroscience : the official journal of the Society for Neuroscience*, *34*(5), 1819–1837. https://doi.org/10.1523/JNEUROSCI.2598-13.2014

Bennett, J. E. M., Philippides, A., & Nowotny, T. (2021). Learning with reinforcement prediction errors in a model of the Drosophila mushroom body. *Nature communications*, *12*(1), 2569. https://doi.org/10.1038/s41467-021-22592-4

Berry, J. A., Cervantes-Sandoval, I., Chakraborty, M., & Davis, R. L. (2015). Sleep Facilitates Memory by Blocking Dopamine Neuron-Mediated Forgetting. *Cell*, *161*(7), 1656–1667. https://doi.org/10.1016/j.cell.2015.05.027

Bilz, F., Geurten, B. R. H., Hancock, C. E., Widmann, A., & Fiala, A. (2020). Visualization of a Distributed Synaptic Memory Code in the Drosophila Brain. *Neuron*, *106*(6), 963–976.e4. https://doi.org/10.1016/j.neuron.2020.03.010

Bitterman, M. E., Menzel, R., Fietz, A., & Schäfer, S. (1983). Classical conditioning of proboscis extension in honeybees (Apis mellifera). *Journal of comparative psychology (Washington, D.C. : 1983)*, *97*(2), 107–119. https://doi.org/10.1037/0735-7036.97.2.107

Boto, T., Stahl, A., & Tomchik, S. M. (2020). Cellular and circuit mechanisms of olfactory associative learning in *Drosophila*. *Journal of neurogenetics*, *34*(1), 36–46. https://doi.org/10.1080/01677063.2020.1715971

Brembs, B., & Heisenberg, M. (2001). Conditioning with compound stimuli in Drosophila melanogaster in the flight simulator. *The Journal of experimental biology*, *204*(Pt 16), 2849–2859. https://doi.org/10.1242/jeb.204.16.2849

Busto, G. U., Cervantes-Sandoval, I., & Davis, R. L. (2010). Olfactory learning in Drosophila. *Physiology (Bethesda, Md.)*, *25*(6), 338–346. https://doi.org/10.1152/physiol.00026.2010

Chen, T. W., Wardill, T. J., Sun, Y., Pulver, S. R., Renninger, S. L., Baohan, A., Schreiter, E. R., Kerr, R. A., Orger, M. B., Jayaraman, V., Looger, L. L., Svoboda, K., & Kim, D. S. (2013). Ultrasensitive fluorescent proteins for imaging neuronal activity. *Nature*, *499*(7458), 295–300. https://doi.org/10.1038/nature12354

Craddock, P., Wasserman, J. S., Polack, C. W., Kosinski, T., Renaux, C., & Miller, R. R. (2018). Associative structure of second-order conditioning in humans. *Learning & behavior*, *46*(2), 171–181. https://doi.org/10.3758/s13420-017-0299-5

Dana, H., Sun, Y., Mohar, B., Hulse, B. K., Kerlin, A. M., Hasseman, J. P., Tsegaye, G., Tsang, A., Wong, A., Patel, R., Macklin, J. J., Chen, Y., Konnerth, A., Jayaraman, V., Looger, L. L., Schreiter, E. R., Svoboda, K., & Kim, D. S. (2019). High-performance calcium sensors for imaging activity in neuronal populations and microcompartments. *Nature methods*, *16*(7), 649–657. https://doi.org/10.1038/s41592-019-0435-6

Dubnau, J., & Chiang, A. S. (2013). Systems memory consolidation in Drosophila. *Current opinion in neurobiology*, *23*(1), 84–91. https://doi.org/10.1016/j.conb.2012.09.006

Dubnau, J., Grady, L., Kitamoto, T., & Tully, T. (2001). Disruption of neurotransmission in Drosophila mushroom body blocks retrieval but not acquisition of memory. *Nature*, *411*(6836), 476–480. https://doi.org/10.1038/35078077

Dylla, K. V., Raiser, G., Galizia, C. G., & Szyszka, P. (2017). Trace Conditioning in *Drosophila* Induces Associative Plasticity in Mushroom Body Kenyon Cells and Dopaminergic Neurons. *Frontiers in neural circuits*, *11*, 42. https://doi.org/10.3389/fncir.2017.00042

Faghihi, F., Moustafa, A. A., Heinrich, R., & Wörgötter, F. (2017). A computational model of conditioning inspired by Drosophila olfactory system. *Neural networks : the official journal of the International Neural Network Society*, *87*, 96–108. https://doi.org/10.1016/j.neunet.2016.11.002

Feinberg, E. H., Vanhoven, M. K., Bendesky, A., Wang, G., Fetter, R. D., Shen, K., & Bargmann, C. I. (2008). GFP Reconstitution Across Synaptic Partners (GRASP) defines cell contacts and synapses in living nervous systems. *Neuron*, *57*(3), 353–363. https://doi.org/10.1016/j.neuron.2007.11.030

Felsenberg, J., Barnstedt, O., Cognigni, P., Lin, S., & Waddell, S. (2017). Re-evaluation of learned information in Drosophila. *Nature*, *544*(7649), 240–244. https://doi.org/10.1038/nature21716

Felsenberg, J., Jacob, P. F., Walker, T., Barnstedt, O., Edmondson-Stait, A. J., Pleijzier, M. W., Otto, N., Schlegel, P., Sharifi, N., Perisse, E., Smith, C. S., Lauritzen, J. S., Costa, M., Jefferis, G. S. X. E., Bock, D. D., & Waddell, S. (2018). Integration of Parallel Opposing Memories Underlies Memory Extinction. *Cell*, *175*(3), 709–722.e15. https://doi.org/10.1016/j.cell.2018.08.021

Fiala, A., and Riemensperger, T. (2017). Localization of a memory trace: Aversive associative olfactory learning and short-term memory in Drosophila. In Learning and Memory: A Comprehensive Reference, Vol.1, Learning Theory and Behavior, R.

Menzel, J.H. Byrne, eds. (Oxford: Academic Press), pp. 475-482. ISBN-13: 9780128051597

Gilboa, A., Sekeres, M., Moscovitch, M., & Winocur, G. (2014). Higher-order conditioning is impaired by hippocampal lesions. *Current biology : CB*, *24*(18), 2202–2207. https://doi.org/10.1016/j.cub.2014.07.078

Gostolupce, D., Iordanova, M. D., & Lay, B. P. P. (2021). Mechanisms of higher-order learning in the amygdala. *Behavioural brain research*, *414*, 113435. https://doi.org/10.1016/j.bbr.2021.113435

Hancock, C. E., Bilz, F., & Fiala, A. (2019). In Vivo Optical Calcium Imaging of Learning-Induced Synaptic Plasticity in Drosophila melanogaster. *Journal of visualized experiments : JoVE*, (152), 10.3791/60288. https://doi.org/10.3791/60288

Hancock, C. E., Geurten, B. R. H., & Fiala, A. (2020). Visualization of naive and learned odor representations using *in vivo* calcium imaging and immunohistochemical bouton mapping of single *Drosophila* mushroom body neurons. *STAR protocols*, *1*(3), 100210. https://doi.org/10.1016/j.xpro.2020.100210

Hancock, C. E., Rostami, V., Rachad, E. Y., Deimel, S. H., Nawrot, M. P., & Fiala, A. (2022). Visualization of learning-induced synaptic plasticity in output neurons of the Drosophila mushroom body γ-lobe. *Scientific reports*, *12*(1), 10421. https://doi.org/10.1038/s41598-022-14413-5

Handler, A., Graham, T. G. W., Cohn, R., Morantte, I., Siliciano, A. F., Zeng, J., Li, Y., & Ruta, V. (2019). Distinct Dopamine Receptor Pathways Underlie the Temporal Sensitivity of Associative Learning. *Cell*, *178*(1), 60–75.e19. https://doi.org/10.1016/j.cell.2019.05.040

Hawkins, R. D., Greene, W., & Kandel, E. R. (1998). Classical conditioning, differential conditioning, and second-order conditioning of the Aplysia gill-withdrawal reflex in a simplified mantle organ preparation. *Behavioral neuroscience*, *112*(3), 636–645. https://doi.org/10.1037//0735-7044.112.3.636

Heisenberg M. (2003). Mushroom body memoir: from maps to models. *Nature reviews. Neuroscience*, *4*(4), 266–275. https://doi.org/10.1038/nrn1074

Hige, T., Aso, Y., Modi, M. N., Rubin, G. M., & Turner, G. C. (2015b). Heterosynaptic Plasticity Underlies Aversive Olfactory Learning in Drosophila. *Neuron*, *88*(5), 985–998. https://doi.org/10.1016/j.neuron.2015.11.003

Hige, T., Aso, Y., Rubin, G. M., & Turner, G. C. (2015a). Plasticity-driven individualization of olfactory coding in mushroom body output neurons. *Nature*, *526*(7572), 258–262. https://doi.org/10.1038/nature15396

Honegger, K. S., Campbell, R. A., & Turner, G. C. (2011). Cellular-resolution population imaging reveals robust sparse coding in the Drosophila mushroom body. *The Journal of neuroscience : the official journal of the Society for Neuroscience*, *31*(33), 11772–11785. https://doi.org/10.1523/JNEUROSCI.1099-11.2011

Hoskins, R. A., Phan, A. C., Naeemuddin, M., Mapa, F. A., Ruddy, D. A., Ryan, J. J., Young, L. M., Wells, T., Kopczynski, C., & Ellis, M. C. (2001). Single nucleotide polymorphism markers for genetic mapping in Drosophila melanogaster. *Genome research*, *11*(6), 1100–1113. https://doi.org/10.1101/gr.gr-1780r

Hussaini, S. A., Komischke, B., Menzel, R., & Lachnit, H. (2007). Forward and backward second-order Pavlovian conditioning in honeybees. *Learning & memory (Cold Spring Harbor, N.Y.)*, *14*(10), 678–683. https://doi.org/10.1101/lm.471307

Jenett, A., Rubin, G. M., Ngo, T. T., Shepherd, D., Murphy, C., Dionne, H., Pfeiffer, B. D., Cavallaro, A., Hall, D., Jeter, J., Iyer, N., Fetter, D., Hausenfluck, J. H., Peng, H., Trautman, E. T., Svirskas, R. R., Myers, E. W., Iwinski, Z. R., Aso, Y., DePasquale, G. M., … Zugates, C. T. (2012). A GAL4-driver line resource for Drosophila neurobiology. *Cell reports*, *2*(4), 991–1001. https://doi.org/10.1016/j.celrep.2012.09.011

Jovanic, T., Schneider-Mizell, C. M., Shao, M., Masson, J. B., Denisov, G., Fetter, R. D., Mensh, B. D., Truman, J. W., Cardona, A., & Zlatic, M. (2016). Competitive Disinhibition Mediates Behavioral Choice and Sequences in Drosophila. *Cell*, *167*(3), 858–870.e19. https://doi.org/10.1016/j.cell.2016.09.009

Kasuya, J., Ishimoto, H., & Kitamoto, T. (2009). Neuronal mechanisms of learning and memory revealed by spatial and temporal suppression of neurotransmission using shibire, a temperature-sensitive dynamin mutant gene in Drosophila melanogaster. *Frontiers in molecular neuroscience*, *2*, 11. https://doi.org/10.3389/neuro.02.011.2009

Kitamoto T. (2001). Conditional modification of behavior in Drosophila by targeted expression of a temperature-sensitive shibire allele in defined neurons. *Journal of neurobiology*, *47*(2), 81–92. https://doi.org/10.1002/neu.1018

Kitamoto T. (2002). Targeted expression of temperature-sensitive dynamin to study neural mechanisms of complex behavior in Drosophila. *Journal of neurogenetics*, *16*(4), 205–228. https://doi.org/10.1080/01677060216295

Klapoetke, N. C., Murata, Y., Kim, S. S., Pulver, S. R., Birdsey-Benson, A., Cho, Y. K., Morimoto, T. K., Chuong, A. S., Carpenter, E. J., Tian, Z., Wang, J., Xie, Y., Yan, Z., Zhang, Y., Chow, B. Y., Surek, B., Melkonian, M., Jayaraman, V., Constantine-Paton, M., Wong, G. K., … Boyden, E. S. (2014). Independent optical excitation of distinct neural populations. *Nature methods*, *11*(3), 338–346. https://doi.org/10.1038/nmeth.2836

König, C., Khalili, A., Niewalda, T., Gao, S., & Gerber, B. (2019). An optogenetic analogue of second-order reinforcement in Drosophila. *Biology letters*, *15*(7), 20190084. https://doi.org/10.1098/rsbl.2019.0084

Lee J. C. (2021). Second-Order Conditioning in Humans. *Frontiers in behavioral neuroscience*, *15*, 672628. https://doi.org/10.3389/fnbeh.2021.672628

Lindsley, D.L., Grell, E.H. (1968). Genetic variations of Drosophila melanogaster. *Publs Carnegie Instn* **627**: 469pp. https://doi.org/10.1126/science.162.3857.993

Loy, I., Fernández, V., & Acebes, F. (2006). Conditioning of tentacle lowering in the snail (Helix aspersa): acquisition, latent inhibition, overshadowing, second-order conditioning, and sensory preconditioning. *Learning & behavior*, *34*(3), 305–314. https://doi.org/10.3758/bf03192885

Luo, L., Callaway, E. M., & Svoboda, K. (2018). Genetic Dissection of Neural Circuits: A Decade of Progress. *Neuron*, *98*(2), 256–281. https://doi.org/10.1016/j.neuron.2018.03.040

Margulies, C., Tully, T., & Dubnau, J. (2005). Deconstructing memory in Drosophila. *Current biology : CB*, *15*(17), R700–R713. https://doi.org/10.1016/j.cub.2005.08.024

Marin, E. C., Jefferis, G. S., Komiyama, T., Zhu, H., & Luo, L. (2002). Representation of the glomerular olfactory map in the Drosophila brain. *Cell*, *109*(2), 243–255. https://doi.org/10.1016/s0092-8674(02)00700-6

McGuire, S. E., Le, P. T., & Davis, R. L. (2001). The role of Drosophila mushroom body signaling in olfactory memory. *Science (New York, N.Y.)*, *293*(5533), 1330–1333. https://doi.org/10.1126/science.1062622

Miller, R. R., Barnet, R. C., & Grahame, N. J. (1995). Assessment of the Rescorla-Wagner model. *Psychological bulletin*, *117*(3), 363–386. https://doi.org/10.1037/0033-2909.117.3.363

Pavlov, I. (1927). Conditioned reflexes: an investigation of the physiological activity of the cerebral cortex (Oxford University Press). ISBN-13: 9781614277989

Pech, U., Pooryasin, A., Birman, S., & Fiala, A. (2013). Localization of the contacts between Kenyon cells and aminergic neurons in the Drosophila melanogaster brain using SplitGFP reconstitution. *The Journal of comparative neurology*, *521*(17), 3992–4026. https://doi.org/10.1002/cne.23388

Pech, U., Revelo, N. H., Seitz, K. J., Rizzoli, S. O., & Fiala, A. (2015). Optical dissection of experience-dependent pre- and postsynaptic plasticity in the Drosophila brain. *Cell reports*, *10*(12), 2083–2095. https://doi.org/10.1016/j.celrep.2015.02.065

Qin, H., Cressy, M., Li, W., Coravos, J. S., Izzi, S. A., & Dubnau, J. (2012). Gamma neurons mediate dopaminergic input during aversive olfactory memory formation in Drosophila. *Current biology : CB*, *22*(7), 608–614. https://doi.org/10.1016/j.cub.2012.02.014

Rescorla, R.A. (1980): Pavlovian second-order conditioning: Studies in associative learning. Psychology Press, N.Y, 2014. ISBN-13: 9781848724440

Riemensperger, T., Issa, A. R., Pech, U., Coulom, H., Nguyễn, M. V., Cassar, M., Jacquet, M., Fiala, A., & Birman, S. (2013). A single dopamine pathway underlies progressive locomotor deficits in a Drosophila model of Parkinson disease. *Cell reports*, *5*(4), 952–960. https://doi.org/10.1016/j.celrep.2013.10.032

Riemensperger, T., Völler, T., Stock, P., Buchner, E., & Fiala, A. (2005). Punishment prediction by dopaminergic neurons in Drosophila. *Current biology : CB*, *15*(21), 1953–1960. https://doi.org/10.1016/j.cub.2005.09.042

Ries, A. S., Hermanns, T., Poeck, B., & Strauss, R. (2017). Serotonin modulates a depression-like state in Drosophila responsive to lithium treatment. *Nature communications*, *8*, 15738. https://doi.org/10.1038/ncomms15738

Rizley, R. C., & Rescorla, R. A. (1972). Associations in second-order conditioning and sensory preconditioning. *Journal of comparative and physiological psychology*, *81*(1), 1–11. https://doi.org/10.1037/h0033333

Scheffer, L. K., Xu, C. S., Januszewski, M., Lu, Z., Takemura, S. Y., Hayworth, K. J., Huang, G. B., Shinomiya, K., Maitlin-Shepard, J., Berg, S., Clements, J., Hubbard,

P. M., Katz, W. T., Umayam, L., Zhao, T., Ackerman, D., Blakely, T., Bogovic, J., Dolafi, T., Kainmueller, D., … Plaza, S. M. (2020). A connectome and analysis of the adult *Drosophila* central brain. *eLife*, *9*, e57443. https://doi.org/10.7554/eLife.57443

Schultz W. (2007). Multiple dopamine functions at different time courses. *Annual review of neuroscience*, *30*, 259–288. https://doi.org/10.1146/annurev.neuro.28.061604.135722

Schultz, W., Dayan, P., & Montague, P. R. (1997). A neural substrate of prediction and reward. *Science (New York, N.Y.)*, *275*(5306), 1593–1599. https://doi.org/10.1126/science.275.5306.1593

Schwaerzel, M., Heisenberg, M., & Zars, T. (2002). Extinction antagonizes olfactory memory at the subcellular level. *Neuron*, *35*(5), 951–960. https://doi.org/10.1016/s0896-6273(02)00832-2

Springer, M., & Nawrot, M. P. (2021). A Mechanistic Model for Reward Prediction and Extinction Learning in the Fruit Fly. *eNeuro*, *8*(3), ENEURO.0549-20.2021. https://doi.org/10.1523/ENEURO.0549-20.2021

Stettler, D. D., & Axel, R. (2009). Representations of odor in the piriform cortex. *Neuron*, *63*(6), 854–864. https://doi.org/10.1016/j.neuron.2009.09.005

Strother, J. A., Wu, S. T., Wong, A. M., Nern, A., Rogers, E. M., Le, J. Q., Rubin, G. M., & Reiser, M. B. (2017). The Emergence of Directional Selectivity in the Visual Motion Pathway of Drosophila. *Neuron*, *94*(1), 168–182.e10. https://doi.org/10.1016/j.neuron.2017.03.010

Tabone, C. J., & de Belle, J. S. (2011). Second-order conditioning in Drosophila. *Learning & memory (Cold Spring Harbor, N.Y.)*, *18*(4), 250–253. https://doi.org/10.1101/lm.2035411

Thévenaz, P., Ruttimann, U. E., & Unser, M. (1998). A pyramid approach to subpixel registration based on intensity. *IEEE transactions on image processing : a publication of the IEEE Signal Processing Society*, *7*(1), 27–41. https://doi.org/10.1109/83.650848

Tully, T., & Quinn, W. G. (1985). Classical conditioning and retention in normal and mutant Drosophila melanogaster. *Journal of comparative physiology. A, Sensory, neural, and behavioral physiology*, *157*(2), 263–277. https://doi.org/10.1007/BF01350033

Turner, G. C., Bazhenov, M., & Laurent, G. (2008). Olfactory representations by Drosophila mushroom body neurons. *Journal of neurophysiology*, *99*(2), 734–746. https://doi.org/10.1152/jn.01283.2007

Ueoka, Y., Hiroi, M., Abe, T., & Tabata, T. (2017). Suppression of a single pair of mushroom body output neurons in *Drosophila* triggers aversive associations. *FEBS open bio*, *7*(4), 562–576. https://doi.org/10.1002/2211-5463.12203

Venken, K. J., Simpson, J. H., & Bellen, H. J. (2011). Genetic manipulation of genes and cells in the nervous system of the fruit fly. *Neuron*, *72*(2), 202–230. https://doi.org/10.1016/j.neuron.2011.09.021

Vosshall, L. B., & Stocker, R. F. (2007). Molecular architecture of smell and taste in Drosophila. *Annual review of neuroscience*, *30*, 505–533. https://doi.org/10.1146/annurev.neuro.30.051606.094306

Vrontou, E., Groschner, L. N., Szydlowski, S., Brain, R., Krebbers, A., & Miesenböck, G. (2021). Response competition between neurons and antineurons in the mushroom body. *Current biology : CB*, *31*(22), 4911–4922.e4. https://doi.org/10.1016/j.cub.2021.09.008

Wong, A. M., Wang, J. W., & Axel, R. (2002). Spatial representation of the glomerular map in the Drosophila protocerebrum. *Cell*, *109*(2), 229–241. https://doi.org/10.1016/s0092-8674(02)00707-9

Yamada, D., Bushey, D., Li, F., Hibbard, K. L., Sammons, M., Funke, J., Litwin-Kumar, A., Hige, T., & Aso, Y. (2023). Hierarchical architecture of dopaminergic circuits enables second-order conditioning in *Drosophila*. *eLife*, *12*, e79042. Advance online publication. https://doi.org/10.7554/eLife.79042

Yamagata, N., Ichinose, T., Aso, Y., Plaçais, P. Y., Friedrich, A. B., Sima, R. J., Preat, T., Rubin, G. M., & Tanimoto, H. (2015). Distinct dopamine neurons mediate reward signals for short- and long-term memories. *Proceedings of the National Academy of Sciences of the United States of America*, *112*(2), 578–583. https://doi.org/10.1073/pnas.1421930112

Yang, C. H., Shih, M. F., Chang, C. C., Chiang, M. H., Shih, H. W., Tsai, Y. L., Chiang, A. S., Fu, T. F., & Wu, C. L. (2016). Additive Expression of Consolidated Memory through Drosophila Mushroom Body Subsets. *PLoS genetics*, *12*(5), e1006061. https://doi.org/10.1371/journal.pgen.1006061

Zars, T., Fischer, M., Schulz, R., & Heisenberg, M. (2000). Localization of a short-term memory in Drosophila. *Science (New York, N.Y.)*, *288*(5466), 672–675. https://doi.org/10.1126/science.288.5466.672

Zhao, C., Widmer, Y. F., Diegelmann, S., Petrovici, M. A., Sprecher, S. G., & Senn, W. (2021). Predictive olfactory learning in Drosophila. *Scientific reports*, *11*(1), 6795. https://doi.org/10.1038/s41598-021-85841-y

V. General discussion

In the framework of this thesis, I scrutinized neuronal activity and connectivity underlying different mechanisms of *Drosophila*'s physiology to make a dent in unraveling the "cognition" of complex behaviors in this insect. The study of the predominant structure in olfactory associative learning, called the mushroom body, revealed to be a practical methodology in uncovering such aspects of learning and memory.

In the first manuscript, we conducted a developmental approach to allow us a better understanding of the structural properties of the MB during its formation. We propose that developmental axon and synapse degradation of the MB γ-KCs during metamorphosis, colloquially known as pruning, is highly linked to the fluctuations of the neuronal activity of this structure. From anatomical to functional imaging experiments, we could show that in order for these γ neurons to undergo pruning, their activity sustains a reduction in the time-window that marks the beginning of metamorphosis (pupariation). We could also suggest two instigators acting in synergy to achieve this decrease in neuronal activity: inhibitory signaling from the GABAergic anterior paired lateral (APL) neuron, and the expression of cell autonomous inwardly rectifying potassium channel 1 (Irk1).

Moreover, we undertook a more synaptic plasticity-oriented approach in the second manuscript, to investigate the coincident detection of sensory cues related to associative olfactory conditioning. In this study, we could show that synaptic changes engendered by classical aversive conditioning are localized to one distinct MB γ-lobe compartment and are caused by odor-reinforcement associations. This could be achieved by expressing post-synaptically localized calcium indicators in different γ lobe-innervating MBONs along with subjecting the flies to an aversive conditioning

paradigm. Behavioral experiments mirroring the imaging ones were performed where the synaptic output of said MBONs was blocked and the behavioral consequences were assessed. The key finding of this study is that forming an aversive olfactory memory depends on the suppression of the synapses between MBON-γ1pedc>α/β or MBON11 (γ1-pedc MBON) and KCs of the γ-lobe.

In the third and last manuscript, we worked towards an understanding of the mechanisms underlying higher-order associative learning in *Drosophila melanogaster*. Since classical conditioning merely consists on one association between a conditioned stimulus and a reinforcing signal, the neuronal circuitry mediating this type of Pavlovian conditioning has been extensively studied, and neuronal circuits underlying aversive or appetitive olfactory learning have been characterized to a fair degree. However, the neuronal circuits mediating the formation of association chains through SOC remain unknown. This type of higher-order conditioning offers the opportunity to examine how the internal transfer of predictive information from a previously conditioned odorant (CS1) to novel stimulus (CS2) occurs at the cellular level. By selective thermo-genetic manipulation of distinct neuronal populations of the mushroom body circuitry during the different phases of first-order training, second order training or in the test situation, we dissected the neuronal circuits that are required for aversive second-order learning. Functional imaging along with optogenetics were used to visualize synaptic plasticity and hunt for the memory traces left by this higher-order paradigm. To summarize the take-away messages of this study, we characterize mushroom body-associated neuronal feedback loops that necessitate the dual implication of two different mushroom body compartments functioning in parallel to enable a learned odor stimulus to take control

over punishment-mediating dopaminergic neurons, thereby mediating associative learning of higher order.

1. The neuronal activity of the γ-lobe Kenyon cells during metamorphosis is crucial for its proper development

The mushroom body is the central hub for associative olfactory learning in the fruit fly (Heisenberg et al., 1985) and other insects (Menzel & Erber, 1978). Genetic manipulation of this structure and impairing its activity leads to a deficit in memory formation and recall (Zars et al., 2000; Dubnau et al., 2001; Schwaerzel et al., 2003; Krashes et al., 2007; Rachad et al., manuscript 3, page 88). Moreover, the pruning and regrowth of the axonal branches of the γ-lobe of the MB during metamorphosis is an essential process for developing a functioning adult MB (Yu & Schuldiner, 2014). In addition, it has been shown that neuronal activity is a key factor in the remodeling of several nervous systems (Duch & Mentel, 2004; Kano et al., 2018; Mayseless et al., 2018; Golovin et al., 2019). However, the interaction between structural remodeling and neuronal activity fluctuations remains unknown. Therefore, what are the mechanisms by which neuronal activity of the MB, autonomously and/or via synaptic partners, influence its remodeling during metamorphosis?

In the first manuscript of this thesis, we propose that chronic activation of these γ-lobe KCs inhibits their pruning, and monitoring cellular activity during different time-points of metamorphosis using the transgenic tool CaMPARI shows a decrease in the activity of the MB at 0h after pupa formation (APF) that regains and surpasses its initial levels at 3h and 6h APF (Figure 1B). The use of such a calcium indicator reflects its advantages; its experimenter-induced temporal control properties and linking high calcium levels with highly active neurons. This means that

hyperpolarization during metamorphosis is crucial for developing a normally functioning MB (Figure 1C-I; Figure 2A-D).

Furthermore, it has been reported that inhibition of γ-lobe KCs pruning exhibits a pruning deficit of one of its intermingled synaptic partner the APL neuron, suggesting that inhibiting remodeling of one neuronal population can affect the functional wiring of the entire microcircuit (Mayseless et al., 2018). In our study, we add to the latter by demonstrating that silencing APL neuronal activity leads to moderate yet quantifiably significant pruning defects, and simultaneous inhibition of both APL and γ KCs suppressed these defects (Figure 3). This signifies that this pruning defect is appropriate to the hyperactive MB γ-lobe. The APL neuron has been shown to be the only inhibitory input to the MB in the early stages of *Drosophila*'s larval development (Masuda-Nakagawa et al., 2014). Therefore, we knocked-down the expression of the metabotropic GABA-B-R1 receptor, that is high expressed in the mushroom body (Figure S3A) and has not been proven to possess excitatory properties during early development as opposed to the ionotropic GABA-A receptor (Ryglewski et al., 2017). This knockdown induced mild pruning defects of the MB (Figure 4; Figure S3J-I). This led us to believe that the APL induces hyperpolarization of the MB via the GABA-B-R1 receptor to initiate its pruning. However, increasing the activity of the APL did not result in premature or severe pruning (Figure S2C-I). This raises a question about the dichotomous notions sufficiency and necessity in the role of the APL in pruning, proving that this neuron is not the only catalyst of the MB γ-lobe remodeling. To verify whether the γ-KCs exhibit any self-regulating mechanisms to reduce their own activity, a potent candidate named irk1 comes to light and displays distinguished expression levels initiated with metamorphosis (Figure 2E). Knocking-down the expression of these inwardly rectifying potassium channels using RNAi altered the

pruning of the MB to a fair degree (Figure 4). Including all aspects of this study, the remodeling of the MB depends on the dual activity of the APL neuron via its GABAergic output and the self-regulatory activity of the irk1 potassium channels.

Consequently, the MB's importance in olfactory learning arises in early developmental stages since pruning deficits of the developing MB lead to an impairment associative odor conditioning (Poppinga et al., 2022). Furthermore, the constantly high activity of the MB during metamorphosis affects its remodeling along with its synaptic partners, notably the APL (Mayseless et al., 2018). Therefore, it is only fair to assume that developing neurons synergistically employ a coordination mechanism to allow for the formation and development of complete and functional circuits, thus an unpruned MB leads to a deficit in the circuitry's architecture, and thus an impairment of olfactory associative learning establishment.

2. Localized synaptic plasticity behind "simple" classical conditioning in the adult *Drosophila* mushroom body

When a learned olfactory memory is acquired, its traces are preserved through synaptic transmission changes in the appropriate microcircuit responsible for evoking distinct behaviors (Magee & Grienberger 2020). Here we ponder over the vast knowledge about aversive olfactory conditioning and utilize it as a behavioral model approach to dissect the neuronal candidates behind it, and visualize the plastic changes occurring in their connectivity. Although, how does the coincident detection of olfactory stimuli along with punishing cues regarding aversive olfactory conditioning facilitates the accomplishment of a learned behavior, and where does the synaptic plasticity underlying such a paradigm occur? In the second manuscript reported in this thesis, we hypothesize that synaptic modifications upon classical

conditioning occur in the connections between KC, DANs and MBONs encoding the simultaneous sensory information from the conditioned stimulus (CS^+) and the unconditioned stimulus (US), also known respectively as odors and electric shocks.

To obtain a reliably restricted readout of this plasticity, we expressed the post-synaptic calcium indicator UAS-dHomer-GCaMP3 that is fused to the C-terminal of the post-synaptic protein Homer (Pech et al., 2015) in different MBONs innervating the MB γ lobe, to visualize and quantify such synaptic changes after odor-shock learning. First, we needed to validate this transgenic tool in localizing odor representations in MBON synapses by comparing its expression pattern and fluorescence changes in reaction to odorants to other calcium sensors that are cytosolic (UAS-GCaMP3 and UAS-GCaMP6f) (Figure 1). Indeed, the post-synaptic dHomer-GCaMP3 shows restricted expression in the MBONs dendritic arborizations that fits the perimeter of the MB compartments and lower baseline/odor-evoked fluorescence than the two cytosolic calcium sensors (Figure 1D-G). Odors responses are widely represented in the MBONs innervating the MB lobes (Hige et al., 2015). Therefore, we analyzed odor-evoked responses in the post-synapses of the different MBONs innervating the γ lobe and found out the presence of a heterogeneous response profile in these neurons. MBONs innervating the γ1, γ3 and γ4 compartments of the MB exhibit strong odor-evoked responses to both used odors in most flies (4-methylcyclohexanol (MCH) and 3-Octanol (3-OCT)) with higher amplitudes in reaction to MCH (Figure 2A, 2C-D). While it has been previously demonstrated and in addition shown by our study that MBON innervating the γ5 compartment show minimal to no odor response (Perisse et al., 2016) (Figure 2E), the γ2 MBON reacts robustly to MCH in the majority of the measured flies as opposed to 3-OCT (Figure 2B). This across-MBON heterogeneity in odor-evoked

response profiles indicates a uniqueness of MBONs activity in reaction to an odor and might impact olfactory associative learning. This MBON individuality in odor responses was also reported using a cytosolic GCaMP (Hige et al., 2015).

Moreover, behavioral assays where flies were differentially trained using an aversive classical conditioning paradigm (Tully & Quinn, 1985) and blocking synaptic transmission of different MBONs innervating the γ lobe using UAS-*Shibire*^{ts} revealed the potential role of γ1-pedc and γ5 MBONs in short-term olfactory memory formation and recall (Figure 6B, 6F). This concurs with studies reporting impairment of memory formation upon blocking synaptic transmission of γ1-pedc MBON (Aso et al., 2014b; Owald et al., 2015). Blocking the individual synaptic output of the remaining MBONs of the γ MB lobe show no interference with odor learning, at least in this paradigm (Figure 6C-E). Once these two neurons were deemed necessary for olfactory learning at the behavioral level, the next logical step was to explore the plasticity in the post-synapses of γ-innervating MBONs after aversive conditioning.

During aversive classical conditioning in flies, the mushroom body intrinsic KCs convey odor information that undergoes modulation from the punishment mediating PPL1-DANs upon reinforcement association from an unconditioned stimulus (US), which leads to conformational changes in the synapses between KCs and MBONs (Aso et al., 2014a; Hige et al., 2015). When optogenetically activated, each of these MBONs possesses the ability to induce an approach or avoidance action and thus behaviorally guiding the animal towards or away from the stimulus (Aso et al., 2014b). Models show that the opposing valence-promoting mirrored connectivity of MBONs and DANs innervating the same MB compartments proposes an antagonistic action between MBONs, i.e. punishment-mediating DANs reduce the activity in their respective compartments, leading to a suppression of its approach-promoting

corresponding MBONs and a higher activity in the opposing ones (avoidance-promoting) (Heisenberg, 2003; Springer & Nawrot, 2021). In addition, it has been reported that γ KCs display synaptic plasticity as a result of odor-differential learning (Bilz et al., 2020). Therefore, we expressed once more the post-synaptic UAS-dHomer-GCaMP3 in the different γ lobe MBONs and subjected the experimental flies to an aversive classical conditioning paradigm. In the post-synapses of the γ1-pedc MBON, we could show that association of CS^+ and US resulted in a decrease in the odor-evoked calcium activity from pre- to post-training, as opposed to the CS^- odor (Figure 3B). In contrast, γ2-through-5 MBONs reveal no significant calcium changes from pre- to post-training solemnly appropriate to CS^+, but rather a generalized adaptive decrease in reaction to both odors specifically in γ3 and γ4 MBONs and little to no odor response in the γ5 MBON (Figure 4A,C,E and G). The control experiments in all the tested MBONs display no significant difference in the calcium activity in the case of presenting the odors without reinforcement from the US, or the shock only (Figure 3D-E; Figure 4B, D, F and H). The question that materializes when pooling both the behavioral assays results and the odor-shock induced synaptic plasticity data: Why is the neuronal transmission from two distinct MBONs required for memory formation in a behavioral paradigm, but only one of these two undergoes post-synaptic plastic changes upon aversive differential training?

Optogenetic activation of γ1-pedc and γ5 MBONs reveals conflicting roles in behavioral guidance of the flies, i.e. exhibiting positive and negative valences respectively upon stimulation (Aso et al., 2014b). Also, the GABAergic γ1-pedc MBON shows significant projections to the γ5 compartment (Aso et al., 2014a) Eichler et al., 2017; Li et al., 2020). In the case of opposing memories, it was shown that γ1-pedc MBON shows reduced calcium activity in its synaptic connections to the

KCs in reaction to CS1 after aversive conditioning, while the γ5 MBON compartment authenticates the same effect after extinction of the aversively learned memory (Felsenberg et al., 2018). This bidirectional activity, along with our data stating the decreased restricted activity in the γ1-pedc MBON post-synapses after olfactory conditioning, suggest that this γ1 region is responsible for CS^+-US association and thus the synaptic plasticity underlying learning an aversively conditioned odor CS^+, whereas the opposing avoidance-promoting γ5 MBON is disinhibited to guide the fly away from CS^+.

A computational approach using a classifier that could be trained (machine learning) by feeding it pseudo-data generated from acquired raw data of calcium imaging experiments (normalized area under the curve AUC of the calcium evoked-responses) of each of the recorded γ-lobe MBONs, supports our findings. First, this classifier was trained such as to predict a response and differentiate it to either CS^+ or CS^- after aversive learning (Figure 5A). We demonstrate, and with a higher significant accuracy, that this model could unambiguously distinguish the readout of CS^+ from CS^- in the trained group (paired CS^+ with US), but not in the control groups (Figure 5B). Furthermore, we trained this same classifier but with individually omitting one of the γ-lobe MBONs and assay the accuracy of prediction. Leaving out the γ1-pedc MBON was the only condition that displayed a lower accuracy rate in predicting CS^+ vs. CS^- (Figure 5C). Taken all of these results together, olfactory aversive conditioning in fruit flies is mediated by localized suppression of γ1-pedc MBON - KC synapses amid CS^+-US association.

3. Higher-order associative learning requires several mushroom body compartments working in parallel

The fly's ability to perceive environmental stimuli of different natures with such a primitive and minuscule brain to process them into promoting complex higher-order associative learning is a fascinating phenomenon in behavioral neuroscience. Such elaborate processes have been the focal point in the context of understanding the cellular and sub-cellular mechanisms underlying higher-order learning in simple model organisms such as *Drosophila*, bringing scientific research a step closer into untangle the essence of "cognition" in perplexing mammalian brains. SOC, an example of higher-order conditioning, consists of two training stages where the first one resembles a classical conditioning protocol (CS1-US association, followed by a break, then a presentation of CS^-), and the second one pairs the previously conditioned stimulus CS1 with a novel stimulus CS2, thus transferring the aversive information to this CS2 (Pavlov, 1927; Tabone & de Belle., 2011). In contrast to classical conditioning, also known as first-order conditioning (FOC), the neuronal circuits, connections, and their roles in SOC memory formation remain unknown. What are the neuronal mechanisms (from activity, connectivity, to plasticity) underlying the establishment of such a higher-order form of learning in the fruit fly?

First and foremost, we needed to conceptualize and design a new automatized and custom-built apparatus for higher-order learning in *Drosophila* (Supplementary Figure 1A-B) to reproduce SOC as described by Tabone and de Belle in 2011. The necessity of creating such a machine sprouted from the idea that classic T-mazes used for olfactory conditioning in flies (Tully & Quinn, 1985; Schwaerzel et al., 2002; Barth et al., 2014; Malik & Hodge, 2014; Ichinose & Tanimoto, 2016) lack the precise temporal control of pulsing one odor over the other to prevent a mixture that could

cloud the differentiation between the stimuli. Establishing such a machine transpired to be a mighty ordeal on account of the different parameters that need to be optimized for such a paradigm to work (odor concentrations, air pressure, etc…) (Supplementary Figure 1C-E). Since then, we could demonstrate that flies are capable of such higher-order associative learning with this apparatus; SOC can be achieved only when both the reinforcements (electric shocks as US in the first training phase, and the previously learned odor CS1 in the second training phase) are paired with their respective conditioned stimulus (CS1 and CS2) (Figure 1B). These results align with the study of Tabone and de Belle conducted in 2011.

We genetically manipulated the different lobes of the MB and the neuronal populations associated to it, notably DANs and MBONs, in the context of olfactory aversive conditioning by blocking their synaptic transmission using UAS-Shi^{ts} in the different phases of SOC (Figure 1C-D). First, we revealed that the MB, especially the γ lobe, is required to form a higher-order memory only during the second training phase of SOC and to retrieve it in the test phase. Its output is not required for SOC memory during the first training phase implicating the CS1-US association (Figure 1E-F). This goes in line with previous results suggesting that the synaptic transmission of KCs of the MB is required for retrieving a short-term memory but not for forming it (Dubnau et al., 2001; McGuire et al., 2003). Surprisingly, the output from another lobe (α′/β′) is required exclusively during the second training phase of SOC (Figure 1G). Similarly, studies reveal the importance of the α'/β' lobe in early memory formation and consolidation, but not in retrieving it (Krashes et al., 2007; Wang et al., 2008). Moreover, output from α/β lobe is not necessary for our SOC paradigm (Figure 1H), which corroborates studies that suggest its role in long-term memory (McGuire et al., 2001; Krashes & Waddell, 2008).

Through a screening of potential MBONs innervating the different compartments of the γ and α′/β′ lobes, thus mediating behavioral output in the different phase of the SOC paradigm, we found two candidates in two different lobes: γ1-pedc (MBON-γ1pedc>α/β or MBON11) and α′2 (MBON-α′2 or MBON13) MBONs. Neurotransmission of γ1-pedc MBON is indispensable in both the second phase of SOC training and retrieving the learned behavior in the test phase (Figure 2A), while output from α′2 MBON is only necessary during that second phase (Figure 2G). These MBONs demonstrate a similar trend to the behavioral results of the MB lobe that they innervate, meaning that these two compartments are highlighted for their role in establishing such a higher-order associative learning. While the α′2 MBON's implication in such a paradigm is of novelty, the γ1-pedc role in associative olfactory conditioning has been described in many studies (Aso et al., 2014b; Owald et al., 2015; Ueoka et al., 2017; Hancock et al., 2022, manuscript 2, page 73).

Furthermore, modulation from DANs during this SOC protocol was investigated by selectively blocking their synaptic outputs as well through thermo-genetic manipulations in the SOC phases. We discovered that the punishment-mediating PPL1 DANs are required in both of the training phases of the SOC paradigm but not during memory recall (Figure 3A), whilst the reward-conveying PAM DANs were dispensable in aversive SOC establishment (Figure 3B). On the same wavelength, our results validate previous findings demonstrating the necessity of the PPL1 cluster in mediating punishing signals for aversive associative olfactory learning (Claridge-Chang et al., 2009; Aso et al., 2010; Aso et al., 2014a), along with the role of the PAM cluster in appetitive odor memory formation (Liu et al., 2012; Aso et al., 2014a). We then performed the same previously mentioned behavioral screening on individual PPL1 cluster neurons to meticulously identify single DANs potentially

involved in higher-order memory formation. As a first result, we observed that the synaptic outputs from both γ1-pedc and γ2-α′1 (PPL1-γ2α′1 DAN or PPL1-03) DANs are partially required in the first training phase of SOC, i.e. blocking their individual output reduces the performance index but does not completely abolish the flies' ability to form a higher-order association (Figure 3C-D). This could be explained by the nature of the US presented in the first training phase of this paradigm; strong electric shocks lead to activation of a wide range of the PPL1 DANs creating a compensatory effect when one of the latter is inoperative. On the other hand, we could show that the neurotransmission of PPL1-01 or PPL1-γ1pedc DAN (γ1-pedc DAN) is required for SOC to take place (Figure 3C). Therefore and taken these results together, it is only fair to speculate that a higher-order association is much more localized and neuron-specific, at least in this paradigm.

Previous findings validate the synaptic changes that KC-MBON connectivity endures from a simultaneous representation of an odor at the KC level along with reinforcing signals mediated by DANs (Hige et al., 2015; Vrontou et al., 2021; Hancock et al., 2022, manuscript 2, page 73). At the cellular level, this CS1-US association that modifies the exceptionally plastic synapses of MBONs has been suggested as a mechanism influencing the valence of stimuli after olfactory conditioning (Owald & Waddell, 2015; Hancock et al., 2022, manuscript 2, page 73). After determining the output from neuronal populations that are required for this higher-order associative learning, the next piece of the SOC puzzle is to validate the connectivity along with the functional roles of said neurons constituting the defined microcircuit. We began in the first place with subjecting the flies to a shock-only protocol and simultaneously monitoring calcium activity in the synaptic terminals of PPL1 DANs in the MB by using the pre-synaptic calcium sensor UAS-Syp-GCaMP3.

We could demonstrate that while both γ1-pedc and γ2-α′1 DANs reliably react to the electric pulsations, the other two DANs (α2-α′2 PPL1 DAN and the negative control γ5 PAM DAN) are unresponsive to electric shocks, meaning that every pulse correlates with a peak in calcium activity in the pre-synaptic site of the reacting neurons (Figure 4A). The same results were obtained while using the neurotransmitter vesicle release sensor UAS-Syp-pHTomato (Figure 4B). These findings concur with a very recent publication showing the implication of γ1-pedc and γ2-α′1 DANs in aversive associative learning by voltage imaging and their reaction to the punishing reinforcement of the US (Schnitzer et al., under review). Comparing these imaging results with the behavioral data, a question surges into mind: How come α′2 MBON is required in the second training phase of SOC while its compartment-specific α2-α′2 DAN is not? We hypothesized that while α2-α′2 DAN does not exhibit any shock-induced calcium responses, α′2 MBON receives input and is modulated by another PPL1 DAN in the CS1-US association. We then performed connectomics analysis using the neuPrint database (Clements et al., 2020) to discover one candidate that might mediate such reinforcement, none other than γ2-α′1 DAN (Figure 4D). We could also authenticate this outcome by finding a few synaptic arborizations from γ2-α′1 DAN that leak onto the bottom of the α′2 compartment using the GRASP technique (Figure 4C).

Since PPL1 DANs modulate the different compartments *via* DA G-protein coupled receptors that increase cAMP concentrations by the adenylyl cyclase Rutabaga pathway (Levin et al., 1992), we postulated that electric shock-inducible PPL1-DANs should elevate cAMP levels in the compartments that they innervate. Upon cAMP imaging using the G-Flamp1 sensor, we observed a variability in response amplitudes and peaks to the electric shocks mediated by PPL1 DANs

innervating the γ-lobe compartments (γ1 and γ2) compared to the α′2 (data not shown). Since we hypothesize that MB α′2 compartment receives punishing information from the γ2-α′1 DAN in the first training phase, a correlation analysis between the peaks in cAMP levels and each electric pulse was performed and shows an accurate shock-inudced cAMP changes in γ1 and γ2 compartments but not in the α′2 region (Data not shown). To speculate on the matter, the observable difference between the two γ-lobe and α′2 compartments might be explained by the presence of a different GPCR dopamine receptor (Dop1R2) exclusively expressed in the α′/β′ lobe. Dop1R2 differs in its signaling cascade from Dop1R1 that is pan-neuronal in the MB (Sun et al., 2020). Therefore, we anticipate that calcium monitoring in said MB compartments in reaction to the shock protocol is necessary for such a claim as well.

From connectivity to function, we generated data validating the existence of distinct microcircuits responsible for our SOC paradigm, but one piece of the puzzle is missing: the hunt for the memory trace. Consequently, we wanted to assess the synaptic changes in the post-synapses of γ1-pedc and α′2 MBONs after higher-order learning. We expressed the post-synaptic UAS-dHomer-GCaMP3 in these MBONs and exposed the flies naively to the odorants to image baseline pre-training calcium responses, then performed SOC to later on present the odors again and image post-training calcium traces (Figure 5A-B). Due to the weak to non-existing odor-evoked activity using dHomer-GCaMP3 in α′2 MBON during pre- and post-training odor presentations (Supplementary Figure 4C) and during SOC training as opposed to the γ1-pedc MBON (Supplementary Figure 4D), we used UAS-GCaMP6f that displays high kinetics in calcium binding to quantify before and after SOC calcium responses in α′2 MBON (Figure 5C-D). Because of time restrictions, reproducing the same experiments while expressing UAS-GCaMP6f in the γ1-pedc MBON for consistency

reasons could not meet the deadline of this thesis submission and are planned to take place in the following weeks. We observed in the case of pairing CS1 and US in the first training phase of SOC, odor-evoked calcium activity decreases post-training in reaction to CS1, but remains unchanged for CS^- in the post-synaptic sites of γ1-pedc MBON (Figure 5F, CS1 and CS^- panels). This aligns with one of the key findings in manuscript 2 demonstrating the localized synaptic plasticity appropriate to CS1-US association (Hancock et al., 2022, manuscript 2, page 73). What we add to the latter as a novel finding is the γ1-pedc MBON post-synapses are depressed after SOC training in reaction to the CS2 odor only when CS1 and US are presented simultaneously in the first training phase of SOC, followed by pairing of CS2 and CS1 in the second training phase (Figure 5F, CS2 panel). We conclude that the coincidence of the conditioned stimulus and the reinforcement in both training phases of SOC is responsible for decrease of the calcium response in reaction to CS2 after training. In line with these results, electrophysiological recordings show that only when an odor (CS1) is simultaneously presented with optogenetic activation of γ1-pedc DAN (mimicking the US), activity of the γ1-pedc MBON is suppressed (Hige et al., 2015).

Moreover and concerning α′2 MBON post-synaptic changes, we could show an increase in odor-evoked calcium levels in reaction to the CS1 odor after SOC only when CS1 and US were paired in the first training phase (Figure 5D, CS1 panel). We report no observable changes from pre- to post-training in odor-evoked calcium activity in reaction to neither CS^- nor CS2 (Figure 5D, CS^- and CS2 panels). From this we deduce that pairing the stimulus and the reinforcement in the first training phase of the SOC paradigm results in a potentiation at the level of the α'2-MBON post-synaptic dendrites. The opposite synaptic plasticity engendered in these two

post-synaptic MBON sites, facilitation in α'2 and depression in γ1-pedc, could potentially be explained by two arguments. First, different DA receptors are expressed in the α′/β′ and γ lobes signaling different protein cascades (Sun et al., 2020), and thereby inducing different plastic changes at the post-synaptic level during the CS1-US association in the first training phase. Second, it has been shown that inhibitory metabotropic receptors (mAChR-A and mAChR-B), exclusively expressed in the γ and α/β lobe KCs, enhance aversive olfactory learning by inducing lateral axo-axonal inhibition in stimulus-specific conditioning that translate to suppression of odor-evoked calcium responses and dopamine-evoked cAMP (Bielopolski et al., 2019; Manoim et al., 2022). Both the lack of these inhibitory mAChRs and the exclusive expression of Dop1R2 in the α'/β' lobe provide insights on explaining the opposing synaptic changes in KC-MBON connectivity in these two compartments.

Well-established results demonstrate the existence of direct and indirect feedback from MBONs to DANs using excitatory and inhibitory neurotransmitters (Li et al., 2020) suggesting a role for these feedback loops as one of the mechanisms underlying higher-order learning. Recent findings demonstrate the shaping of an aversive memory to an odor upon simultaneous optogenetic inhibition of the γ1-pedc MBON or optogenetic activation of γ1-pedc DAN (König et al., 2019). In our study, we optogenetically activated the two key MBONs in establishing SOC (γ1-pedc and α′2 MBONs) using UAS-CsChrimson and monitored the calcium activity, using UAS-GCaMP6m, of the sole PPL1 DAN implicated in the second training phase of CS1-CS2 association in the SOC paradigm, the γ1-pedc DAN. We found that procuring red light stimulations to the α′2 MBON induced activation of the γ1-pedc DAN, and *vice versa* for the γ1-pedc MBON (Figure 6A-D). It was shown that γ1-pedc MBON

has direct GABAergic feedback to the γ1-pedc DAN (Aso et al., 2014b; Ueoka et al., 2017; Pavlowsky et al., 2018), whereas no direct connection was found from the cholinergic α′2 MBON. Nevertheless, indirect connections *via* interneurons from MBONs to DANs were shown to exist in flies (Li et al., 2020). We suggest that γ1-pedc and α′2 MBONs create opposing feedback loops to γ1-pedc DAN and hypothesize about their role in the CS1-CS2 association to allow a learned odor (CS1) to reinforce a novel conditioned stimulus (CS2). Next and as an outlook, we want to confirm that indeed the learned odor hijacks the γ1-pedc DAN during the second training phase of SOC by monitoring the pre-synaptic calcium activity of this punishment-mediating DAN and hypothesizing an increased odor-evoked calcium activity in response to CS1 after SOC training.

To recapitulate the model that we propose for our SOC paradigm, the CS1-US association leads to a localized depression of the post-synaptic γ1-pedc MBON via modulation from γ1-pedc DAN while priming the α′2 compartment via the γ2-α′1 DAN in the first training phase. During the second training phase and through potentiated α′2 KCs, the conditioned odor CS1 activates the α′2 MBON in and of itself activates the γ1-pedc DAN along with coincidental activation of γ-KC by CS2, leading to a depression at the post-synaptic γ1-pedc MBON (Figure 6E). In *Aplysia*, a theoretical model proposes that the learning rules responsible for synaptic plasticity underlying associative classical conditioning may serve as a primer for establishing higher-order learning (Hawkins & Kandel, 1984). They propose that their SOC model in the gill- and siphon-withdrawal reflex of the sea slug relies on two parallel cellular processes; facilitation in the synapses between modulatory and sensory neurons upon CS1-US association, along with synaptic depression at the motor-interneuron connections (Hawkins & Kandel, 1984). To sum this conceptual model up, the authors suggest

that SOC changes the ability of CS1 to gain access to the internal mechanisms over which the US previously acted and modulated the sensory input (Hawkins & Kandel, 1984). In addition, a more recent computational model called the *simulated fly* is in accordance with our overall findings in terms of the existence of retrograde signaling as a feedback to the MB in order for SOC to take place (Faghihi et al., 2017). Overall, in this third and last manuscript, we describe two opposing mushroom body compartments working in parallel through bidirectional feedback loops, allowing a previously learned odor to take control of the punishment-mediating dopaminergic system, thereby justifying the mechanisms underlying associative learning of a higher order.

One last and exciting finding in our study is the fly's ability to perform an even higher form of olfactory associative learning, called third-order conditioning (TOC). In this paradigm, the animals were subjected to a third training phase on top of SOC, consisting of overlaying pulses of the CS2 on top of a fourth and novel odor (CS3), leading to transfer of the aversive information to the latter and avoiding it in a choice situation with CS^- (Figure 7B, "Paired-Paired-Paired"). No TOC memory formation was observed in all the three controls where dissociation between the conditioned stimulus and the reinforcement happened either during the first, second or third training phases (Figure 7B, "Paired-Paired-Unpaired", "Paired-Unpaired-Paired" and "Unpaired-Paired-Paired"). Investigating complex behaviors such as TOC might be the gateway into understanding associative chains and unpacking the essence of cognitive neuroscience.

Summary

Despite its small brain and its succinct life cycle, the fruit fly *Drosophila melanogaster* is a versatile model organism in behavioral and molecular neuroscience. From understanding the molecular machinery behind development and cell differentiation to the investigation of neuronal mechanisms underlying complex behaviors of higher-order, this animal was and remains an indispensable specimen in scientific research due its vast and extensive arsenal of transgenetic tools. Understanding the principles behind olfactory higher-order associative chains formation in *Drosophila* is one step further into unraveling the essence of learning and memory. However, the rationale behind such mechanisms sprouts since the development of the young brain to its full potential and its ability form complex and intermingled connections governing this type of higher-order learning.

First, we took a developmental approach to assess the activity behind neuronal development of the center of olfactory learning in the fruit fly, the mushroom body (MB). In the first manuscript, we could demonstrate that in order for the MB to undergo a series of degeneration and regrowth of axon terminals and synapses that are necessary for its healthy development (also called remodeling), its activity needs to be hyperpolarized by cell-autonomous and external factors. The interruption of such processes leads to the poor development of the MB along with its synaptic partners, thus translating to a deficit in olfactory memory formation in the adult stage.

Then, we worked towards scrutinizing the synaptic plasticity instigating olfactory learning in the context of a classical aversive conditioning paradigm in the second manuscript. Aversive olfactory conditioning in Drosophila consists of training the animals to associate a neutral stimulus (that later becomes the conditioned stimulus

CS1), independently of its innate valence, to a punishing reinforcement (e.g. electric shocks also called unconditioned stimulus US), leading to its avoidance in the memory recall phase. We demonstrate that CS1-US association effectuates localized synaptic changes between odor encoding cells (Kenyon cells KCs) and behavioral mediating output neurons (MB output neurons MBONs) in one distinct compartment of the MB, the γ1.

In the third and last manuscript, we designated second-order conditioning (SOC) as a higher-order form of learning to unravel and get one step closer to understanding the principles of associative chains in learning. SOC can be achieved when a previously conditioned stimulus (CS1) is paired with a second-conditioned stimulus (CS2), eliciting a conditioned response to the CS2. This type of conditioning offers the opportunity to examine how the internal transfer of information from CS1 to CS2 occurs on cellular and molecular levels. Therefore, investigating the yet unclear neuronal microcircuit that underlies this behavior is of importance. By thermo-genetically manipulating a panoply of MB neuronal populations, we could show a distinct microcircuits that are implicated in aversive olfactory learning during different phases of training and test in SOC. Then, functional imaging along with connectomics analysis procured a better understanding of the dynamics between the candidate neurons, from which emerges a proposed model for SOC. We suggest that two parallel MB compartments work in synergy allowing a previously conditioned odor through bidirectional feedback loops to hijack the punishment-mediating dopaminergic neurons, and thus formation of higher-order associations.

References

Abrams, T. W., & Kandel, E. R. (1988). Is contiguity detection in classical conditioning a system or a cellular property? Learning in Aplysia suggests a possible molecular site. *Trends in neurosciences*, *11*(4), 128–135. https://doi.org/10.1016/0166-2236(88)90137-3

Adams, M. D., Celniker, S. E., Holt, R. A., Evans, C. A., Gocayne, J. D., Amanatides, P. G., Scherer, S. E., Li, P. W., Hoskins, R. A., Galle, R. F., George, R. A., Lewis, S. E., Richards, S., Ashburner, M., Henderson, S. N., Sutton, G. G., Wortman, J. R., Yandell, M. D., Zhang, Q., Chen, L. X., … Venter, J. C. (2000). The genome sequence of *Drosophila melanogaster*. *Science (New York, N.Y.)*, *287*(5461), 2185–2195. https://doi.org/10.1126/science.287.5461.2185

Aimon, S., Katsuki, T., Jia, T., Grosenick, L., Broxton, M., Deisseroth, K., Sejnowski, T. J., & Greenspan, R. J. (2019). Fast near-whole-brain imaging in adult Drosophila during responses to stimuli and behavior. *PLoS biology*, *17*(2), e2006732. https://doi.org/10.1371/journal.pbio.2006732

Amiro, T. W., & Bitterman, M. E. (1980). Second-order appetitive conditioning in goldfish. *Journal of experimental psychology. Animal behavior processes*, *6*(1), 41–48. https://doi.org/10.1037/0097-7403.6.1.41

Arias A. M. (2008). Drosophila melanogaster and the development of biology in the 20th century. *Methods in molecular biology (Clifton, N.J.)*, *420*, 1–25. https://doi.org/10.1007/978-1-59745-583-1_1

Aso, Y., & Rubin, G. M. (2016). Dopaminergic neurons write and update memories with cell-type-specific rules. *eLife*, *5*, e16135. https://doi.org/10.7554/eLife.16135

Aso, Y., Grübel, K., Busch, S., Friedrich, A. B., Siwanowicz, I., & Tanimoto, H. (2009). The mushroom body of adult Drosophila characterized by GAL4 drivers. *Journal of neurogenetics*, *23*(1-2), 156–172. https://doi.org/10.1080/01677060802471718

Aso, Y., Hattori, D., Yu, Y., Johnston, R. M., Iyer, N. A., Ngo, T. T., Dionne, H., Abbott, L. F., Axel, R., Tanimoto, H., & Rubin, G. M. (2014a). The neuronal architecture of the mushroom body provides a logic for associative learning. *eLife*, *3*, e04577. https://doi.org/10.7554/eLife.04577

Aso, Y., Sitaraman, D., Ichinose, T., Kaun, K. R., Vogt, K., Belliart-Guérin, G., Plaçais, P. Y., Robie, A. A., Yamagata, N., Schnaitmann, C., Rowell, W. J., Johnston, R. M., Ngo, T. T., Chen, N., Korff, W., Nitabach, M. N., Heberlein, U., Preat, T., Branson, K.

M., Tanimoto, H., … Rubin, G. M. (2014b). Mushroom body output neurons encode valence and guide memory-based action selection in *Drosophila*. *eLife*, *3*, e04580. https://doi.org/10.7554/eLife.04580

Aso, Y., Siwanowicz, I., Bräcker, L., Ito, K., Kitamoto, T., & Tanimoto, H. (2010). Specific dopaminergic neurons for the formation of labile aversive memory. *Current biology : CB*, *20*(16), 1445–1451. https://doi.org/10.1016/j.cub.2010.06.048

Barnstedt, O., Owald, D., Felsenberg, J., Brain, R., Moszynski, J. P., Talbot, C. B., Perrat, P. N., & Waddell, S. (2016). Memory-Relevant Mushroom Body Output Synapses Are Cholinergic. *Neuron*, *89*(6), 1237–1247. https://doi.org/10.1016/j.neuron.2016.02.015

Barth, J., Dipt, S., Pech, U., Hermann, M., Riemensperger, T., & Fiala, A. (2014). Differential associative training enhances olfactory acuity in *Drosophila melanogaster*. *The Journal of neuroscience : the official journal of the Society for Neuroscience*, *34*(5), 1819–1837. https://doi.org/10.1523/JNEUROSCI.2598-13.2014

Bellen, H. J., Tong, C., & Tsuda, H. (2010). 100 years of *Drosophila* research and its impact on vertebrate neuroscience: a history lesson for the future. *Nature reviews. Neuroscience*, *11*(7), 514–522. https://doi.org/10.1038/nrn2839

Benton, R., Vannice, K. S., Gomez-Diaz, C., & Vosshall, L. B. (2009). Variant ionotropic glutamate receptors as chemosensory receptors in Drosophila. *Cell*, *136*(1), 149–162. https://doi.org/10.1016/j.cell.2008.12.001

Bidaye, S. S., Machacek, C., Wu, Y., & Dickson, B. J. (2014). Neuronal control of *Drosophila* walking direction. *Science (New York, N.Y.)*, *344*(6179), 97–101. https://doi.org/10.1126/science.1249964

Bielopolski, N., Amin, H., Apostolopoulou, A. A., Rozenfeld, E., Lerner, H., Huetteroth, W., Lin, A. C., & Parnas, M. (2019). Inhibitory muscarinic acetylcholine receptors enhance aversive olfactory learning in adult *Drosophila*. *eLife*, *8*, e48264. https://doi.org/10.7554/eLife.48264

Bilz, F. (2018). *Optical Analysis of Synaptic Plasticity Underlying Associative Learning in Drosophila Melanogaster* (Doctoral dissertation, Georg-August-Universität Göttingen). http://dx.doi.org/10.53846/goediss-7088

Bilz, F., Geurten, B. R. H., Hancock, C. E., Widmann, A., & Fiala, A. (2020). Visualization of a Distributed Synaptic Memory Code in the *Drosophila* Brain. *Neuron*, *106*(6), 963–976.e4. https://doi.org/10.1016/j.neuron.2020.03.010

Boeckh, J., Distler, P., Ernst, K. D., Hösl, M., & Malun, D. (1990). Olfactory bulb and antennal lobe. In *Chemosensory information processing* (pp. 201-227). Springer, Berlin, Heidelberg. ISBN: 978-3-642-75127-1

Boto, T., Stahl, A., Zhang, X., Louis, T., & Tomchik, S. M. (2019). Independent Contributions of Discrete Dopaminergic Circuits to Cellular Plasticity, Memory Strength, and Valence in Drosophila. *Cell reports*, *27*(7), 2014–2021.e2. https://doi.org/10.1016/j.celrep.2019.04.069

Brand, A. H., & Perrimon, N. (1993). Targeted gene expression as a means of altering cell fates and generating dominant phenotypes. *Development (Cambridge, England)*, *118*(2), 401–415. https://doi.org/10.1242/dev.118.2.401

Buchner, E., & Wu, C. F. (2009). Drosophila neurogenetics--the Heisenberg impact. *Journal of neurogenetics*, *23*(1-2), 1–2. https://doi.org/10.1080/01677060802687701

Bülthoff, H., Götz, K. G., & Herre, M. (1982). Recurrent inversion of visual orientation in the walking fly, Drosophila melanogaster. *Journal of comparative physiology*, *148*(4), 471-481. https://doi.org/10.1007/BF00619785

Busto, G. U., Cervantes-Sandoval, I., & Davis, R. L. (2010). Olfactory learning in *Drosophila*. *Physiology (Bethesda, Md.)*, *25*(6), 338–346. https://doi.org/10.1152/physiol.00026.2010

Cachero, S., Gkantia, M., Bates, A. S., Frechter, S., Blackie, L., McCarthy, A., Sutcliffe, B., Strano, A., Aso, Y., & Jefferis, G. S. X. E. (2020). BAcTrace, a tool for retrograde tracing of neuronal circuits in *Drosophila*. *Nature methods*, *17*(12), 1254–1261. https://doi.org/10.1038/s41592-020-00989-1

Cadd, G., & McKnight, G. S. (1989). Distinct patterns of cAMP-dependent protein kinase gene expression in mouse brain. *Neuron*, *3*(1), 71–79. https://doi.org/10.1016/0896-6273(89)90116-5

Cassenaer, S., & Laurent, G. (2012). Conditional modulation of spike-timing-dependent plasticity for olfactory learning. *Nature*, *482*(7383), 47–52. https://doi.org/10.1038/nature10776

Claridge-Chang, A., Roorda, R. D., Vrontou, E., Sjulson, L., Li, H., Hirsh, J., & Miesenböck, G. (2009). Writing memories with light-addressable reinforcement circuitry. *Cell*, *139*(2), 405–415. https://doi.org/10.1016/j.cell.2009.08.034

Cocchi, E., Drago, A., & Serretti, A. (2016). Hippocampal Pruning as a New Theory of Schizophrenia Etiopathogenesis. *Molecular neurobiology*, *53*(3), 2065–2081. https://doi.org/10.1007/s12035-015-9174-6

Cong, J., Geng, W., He, B., Liu, J., Charlton, J., & Adler, P. N. (2001). The furry gene of Drosophila is important for maintaining the integrity of cellular extensions during morphogenesis. *Development (Cambridge, England)*, *128*(14), 2793–2802. https://doi.org/10.1242/dev.128.14.2793

Corbit, L. H., & Balleine, B. W. (2005). Double dissociation of basolateral and central amygdala lesions on the general and outcome-specific forms of pavlovian-instrumental transfer. *The Journal of neuroscience : the official journal of the Society for Neuroscience*, *25*(4), 962–970. https://doi.org/10.1523/JNEUROSCI.4507-04.2005

Couto, A., Alenius, M., & Dickson, B. J. (2005). Molecular, anatomical, and functional organization of the *Drosophila* olfactory system. *Current biology : CB*, *15*(17), 1535–1547. https://doi.org/10.1016/j.cub.2005.07.034

Craddock, P., Wasserman, J. S., Polack, C. W., Kosinski, T., Renaux, C., & Miller, R. R. (2018). Associative structure of second-order conditioning in humans. *Learning & behavior*, *46*(2), 171–181. https://doi.org/10.3758/s13420-017-0299-5

Crittenden, J. R., Skoulakis, E. M., Han, K. A., Kalderon, D., & Davis, R. L. (1998). Tripartite mushroom body architecture revealed by antigenic markers. *Learning & memory (Cold Spring Harbor, N.Y.)*, *5*(1-2), 38–51. doi:10.1101/lm.5.1.38

DasGupta, S., Ferreira, C. H., & Miesenböck, G. (2014). FoxP influences the speed and accuracy of a perceptual decision in Drosophila. *Science (New York, N.Y.)*, *344*(6186), 901–904. https://doi.org/10.1126/science.1252114

Davis R. L. (2004). Olfactory learning. *Neuron*, *44*(1), 31–48. https://doi.org/10.1016/j.neuron.2004.09.008

Davis, R. L., & Han, K. A. (1996). Neuroanatomy: mushrooming mushroom bodies. *Current biology : CB*, *6*(2), 146–148. https://doi.org/10.1016/s0960-9822(02)00447-5

Dayan, P., & Balleine, B. W. (2002). Reward, motivation, and reinforcement learning. *Neuron*, *36*(2), 285–298. https://doi.org/10.1016/s0896-6273(02)00963-7

de Belle, J. S., & Heisenberg, M. (1994). Associative odor learning in *Drosophila* abolished by chemical ablation of mushroom bodies. *Science (New York, N.Y.)*, *263*(5147), 692–695. https://doi.org/10.1126/science.8303280

Dubnau, J., Grady, L., Kitamoto, T., & Tully, T. (2001). Disruption of neurotransmission in *Drosophila* mushroom body blocks retrieval but not acquisition of memory. *Nature*, *411*(6836), 476–480. https://doi.org/10.1038/35078077

Duch, C., & Mentel, T. (2004). Activity affects dendritic shape and synapse elimination during steroid controlled dendritic retraction in Manduca sexta. *The Journal of neuroscience : the official journal of the Society for Neuroscience*, *24*(44), 9826–9837. https://doi.org/10.1523/JNEUROSCI.3189-04.2004

Eichler, K., Li, F., Litwin-Kumar, A., Park, Y., Andrade, I., Schneider-Mizell, C. M., Saumweber, T., Huser, A., Eschbach, C., Gerber, B., Fetter, R. D., Truman, J. W., Priebe, C. E., Abbott, L. F., Thum, A. S., Zlatic, M., & Cardona, A. (2017). The complete connectome of a learning and memory centre in an insect brain. *Nature*, *548*(7666), 175–182. https://doi.org/10.1038/nature23455

Faghihi, F., Moustafa, A. A., Heinrich, R., & Wörgötter, F. (2017). A computational model of conditioning inspired by Drosophila olfactory system. *Neural networks : the official journal of the International Neural Network Society*, *87*, 96–108. https://doi.org/10.1016/j.neunet.2016.11.002

Feinberg, E. H., Vanhoven, M. K., Bendesky, A., Wang, G., Fetter, R. D., Shen, K., & Bargmann, C. I. (2008). GFP Reconstitution Across Synaptic Partners (GRASP) defines cell contacts and synapses in living nervous systems. *Neuron*, *57*(3), 353–363. https://doi.org/10.1016/j.neuron.2007.11.030

Felsenberg, J., Jacob, P. F., Walker, T., Barnstedt, O., Edmondson-Stait, A. J., Pleijzier, M. W., Otto, N., Schlegel, P., Sharifi, N., Perisse, E., Smith, C. S., Lauritzen, J. S., Costa, M., Jefferis, G. S. X. E., Bock, D. D., & Waddell, S. (2018). Integration of Parallel Opposing Memories Underlies Memory Extinction. *Cell*, *175*(3), 709–722.e15. https://doi.org/10.1016/j.cell.2018.08.021

Fernández-Moreno, M. A., Farr, C. L., Kaguni, L. S., & Garesse, R. (2007). *Drosophila melanogaster* as a model system to study mitochondrial biology. *Methods in molecular biology (Clifton, N.J.)*, *372*, 33–49. https://doi.org/10.1007/978-1-59745-365-3_3

Fiala A. (2007). Olfaction and olfactory learning in *Drosophila*: recent progress. *Current opinion in neurobiology*, *17*(6), 720–726. https://doi.org/10.1016/j.conb.2007.11.009

Fiala, A., Spall, T., Diegelmann, S., Eisermann, B., Sachse, S., Devaud, J. M., Buchner, E., & Galizia, C. G. (2002). Genetically expressed cameleon in *Drosophila melanogaster* is used to visualize olfactory information in projection neurons. *Current biology : CB*, *12*(21), 1877–1884. https://doi.org/10.1016/s0960-9822(02)01239-3

Fishilevich, E., & Vosshall, L. B. (2005). Genetic and functional subdivision of the *Drosophila* antennal lobe. *Current biology : CB*, *15*(17), 1548–1553. https://doi.org/10.1016/j.cub.2005.07.066

Galizia, C. G., & Sachse, S. (2010). Odor Coding in Insects. In A. Menini (Ed.), *The Neurobiology of Olfaction*. CRC Press/Taylor & Francis. ISBN-13: 978-1-4200-7197-9

Gao, F., Yang, S., Wang, J., & Zhu, G. (2022). cAMP-PKA cascade: An outdated topic for depression?. *Biomedicine & pharmacotherapy = Biomedecine & pharmacotherapie*, *150*, 113030. https://doi.org/10.1016/j.biopha.2022.113030

Gerber, B., Tanimoto, H., & Heisenberg, M. (2004). An engram found? Evaluating the evidence from fruit flies. *Current opinion in neurobiology*, *14*(6), 737–744. https://doi.org/10.1016/j.conb.2004.10.014

Gervasi, N., Tchénio, P., & Preat, T. (2010). PKA dynamics in a Drosophila learning center: coincidence detection by rutabaga adenylyl cyclase and spatial regulation by dunce phosphodiesterase. *Neuron*, *65*(4), 516–529. https://doi.org/10.1016/j.neuron.2010.01.014

Giurfa M. (2013). Cognition with few neurons: higher-order learning in insects. *Trends in neurosciences*, *36*(5), 285–294. https://doi.org/10.1016/j.tins.2012.12.011

Golovin, R. M., Vest, J., Vita, D. J., & Broadie, K. (2019). Activity-Dependent Remodeling of *Drosophila* Olfactory Sensory Neuron Brain Innervation during an Early-Life Critical Period. *The Journal of neuroscience : the official journal of the Society for Neuroscience*, *39*(16), 2995–3012. https://doi.org/10.1523/JNEUROSCI.2223-18.2019

Gordon, M. D., & Scott, K. (2009). Motor control in a Drosophila taste circuit. *Neuron*, *61*(3), 373–384. https://doi.org/10.1016/j.neuron.2008.12.033

Groth, A. C., Fish, M., Nusse, R., & Calos, M. P. (2004). Construction of transgenic *Drosophila* by using the site-specific integrase from phage phiC31. *Genetics*, *166*(4), 1775–1782. https://doi.org/10.1534/genetics.166.4.1775

Gruntman, E., & Turner, G. C. (2013). Integration of the olfactory code across dendritic claws of single mushroom body neurons. *Nature neuroscience*, *16*(12), 1821–1829. https://doi.org/10.1038/nn.3547

Hamada, F. N., Rosenzweig, M., Kang, K., Pulver, S. R., Ghezzi, A., Jegla, T. J., & Garrity, P. A. (2008). An internal thermal sensor controlling temperature preference in Drosophila. *Nature*, *454*(7201), 217–220. https://doi.org/10.1038/nature07001

Han, P. L., Levin, L. R., Reed, R. R., & Davis, R. L. (1992). Preferential expression of the Drosophila rutabaga gene in mushroom bodies, neural centers for learning in insects. *Neuron*, *9*(4), 619–627. https://doi.org/10.1016/0896-6273(92)90026-a

Han, R., Wei, T. M., Tseng, S. C., & Lo, C. C. (2021). Characterizing approach behavior of Drosophila melanogaster in Buridan's paradigm. *PloS one*, *16*(1), e0245990. https://doi.org/10.1371/journal.pone.0245990

Hartenstein, V., Spindler, S., Pereanu, W., & Fung, S. (2008). The development of the *Drosophila* larval brain. *Advances in experimental medicine and biology*, *628*, 1–31. https://doi.org/10.1007/978-0-387-78261-4_1

Hawkins, R. D., & Kandel, E. R. (1984). Is there a cell-biological alphabet for simple forms of learning?. *Psychological review*, *91*(3), 375–391.

Hawkins, R. D., Greene, W., & Kandel, E. R. (1998). Classical conditioning, differential conditioning, and second-order conditioning of the Aplysia gill-withdrawal reflex in a simplified mantle organ preparation. *Behavioral neuroscience*, *112*(3), 636–645. https://doi.org/10.1037//0735-7044.112.3.636

Hearn, M. G., Ren, Y., McBride, E. W., Reveillaud, I., Beinborn, M., & Kopin, A. S. (2002). A Drosophila dopamine 2-like receptor: Molecular characterization and identification of multiple alternatively spliced variants. *Proceedings of the National Academy of Sciences of the United States of America*, *99*(22), 14554–14559. https://doi.org/10.1073/pnas.202498299

Heinz, A., & Schlagenhauf, F. (2010). Dopaminergic dysfunction in schizophrenia: salience attribution revisited. *Schizophrenia bulletin*, *36*(3), 472–485. https://doi.org/10.1093/schbul/sbq031

Heisenberg M. (2003). Mushroom body memoir: from maps to models. *Nature reviews. Neuroscience*, *4*(4), 266–275. https://doi.org/10.1038/nrn1074

Heisenberg, M., & Buchner, E. (1977). The role of retinula cell types in visual behavior of Drosophila melanogaster. *Journal of comparative physiology*, *117*(2), 127-162. https://doi.org/10.1007/BF00612784

Heisenberg, M., & Götz, K. G. (1975). The use of mutations for the partial degradation of vision inDrosophila melanogaster. *Journal of comparative physiology*, *98*(3), 217-241. https://doi.org/10.1007/BF00656971

Heisenberg, M., Borst, A., Wagner, S., & Byers, D. (1985). *Drosophila* mushroom body mutants are deficient in olfactory learning. *Journal of neurogenetics*, *2*(1), 1–30. https://doi.org/10.3109/01677068509100140

Hidalgo, A., Urban, J., & Brand, A. H. (1995). Targeted ablation of glia disrupts axon tract formation in the *Drosophila* CNS. *Development (Cambridge, England)*, *121*(11), 3703–3712. https://doi.org/10.1242/dev.121.11.3703

Hige, T., Aso, Y., Rubin, G. M., & Turner, G. C. (2015). Plasticity-driven individualization of olfactory coding in mushroom body output neurons. *Nature*, *526*(7572), 258–262. https://doi.org/10.1038/nature15396

Holmes, N. M., Parkes, S. L., Killcross, A. S., & Westbrook, R. F. (2013). The basolateral amygdala is critical for learning about neutral stimuli in the presence of danger, and the perirhinal cortex is critical in the absence of danger. *The Journal of neuroscience : the official journal of the Society for Neuroscience*, *33*(32), 13112–13125. https://doi.org/10.1523/JNEUROSCI.1998-13.2013

Hong, S., Beja-Glasser, V. F., Nfonoyim, B. M., Frouin, A., Li, S., Ramakrishnan, S., Merry, K. M., Shi, Q., Rosenthal, A., Barres, B. A., Lemere, C. A., Selkoe, D. J., & Stevens, B. (2016). Complement and microglia mediate early synapse loss in Alzheimer mouse models. *Science (New York, N.Y.)*, *352*(6286), 712–716. https://doi.org/10.1126/science.aad8373

Huang, T. H., Niesman, P., Arasu, D., Lee, D., De La Cruz, A. L., Callejas, A., Hong, E. J., & Lois, C. (2017). Tracing neuronal circuits in transgenic animals by transneuronal control of transcription (*TRACT*). *eLife*, *6*, e32027. https://doi.org/10.7554/eLife.32027

Hussaini, S. A., Komischke, B., Menzel, R., & Lachnit, H. (2007). Forward and backward second-order Pavlovian conditioning in honeybees. *Learning & memory (Cold Spring Harbor, N.Y.)*, *14*(10), 678–683. https://doi.org/10.1101/lm.471307

Ichinose, T., & Tanimoto, H. (2016). Dynamics of memory-guided choice behavior in Drosophila. *Proceedings of the Japan Academy. Series B, Physical and biological sciences*, *92*(8), 346–357. https://doi.org/10.2183/pjab.92.346

Ichinose, T., Aso, Y., Yamagata, N., Abe, A., Rubin, G. M., & Tanimoto, H. (2015). Reward signal in a recurrent circuit drives appetitive long-term memory formation. *eLife*, *4*, e10719. https://doi.org/10.7554/eLife.10719

Inami, S., Sato, S., Kondo, S., Tanimoto, H., Kitamoto, T., & Sakai, T. (2020). Environmental Light Is Required for Maintenance of Long-Term Memory in *Drosophila*. *The Journal of neuroscience : the official journal of the Society for Neuroscience*, *40*(7), 1427–1439. https://doi.org/10.1523/JNEUROSCI.1282-19.2019

Issa, A. R., Sun, J., Petitgas, C., Mesquita, A., Dulac, A., Robin, M., Mollereau, B., Jenny, A., Chérif-Zahar, B., & Birman, S. (2018). The lysosomal membrane protein LAMP2A promotes autophagic flux and prevents SNCA-induced Parkinson disease-like symptoms in the Drosophila brain. *Autophagy*, *14*(11), 1898–1910. https://doi.org/10.1080/15548627.2018.1491489

Ito, K., Awano, W., Suzuki, K., Hiromi, Y., & Yamamoto, D. (1997). The *Drosophila* mushroom body is a quadruple structure of clonal units each of which contains a virtually identical set of neurones and glial cells. *Development (Cambridge, England)*, *124*(4), 761–771. https://doi.org/10.1242/dev.124.4.761

Jenett, A., Rubin, G. M., Ngo, T. T., Shepherd, D., Murphy, C., Dionne, H., Pfeiffer, B. D., Cavallaro, A., Hall, D., Jeter, J., Iyer, N., Fetter, D., Hausenfluck, J. H., Peng, H., Trautman, E. T., Svirskas, R. R., Myers, E. W., Iwinski, Z. R., Aso, Y., DePasquale, G. M., … Zugates, C. T. (2012). A GAL4-driver line resource for *Drosophila* neurobiology. *Cell reports*, *2*(4), 991–1001. https://doi.org/10.1016/j.celrep.2012.09.011

Jennings, D., & Kirkpatrick, K. (2018). Temporal map formation in appetitive second-order conditioning in rats. *Behavioural processes*, *154*, 60–72. https://doi.org/10.1016/j.beproc.2018.02.001

Johard, H. A., Enell, L. E., Gustafsson, E., Trifilieff, P., Veenstra, J. A., & Nässel, D. R. (2008). Intrinsic neurons of Drosophila mushroom bodies express short neuropeptide F: relations to extrinsic neurons expressing different neurotransmitters. *The Journal of comparative neurology*, *507*(4), 1479–1496. https://doi.org/10.1002/cne.21636

Johnson, O., Becnel, J., & Nichols, C. D. (2011). Serotonin receptor activity is necessary for olfactory learning and memory in Drosophila melanogaster. *Neuroscience*, *192*, 372–381. https://doi.org/10.1016/j.neuroscience.2011.06.058

Joshua, M., Adler, A., & Bergman, H. (2009). The dynamics of dopamine in control of motor behavior. *Current opinion in neurobiology*, *19*(6), 615–620. https://doi.org/10.1016/j.conb.2009.10.001

Jung, J. E., Lee, J. Y., Kim, I. R., Park, S. M., Kang, J. W., Kim, Y. H., Park, H. R., & Lee, J. H. (2020). MicroRNA-31 Regulates Expression of *Wntless* in Both *Drosophila melanogaster* and Human Oral Cancer Cells. *International journal of molecular sciences*, *21*(19), 7232. https://doi.org/10.3390/ijms21197232

Jürgensen, A. M., Khalili, A., Chicca, E., Indiveri, G., & Nawrot, M. P. (2021). A neuromorphic model of olfactory processing and sparse coding in the Drosophila larva brain. *Neuromorphic Computing and Engineering*, *1*(2), 024008. 10.1088/2634-4386/ac3ba6

Kano, M., Watanabe, T., Uesaka, N., & Watanabe, M. (2018). Multiple Phases of Climbing Fiber Synapse Elimination in the Developing Cerebellum. *Cerebellum (London, England)*, *17*(6), 722–734. https://doi.org/10.1007/s12311-018-0964-z

Kasuya, J., Ishimoto, H., & Kitamoto, T. (2009). Neuronal mechanisms of learning and memory revealed by spatial and temporal suppression of neurotransmission using shibire, a temperature-sensitive dynamin mutant gene in *Drosophila melanogaster. Frontiers in molecular neuroscience*, *2*, 11. https://doi.org/10.3389/neuro.02.011.2009

Kitamoto T. (2001). Conditional modification of behavior in Drosophila by targeted expression of a temperature-sensitive shibire allele in defined neurons. *Journal of neurobiology*, *47*(2), 81–92. https://doi.org/10.1002/neu.1018

Kitamoto T. (2002). Conditional disruption of synaptic transmission induces male-male courtship behavior in *Drosophila*. *Proceedings of the National Academy of Sciences*

of the United States of America, *99*(20), 13232–13237. https://doi.org/10.1073/pnas.202489099

Klapoetke, N. C., Murata, Y., Kim, S. S., Pulver, S. R., Birdsey-Benson, A., Cho, Y. K., Morimoto, T. K., Chuong, A. S., Carpenter, E. J., Tian, Z., Wang, J., Xie, Y., Yan, Z., Zhang, Y., Chow, B. Y., Surek, B., Melkonian, M., Jayaraman, V., Constantine-Paton, M., Wong, G. K., … Boyden, E. S. (2014). Independent optical excitation of distinct neural populations. *Nature methods*, *11*(3), 338–346. https://doi.org/10.1038/nmeth.2836

Knapp, E. M., Kaiser, A., Arnold, R. C., Sampson, M. M., Ruppert, M., Xu, L., Anderson, M. I., Bonanno, S. L., Scholz, H., Donlea, J. M., & Krantz, D. E. (2022). Mutation of the *Drosophila melanogaster* serotonin transporter dSERT impacts sleep, courtship, and feeding behaviors. *PLoS genetics*, *18*(11), e1010289. https://doi.org/10.1371/journal.pgen.1010289

Kong, E. C., Woo, K., Li, H., Lebestky, T., Mayer, N., Sniffen, M. R., Heberlein, U., Bainton, R. J., Hirsh, J., & Wolf, F. W. (2010). A pair of dopamine neurons target the D1-like dopamine receptor DopR in the central complex to promote ethanol-stimulated locomotion in *Drosophila*. *PloS one*, *5*(4), e9954. https://doi.org/10.1371/journal.pone.0009954

König, C., Khalili, A., Niewalda, T., Gao, S., & Gerber, B. (2019). An optogenetic analogue of second-order reinforcement in *Drosophila*. *Biology letters*, *15*(7), 20190084. https://doi.org/10.1098/rsbl.2019.0084

Krashes, M. J., & Waddell, S. (2008). Rapid consolidation to a radish and protein synthesis-dependent long-term memory after single-session appetitive olfactory conditioning in *Drosophila*. *The Journal of neuroscience : the official journal of the Society for Neuroscience*, *28*(12), 3103–3113. https://doi.org/10.1523/JNEUROSCI.5333-07.2008

Krashes, M. J., DasGupta, S., Vreede, A., White, B., Armstrong, J. D., & Waddell, S. (2009). A neural circuit mechanism integrating motivational state with memory expression in *Drosophila*. *Cell*, *139*(2), 416–427. https://doi.org/10.1016/j.cell.2009.08.035

Krashes, M. J., Keene, A. C., Leung, B., Armstrong, J. D., & Waddell, S. (2007). Sequential use of mushroom body neuron subsets during *Drosophila* odor memory processing. *Neuron*, *53*(1), 103–115. https://doi.org/10.1016/j.neuron.2006.11.021

Lagasse, F., Moreno, C., Preat, T., & Mery, F. (2012). Functional and evolutionary trade-offs co-occur between two consolidated memory phases in Drosophila melanogaster. *Proceedings. Biological sciences*, *279*(1744), 4015–4023. https://doi.org/10.1098/rspb.2012.1457

Lau, C. K. S., Jelen, M., & Gordon, M. D. (2021). A closed-loop optogenetic screen for neurons controlling feeding in *Drosophila*. *G3 (Bethesda, Md.)*, *11*(5), jkab073. https://doi.org/10.1093/g3journal/jkab073

Lebestky, T., Chang, J. S., Dankert, H., Zelnik, L., Kim, Y. C., Han, K. A., Wolf, F. W., Perona, P., & Anderson, D. J. (2009). Two different forms of arousal in *Drosophila* are oppositely regulated by the dopamine D1 receptor ortholog DopR via distinct neural circuits. *Neuron*, *64*(4), 522–536. https://doi.org/10.1016/j.neuron.2009.09.031

Lee, J. C., & Livesey, E. J. (2012). Second-order conditioning and conditioned inhibition: influences of speed versus accuracy on human causal learning. *PloS one*, *7*(11), e49899. https://doi.org/10.1371/journal.pone.0049899

Levin, L. R., Han, P. L., Hwang, P. M., Feinstein, P. G., Davis, R. L., & Reed, R. R. (1992). The Drosophila learning and memory gene rutabaga encodes a Ca2+/Calmodulin-responsive adenylyl cyclase. *Cell*, *68*(3), 479–489. https://doi.org/10.1016/0092-8674(92)90185-f

Li, B. X., Satoh, A. K., & Ready, D. F. (2007). Myosin V, Rab11, and dRip11 direct apical secretion and cellular morphogenesis in developing Drosophila photoreceptors. *The Journal of cell biology*, *177*(4), 659–669. https://doi.org/10.1083/jcb.200610157

Li, F., Lindsey, J. W., Marin, E. C., Otto, N., Dreher, M., Dempsey, G., Stark, I., Bates, A. S., Pleijzier, M. W., Schlegel, P., Nern, A., Takemura, S. Y., Eckstein, N., Yang, T., Francis, A., Braun, A., Parekh, R., Costa, M., Scheffer, L. K., Aso, Y., … Rubin, G. M. (2020). The connectome of the adult *Drosophila* mushroom body provides insights into function. *eLife*, *9*, e62576. https://doi.org/10.7554/eLife.62576

Lima, S. Q., & Miesenböck, G. (2005). Remote control of behavior through genetically targeted photostimulation of neurons. *Cell*, *121*(1), 141–152. https://doi.org/10.1016/j.cell.2005.02.004

Lin, A. C., Bygrave, A. M., de Calignon, A., Lee, T., & Miesenböck, G. (2014). Sparse, decorrelated odor coding in the mushroom body enhances learned odor

discrimination. *Nature neuroscience*, *17*(4), 559–568. https://doi.org/10.1038/nn.3660

Liu, C., Plaçais, P. Y., Yamagata, N., Pfeiffer, B. D., Aso, Y., Friedrich, A. B., Siwanowicz, I., Rubin, G. M., Preat, T., & Tanimoto, H. (2012). A subset of dopamine neurons signals reward for odour memory in *Drosophila*. *Nature*, *488*(7412), 512–516. https://doi.org/10.1038/nature11304

Liu, Q., Yang, X., Tian, J., Gao, Z., Wang, M., Li, Y., & Guo, A. (2016). Gap junction networks in mushroom bodies participate in visual learning and memory in *Drosophila*. *eLife*, *5*, e13238. https://doi.org/10.7554/eLife.13238

Luan, H., Peabody, N. C., Vinson, C. R., & White, B. H. (2006). Refined spatial manipulation of neuronal function by combinatorial restriction of transgene expression. *Neuron*, *52*(3), 425–436. https://doi.org/10.1016/j.neuron.2006.08.028

Luo, L., & O'Leary, D. D. (2005). Axon retraction and degeneration in development and disease. *Annual review of neuroscience*, *28*, 127–156. https://doi.org/10.1146/annurev.neuro.28.061604.135632

Luo, S. X., Axel, R., & Abbott, L. F. (2010). Generating sparse and selective third-order responses in the olfactory system of the fly. *Proceedings of the National Academy of Sciences of the United States of America*, *107*(23), 10713–10718. https://doi.org/10.1073/pnas.1005635107

Ma, J., & Ptashne, M. (1987). The carboxy-terminal 30 amino acids of GAL4 are recognized by GAL80. *Cell*, *50*(1), 137–142. https://doi.org/10.1016/0092-8674(87)90670-2

Magee, J. C., & Grienberger, C. (2020). Synaptic Plasticity Forms and Functions. *Annual review of neuroscience*, *43*, 95–117. https://doi.org/10.1146/annurev-neuro-090919-022842

Malik, B. R., & Hodge, J. J. (2014). Drosophila adult olfactory shock learning. *Journal of visualized experiments : JoVE*, (90), e50107. https://doi.org/10.3791/50107

Manoim, J. E., Davidson, A. M., Weiss, S., Hige, T., & Parnas, M. (2022). Lateral axonal modulation is required for stimulus-specific olfactory conditioning in Drosophila. *Current biology : CB*, *32*(20), 4438–4450.e5. https://doi.org/10.1016/j.cub.2022.09.007

Marin, E. C., Jefferis, G. S., Komiyama, T., Zhu, H., & Luo, L. (2002). Representation of the glomerular olfactory map in the *Drosophila* brain. *Cell*, *109*(2), 243–255. https://doi.org/10.1016/s0092-8674(02)00700-6

Mark Schnitzer, Cheng Huang, Junjie Luo et al. Dopamine signals integrate innate and learnt valences to regulate memory dynamics, 11 August 2022, PREPRINT (Version 1) available at Research Square. https://doi.org/10.21203/rs.3.rs-1915648/v1

Martinez-Cervantes, J., Shah, P., Phan, A., & Cervantes-Sandoval, I. (2022). Higher-order unimodal olfactory sensory preconditioning in *Drosophila*. *eLife*, *11*, e79107. https://doi.org/10.7554/eLife.79107

Masuda-Nakagawa, L. M., Ito, K., Awasaki, T., & O'Kane, C. J. (2014). A single GABAergic neuron mediates feedback of odor-evoked signals in the mushroom body of larval Drosophila. *Frontiers in neural circuits*, *8*, 35. https://doi.org/10.3389/fncir.2014.00035

Mayseless, O., Berns, D. S., Yu, X. M., Riemensperger, T., Fiala, A., & Schuldiner, O. (2018). Developmental Coordination during Olfactory Circuit Remodeling in *Drosophila*. *Neuron*, *99*(6), 1204–1215.e5. https://doi.org/10.1016/j.neuron.2018.07.050

McGuire, S. E., Le, P. T., & Davis, R. L. (2001). The role of *Drosophila* mushroom body signaling in olfactory memory. *Science (New York, N.Y.)*, *293*(5533), 1330–1333. https://doi.org/10.1126/science.1062622

McGuire, S. E., Mao, Z., & Davis, R. L. (2004). Spatiotemporal gene expression targeting with the TARGET and gene-switch systems in Drosophila. *Science's STKE : signal transduction knowledge environment*, *2004*(220), pl6. https://doi.org/10.1126/stke.2202004pl6

McGuire, S. E., Le, P. T., Osborn, A. J., Matsumoto, K., & Davis, R. L. (2003). Spatiotemporal rescue of memory dysfunction in Drosophila. *Science (New York, N.Y.)*, *302*(5651), 1765–1768. https://doi.org/10.1126/science.1089035

Menzel, R., & Erber, J. (1978). Learning and memory in bees. *Scientific American*, *239*(1), 102-111. http://www.jstor.org/stable/24955780

Miesenböck, G., De Angelis, D. A., & Rothman, J. E. (1998). Visualizing secretion and synaptic transmission with pH-sensitive green fluorescent proteins. *Nature*, *394*(6689), 192–195. https://doi.org/10.1038/28190

Mirzoyan, Z., Sollazzo, M., Allocca, M., Valenza, A. M., Grifoni, D., & Bellosta, P. (2019). *Drosophila melanogaster*: A Model Organism to Study Cancer. *Frontiers in genetics*, *10*, 51. https://doi.org/10.3389/fgene.2019.00051

Montague, P. R., Hyman, S. E., & Cohen, J. D. (2004). Computational roles for dopamine in behavioural control. *Nature*, *431*(7010), 760–767. https://doi.org/10.1038/nature03015

Nagel, G., Ollig, D., Fuhrmann, M., Kateriya, S., Musti, A. M., Bamberg, E., & Hegemann, P. (2002). Channelrhodopsin-1: a light-gated proton channel in green algae. *Science (New York, N.Y.)*, *296*(5577), 2395–2398. https://doi.org/10.1126/science.1072068

Nakai, J., Ohkura, M., & Imoto, K. (2001). A high signal-to-noise Ca(2+) probe composed of a single green fluorescent protein. *Nature biotechnology*, *19*(2), 137–141. https://doi.org/10.1038/84397

neuPrint: Analysis Tools for EM Connectomics. Jody Clements, Tom Dolafi, Lowell Umayam, Nicole L. Neubarth, Stuart Berg, Louis K. Scheffer, Stephen M. Plaza bioRxiv 2020.01.16.909465; doi: https://doi.org/10.1101/2020.01.16.909465

Ni L. (2021). Genetic Transsynaptic Techniques for Mapping Neural Circuits in *Drosophila*. *Frontiers in neural circuits*, *15*, 749586. https://doi.org/10.3389/fncir.2021.749586

Nighorn, A., Healy, M. J., & Davis, R. L. (1991). The cyclic AMP phosphodiesterase encoded by the Drosophila dunce gene is concentrated in the mushroom body neuropil. *Neuron*, *6*(3), 455–467. https://doi.org/10.1016/0896-6273(91)90253-v

Ong, C., Yung, L. Y., Cai, Y., Bay, B. H., & Baeg, G. H. (2015). *Drosophila melanogaster* as a model organism to study nanotoxicity. *Nanotoxicology*, *9*(3), 396–403. https://doi.org/10.3109/17435390.2014.940405

Oshima, K., Takeda, M., Kuranaga, E., Ueda, R., Aigaki, T., Miura, M., & Hayashi, S. (2006). IKK epsilon regulates F actin assembly and interacts with Drosophila IAP1 in cellular morphogenesis. *Current biology : CB*, *16*(15), 1531–1537. https://doi.org/10.1016/j.cub.2006.06.032

Owald, D., & Waddell, S. (2015). Olfactory learning skews mushroom body output pathways to steer behavioral choice in *Drosophila*. *Current opinion in neurobiology*, *35*, 178–184. https://doi.org/10.1016/j.conb.2015.10.002

Owald, D., Felsenberg, J., Talbot, C. B., Das, G., Perisse, E., Huetteroth, W., & Waddell, S. (2015). Activity of defined mushroom body output neurons underlies learned

olfactory behavior in *Drosophila*. *Neuron*, *86*(2), 417–427. https://doi.org/10.1016/j.neuron.2015.03.025

Pandey, A., Saini, S., Khatoon, R., Sharma, D., Narayan, G., & Kar Chowdhuri, D. (2016). Overexpression of hsp27 Rescued Neuronal Cell Death and Reduction in Life- and Health-Span in Drosophila melanogaster Against Prolonged Exposure to Dichlorvos. *Molecular neurobiology*, *53*(5), 3179–3193. https://doi.org/10.1007/s12035-015-9221-3

Paradis, S., Sweeney, S. T., & Davis, G. W. (2001). Homeostatic control of presynaptic release is triggered by postsynaptic membrane depolarization. *Neuron*, *30*(3), 737–749. https://doi.org/10.1016/s0896-6273(01)00326-9

Pavlov, I. P. (1927). Conditioned reflexes: an investigation of the physiological activity of the cerebral cortex. Oxford Univ. Press.

Pavlowsky, A., Schor, J., Plaçais, P. Y., & Preat, T. (2018). A GABAergic Feedback Shapes Dopaminergic Input on the *Drosophila* Mushroom Body to Promote Appetitive Long-Term Memory. *Current biology : CB*, *28*(11), 1783–1793.e4. https://doi.org/10.1016/j.cub.2018.04.040

Pendleton, R. G., Rasheed, A., Sardina, T., Tully, T., & Hillman, R. (2002). Effects of tyrosine hydroxylase mutants on locomotor activity in *Drosophila*: a study in functional genomics. *Behavior genetics*, *32*(2), 89–94. https://doi.org/10.1023/a:1015279221600

Perisse, E., Owald, D., Barnstedt, O., Talbot, C. B., Huetteroth, W., & Waddell, S. (2016). Aversive Learning and Appetitive Motivation Toggle Feed-Forward Inhibition in the Drosophila Mushroom Body. *Neuron*, *90*(5), 1086–1099. https://doi.org/10.1016/j.neuron.2016.04.034

Pfeiffer, B. D., Ngo, T. T., Hibbard, K. L., Murphy, C., Jenett, A., Truman, J. W., & Rubin, G. M. (2010). Refinement of tools for targeted gene expression in *Drosophila*. *Genetics*, *186*(2), 735–755. https://doi.org/10.1534/genetics.110.119917

Pihán, P., Lisbona, F., Borgonovo, J., Edwards-Jorquera, S., Nunes-Hasler, P., Castillo, K., Kepp, O., Urra, H., Saarnio, S., Vihinen, H., Carreras-Sureda, A., Forveille, S., Sauvat, A., De Giorgis, D., Pupo, A., Rodríguez, D. A., Quarato, G., Sagredo, A., Lourido, F., Letai, A., … Hetz, C. (2021). Control of lysosomal-mediated cell death by the pH-dependent calcium channel RECS1. *Science advances*, *7*(46), eabe5469. https://doi.org/10.1126/sciadv.abe5469

Poppinga, H., Çoban, B., Meltzer, H., Mayseless, O., Widmann, A., Schuldiner, O., & Fiala, A. (2022). Pruning deficits of the developing *Drosophila* mushroom body result in mild impairment in associative odour learning and cause hyperactivity. *Open biology*, *12*(9), 220096. https://doi.org/10.1098/rsob.220096

Potter, C. J., & Luo, L. (2011). Using the Q system in *Drosophila melanogaster*. *Nature protocols*, *6*(8), 1105–1120. https://doi.org/10.1038/nprot.2011.347

Prévost, C., Liljeholm, M., Tyszka, J. M., & O'Doherty, J. P. (2012). Neural correlates of specific and general Pavlovian-to-Instrumental Transfer within human amygdalar subregions: a high-resolution fMRI study. *The Journal of neuroscience : the official journal of the Society for Neuroscience*, *32*(24), 8383–8390. https://doi.org/10.1523/JNEUROSCI.6237-11.2012

Qin, H., Cressy, M., Li, W., Coravos, J. S., Izzi, S. A., & Dubnau, J. (2012). Gamma neurons mediate dopaminergic input during aversive olfactory memory formation in Drosophila. *Current biology : CB*, *22*(7), 608–614. https://doi.org/10.1016/j.cub.2012.02.014

Rabinovich, D., Yaniv, S. P., Alyagor, I., & Schuldiner, O. (2016). Nitric Oxide as a Switching Mechanism between Axon Degeneration and Regrowth during Developmental Remodeling. *Cell*, *164*(1-2), 170–182. https://doi.org/10.1016/j.cell.2015.11.047

Rachidi, M., Lopes, C., & Benichou, J. C. (1997). Genetical analysis of visual system disorganizer (vid), a new gene involved in normal development of eye and optic lobe of the brain in Drosophila melanogaster. *Genetica*, *99*(1), 31–45. https://doi.org/10.1007/BF02259496

Redt-Clouet, C., Trannoy, S., Boulanger, A., Tokmatcheva, E., Savvateeva-Popova, E., Parmentier, M. L., Preat, T., & Dura, J. M. (2012). Mushroom body neuronal remodelling is necessary for short-term but not for long-term courtship memory in *Drosophila*. *The European journal of neuroscience*, *35*(11), 1684–1691. https://doi.org/10.1111/j.1460-9568.2012.08103.x

Riemensperger, T., Issa, A. R., Pech, U., Coulom, H., Nguyễn, M. V., Cassar, M., Jacquet, M., Fiala, A., & Birman, S. (2013). A single dopamine pathway underlies progressive locomotor deficits in a Drosophila model of Parkinson disease. *Cell reports*, *5*(4), 952–960. https://doi.org/10.1016/j.celrep.2013.10.032

Riemensperger, T., Völler, T., Stock, P., Buchner, E., & Fiala, A. (2005). Punishment prediction by dopaminergic neurons in Drosophila. *Current biology : CB*, *15*(21), 1953–1960. https://doi.org/10.1016/j.cub.2005.09.042

Rister, J., Pauls, D., Schnell, B., Ting, C. Y., Lee, C. H., Sinakevitch, I., Morante, J., Strausfeld, N. J., Ito, K., & Heisenberg, M. (2007). Dissection of the peripheral motion channel in the visual system of Drosophila melanogaster. *Neuron*, *56*(1), 155–170. https://doi.org/10.1016/j.neuron.2007.09.014

Robert A Rescorla, Second-order conditioning of Pavlovian conditioned inhibition, Learning and Motivation, Volume 7, Issue 2, 1976, Pages 161-172, ISSN 0023-9690, https://doi.org/10.1016/0023-9690(76)90025-4.

Rosenzweig, M., Brennan, K. M., Tayler, T. D., Phelps, P. O., Patapoutian, A., & Garrity, P. A. (2005). The *Drosophila* ortholog of vertebrate TRPA1 regulates thermotaxis. *Genes & development*, *19*(4), 419–424. https://doi.org/10.1101/gad.1278205

Ryglewski, S., Vonhoff, F., Scheckel, K., & Duch, C. (2017). Intra-neuronal Competition for Synaptic Partners Conserves the Amount of Dendritic Building Material. *Neuron*, *93*(3), 632–645.e6. https://doi.org/10.1016/j.neuron.2016.12.043

Sabandal, J. M., Berry, J. A., & Davis, R. L. (2021). Dopamine-based mechanism for transient forgetting. *Nature*, *591*(7850), 426–430. https://doi.org/10.1038/s41586-020-03154-y

Saumweber, T., Rohwedder, A., Schleyer, M., Eichler, K., Chen, Y. C., Aso, Y., Cardona, A., Eschbach, C., Kobler, O., Voigt, A., Durairaja, A., Mancini, N., Zlatic, M., Truman, J. W., Thum, A. S., & Gerber, B. (2018). Functional architecture of reward learning in mushroom body extrinsic neurons of larval *Drosophila*. *Nature communications*, *9*(1), 1104. https://doi.org/10.1038/s41467-018-03130-1

Sayin, S., De Backer, J. F., Siju, K. P., Wosniack, M. E., Lewis, L. P., Frisch, L. M., Gansen, B., Schlegel, P., Edmondson-Stait, A., Sharifi, N., Fisher, C. B., Calle-Schuler, S. A., Lauritzen, J. S., Bock, D. D., Costa, M., Jefferis, G. S. X. E., Gjorgjieva, J., & Grunwald Kadow, I. C. (2019). A Neural Circuit Arbitrates between Persistence and Withdrawal in Hungry *Drosophila*. *Neuron*, *104*(3), 544–558.e6. https://doi.org/10.1016/j.neuron.2019.07.028

Scheffer, L. K., Xu, C. S., Januszewski, M., Lu, Z., Takemura, S. Y., Hayworth, K. J., Huang, G. B., Shinomiya, K., Maitlin-Shepard, J., Berg, S., Clements, J., Hubbard,

P. M., Katz, W. T., Umayam, L., Zhao, T., Ackerman, D., Blakely, T., Bogovic, J., Dolafi, T., Kainmueller, D., … Plaza, S. M. (2020). A connectome and analysis of the adult *Drosophila* central brain. *eLife*, *9*, e57443. https://doi.org/10.7554/eLife.57443

Schroll, C., Riemensperger, T., Bucher, D., Ehmer, J., Völler, T., Erbguth, K., Gerber, B., Hendel, T., Nagel, G., Buchner, E., & Fiala, A. (2006). Light-induced activation of distinct modulatory neurons triggers appetitive or aversive learning in Drosophila larvae. *Current biology : CB*, *16*(17), 1741–1747. https://doi.org/10.1016/j.cub.2006.07.023

Schultz, W., Dayan, P., & Montague, P. R. (1997). A neural substrate of prediction and reward. *Science (New York, N.Y.)*, *275*(5306), 1593–1599. https://doi.org/10.1126/science.275.5306.1593

Schwaerzel, M., Heisenberg, M., & Zars, T. (2002). Extinction antagonizes olfactory memory at the subcellular level. *Neuron*, *35*(5), 951–960. https://doi.org/10.1016/s0896-6273(02)00832-2

Schwaerzel, M., Monastirioti, M., Scholz, H., Friggi-Grelin, F., Birman, S., & Heisenberg, M. (2003). Dopamine and octopamine differentiate between aversive and appetitive olfactory memories in *Drosophila*. *The Journal of neuroscience : the official journal of the Society for Neuroscience*, *23*(33), 10495–10502. https://doi.org/10.1523/JNEUROSCI.23-33-10495.2003

Sekar, A., Bialas, A. R., de Rivera, H., Davis, A., Hammond, T. R., Kamitaki, N., Tooley, K., Presumey, J., Baum, M., Van Doren, V., Genovese, G., Rose, S. A., Handsaker, R. E., Schizophrenia Working Group of the Psychiatric Genomics Consortium, Daly, M. J., Carroll, M. C., Stevens, B., & McCarroll, S. A. (2016). Schizophrenia risk from complex variation of complement component 4. *Nature*, *530*(7589), 177–183. https://doi.org/10.1038/nature16549

Shanbhag, S. R., Müller, B., & Steinbrecht, R. A. (2000). Atlas of olfactory organs of *Drosophila melanogaster* 2. Internal organization and cellular architecture of olfactory sensilla. *Arthropod structure & development*, *29*(3), 211–229. https://doi.org/10.1016/s1467-8039(00)00028-1.

Siegenthaler, D., Escribano, B., Bräuler, V., & Pielage, J. (2019). Selective suppression and recall of long-term memories in Drosophila. *PLoS biology*, *17*(8), e3000400. https://doi.org/10.1371/journal.pbio.3000400

Silbering, A. F., Rytz, R., Grosjean, Y., Abuin, L., Ramdya, P., Jefferis, G. S., & Benton, R. (2011). Complementary function and integrated wiring of the evolutionarily distinct Drosophila olfactory subsystems. *The Journal of neuroscience : the official journal of the Society for Neuroscience*, *31*(38), 13357–13375. https://doi.org/10.1523/JNEUROSCI.2360-11.2011

Skoulakis, E. M., Kalderon, D., & Davis, R. L. (1993). Preferential expression in mushroom bodies of the catalytic subunit of protein kinase A and its role in learning and memory. *Neuron*, *11*(2), 197–208. https://doi.org/10.1016/0896-6273(93)90178-t

Springer, M., & Nawrot, M. P. (2021). A Mechanistic Model for Reward Prediction and Extinction Learning in the Fruit Fly. *eNeuro*, *8*(3), ENEURO.0549-20.2021. https://doi.org/10.1523/ENEURO.0549-20.2021

Stanhope K. J. (1992). The representation of the reinforcer and the force of the pigeon's keypeck in first- and second-order conditioning. *The Quarterly journal of experimental psychology. B, Comparative and physiological psychology*, *44*(2), 137–158. https://doi.org/10.1080/02724999208250607

Sugamori, K. S., Demchyshyn, L. L., McConkey, F., Forte, M. A., & Niznik, H. B. (1995). A primordial dopamine D1-like adenylyl cyclase-linked receptor from Drosophila melanogaster displaying poor affinity for benzazepines. *FEBS letters*, *362*(2), 131–138. https://doi.org/10.1016/0014-5793(95)00224-w

Sun, H., Nishioka, T., Hiramatsu, S., Kondo, S., Amano, M., Kaibuchi, K., Ichinose, T., & Tanimoto, H. (2020). Dopamine Receptor Dop1R2 Stabilizes Appetitive Olfactory Memory through the Raf/MAPK Pathway in *Drosophila*. *The Journal of neuroscience : the official journal of the Society for Neuroscience*, *40*(14), 2935–2942. https://doi.org/10.1523/JNEUROSCI.1572-19.2020

Suzuki, Y., Kurata, Y., & Sakai, T. (2022). Dorsal-lateral clock neurons modulate consolidation and maintenance of long-term memory in *Drosophila*. *Genes to cells : devoted to molecular & cellular mechanisms*, *27*(4), 266–279. https://doi.org/10.1111/gtc.12923

Sweeney, S. T., Broadie, K., Keane, J., Niemann, H., & O'Kane, C. J. (1995). Targeted expression of tetanus toxin light chain in *Drosophila* specifically eliminates synaptic transmission and causes behavioral defects. *Neuron*, *14*(2), 341–351. https://doi.org/10.1016/0896-6273(95)90290-2

Szüts, D., & Bienz, M. (2000). LexA chimeras reveal the function of *Drosophila* Fos as a context-dependent transcriptional activator. *Proceedings of the National Academy of Sciences of the United States of America*, *97*(10), 5351–5356. https://doi.org/10.1073/pnas.97.10.5351

Takeuchi, K. I., Honda, D., Okumura, M., Miura, M., & Chihara, T. (2022). Systemic innate immune response induces death of olfactory receptor neurons in Drosophila. *Genes to cells : devoted to molecular & cellular mechanisms*, *27*(2), 113–123. https://doi.org/10.1111/gtc.12914

Talay, M., Richman, E. B., Snell, N. J., Hartmann, G. G., Fisher, J. D., Sorkaç, A., Santoyo, J. F., Chou-Freed, C., Nair, N., Johnson, M., Szymanski, J. R., & Barnea, G. (2017). Transsynaptic Mapping of Second-Order Taste Neurons in Flies by trans-Tango. *Neuron*, *96*(4), 783–795.e4. https://doi.org/10.1016/j.neuron.2017.10.011

Tempel, B. L., Livingstone, M. S., & Quinn, W. G. (1984). Mutations in the dopa decarboxylase gene affect learning in *Drosophila*. *Proceedings of the National Academy of Sciences of the United States of America*, *81*(11), 3577–3581. https://doi.org/10.1073/pnas.81.11.3577

Theobald, J. C., Duistermars, B. J., Ringach, D. L., & Frye, M. A. (2008). Flies see second-order motion. *Current biology : CB*, *18*(11), R464–R465. https://doi.org/10.1016/j.cub.2008.03.050

Theobald, J. C., Shoemaker, P. A., Ringach, D. L., & Frye, M. A. (2010). Theta motion processing in fruit flies. *Frontiers in behavioral neuroscience*, *4*, 35. https://doi.org/10.3389/fnbeh.2010.00035

Thomas, M. S., Davis, R., Karmiloff-Smith, A., Knowland, V. C., & Charman, T. (2016). The over-pruning hypothesis of autism. *Developmental science*, *19*(2), 284–305. https://doi.org/10.1111/desc.12303

Tissot, M., & Stocker, R. F. (2000). Metamorphosis in *drosophila* and other insects: the fate of neurons throughout the stages. *Progress in neurobiology*, *62*(1), 89–111. https://doi.org/10.1016/s0301-0082(99)00069-6

Tolwinski N. S. (2017). Introduction: Drosophila-A Model System for Developmental Biology. *Journal of developmental biology*, *5*(3), 9. https://doi.org/10.3390/jdb5030009

Tomchik S. M. (2013). Dopaminergic neurons encode a distributed, asymmetric representation of temperature in Drosophila. *The Journal of neuroscience : the*

official journal of the Society for Neuroscience, *33*(5), 2166–76a. https://doi.org/10.1523/JNEUROSCI.3933-12.2013

Tomchik, S. M., & Davis, R. L. (2009). Dynamics of learning-related cAMP signaling and stimulus integration in the Drosophila olfactory pathway. *Neuron*, *64*(4), 510–521. https://doi.org/10.1016/j.neuron.2009.09.029

Tully, T., & Quinn, W. G. (1985). Classical conditioning and retention in normal and mutant *Drosophila melanogaster*. *Journal of comparative physiology. A, Sensory, neural, and behavioral physiology*, *157*(2), 263–277. https://doi.org/10.1007/BF01350033

Turner, G. C., Bazhenov, M., & Laurent, G. (2008). Olfactory representations by *Drosophila* mushroom body neurons. *Journal of neurophysiology*, *99*(2), 734–746. https://doi.org/10.1152/jn.01283.2007

Twitmyer, E. B. (1905) Knee-jerks without stimulation of the patellar tendon. *Psychological Bulletin*, *2*, 43–44. https://doi.org/10.1037/h0037386

Ueoka, Y., Hiroi, M., Abe, T., & Tabata, T. (2017). Suppression of a single pair of mushroom body output neurons in *Drosophila* triggers aversive associations. *FEBS open bio*, *7*(4), 562–576. https://doi.org/10.1002/2211-5463.12203

Venken, K. J., Simpson, J. H., & Bellen, H. J. (2011). Genetic manipulation of genes and cells in the nervous system of the fruit fly. *Neuron*, *72*(2), 202–230. https://doi.org/10.1016/j.neuron.2011.09.021

Vrontou, E., Groschner, L. N., Szydlowski, S., Brain, R., Krebbers, A., & Miesenböck, G. (2021). Response competition between neurons and antineurons in the mushroom body. *Current biology : CB*, *31*(22), 4911–4922.e4. https://doi.org/10.1016/j.cub.2021.09.008

Wang, J. W., Wong, A. M., Flores, J., Vosshall, L. B., & Axel, R. (2003). Two-photon calcium imaging reveals an odor-evoked map of activity in the fly brain. *Cell*, *112*(2), 271–282. https://doi.org/10.1016/s0092-8674(03)00004-7

Wang, L., Wu, C., Peng, W., Zhou, Z., Zeng, J., Li, X., Yang, Y., Yu, S., Zou, Y., Huang, M., Liu, C., Chen, Y., Li, Y., Ti, P., Liu, W., Gao, Y., Zheng, W., Zhong, H., Gao, S., Lu, Z., … Chu, J. (2022). A high-performance genetically encoded fluorescent indicator for in vivo cAMP imaging. *Nature communications*, *13*(1), 5363. https://doi.org/10.1038/s41467-022-32994-7

Wang, M., Li, A., Sekiya, M., Beckmann, N. D., Quan, X., Schrode, N., Fernando, M. B., Yu, A., Zhu, L., Cao, J., Lyu, L., Horgusluoglu, E., Wang, Q., Guo, L., Wang, Y. S.,

Neff, R., Song, W. M., Wang, E., Shen, Q., Zhou, X., … Zhang, B. (2021). Transformative Network Modeling of Multi-omics Data Reveals Detailed Circuits, Key Regulators, and Potential Therapeutics for Alzheimer's Disease. *Neuron*, *109*(2), 257–272.e14. https://doi.org/10.1016/j.neuron.2020.11.002

Wang, Y., Mamiya, A., Chiang, A. S., & Zhong, Y. (2008). Imaging of an early memory trace in the *Drosophila* mushroom body. *The Journal of neuroscience : the official journal of the Society for Neuroscience*, *28*(17), 4368–4376. https://doi.org/10.1523/JNEUROSCI.2958-07.2008

Watts, R. J., Hoopfer, E. D., & Luo, L. (2003). Axon pruning during Drosophila metamorphosis: evidence for local degeneration and requirement of the ubiquitin-proteasome system. *Neuron*, *38*(6), 871–885. https://doi.org/10.1016/s0896-6273(03)00295-2

Wise R. A. (2004). Dopamine, learning and motivation. *Nature reviews. Neuroscience*, *5*(6), 483–494. https://doi.org/10.1038/nrn1406

Wong, A. M., Wang, J. W., & Axel, R. (2002). Spatial representation of the glomerular map in the *Drosophila* protocerebrum. *Cell*, *109*(2), 229–241. https://doi.org/10.1016/s0092-8674(02)00707-9

Wu, L., Dong, A., Dong, L., Wang, S. Q., & Li, Y. (2019). PARIS, an optogenetic method for functionally mapping gap junctions. *eLife*, *8*, e43366. https://doi.org/10.7554/eLife.43366

Xia, S., Liu, L., Feng, C., & Guo, A. (1997). Memory consolidation in Drosophila operant visual learning. *Learning & memory (Cold Spring Harbor, N.Y.)*, *4*(2), 205–218. https://doi.org/10.1101/lm.4.2.205

Xia, Z. G., Refsdal, C. D., Merchant, K. M., Dorsa, D. M., & Storm, D. R. (1991). Distribution of mRNA for the calmodulin-sensitive adenylate cyclase in rat brain: expression in areas associated with learning and memory. *Neuron*, *6*(3), 431–443. https://doi.org/10.1016/0896-6273(91)90251-t

Xie, Z., Huang, C., Ci, B., Wang, L., & Zhong, Y. (2013). Requirement of the combination of mushroom body γ lobe and α/β lobes for the retrieval of both aversive and appetitive early memories in *Drosophila*. *Learning & memory (Cold Spring Harbor, N.Y.)*, *20*(9), 474–481. https://doi.org/10.1101/lm.031823.113

Yamada, D., Bushey, D., Li, F., Hibbard, K. L., Sammons, M., Funke, J., Litwin-Kumar, A., Hige, T., & Aso, Y. (2023). Hierarchical architecture of dopaminergic circuits enables second-order conditioning in *Drosophila*. *eLife*, *12*, e79042. Advance online publication. https://doi.org/10.7554/eLife.7904.

Yamanaka, N., Rewitz, K. F., & O'Connor, M. B. (2013). Ecdysone control of developmental transitions: lessons from *Drosophila* research. *Annual review of entomology*, *58*, 497–516. https://doi.org/10.1146/annurev-ento-120811-153608

Yaron, A., & Schuldiner, O. (2016). Common and Divergent Mechanisms in Developmental Neuronal Remodeling and Dying Back Neurodegeneration. *Current biology : CB*, *26*(13), R628–R639. https://doi.org/10.1016/j.cub.2016.05.025

Yost, R. T., Robinson, J. W., Baxter, C. M., Scott, A. M., Brown, L. P., Aletta, M. S., Hakimjavadi, R., Lone, A., Cumming, R. C., Dukas, R., Mozer, B., & Simon, A. F. (2020). Abnormal Social Interactions in a *Drosophila* Mutant of an Autism Candidate Gene: *Neuroligin 3*. *International journal of molecular sciences*, *21*(13), 4601. https://doi.org/10.3390/ijms21134601

Yu, D., Keene, A. C., Srivatsan, A., Waddell, S., & Davis, R. L. (2005). *Drosophila* DPM neurons form a delayed and branch-specific memory trace after olfactory classical conditioning. *Cell*, *123*(5), 945–957. https://doi.org/10.1016/j.cell.2005.09.037

Yu, F., & Schuldiner, O. (2014). Axon and dendrite pruning in Drosophila. *Current opinion in neurobiology*, *27*, 192–198. https://doi.org/10.1016/j.conb.2014.04.005

Yu, X. M., Gutman, I., Mosca, T. J., Iram, T., Ozkan, E., Garcia, K. C., Luo, L., & Schuldiner, O. (2013). Plum, an immunoglobulin superfamily protein, regulates axon pruning by facilitating TGF-β signaling. *Neuron*, *78*(3), 456–468. https://doi.org/10.1016/j.neuron.2013.03.004

Zars, T., Fischer, M., Schulz, R., & Heisenberg, M. (2000). Localization of a short-term memory in *Drosophila*. *Science (New York, N.Y.)*, *288*(5466), 672–675. https://doi.org/10.1126/science.288.5466.672

Zatsepina, O. G., Nikitina, E. A., Shilova, V. Y., Chuvakova, L. N., Sorokina, S., Vorontsova, J. E., Tokmacheva, E. V., Funikov, S. Y., Rezvykh, A. P., & Evgen'ev, M. B. (2021). Hsp70 affects memory formation and behaviorally relevant gene expression in Drosophila melanogaster. *Cell stress & chaperones*, *26*(3), 575–594. https://doi.org/10.1007/s12192-021-01203-7

Zhang, X., Liu, H., Lei, Z., Wu, Z., & Guo, A. (2013). Lobula-specific visual projection neurons are involved in perception of motion-defined second-order motion in Drosophila. *The Journal of experimental biology*, *216*(Pt 3), 524–534. https://doi.org/10.1242/jeb.079095

Zhang, Y., Zhou, Y., Zhang, X., Wang, L., & Zhong, Y. (2021). Clock neurons gate memory extinction in Drosophila. *Current biology : CB*, *31*(6), 1337–1343.e4. https://doi.org/10.1016/j.cub.2021.01.008

Zhao, B., Sun, J., Zhang, X., Mo, H., Niu, Y., Li, Q., Wang, L., & Zhong, Y. (2019). Long-term memory is formed immediately without the need for protein synthesis-dependent consolidation in *Drosophila*. *Nature communications*, *10*(1), 4550. https://doi.org/10.1038/s41467-019-12436-7

Zhu Y. (2013). The Drosophila visual system: From neural circuits to behavior. *Cell adhesion & migration*, *7*(4), 333–344. https://doi.org/10.4161/cam.25521

Zhu, Y., Nern, A., Zipursky, S. L., & Frye, M. A. (2009). Peripheral visual circuits functionally segregate motion and phototaxis behaviors in the fly. *Current biology : CB*, *19*(7), 613–619. https://doi.org/10.1016/j.cub.2009.02.053

Appendix (Abbreviations list)

3-OCT	3-Octanol
Ach	Acetylcholine
AL	Antennal lobe
APF	After pupa formation
APL	Anterior paired lateral
BenzA	Benzaldehyde
cAMP	3’5’-cyclic adenosine monophosphate
CaMPARI	Calcium modulated photoactivatable ratiometric integrator
CS	Conditioned stimulus
DA	Dopamine
DAN	Dopaminergic neuron
DPM	Dorsal paired medial
dTrpA1	*Drosophila* transient receptor potential A1
FLP	Flipase
FOC	First-order conditioning
FRT	Flipase recognition target
GABA	Gamma-aminobutyric acid
GABA-B-R1	Gamma-aminobutyric acid-B-receptor 1
GFP	Green fluorescent protein
GRASP	GFP reconstitution across synaptic partners
Irk1/Kir2.1	Inwardly rectifying potassium channel 1
KC	Kenyon cell
lexAop	lexA operator

LH	Lateral horn
MB	Mushroom body
MBON	Mushroom body output neuron
MCH	4-Methylcyclohexanol
OR	Olfactory receptor
OSN	Olfactory sensory neuron
PA	Pentyl acetate
PAM	Protocerebral anterior medial
PN	Projection neuron
PPL	Protocerebral posterior lateral
QUAS	QF upstream activation sequence
Shi^{ts}	Temperature-sensitive Shibire
SOC	Second-order conditioning
Syp	Synaptophysin
TOC	Third-order conditioning
UAS	Upstream activation sequence
US	Unconditioned stimulus

Acknowledgments

First, I would like to thank my supervisor Prof. Dr. André Fiala for providing me with the opportunity to work in his lab along with his precious help and support. He never hesitated to procure me with his exceptional scientific knowledge and input in case of need for guidance.

In addition, I would to thank my thesis committee members Prof. Dr. Ralf Heinrich and Prof. Dr. Siegrid Löwel for their valuable support and feedback during our thorough discussions in our TAC meetings. Special thanks go Prof. Dr. Ralf Heinrich for reviewing this thesis.

I am also grateful for Dr. Annekathrin Widmann and Dr. Clare Elizabeth Hancock for their technical help in learning various techniques employed in the scope of this work, along with their scientific input and support.

I am grateful to our collaborators in the Nawrot workgroup at the University of Cologne - Prof. Martin Nawrot, Anna-Maria Jürgensen, and Magdalena Springer - together with Suewei Lin and Chen-Han Lin from Academia Sinica in Tapei- Taiwan, for their work and discussions involving the third manuscript of this thesis.

I am very lucky to have supervised numerous students who contributed in one way or the other in my doctoral research in the past years - Eva Küsters, Marie Eileen Wiesenhavern, Julia Kniep, Tim Wellinghof, Johanna-Marie Hunke, and Tejas Nair.

I am tremendously thankful for Jutta Böker for being my savior in my daily lab life and her warm welcoming smile in the face of any challenge. I am particularly grateful for Annegret Lattner for helping me navigate through all aspects of bureaucracy as an expat and for always going the extra mile in making sure that I was well integrated.

I am grateful for having such wonderful fellow PhD students - Hanna Rebekka Franz, Stephan Hubertus Deimel, Lisa Epple and Yogesh Gadgil. Thank you for your kindness and companionship. In particular, I would like to thank Hanna and Stephan for their stimulating scientific discussions and their support but above all for all the joy, the laughter and the fun we had during these past few years.

Furthermore, I would like to especially thank Dr. Annekathrin Widmann Hanna Rebekka Franz for reviewing and proofreading this thesis, giving me very helpful suggestions and corrections.

Special thanks go to our workshop - notably Jan Hoffman and Tobias Mühmer - for all their help and their welcoming kindness.

I am grateful for my two best-friends, nay brothers, Nabil Zniber and Noureddine Raïss for their love and support. Even though our journeys have diverged, you will always be a part of my life.

Above all else, I am grateful for my family: My parents, Naima Simou and Allal Rachad, for their unconditional and boundless love and support, for giving me strength, and for making me the person that I am today, along with my sister Kawtar Ezzemrani and nephews, Jad and Amir Fakir, for being the bright spots in my rainy days.

One last and prominent thank you goes to my wife Habiba Lahlal for her support in every step that I make, for her love and affection and for her patience in dealing with my travails, my absences, my fits of pique and impatience during my doctoral research.